CO_2 Sequestration via Gas Hydrates

AERI/COURSE Agreement Number: 1569

Graduate Students: Faisal Al-Otabi,

Chee Wee Sia, Carlos Giraldo Sierra and Kasif Khan

Academic Advisors: Raj Bishnoi, Matthew Clarke

And Brij Maini

FINAL REPORT

March 15, 2010

Abstract

This project was aimed at evaluating the feasibility of storing CO2 in underground porous formations in the form of CO_2 hydrate. The main objectives were to investigate the conditions needed to form CO_2 hydrate in porous media, determine the intrinsic kinetics of CO_2 hydrate formation, develop experimental techniques for creating hydrate saturated porous media in the laboratory and investigate the formation and decomposition of hydrates under controlled conditions using well characterized sand-packs.

Significant progress was made towards developing an improved understanding of hydrate behaviour in porous media. An experimental rig and experimental methodology was developed for generating uniformly distributed hydrate saturation in sand-packs at desired levels of hydrate saturation. The rig was used extensively to study the formation and decomposition of hydrates in porous media and to measure the effect of hydrate saturation on the permeability of the sand. An experimental methodology to study the replacement of methane with CO_2 in methane hydrate containing porous media, which would permit the recovery of methane and sequestration of CO_2 in the same process, was also developed. Numerical simulation models were also used to study this process. The work has generated one completed Ph.D. thesis and two interim reports by Ph.D. candidates that will form the backbone of their Ph.D. theses.

The project has supported four graduate students in their research. One Ph.D. student, Faisal Al-Otabi, graduated in November 2009 and two PhD students, Chee Wee Sia and Carlos Giraldo Sierra, are continuing with their experimental work. One M.Sc. student, Mr. Kasif Khan is near the end of his program and will graduate later this year. The project has also supported work of a post-doctoral fellow, Dr. Amit Majumdar.

This project has generated much important information on evaluating the potential of forming CO_2 hydrates in underground porous formations. Many of the basic thermodynamic and kinetic parameters, that were not available at the start of this work, have been successfully measured. Experimental data on formation and decomposition of CO_2 hydrates in porous media have been generated. Numerical models of hydrate formation in porous media have been developed. Thus all objectives of the project have been met.

Keywords: CO_2 Sequestration, gas hydrates, porous media, hydrate formation kinetics, numerical simulation, laboratory studies.

Table of Contents

Experimental results obtained by Lee et al. (2003) show that this replacement is favoured in the laboratory setting. Also, molecular dynamics simulation of the guest's replacement in the hydrate structure shows thermodynamic feasibility of the process (Yezdimer et al., 2002). This simulation was done using the approach of pure gas components and the ideal filling of cages, with hypothetical mutation when CH_4 in hydrate cages is substituted by CO_2 in the cages. In natural settings, electrolytes are usually present to affect the phase equilibrium, while cages are only partially filled. Also, it is aqueous CO_2 that pushes CH_4 from cages to become, first, aqueous and then gaseous CH_4.

In assessing this technology, first, equilibrium composition of mixed hydrate and vapour phase as well as the occupancy needs to be predicted at different thermodynamic conditions. Then, influence of electrolytes on the equilibrium must be estimated. Kinetics of conversion is a key factor in this problem and needs to be understood. In addition, the replacement reaction rate and net amount in natural environment will depend not only on gas transport but also on dispersion of hydrate in sediments and hydrate particle size. The latter two factors depend on the pore size because the size affects the total gas content in the pore. For example, the amount of gas in small pores may be simply insufficient to initiate nucleation and to maintain equilibrium concentration. Consequently, hydrate may not form there although P-T conditions correspond to their stability. This agrees with observations that hydrates tend to be less abundant in clays compared to the larger pore sediments at the same depth.

The Original Project Goals

The goals set at the beginning of the project were:

1. To investigate the hydrate formation kinetics of CO_2, CH_4, C_2H_6, propane and their mixtures.
2. To determine the crystalline properties of hydrates using a Raman Spectrometer.
3. To collect experimental data on formation and decomposition of CO_2 and CH_4-CO_2 hydrates in porous media.
4. To evaluate the feasibility of recovering CH_4 from naturally occurring hydrate deposits by injecting CO_2 to replace CH_4 by CO_2.
5. To develop a mathematical model for hydrate formation and decomposition in porous media.

Experimental Investigation of the Formation of CO_2 hydrate in Porous Media and Its Impact on Formation Permeability

An experimental study of CO_2 hydrate formation and decomposition in porous media has been completed. An important objective of this work was to evaluate the loss of formation permeability resulting from the formation of CO_2 hydrate in the sand. For CO_2 sequestration, it is essential to ensure that the formation of hydrate in the vicinity of injection wells does not result in complete loss of permeability. It was found that appreciable permeability can be maintained after formation of CO_2 hydrate in sand-packs provided the hydrate saturation does not exceed certain threshold value, which would depend on the original sand permeability. It was also found that the hydrate saturation can be kept low by reducing the water saturation in the sand before forming the hydrates.

Details of this work are presented in Appendix B of this report. The following provides a brief overview of the important findings.

Hydrate Formation Experiments

Hydrate formation experiments were carried out in a sand-pack prepared in a windowed cell. The cell was equipped with several thermocouples and the local change of temperature in the sand served as an indicator of hydrate formation or decomposition. Hydrate formation is exothermic in nature and hydrate decomposition is strongly endothermic. Therefore, an increase in local temperature indicates hydrate formation while the decrease would indicate decomposition of hydrate. Temperatures at several locations in the sand-pack were recorded. When the pressure of the cell was increased above the hydrate formation pressure, and hydrate was expected to form.

Figures 1 and 2 show the formation characteristics. The samples have different initial water saturations, 45% and 60% respectively. Based on the temperatures recorded by the thermocouples and gas inflow recorded by the mass flow meter these two samples can be compared.

Referring to Figure 1, when the pressure was increased to 350 psi, the start of the hydrate growth occurred after 14 minutes. The continuous supply of CO_2 gas maintained the pressure above the hydrate formation pressure. The peak temperature recorded by each of the thermocouple was different. Even the initiation periods of hydrate formation at different locations were different. Random smaller peaks of temperature can be observed thereafter. No general order can be observed. After 2.5 hours, no obvious new peaks were recorded.

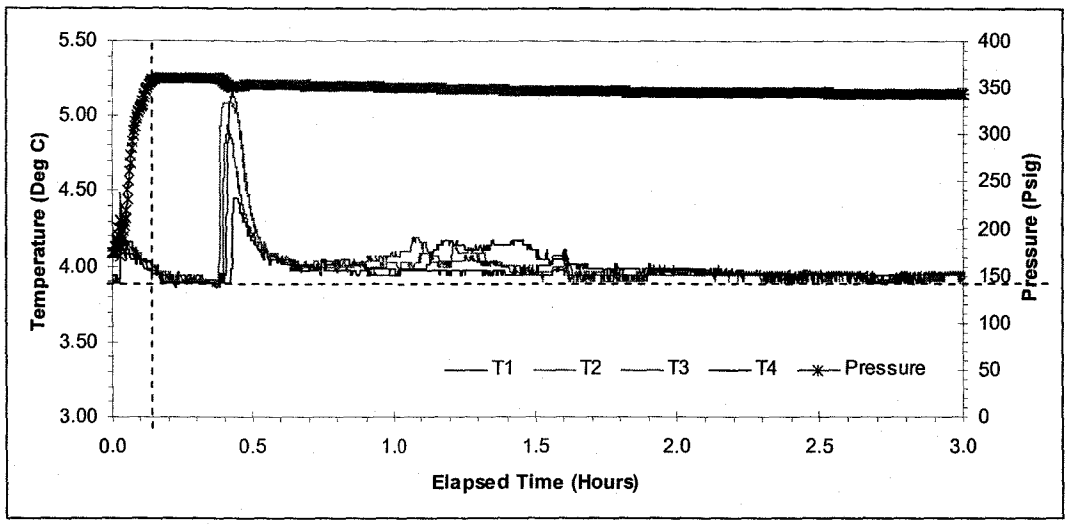

Figure 1: Temperature and Pressure versus Elapsed time during formation of hydrate (S_{wi} = 45%)

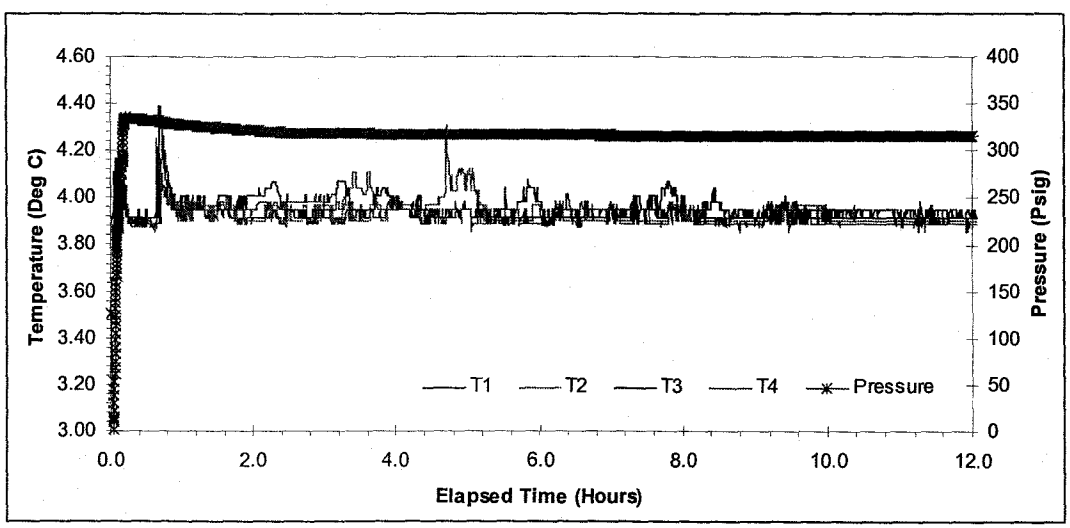

Figure 2: Temperature and Pressure versus Elapsed time during formation of hydrate (S_{wi} = 62%)

Figure 2 shows the graph of temperature and pressure versus elapsed time during hydrate formation for sample with 60% initial water saturation. More random peaks can be observed. Similar to Figure 1, no general temperature patterns can be observed.

Permeability of Hydrate Saturated Sand

Permeability of the porous medium in the presence of hydrate was measured by varying the gas flow rate and measuring the pressure gradient.

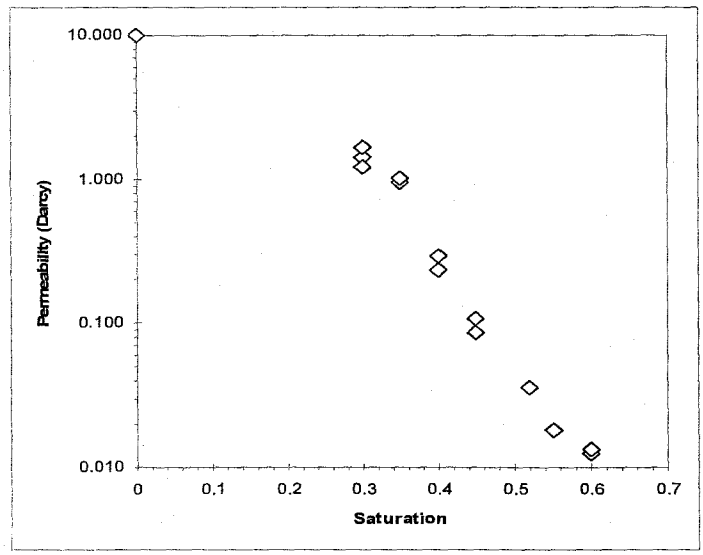

Figure 3: Graph of Permeability versus initial water saturation

Figure 3 shows the graph of permeability of the porous medium in the presence of hydrate versus the initial water saturation used for forming the hydrate. The investigation was conducted for the saturation varying from 30% to 62%. The absolute permeability of the porous medium is 10 Darcy. With 30% hydrate formed in the system, the permeability dropped below 2 Darcy, and the porous medium is almost impermeable when the hydrate saturation is above 60%. Each of the run was repeated twice, and the results are repeatable. The repeatability was not an issue when the distribution of water in the porous medium was uniform.

Existing permeability models versus experimental results

Kleinberg *et al.* (2003) reviewed the existing permeability models to study the formation habit of gas hydrates in natural environment. In the current study, such models are compared with the measured permeability.

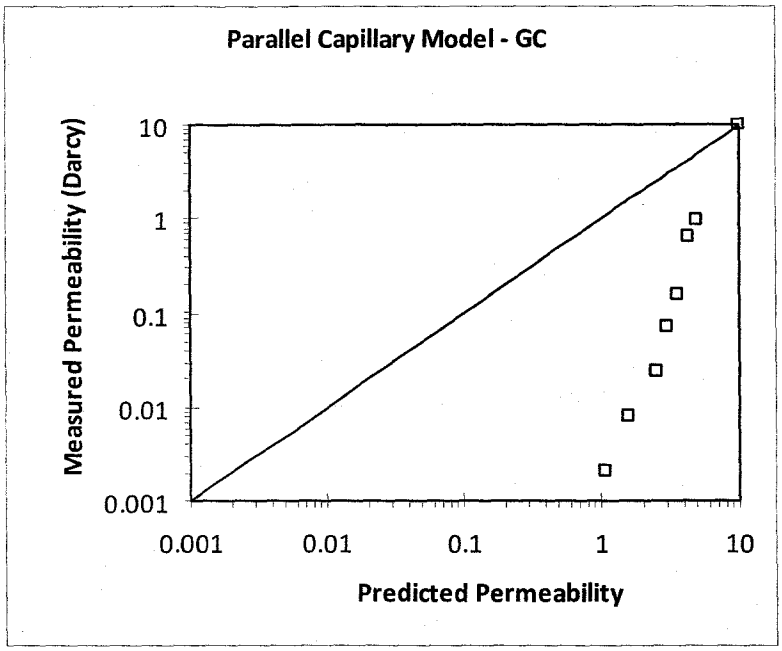

Figure 4: Measured permeability versus predicted permeability using parallel capillary model (grain coating)

Figure 4 is the graph of measured permeability versus predicted permeability using parallel capillary model for grain coating formation habit. From the comparison, it is obvious that either the capillary permeability model is not a good model for permeability prediction or the hydrate formed in the system under study is not grain coating. Based on the published results by Kleinberg *et al.* (2003) and Kumar *et al.*, (2010) the performance of this model is questionable. This is due to the omission of the tortuosity and the control of pore throats on the permeability.

Kozeny Grain model, does take into account the tortuosity. However, it is kept constant *i.e.* the tortuosity does not vary with the hydrate saturation. The predicted permeability using this model is compared to the measured permeability from the current study. Figures 5 and 6 show graphs of measured permeability versus predicted permeability using Kozeny grain model for grain coating and pore filling formation habit respectively. From the comparison, neither the grain coating nor the pore filling model describes the observed behaviour.

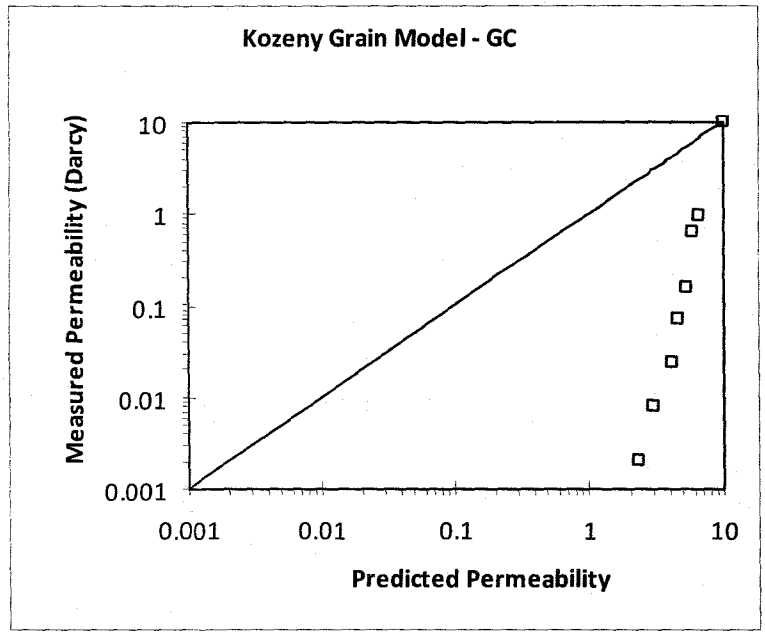

Figure 5: Graph of measured permeability versus predicted permeability using Kozeny Grain Model (Grain coating)

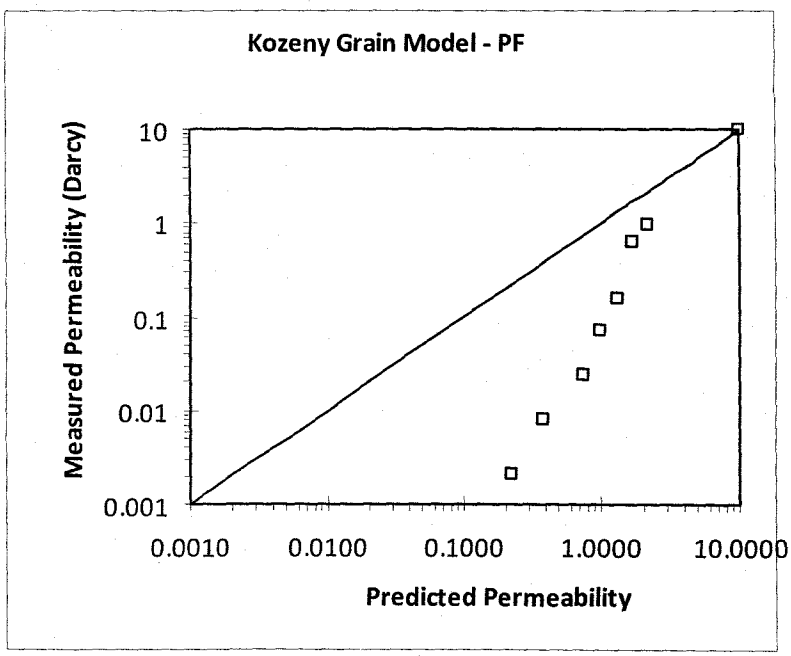

Figure 6: Graph of measured permeability versus predicted permeability using Kozeny Grain Model (Pore Filling)

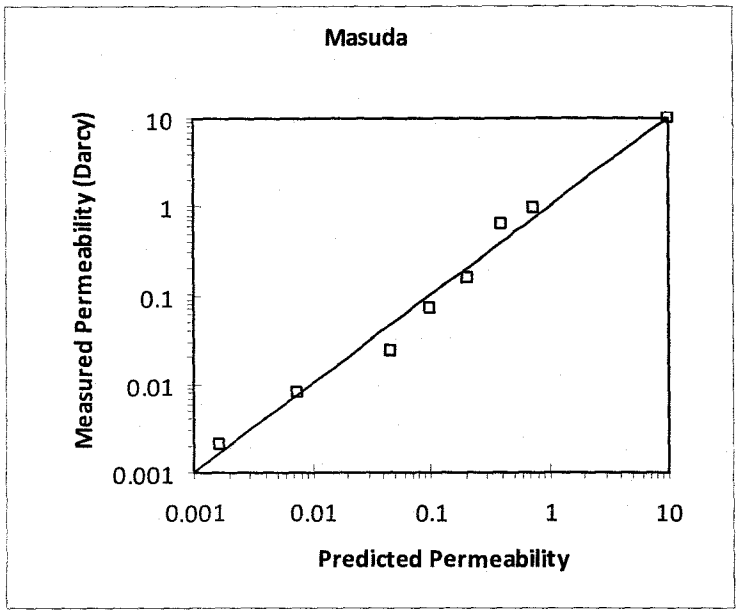

Figure 7: Graph of measured permeability versus predicted permeability using University of Tokyo Model

Figure 7 shows the graph of measured permeability versus predicted permeability using University of Tokyo model. By varying the Masuda permeability reduction exponent value, N, a very good match is achieved when $N = 9$.

As mentioned by Kleinberg *et al.* (2003) this model is very versatile, but cannot explain the formation habit of the gas hydrate in porous media. We believe that the permeability reduction exponent can be related to the properties of the porous media. However, further investigation is required before any firm conclusion can be made.

The dissociation of hydrates and cumulative gas production

In the experimental study, the gas was collected during dissociation by lowering the output pressure below the hydrate formation pressure.

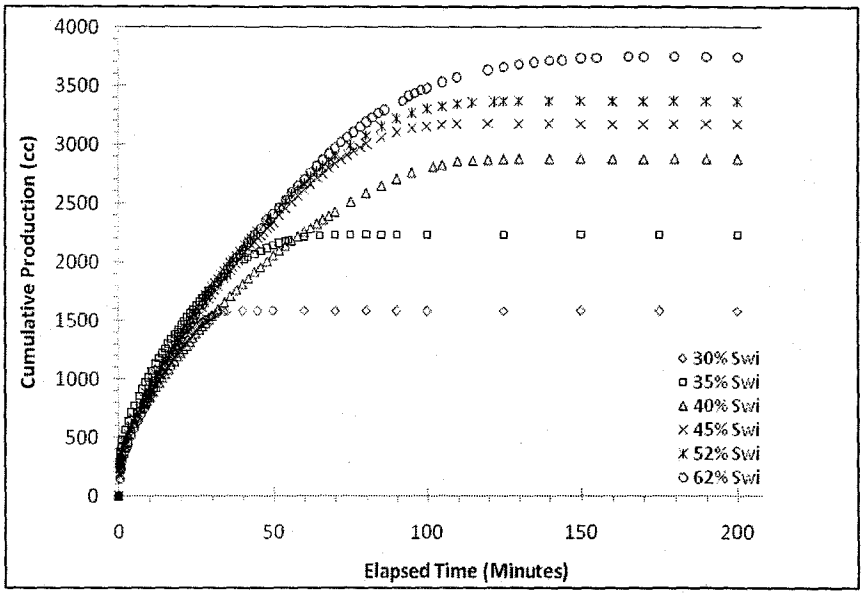

Figure 8: Graph of Cumulative Gas Production during Hydrate dissociation

Figure 8 is a graph of cumulative gas production from hydrate dissociation for different initial hydrate saturation. Higher the initial hydrate saturation produces more gas during dissociation. The outlet pressure was set around 200 - 250 psi for all the runs. The rate of gas production for all the run at the early time of dissociation was almost the same.

Temperature Profile during Dissociation

Dissociation of gas hydrate is endothermic in nature. Figures 9 and 10 show the graph of the temperature recorded by the designated thermocouples during dissociation of gas hydrate for two runs (S_h = 35% and S_h = 62%).

Prior to dissociation, the pressure in the cell for the system presented in Figure 9 is 366 psi. When the outlet back pressure was reduced to 208 psi, the temperature in the cell dropped to 3.3 degree Celsius from 3.9 degree Celsius immediately. Within tens of seconds, the temperature went back to near original temperature.

Figure 10 is the temperature recorded during dissociation of gas hydrate with initial hydrate saturation of 62%. The initial pressure in the cell was 336 psi before the system was depressurised to 259 psi. The temperature drop during the dissociation is not as big as the one shown in Figure 9 because of the depressurization is to a higher pressure level.

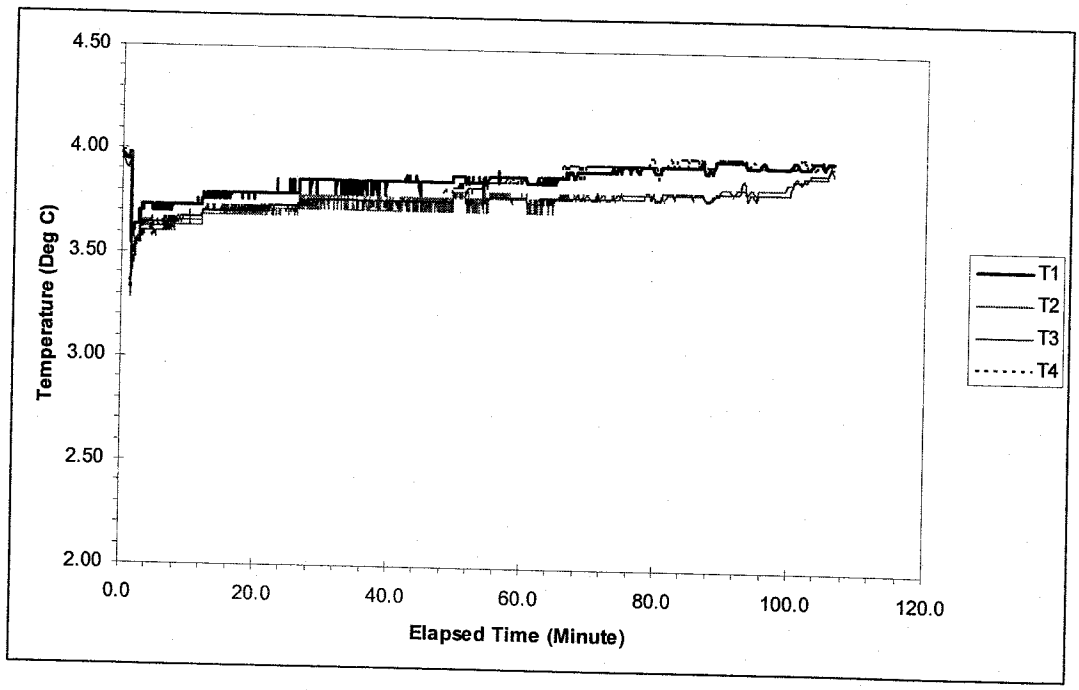

Figure 9: Graph of Temperature versus Elapsed Time during dissociation of Gas Hydrate (S_h = 35%)

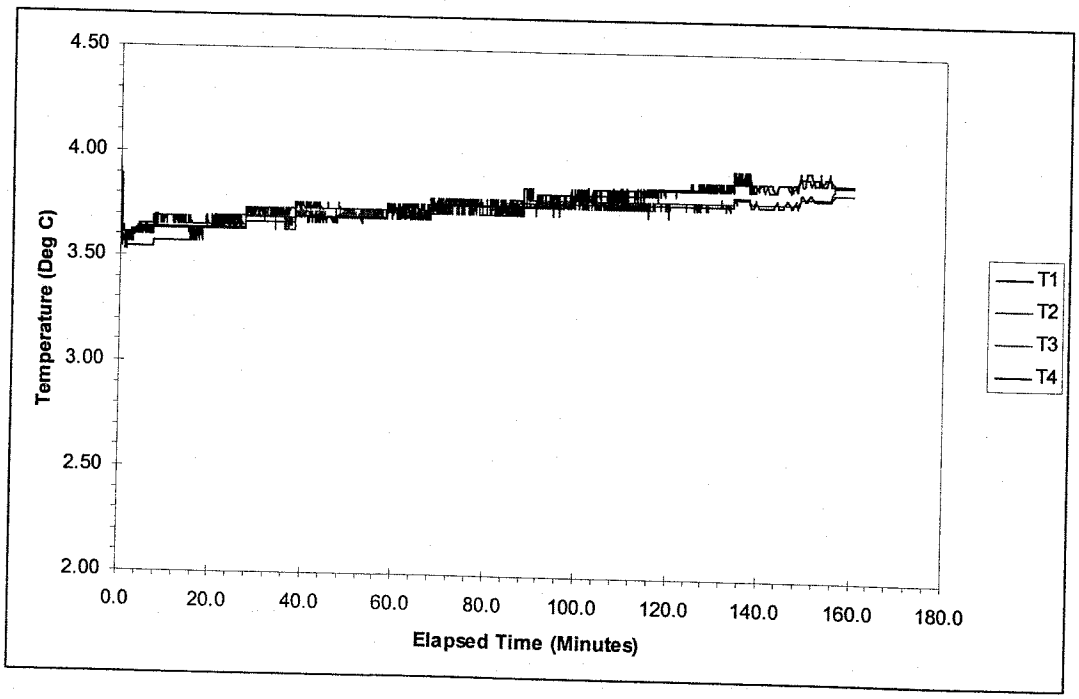

Figure 10: Graph of Temperature versus Elapsed Time during dissociation of Gas Hydrate (S_h = 62%)

These temperature profiles and the gas production profiles provide a data-set that can be used to test the validity of hydrate decomposition models and fine tune such models for more accurate predictions.

Evaluation of CO_2 Sequestration by Replacement of CH_4 with CO_2 in Methane Hydrate Deposits

A systematic study of this process involving numerical simulation and laboratory experiments forms the backbone of Ph.D. thesis of Mr. Carlos Alberto Giraldo Sierra. He is expected to finish the thesis research in 2011. A detailed report on this work is included as Appendix C. The following presents a brief overview of the accomplishments.

A general model was developed to study the characteristics of CO_2-CH_4 replacement reaction when a CO_2 gas is injected at constant flow rate. The numerical results of the methane produced in the cell during the exchange will then be compared to the experimental data in order to get a better understating of this phenomenon.

The model considers the following assumptions:

1. Steady-state of CO_2 injection is supplied
2. Reactor is an unsteady-state open system
3. Phases involved are: gas/aqueous/hydrate
4. Components: CH_4, CO_2, H_2O, CH_4HYD, CO_2HYD
5. Darcy's law describes the fluid flow in porous media.
6. Relative permeability curves and capillary pressure calculated using Hong's correlation (Hong, 2003) are applicable.

CMG's STARS was chosen as the tool to solve the mass and energy balances. Its suitability to represent gas hydrates has been proven by others authors (Wilder, 2008; Uddin et al[a, b], 2008; Uddin et al, 2006). In order to use STARS as a modeling tool, the kinetics of gas hydrate decomposition has to be transformed into a suitable format.

Kinetics of methane hydrate decomposition follows the Kim-Bishnoi model:

$$-\frac{1}{V}\frac{dn_{CH4HYD}}{dt} = k_d A_{dec}(f_e - f_{CH4})$$

$A_{dec} = \Phi_f S_H A_{SH}$; A_{SH}=3.75*10^5 m^2 of hydrate/m^3 of hydrate (Matsuda, 2002)

$$k_d = k_d^0 \exp\left(\frac{-E}{RT}\right)$$ where E=81kJ/mol and k_d^0= 3.6*10^4 mol/m^{2}Pa s

$f_{CH4}=\varphi P$; $f_e=\varphi P_e$. ; Assuming that the system behaves as an ideal gas the φ=1. This assumption will be verified according to the experimental conditions (see results section).

$$-\frac{1}{V}\frac{dn_{CH4HYD}}{dt} = k_d^0 \exp\left(\frac{-E}{RT}\right)(\Phi_f S_H A_{SH})(P_e - P_{CH4})$$

$$-\frac{1}{V}\frac{dn_{CH4HYD}}{dt} = \frac{k_d^0 A_{SH}}{\rho_{CH4HYD}} \exp\left(\frac{-E}{RT}\right)(\Phi_f S_H \rho_{CH4HYD}) P_e\left(1-\frac{P_{CH4}}{P_e}\right)$$

$$P_e(kPa) = a\exp\left(\frac{b}{T(^\circ C)-C}\right) = 9.02E15\exp\left(\frac{-7881.79}{T+273.15}\right)$$

$$-\frac{1}{V}\frac{dn_{CH4HYD}}{dt} = \frac{k_d^0 A_{SH} a}{\rho_{CH4HYD}} \exp\left(\frac{-E-bR}{RT(K)}\right)(\Phi_f S_H \rho_{CH4HYD})\left(1-\frac{P_{CH4}}{P_e}\right)$$

For CO_2 decomposition:

$$P_e(kPa) = 9.02E15\exp\left(\frac{-8073.66}{T+273.15}\right)$$; E=103kJ/mol and k_d^0= 1.83*10^8 mol/m^{2}Pa s.

Modeling CH_4-CO_2 replacement in CH_4-hydrates.

This model includes all three rate-controlling mechanisms (multiphase fluid flow in porous media, kinetics of replacement and heat transfer) that govern CO_2-CH_4 replacement reaction.

Governing Equations

The equations that govern the process of CH_4-CO_2 replacement in CH_4-hydrate are:

1. *Material Balance:* Accumulation=input-output+production

- For CH_4:

$$\frac{\partial(\rho_{CH_4}\Phi_f S_g)}{\partial t} = -\frac{\partial(\rho_{CH_4}u_g)}{\partial x} + r_{CH_4}$$

- For CO_2:

$$\frac{\partial(\rho_{CO_2}\Phi_f S_g)}{\partial t} = -\frac{\partial(\rho_{CO_2}u_g)}{\partial x} - r_{CO_2}$$

- For water: It would depend if there is a production or consumption

$$\frac{\partial(\rho_w\Phi_f S_w)}{\partial t} = -\frac{\partial(\rho_w u_w)}{\partial x} - (r_{CO_2} - r_{CH_4})$$

- For CH_4HYD

$$\frac{\partial(\rho_{CH_4HYD}\Phi_f S_H)}{\partial t} = -r_{CH_4}$$

- For CO_2HYD

$$\frac{\partial(\rho_{CO_2HYD}\Phi_f S_H)}{\partial t} = r_{CO_2}$$

2. *Energy Balance*: Accumulation= input-output+production+Q-W

$$\frac{\partial(\rho_{rock}(1-\Phi_f)U_{rock} + \rho_H\Phi_f S_H U_H + \rho_g\Phi_f S_g U_g + \rho_w\Phi_f S_w U_w)}{\partial t}$$
$$= -\frac{\partial(\rho_g u_g H_g + \rho_w u_w H_w)}{\partial x} + \frac{\partial}{\partial x}\left(k_m\frac{\partial T}{\partial x}\right) + Q + \Delta H_R r_{CH4} + \Delta H_R r_{CO2}$$

Kinetics

Although, the kinetics of this process is not well understood, it is likely that CH_4-hydrate dissociates before CO_2 hydrate forms in the operating region chosen. In addition, CH_4-hydrate decomposition is stimulated by the heat released by CO_2-hydrate formation (Oghaki et al. 1996).

$CH_4(H_2O)_n \rightarrow CH_4 + nH_2O$ ΔH_d=54.19kJ/mol

$CO_2 + nH_2O \rightarrow CO_2(H_2O)_n$ ΔH_f=-57.66 kJ/mol

The kinetics of CH_4 hydrate decomposition will be compositional dependent since a mixture of gases is present in the gas phase, thus:

$f_{CH4}=\varphi y_{CH4}P$; $f_{CO2}=\varphi y_{CO2}P$; following the same procedure showed before, it is possible to obtain the following expression:

$$-\frac{1}{V}\frac{dn_{CH4HYD}}{dt}=\frac{k_d^0 A_{SH} a}{\rho_{CH4HYD} P}\exp\left(\frac{-E-bR}{RT(K)}\right)(\Phi_f S_{CH4HYD}\rho_{CH4HYD})(y_{CH4}P)\left(1-\frac{P}{P_e}\right)$$

For CO_2 hydrate formation, the procedure is analogous to the dissociation, however $A_{dec}=\Phi_f S_w A_{SH}$

$$\frac{1}{V}\frac{dn_{CO2HYD}}{dt}=k_{fCO2}A_{dec}(f_{CO2}-f_e)$$

$$\frac{1}{V}\frac{dn_{CO2HYD}}{dt}=\frac{k_{fCO2}A_{SH}}{\rho_W P}P_e(\Phi_f S_W\rho_W)(y_{CO2}P)\left(\frac{P}{P_e}-1\right)$$

In this case, the CO_2 hydrate formation is inhibited by the presence of CH_4 in the gas mixture (equilibrium curve shifts depending on the gas composition) which implies that some CH_4 will be reacting with water to form the hydrate structure. Thus, the formation of CH_4-hydrate also has to be considered taking into account that the equilibrium pressure would be the one in the mixture.

$CH_4 + nH_2O \rightarrow CH_4(H_2O)_n \quad \Delta H_d=-54.19kJ/mol$

$$\frac{1}{V}\frac{dn_{CH4HYD}}{dt}=\frac{k_{fCH4}A_{SH}}{\rho_W P}P_e(\Phi_f S_W\rho_W)(y_{CH4}P)\left(\frac{P}{P_e}-1\right)$$

Kinetics constants for CH_4 hydrate and CO_2 hydrate formation are taken from Englezos (1987) and Clarke (2005) respectively.

The equation for the equilibrium pressure presented below was fitted to the correlation reported by Adisasmito (1991)

$$P_e(kPa) = \frac{9.02E15}{(1+1.0511y_{CO2})^{0.9585}} \exp\left(\frac{-7896.076}{T+273.15}\right)$$

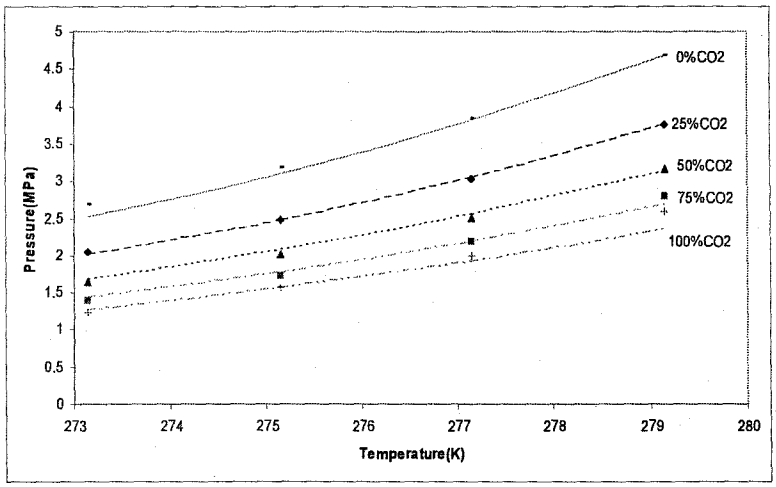

Figure 11: Phase Equilibrium of mixtures CO_2 and CH_4. Data points represent results obtained using Adisasmito's correlation.

Results

In order to verify the suitability of STARS to simulate this type of process, initially the CH_4-hydrate and CO_2-hydrate decomposition was simulated and compared with previous works (Hong, 2003; Kumar, 2005). The results presented below are modeled as one-dimensional processes for comparison purposes (previous works were done this way) and because experimentally it will only be possible to obtain information in one direction.

a. Modeling CH_4 hydrate decomposition (Hong, 2003)

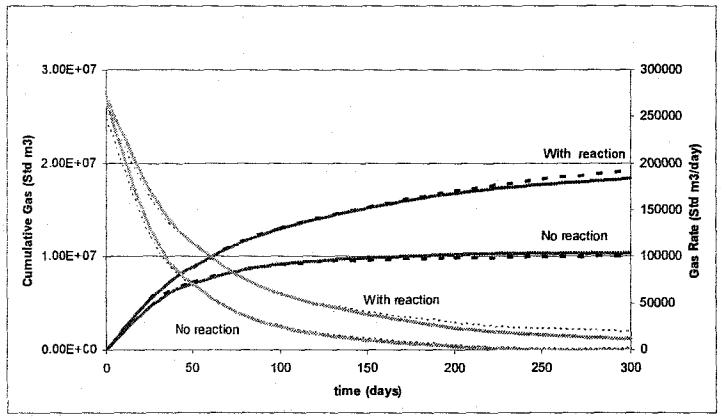

Figure 12: Gas production in CH4 hydrate dissociation. Gas production from a single well located at the centre of a 200m radius cylindrical reservoir. Pi=6913kPa, Ti=10C, BHP=4000kPa, S_H=0.6. Adiabatic system. Dashed lines represent Hong's work.

b. Modeling CO_2 hydrate decomposition (Kumar, 2005)

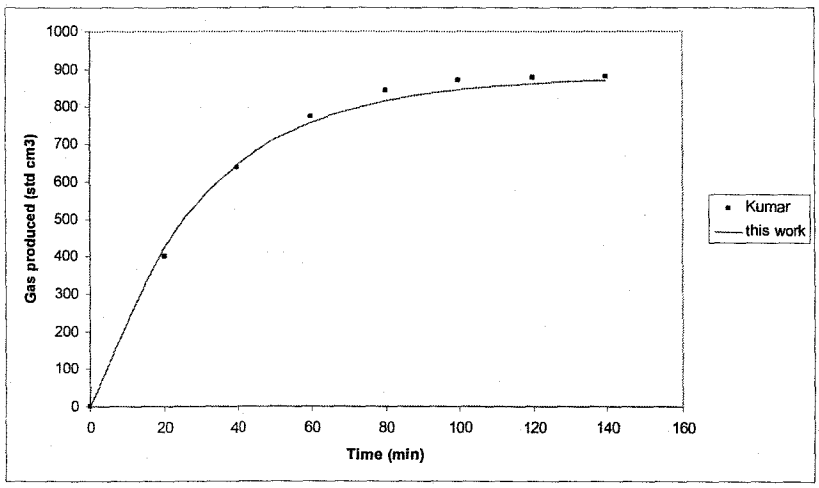

Figure 13: Gas production in CO2 hydrate dissociation. Gas production from a cell packed glass beads. P_i=2412kPa, T_i=3.6C, BHP=1654kPa, SH=0.187, T_{bath}=3.6C. Non-adiabatic system. At these conditions, the fugacity coefficient calculated using the TB EOS is 0.88.

In order to check the behaviour of the system during the replacement reaction, the experimental set up used in the lab and described by Kumar (2005) is modeled in STARS. Operational and initial conditions are shown in Figure 14.

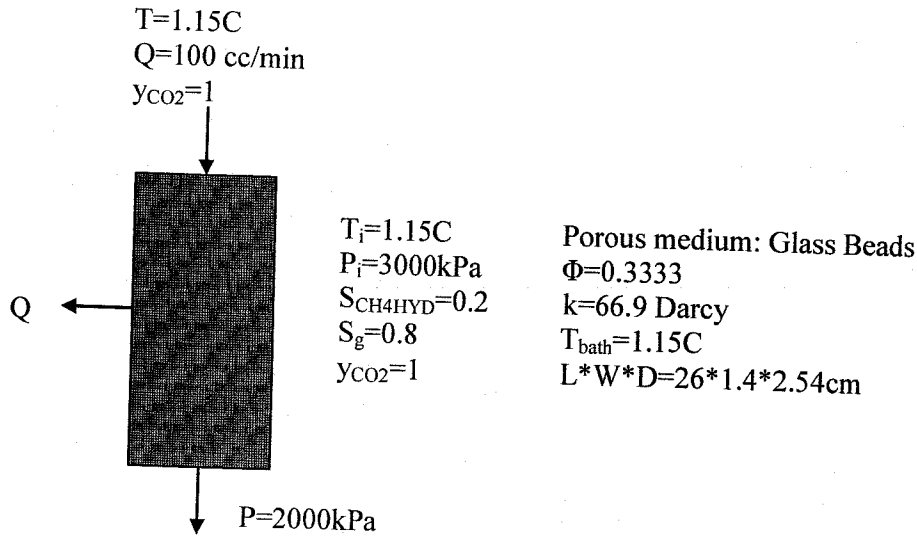

Figure 14: Schematic representation and initial conditions of the replacement experiment (Base Case)

The results are presented in Figures 15 to 17.

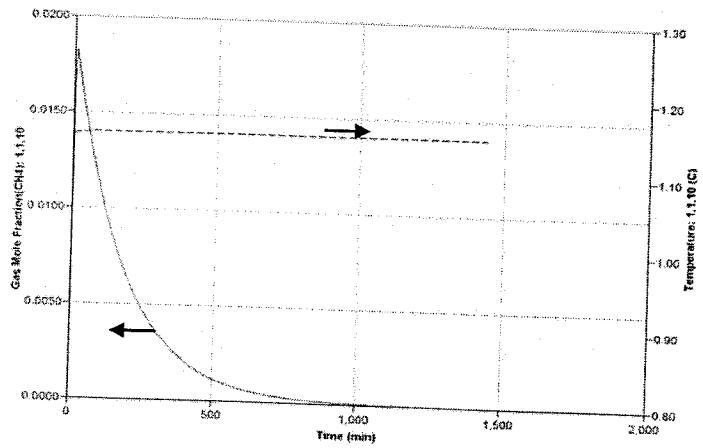

Figure 15: CH4 Mole fraction in the gas phase and Temperature profile during the Base Case

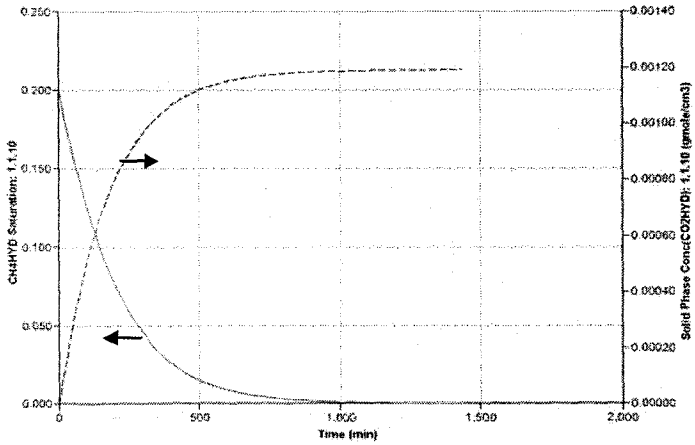

Figure 16: CH_4 and CO_2 Hydrates profile during the Base Case

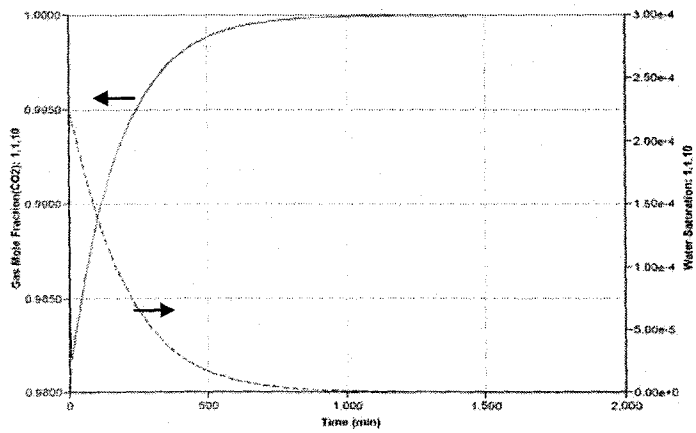

Figure 17: CO_2 Mole fraction in the gas phase and water saturation profile during the Base Case

The following conclusions can be made from the results presented in Figures 15 to 17.

- These graphs show that at the beginning of the process a fast decomposition of CH_4-hydrate occurs followed by the formation of CO_2-hydrate which can be inferred by the temperature drop and the increase of water saturation.
- The system recovers quickly its initial temperature. This is due to the fact that the equipment is immersed in a constant temperature bath and that the CH_4-hydrate heat of decomposition and CO_2-hydrate heat of formation are very similar.

- Water saturation is always very low, meaning that all the water is almost being consumed as soon it is produced.
- Gas composition of CH_4 increases at the beginning of the process and tend to fade with time due to it is constantly removed of the system.
- Total conversion of CH_4-hydrate is achieved at approximately 1000 min

To verify the effect of some of the process variables, four additional cases are presented:

I. Effect of CO_2 flow rate injection: Q_{CO2}=10 cm^3/min

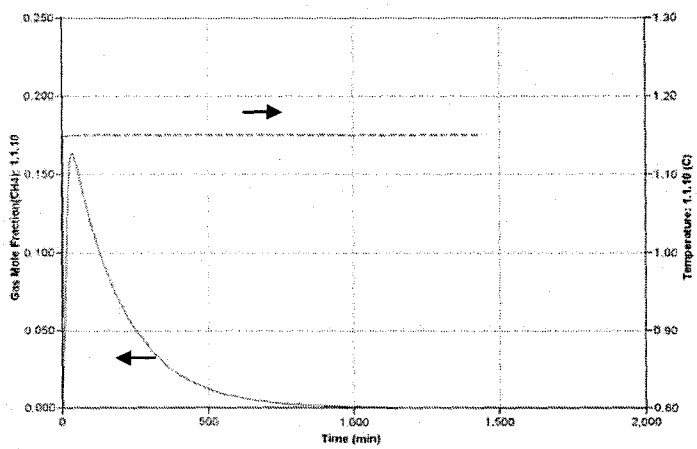

Figure 18: CH4 moles fraction in the gas phase and temperature profile during the alternative I

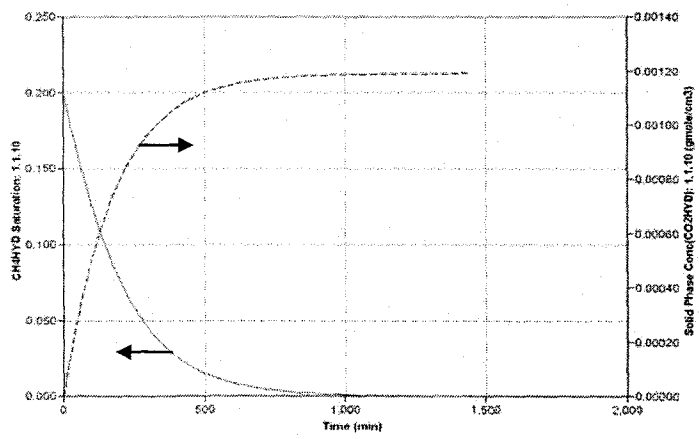

Figure 19: CH_4 and CO_2 hydrates saturation profile during the alternative I

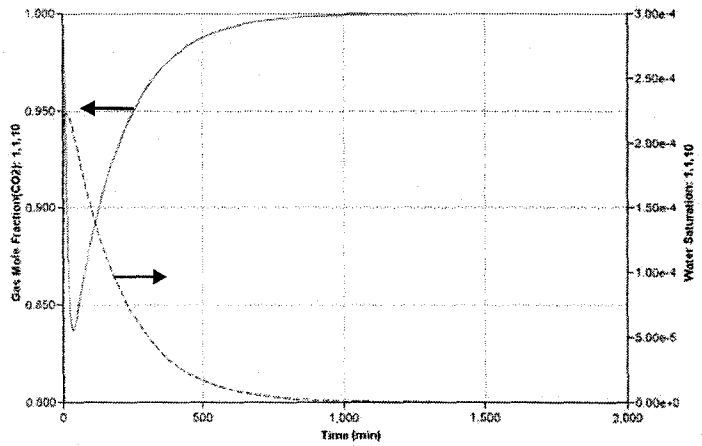

Figure 20: CO_2 moles fraction in the gas phase and water saturation profile during the alternative I

From these graphs, it can be seen that by reducing the CO_2 flow rate from 100 cm^3/min to 10 cm^3/min does not really affect the kinetics of exchange; however, in this case it was assumed that mass transfer resistance is negligible. This will be checked during the experiments. The small variations on the decomposition and formation rates are due to the different composition in the gas mixture.

II. Effect of external heat transfer: Q=0 J/s

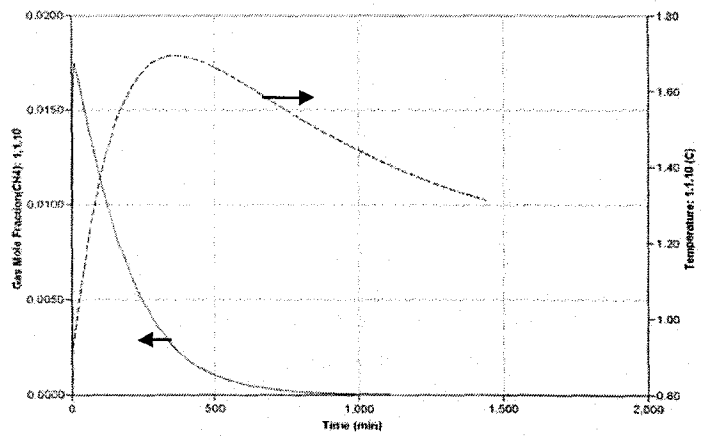

Figure 21: CH4 moles fraction in the gas phase and temperature profile during the alternative II

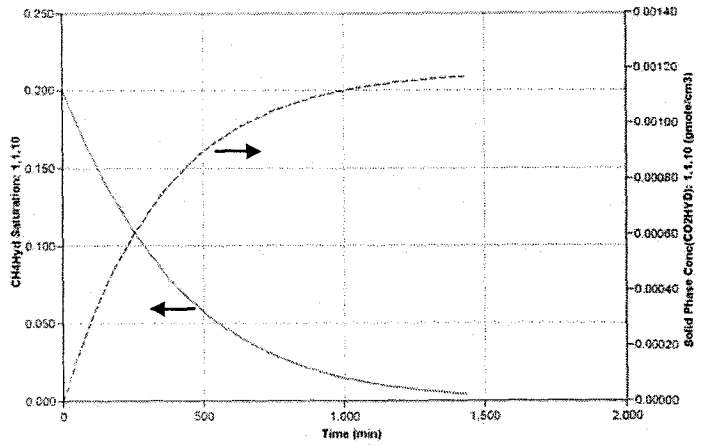

Figure 28: CH_4 and CO_2 Hydrate saturation profile during the alternative IV

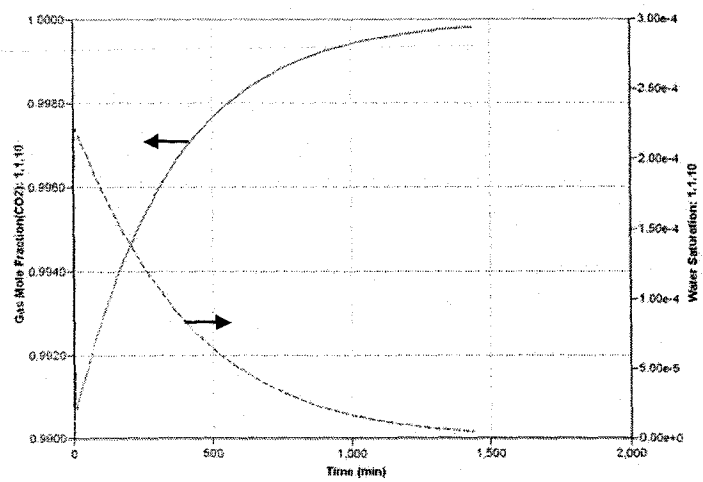

Figure 29: CO_2 mole fraction in the gas phase and water saturation profile during the alternative IV

These graphs show that the effect of the surface plays a key role in the overall process of CH_4-CO_2 replacement, by reducing the reaction area, the rate of decomposition diminishes significantly. The following table, presents some of the results on how CH_4-Hydrate saturation changes with time

Table 1. Comparative table of CH_4 hydrate saturation.

Time (min)	Case Base	Alternative I	Alternative II	Alternative III	Alternative IV
0	0.2	0.2	0.2	0.2	0.2
178	0.084	0.084	0.082	0.088	0.132
536	0.012	0.012	0.010	0.014	0.052
715	0.004	0.004	0.003	0.006	0.032

Based on these results, it is possible to conclude that the controlling mechanism is the intrinsic kinetics; in particular, the reaction area of hydrates in the porous media is an important controlling factor.

Training of HQP

Two PhD students, Chee Wee Sia and Carlos Alberto Giraldo Sierra, continue to work on the project and will include the results in their PhD theses expected to be completed in 2011. One MSc student, Kasif Khan, was also supported by this work. He has completed his experimental work and will defend his thesis in June 2010. The project also partially supported the Ph.D. thesis research of Dr. Faisal Al-Otabi, who finished his graduate program in early 2010 and returned to Saudi Arabia.

Overall Conclusions

1. A more reliable experimental technique has been developed for measuring the kinetics of hydrate formation and extensive data on the hydrate formation kinetics of various gases have been measured.
2. An experimental study on the formation and decomposition of CO_2 hydrate in porous media has been completed. This work has provided valuable information on the impact of hydrate formation on the permeability of sand at different levels of hydrate saturation.
3. Considerable progress has been made in the study of replacement of CH_4 with CO_2 in hydrate bearing formations. A numerical simulation study has been completed and the experimental work has begun.

References:

Adisasmito, S; Frank, R.; Sloan D.; "Hydrates of carbon dioxide and methane mixtures"; Journal of chemical engineering data; v 36; n 1; p 68-71; 1991.

Ahmadi, G., Ji, C., and Smith, D.H., "Natural Gas Production from Hydrate Dissociation: An Axisymmetric Model", Journal of Petroleum Science and Engineering, 58, 245 – 258, (2007).

Al-Otabi, F.; "Determination of the intrinsic kinetics of decomposition of hydrates formed from mixtures of nitrogen and carbon dioxide using in-situ particle size analysis", MSc. Thesis, University of Calgary, 2005.

Al-Otabi, F.; "Kinetics Studies of Gas Hydrate Formation Using In-situ Particle Size Analysis and Raman Spectroscopy", PhD. Thesis, University of Calgary, 2009.

American Association of Petroleum Geologists Bulletin, v 85, n 7, p 1211-1230, 2001

Attia, M.A., "Effects of Petrophysical Rock Properties on Tortuosity Factor", Journal of Petroleum Science and Engineering, 48, 185 – 198, (2005).

Bergeron, S.; Servio, P.; "Reaction rate constant of CO2 hydrate formation and verification of old premises pertaining to hydrate growth kinetics"; AIChE Journal, v 54, n 11, p 2964-2970, 2008.

Clarke, M., and Bishnoi, P.R., "Determination of the Intrinsic Rate of Ethane Gas Hydrate Decomposition", Chemical Engineering Science, 55, 4869 – 4883, (2000).

Clarke, M., and Bishnoi, P.R., 'Measuring and Modelling the Rate of Decomposition of Gas Hydrates Formed from Mixtures of Methane and Ethane" Chemical Engineering Science, 56, 4715 – 4724, (2001).

Clarke, M.; Bishnoi, P.R.; Determination of the activation energy and intrinsic rate constant of methane gas hydrate decomposition; Canadian Journal of Chemical Engineering, v 79, n 1, p 143-147, 2001.

Clarke, M.; Bishnoi, P.R.; "Determination of the intrinsic rate constant and activation energy of CO2 gas hydrate decomposition using in-situ particle size analysis"; Chemical Engineering Science, v 59, n 14, p 2983-2993, 2004

Clarke, M.; Bishnoi, P.R. ; "Determination of the intrinsic kinetics of CO2 gas hydrate formation using in situ particle size analysis"; Chemical Engineering Science, v 60, n 3, p 695-709, 2005

Collett, T. ; Kuuskraa, A.; "Emerging U.S. gas resources - 4. Hydrates contain vast store of world gas resources"; Oil and Gas Journal, v 96, n 19, p 90-95, 1998.

Collett, T.S., "Well log Evaluation of Gas Hydrate Saturation" Transactions SPWLA 39th Annual Logging Symposium, 26 – 29 May, Houston Texas, Society of Petrophysicists and Well Log Analysts, MM1 – MM14, (1998a).

Collett, T.S., " Well Log Characterization of Sediment Porosities in Gas-Hydrate-Bearing Reservoirs", Society of Petroleum Engineers, SPE Paper 49298, 765 – 776, (1998b).

Energy Information Administration form the US government, www. eia.doe.gov/oiaf/ ieo/ nat_gas.html , 2009.

Englezos, P.; Kalogerakis, N.; Dholabhai, P.D.; Bishnoi, P.R. "Kinetics of formation of methane and ethane gas hydrates. Chemical Engineering Science, v 42, n 11, p 2647-2658, 1987.

Giraldo, C.; "Measurement and Thermodynamic Modeling of Ethane and Carbon Dioxide Gas Hydrate Incipient Conditions in Reverse Micelles", MSc. Thesis, University of Calgary, 2008

Goel, N.; In situ methane hydrate dissociation with carbon dioxide sequestration: Current knowledge and issues; Journal of Petroleum Science and Engineering, v 51, n 3-4, p 169-184; 2006

Graue, A.; Kvamme, B.; Baldwin, B.A.; Stevens, J.; Howard, J.; Aspenes, E.; Ersland, G.; Huseb, J.; Zornes, D.; "CO_2 storage in natural-gas-hydrate reservoirs benefits from associated methane production"; JPT, Journal of Petroleum Technology; v 58; n 8; p 65-67; 2006

Gudmundsson, J., Borrehaug, A., "Frozen Hydrate for Transport of Natural Gas", Proc. 2nd Int. Conf. on Natural Gas Hydrates, 415–422, (1996).

Hirohama S., Shimoyama Y., Wakabayashi A., Tatsuta S., and Nishida N., "Conversion of CH4-Hydrate to CO2-Hydrate in liquid CO2", Journal of Chemical Engineering of Japan, v 29, n6, pp 1014-1020, 1996.

Hong, H., and Pooladi-Darvish, M., "A Numerical Study on Gas Production from Formations Containing Gas Hydrate" Paper CIPC 2003 – 60 presented at the 2003 CIPC Conference, Calgary, (2003).

Hong, H., Pooladi-Darvish, M., and Bishnoi, P.R., "Analytical Modelling of Gas Production From Hydrates in Porous Media", Journal of Canadian Petroleum Techology, 42(11), 45 – 56, (2003).

Hong, H.; "Modeling of gas production form hydrates in porous media", MSc. Thesis, University of Calgary, 2003.

Jadhawar P., Yang J., Jadhawar J., and Tohidi B., "Preliminary Experimental Investigation on Replacing Methane in Hydrate Structure with Carbon Dioxide in Porous Media", 5th International Conference on Gas Hydrates, Throndheim, Norway, p 1006-1011, 2005.

Jamaluddin, A.K.M., Kalogerakis, N., Bishnoi, P.R., "Modelling of Decomposition of a Synthetic Core of Methane Gas Hydrate by Coupling Intrinsic Kinetics with Heat Transfer Rates", Canadian Journal of Chemical Engineering, 67, 948 – 954, (1989).

Khairkhah, D., Pooladi-Darvish, M. Bishnoi, P.R., Collet, T.S., and Dallimore, S.R., "Production Potential of the Mallik Field Reservoir", Scientific Results from JAPEX/JNOC/GSC Mallik 2L-38 Gas Hydrate Research Well, Mackenzie Delta, Northwest Territories, Canada, (ed) Dallimore, S.R., Uchida, T., and Collet, T.S., Geological Survey of Canada, Bulletin 544, 377 – 390, (1999).

Kim, H.C. ; Bishnoi, P.R.; Heidemann, R.A.; Rizvi, S.S.H.; Kinetics of methane hydrate decomposition"; Chemical Engineering Science, v 42, n 7, p 1645-1653, 1987.

Kleinberg, R.L., and Griffin, D.D., "NMR Measurements of Permafrost Unfrozen Water Assay, Pore-scale Distribution of Ice and Hydraulic Permeability of Sediments" Cold Regions Science and Technology, 42, 63 -77, (2005)

Kleinberg, R.L., Flaum, C., Griffin, D.D., Brewer, P.G., Malby, G.E., Peltzer, E.T., and Yesinowski, J.P., "Deep sea NMR: Methane Hydrate Growth Habit in Porous Media and its Application to Hydraulic Permeability, Deposit Accumulation, and Submarine Slope Stability" Journal of Geophysical Research, 108(B10), 2508, doi:10.1029/2003JB002389, (2003).

Kneafsey, T.J., Tomutsa, L., Moridis, G.J., Seol, Y., Freifeld, B.M., Taylor, C.E., and Gupta, A., "Methane Hydrate Formation and Dissociation in a Partially saturated Core-Scale Sand Sample", Journal of Petroleum Science and Engineering, 56, 108 – 126, (2007).

Komai, T.; Kawabe, Y.; Kawamura, T; Yoon, J.Extraction of Gas Hydrates Using CO2 Sequestration; Proceedings of the International Offshore and Polar Engineering Conference, p 321-326, 2003

Komai, T.; Yamamoto, Y.; Ohga, K.; "Dynamics of reformation and replacement of CO2 and CH4 gas hydrates"; Third International Conference on Gas Hydrates, Salt Lake City, USA; p 272-280; 1999.

Kumar A.; "Formation and dissociatin of gas hydrates in porous media", MSc. Thesis, University of Calgary, 2005.

Kumar, A., Maini, B.B., Bishnoi, P.R., Clarke, M., Zatsepina, O., Srinivasan, S., "Experimental Determination of Permeability in the Presence of Hydrates and Its Effect on the Dissociation Characteristics of Gas Hydrates in Porous Media" Journal of Petroleum Science and Engineering, 70, 114 – 122, (2010).

Lee H., Seo Y., Moudrakovski I., and Ripmeester J., "Recovering Methane from Solid Methane Hydrate with Carbon Dioxide", Angewwandte Chemie International Edition, v42, p 5048-5051, 2003.

Moridis, G.J., Kneafsey, T. and Pruess, K., "Depressurization – Induced Gas Production from Class 1 Hydrate Deposits", SPE Reservoir Evaluation & Engineering, 10, 458 – 481, (2007).

Murray, D.R., Kleinberg, R.L., Sinha, B.K., Fukuhara, M., Osawa, O., Endo, T., and Namikawa, T., "Saturation, Acoustic Properties, Growth habit, and State of Stress of a Gas Hydrate Reservoir from Well Logs", Petrophysics, 47(2) 129 – 137, (2006).

Nazridoust, K., and Ahmadi, G., "Computational Modelling of Methane Hydrate Dissociation in a Sandstone Core", Chemical Engineering Science, 62, 6155 – 6177, (2007).

Nguyen, H., Phillips, J., John, V.T, "Clathrate Formation in Reversed Micellar Solutions", Journal of Physical chemistry, v93, n25, 8123-8126, 1989.

Ohgaki, K., Takano, K., Sangawa, H., Matsubara, T., Nakano, S., "Methane exploitation by carbon dioxide from gas hydrates – Phase equilibria for CO_2-CH_4 mixed hydrate system," Journal of Chemical Engineering of Japan, Vol 29, 478-483 (1996)

Ota, M.; Abe, Y.; Watanabe, M.; Smith Jr., R..; Inomata, H.;Methane recovery from methane hydrate using pressurized CO2; Fluid Phase Equilibria, v 228-229, p 553-559; 2005.

Ota, M.; Morohashi, K.; Abe, Y.; Watanabe, M.; Lee R.; Innomata, H.; "Replacement of CH_4 in the hydrate by use of liquid CO2"; Energy Conversion and Management, v46, n 11-12, p 1680-1691, 2005.

Ota, M.; Saito, T.; Aida, T.; Watanabe, M.; Sato, Y.i; Smith, L.; Inomata, H.; "Macro and microscopic CH4-CO2 replacement in CH 4 hydrate under pressurized CO2"; AIChE Journal, v 53, n 10, p 2715-2721, 2007.

Park, Y; Kim, Y; Lee, W; Huh, G; Park, P; Lee, J; Lee H; "Sequestering carbon dioxide into complex structures of naturally occurring gas hydrates"; :Proc Natl Acad Sci; v103; n 34; p 12690-12694; U S A; 2006.

Phillips, J., Nguyen, H., John, V.T., "Protein Recovery from Reversed Solutions Through Contact with a Pressurized Gas Phase", Biotechnol. Prog., v7, p 43-48, 1991.

Pooladi-Darvish, M., "Gas Production From Hydrate Reservoirs and Its Modeling", Journal of Petroleum Technology, 56(6), 65 – 71, (2004).

Rao, A., Nguyen, H., John, V.T., "Modification of Enzyme Activity in Reversed Micelles Through Clathrate Hydrate Formation", Biotechnol. Prog., v6, p 465-471, 1990.

Revil, A., "Thermal Conductivity of Unconsolidated Sediments with Geophysical Applications", Journal of Geophysical Research, 105(B7), 16749 – 16768, (2000).

Salem, H.S., "Derivation of the Cementation Factor (Archie's Exponents) and the Kozeny-Carman Constant from Well Log Data and Dependence on Lithology and 39 Other Physical Parameters", Society of Petroleum Engineers, SPE Paper 26309, (1993).

Schultheiss, P.J., and Holland, M.E., "Borehole Pressure and Laboratory Pressure Core Analysis for Gas Hydrate Investigations", Offshore Technology Conference, Houston, Texas, U.S.A., 5 – 8 May 2008, (2008).

Selim, M.S., and Sloan, E.D., "Hydrate Dissociation in Sediment", SPE Reservoir Engineering, 5(2), 245 – 251, (1990).

Spangenberg, E., "Modeling of the Influence of Gas Hydrate Content on the Electrical Properties of Porous Sediment", Journal of Geophysical Research, 106(B4), 6535 – 6548, (2001).

Stevens, J.; Howard, J; Baldwin B.; Ersland, G.; Husebo, J.; Graue, A; " Experimental hydrate formation and gas production scenarios based on CO2 sequestration"; Proceedings of the 6th international conference on gas hydrates; Vancouver, 2008.

Tohidi, B., Anderson, R., Clennel, M.B., Burgass, R.W., and Bikerdab, A.B., "Visual Observation of Gas-Hydrate Formation and Dissociation in Synthetic Porous Media by Means of Glass Micromodels", Geology, 29(9), 867 – 870, (2001).

Uchida, T.; Takeya, S.; Ebimuna, T.; Narita, H.; "Replacing methane with CO2 in clathrate hydrate: Obaservations using raman spectroscopy"; Greenhouse gas control technologies, 2001.

Uddin, M; Coombe D.; Law D.; "Numerical studies of gas hydrate formation and decomposition in a geological reservoir"; Journal of Energy Resources Technology, v 130, p 0325011-03250114; 2008.

Uddin, M; Coombe D.; Law D.; Gunter W.; "Numerical studies of gas hydrate formation and decomposition in a geological reservoir"; SPE Gas Technology Symposium; SPE 100460; Calgary; p 1-13; 2006.

Uddin, M; Coombe D.; Wright F.; "Modeling of CO2-Hydrate formation in geological reservoirs by injection of CO2"; Journal of Energy Resources Technology, v 130, p 0325021-03250211; 2008.

Waite, W.F., deMartin, B.J., Kirby, S.H., Pinkston, J., and Ruppel, C.D., "Thermal Conductivity Measurement in Porous Mixtures of Methane Hydrate and Quartz Sand", Geophysical Research Letters, 29(4), 82(1) – 82(4), (2002).

Waite, W.F., Gilbert, L.Y., Winters, W.J., and Mason, D.H., "Estimating Thermal Diffusivity and Specific Heat from Needle Probe Thermal Conductivity Data", Review of Scientific Instruments, 77, 044904, (2006).

Waite, W.F., Stern, L.A., Kirby, S.H., Winters, W.J., and Mason, D.H., "Simultaneous Determination of Thermal Conductivity, thermal Diffusivity and Specific Heat in sI Methane Hydrate", Geophysical Journal International, 169, 767 – 774, (2007).

Waite, W.F., Winters, W.J., and Mason, D.H., "Methane Hydrate Formation in Partially Water – Saturated Ottawa Sand", American Mineralogist, 89, 1202 – 1207, (2004).

Winters, W.J., Pecher, I.A., Waite, W.F., and Mason, D.H., "Physical Properties and Rock Physics Models of Sediment containing Natural and Laboratory-Formed Methane Gas Hydrate", American Mineralogist, 89, 1221 – 1227, (2004).

Worthington, P.F., "Petrophysical Evaluation of Gas Hydrate Formations" International Petroleum Technology Conference held in Kuala Lumpur, Malaysia, 3 – 5 December 2008, (2008).

Yang J., Chapoy A., and Tohidi B., "Thermodynamic Conditions and Kinetics of Integrated Methane Recovery and Carbon Dioxide Sequestration", Offshore Technology Conference, Houston, USA, p 976-982, 2008.

Yezdimer, E.M., Cunnings, P.T., Chialvo, A.A., "Determination of the Gibbs free energy of gas replacement in sI clathrate hydrate by molecular simulation," Journal of Physical Chemistry A, Vol 106, 7982-7987 (2002)

Yousif, M.H., Abass, H.H., Selim, M.S., Sloan, E.D., "Experimental and Theoretical Investigation of Methane-Gas-Hydrate Dissociation in Porous Media", SPE Reservoir Engineering, 6(1), 69 – 76, (1991).

Appendix A: Ph.D. Thesis of Dr. Faisal Al-Otabi

UNIVERSITY OF CALGARY

Kinetic Studies of Gas Hydrate Formation Using *In Situ* Particle Size Analysis and Raman Spectroscopy

by

Faisal Dulaim Al-Otaibi

A THESIS

SUBMITTED TO THE FACULTY OF GRADUATE STUDIES

IN PARTIAL FULFILMENT OF THE REQUIREMENTS FOR THE

DEGREE OF DOCTOR OF PHILOSOPHY

DEPARTMENT OF CHEMICAL AND PETROLEUM ENGINEERING

CALGARY, ALBERTA

November, 2009

Abstract

In this study, actual particle size measurements were combined with Raman spectroscopy analysis to investigate the kinetics of hydrate formation from various natural gas hydrate formers. Experimental data on gas hydrates formation from methane, ethane, propane, and an equimolar ethane-propane mixture were collected with a semi-batch stirred isothermal-isobaric reactor that incorporates an *in situ* particle size analyzer and a Raman spectrometer. The particle size analyzer used is a Lasentec® FBRM (focused beam reflectance measurement) probe capable of measuring particle chord lengths down to 0.5 μm.

A procedure was developed to use the focused beam reflectance measurement (FBRM) probe to obtain satisfactory particle size measurements of the hydrate particles. Since the experimental measurements were made on the particle sizes and their distribution, the need to make assumptions with regard to initial nuclei size and particle size distribution during hydrate growth was eliminated for modelling the experimental data. The working equations used by Englezos et al. (1987a) were modified to incorporate the particle size measurement information in order to extract the intrinsic kinetic rate constant for hydrate growth by regressing the experimental data. The intrinsic kinetic rate constants for hydrate formation of methane gas in structure I, ethane gas in structure I, and propane gas in structure II were determined. Then, an equimolar mixture of ethane and propane gases was used where the experimental data and the *a priori*

determined rate constant for hydrate formation of propane in structure II were used to extract the intrinsic rate constant of gas hydrate formation for ethane in structure II.

Raman spectroscopy was used to identify the structure in which the gas hydrate former exists during the hydrate formation experiment to ensure that the reported intrinsic rate constant of each gas hydrate former correspond to the right hydrate structure.

The intrinsic rate constant for ethane hydrate formation in structure II hydrate was found to be significantly smaller than that in structure I. The kinetic model successfully captured the intrinsic nature of the hydrate growth phenomenon.

Acknowledgements

I would like to acknowledge my supervisor Dr. P.R. Bishnoi for his continuous support, guidance, patience, and encouragement throughout the course of this study. I am honoured to work under his supervision and gain a little of his remarkable knowledge that extends beyond gas hydrates.

I would also like to thank my co-supervisor, Dr. B.B. Maini for his useful comments and discussions, Dr. M.A. Clarke for his help and suggestions, Dr. A. Majumdar for his help and contribution, and the support staff and technicians in the Department of Chemical and Petroleum Engineering.

The financial support of NSERC throughout the course of the study is highly appreciated.

Last but not least, I am grateful to my sponsor and employer Saudi Aramco Oil Company for their financial support to pursue my graduate studies.

Dedication

This work is dedicated to my parents, my wife, and my children.

Epigraph

تنشد عن الوقت بالتحديد والجيه

وانا على شوفكم يا ابوي شفقاني

مشيت لي درب لو حفين رجليه

والله لاتمه اذا مولايه احياني

Table of Contents

List of Tables

List of Figures and Illustrations

List of Symbols, Abbreviations and Nomenclature

a	Gas liquid interfacial area per unit volume, m^2/m^3.
Å	Ångström, 10^{-10} m.
$A_{(g-l)}$	Gas-liquid interfacial area, m^2.
A_p	Surface area of a particle, m^2.
$C_{k,i}$	Langmuir constant of species "*k*" in cavity of type "*i*", Pa^{-1}.
c	Concentration of the gas in the liquid water, $mole/m^3$.
c_{wo}	Initial concentration of water molecules, $mole/m^3$.
D	Diffusivity of the gas, m^2/s.
d	Diameter, m.
f_{eq}	Equilibrium fugacity, MPa.
f_g	Fugacity of the hydrate former in the vapour phase, MPa.
f_b	Fugacity of the hydrate former in the bulk liquid phase, MPa.
f	Fugacity, MPa.
G	Linear growth rate, m/s.
H	Henry's constant, MPa.
J	Molar flux, $mole/(m^2.s)$.
K^*	Combined rate parameter, $mole/(m^2.MPa.s)$.
K_r	Reaction rate constant, $mole/(m^2.MPa.s)$.
K_d	Mass transfer coefficient for the liquid phase, $mole/(m^2.MPa.s)$.
K_L	Liquid side mass transfer coefficient at g-l interface, m/s.

L	Characteristic length, m.
M	Mass (kg) of hydrate per mole of gas.
N_A	Avogadro's Number, 6.023×10^{23} molecules/mole.
$N_{k,i}$	The number of molecules of species "*k*" in cavity "*i*".
N_w	Number of water molecules in a unit cell.
$n_{H(t)}$	Number of moles of gas in the hydrate phase.
P	Pressure, MPa.
RPM	Revolutions per minute.
R	Universal gas constant, 8.314 J/(mole.K).
$R_y(t)$	Global rate of reactions, mole/(m^3.s).
T	Temperature, K.
t	Time, s.
V	Volume of reaction mass, m^3.
V_{cell}	Volume of a unit cell, m^3.
$y_{k,i}$	Fractional occupancy of cavity "i" by component "k".
z	Compressibility factor.

Greek Letters

φ	Particle density function, m^{-4}.
μ_m	m^{th} moment of the particle size distribution, m^n/m^3.
ρ	Density, kg of hydrate per m^3 of hydrate.
v_i	Number of type "*i*" cavities in unit cell.

CHAPTER ONE: INTRODUCTION

1.1 Background

Gas hydrates fit in a class of solids known as clathrates. They are non-stoichiometric crystalline compounds that occur when hydrogen-bonded water molecules form cavities that can be occupied by a guest molecule under suitable conditions of pressure and temperature. Normally, hydrates form at elevated pressures and low temperatures (not necessarily below the freezing point of water). Light alkanes, carbon dioxide, hydrogen sulphide, nitrogen and oxygen are known to form hydrates at certain conditions of pressure and temperature in the presence of water.

When the guest molecules enter the hydrate cages, there are no chemical bonds between the host and guest molecules. Instead, the guest molecules stabilize the hydrate cages by van der Waals interaction forces. Typically, at normal pressure conditions (less than 0.5 GPa at ambient temperature), a water cage has a maximum occupancy of one guest molecule. It is not necessary for all the cages in the gas hydrate structure to be filled. In fact, the cage filling depends on pressure, temperature, and the nature of the guest species (Sloan and Koh, 2007).

There are three main gas hydrate structures in which gas hydrates can exist: structure I, structure II (Claussen, 1951; von Stackelberg & Muller, 1954; Jeffery & McMullan, 1967), and structure H (Ripmeester et. al. 1988). In addition, at least three new clathrates hydrate structures have been discovered within the last decade, including:

i. Multiple occupancy of water cavities in hydrogen, methane, argon, and xenon hydrates at high pressure (Loveday et al., 2001; Hirari et el., 2004)

ii. A complex clathrates hydrate structure, containing 1.67 choline hydroxide tetra-n-propylammonium fluoride and $30.33H_2O$ (Udachin and Ripmeester, 1999).

iii. Tetragonal structure of bromine hydrate and trigonal sT hydrate structure formed with dimethyl ether guest molecules (Udachin et al.,1997)

In both structure I and II, the water molecules are tetrahedrally coordinated, as in ordinary ice, and the hydrate forming gases are linked to the water lattice by van der Waals forces.

Structure I, a body-centered cubic gas hydrate structure, has two cavities (a and b) as illustrated in Figure 1.1. This structure can be formed with smaller guest molecules (less than 6 Å), such as: methane, ethane, carbon dioxide, and hydrogen sulphide. The unit cell (the smallest repeating unit of a crystal structure) of structure I hydrate consists of 46 water molecules and includes two small and six large cavities. Small cavities have a maximum linear dimension of 5.1 Å while the large cavities have a maximum linear dimension of 5.8 Å.

Structure II, a diamond lattice within a cubic framework, has two cavities (a and c) as seen in Figure 1.1. The unit cell of this structure consists of 136 water molecules and includes sixteen small and eight large cavities. This gas hydrate

structure is formed with somewhat larger single guest molecules (6 Å < d <7 Å) such as: propane, or iso-butane (Sloan, 1997). Nevertheless, it is known that the smallest guests (argon, krypton, nitrogen, and oxygen) form structure II hydrates rather than structure I.

Structure H, a hexagonal, has three cavities denoted by (a), (d), and (e) in Figure 1.1. In this structure, two different sizes of molecules are required to stabilize it. The unit cell of this structure has three molecules in 5^{12} cavity, two molecules in $4^3 5^6 6^3$ cavity, one molecule in $5^{12}6^8$ cavity and 34 water molecules. Molecules typically larger than 7.4 Å, such as neo-hexane, enter the $5^{12}6^8$ cavity.

Factors such as guest molecule size, temperature, pressure, and composition of the hydrate forming gas dictate which hydrate structure is exhibited. Structural transitions between structure I and structure II have been experimentally reported in many gas hydrate systems using Raman spectroscopy, NMR and x-ray diffraction at certain pressure, temperature and compositions regimes (Subramanian et al., 2000a,b).

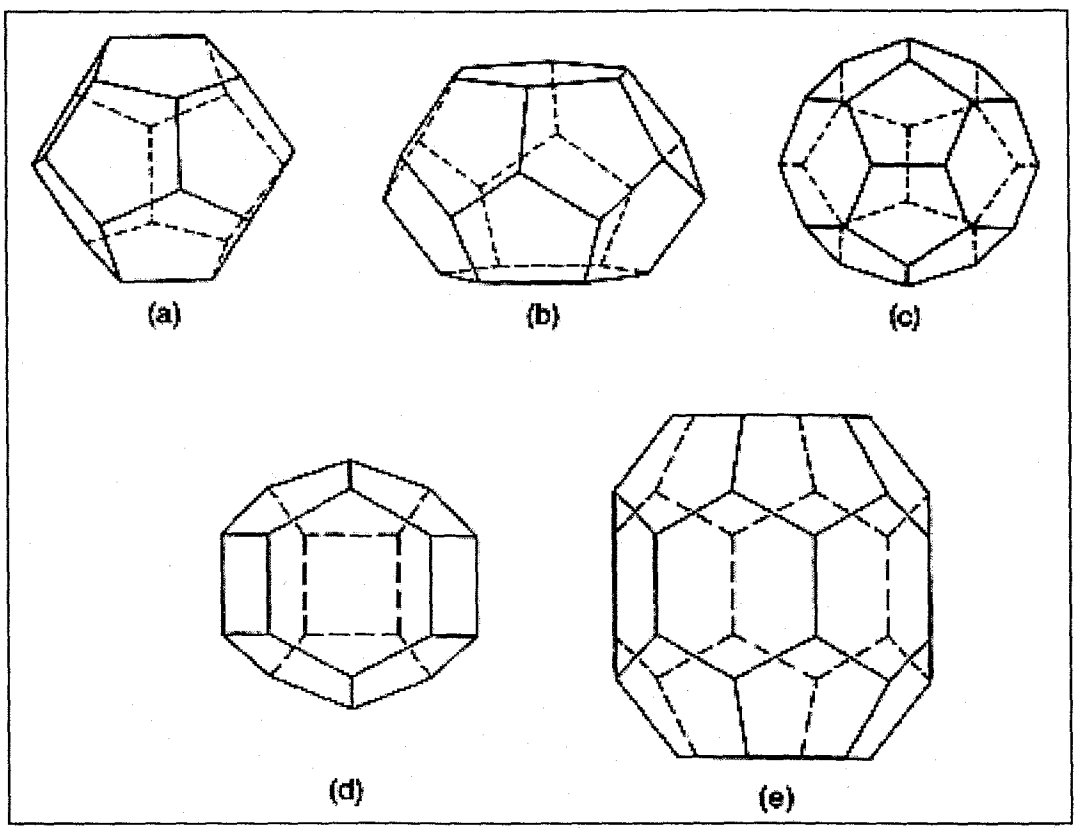

Figure 1.1: Cavities in gas clathrate hydrates (Sloan 1998).

*(a) Pentagonal Dodecahedron (5^{12}), (b) Tetrakaidecahedron ($5^{12}6^2$)

(c) Hexakaidecahedron ($5^{12}6^4$), (d) Irregular Dodecahedron ($4^3 5^6 6^3$)

(e) Icosahedron ($5^{12}6^8$)

1.2 Importance of gas hydrates

Gas hydrates have the potential for significant impact on world energy and the environment. In general, the importance of gas hydrate studies can be summarized as follows:

1.2.1 Gas hydrates as a nuisance in the industry

Gas hydrates can plug pipelines, foul process equipment, cause tubing and casing collapses, and/or cause blowouts or blockages during drilling, which makes them unwanted phenomena in process plants and pipelines operation. Yet, this phenomenon can be avoided by lowering water dew point, and operating outside the hydrate formation range, i.e., high temperatures and low pressures (heating or depressurizing), or can be controlled through thermodynamic inhibition chemicals. However, avoiding hydrates by thermodynamic control can become economically unfavourable especially in deepwater production scenarios. Therefore, the trend of flow assurance is moving towards kinetic control of hydrate formation by use of kinetic hydrate inhibitors and anti-agglomerants.

1.2.2 Gas hydrates and the environment

The presence of hydrates in the earth provides two important items of information. One pertains to possible indicators of current and ancient climate changes due to methane releases and ice hydrates of air from Antarctica (Sloan 1998). The other pertains to geological hazards due to their association with

significant movement of earth in deepwater ocean environment. Nixon and Grozic (2007) stated that "there is substantial evidence from case histories that links gas hydrate dissociation to submarine slope failures and other geohazards". In addition, there is another aspect which deserves attention; that is carbon dioxide sequestering and storage as hydrates in the ocean as a mitigation strategy for carbon dioxide emissions (Shindo et al. 1993).

1.2.3 Gas hydrates as future energy source

It has been confirmed that hydrate deposits exist both offshore and onshore around the globe (Sloan and Koh, 2007). Methane hydrates can exist in oceanic sediments where the ocean is at least 300 meters deep. In the permafrost regions, it is present at depths between 150 and 2000 meters below the surface (Sloan, 1997). It is worth noting that natural gas hydrate deposits are distributed worldwide in contrast to conventional oil and gas deposits. More importantly, it is believed that there is twice as much carbon in hydrates form as in oil, natural gas, and coal combined (Suess et al., 1999). The paradigm has shifted for the recent years from assessment of the hydrate deposits amount to production of gas from hydrate deposits (Sloan and Koh, 2007).

1.2.4 Gas hydrates as alternative for natural gas transportation

Several studies have been reported showing the feasibility of transporting natural gas in the solid hydrates form. A natural gas hydrate (NGH) transportation chain consists of hydrate production, marine transport and re-gasification elements.

Gudmundsson and Borrehaug (1996) found, with a conservative economic analysis, that the capital cost associated with an NGH chain is 28% lower than the equivalent LNG chain. Takaoki et al. (2002) found that storing hydrates as small pellets is a suitable way for transportation.

1.2.5 Gas hydrates as natural gas storage

Natural gas can be stored at low pressures and temperatures in the form of hydrates. Parent (1948) calculated that a natural gas with a volume of 4.42 m^3 at 15 ^0C and atmospheric pressure only requires 0.028 m^3 of volume for storage in the hydrate state. Therefore, only 1/156 of the volume in the free state is needed which makes the use of hydrates a possible alternative to store natural gas.

1.3 Thermodynamic studies of gas hydrates

Thermodynamic analysis of the behaviour of gas hydrates has been reported extensively by several researchers. van der Waals and Platteeuw (1959) were the first to use the Langmuir type adsorption theory for the prediction of gas hydrate equilibria. Then, a numerical procedure based on that model was proposed by Parrish and Prausnitz (1972) to calculate the hydrate formation conditions from gaseous mixtures. Ng and Robinson (1976) and later, John et al. (1985) improved this procedure. Extensive work for predicting gas hydrate equilibrium has been done also by Holder et al. (1980) and Bishnoi et al. (1989) and summarized by Makogan (1981) and Sloan (1991).

1.4 Kinetics studies of gas hydrates

The thermodynamics of gas hydrates have been studied extensively for several decades in contrast to the kinetics of hydrates formation and decomposition. As far as the kinetics of gas hydrates formation is concerned, there are two main steps pertaining to hydrate formation, namely crystal nucleation and growth. A recent paper by Ribeiro and Lage (2008) provides a critical review of the literature on hydrate kinetics with emphasis upon the modelling efforts.

1.4.1 Hydrate nucleation

Hydrate nucleation is the process during which small clusters of water and gas defined as hydrate nuclei grow and disperse in an attempt to achieve critical size for continued growth (Sloan and Koh, 2007). According to Mullin (1993), the nucleation step is a microscopic phenomenon involving tens of thousands of molecules and it is difficult to observe experimentally. Vysniauskas and Bishnoi (1983) pioneered the kinetics of gas hydrate formation by proposing a semi-empirical model to correlate the experimental data. Their model consists of three steps: an initial clustering process, formation of a critical nucleus, and growth of the hydrate crystal around the stable nucleus. They considered the reaction rate to depend on the concentrations of the critical size nucleus and monomers of water and methane at the gas-water interface, and the total area of the water-gas interface. Sloan and Fleyfel proposed a hypothesis to describe the molecular mechanism for gas hydrate nucleation from ice (Sloan, 1990; Sloan and Fleyfel, 1991). The model consists of four steps as follow:

(i) Initially, the ice and gas phases are separated by a thin film of water. Within that liquid film, the basic hydrate cavity (5^{12}) is formed through molecular transitions at the ice interface.

(ii) Then, cavities may link either through vertices to form the Structure I hydrate or through face-sharing to form the Structure II hydrate.

(iii) Unit crystals of either structure are formed, and then combine with other unit crystals.

(iv) Once these crystals grow beyond the critical size, the primary nucleation step ends, and the crystals growth step begins.

The above hypothesis was extended to model hydrate formation from ice by Muller-Bongartz et al. (1992). Parent and Bishnoi (1996) studied hydrate nucleation using light scattering technique and concluded that the thermal history of water and the agitation effects are factors influencing the nucleation phenomenon. Natarajan and Bishnoi (1996) viewed hydrate nucleation as an intrinsically stochastic process involving the formation and growth of gas-water clusters to critical size, stable hydrate nuclei. They suggested that the stochastic nature of the nucleation process could be masked by high nucleation driving forces and the presence of heterogeneities making it a deterministic process.

1.4.2 Hydrate growth

The attempts to establish a kinetic model for hydrate growth started with the work of Glew and Hagget (1968). Based on experimental observations of ethylene oxide hydrates, they found that the rate was directly proportional to the

temperature difference between the reactor and its cooling bath. They identified the driving force for hydrate formation as the difference between the equilibrium and operating temperatures. The same driving force was adopted by Pangborn and Barduhn (1970). Vysniauskas and Bishnoi (1983) analyzed methane hydrate formation in a semi batch isobaric stirred reactor immersed inside an isothermal bath. In their study, a semi-empirical kinetic model was proposed by considering the reaction to depend on the concentrations of the critical size cluster and the monomers of water and methane at the interface. This was the first attempt in the literature to model hydrate formation kinetics specifically for hydrocarbon hydrates. According to Riberio and Lage (2007), there are more than fourteen available models for hydrate formations from which four are considered main and will be discussed briefly in the following sections.

1.4.2.1 The model of Englezos-Kalogerakis-Dholabhai-Bishnoi

Englezos et al. (1987a,b) developed a mechanistic model for the kinetics of the formation of hydrates of methane, ethane and their mixtures in liquid water using the experimental data obtained in the Bishnoi laboratories (Bishnoi et al., 1985 and 1986) utilizing a semi-batch stirred reactor. They considered the hydrate formation as a heterogeneous process involving mass transfers at the gas liquid-interface in the reactor and subsequent crystallization of the gas molecules into the hydrate structure. The model has one fitted parameter; the intrinsic rate constant for the gas hydrate former, to match the experimental data of the hydrate growth. As this model is used in the current study a thorough discussion

is given later in Chapter 2. It is worth mentioning that while writing the initial conditions for the first and second moments of the particle size distribution in the original model of Englezos et al. (1987a) there was an inconsistency in representing the particle size by its radius rather than its diameter. This inconsistency in the model was removed later by Malegaonkar et al. (1997) and the intrinsic rate constants for ethane and methane gas hydrates formation were re-determined. Furthermore, a modification to the model was made to account for the high solubility of carbon dioxide in water, and then, the intrinsic rate constant for carbon dioxide hydrates formation was determined (Malegaonkar et al., 1997). The Englezos et al. Model (1987) laid down the corner stone for all hydrate formation modelling efforts that followed.

1.4.2.2 The model of Skovborg and Rasmussen

Skovborg and Rasmussen (1994) proposed a simplification to the Englezos et al. (1987a) model by removing the population balance equations and assuming that the transport of gas molecules from the gas phase to the liquid water phase is the rate-determining step in the overall hydrate formation process. In their effort to simplify the model, they used the same experimental data produced from the Bishnoi laboratory. Unlike the original model by Englezos et al. (1987), there is no published evidence that the parameters of the simplified model by Skovborg-Rasmussen are apparatus independent (Sloan and Koh, 2007). The model appears to be a data fit rather than have theoretical significance (Sloan and Koh, 2007). In fact, Gnanendran and Amin (2004) simulated natural gas hydrate

formation using the Skovborg and Rasmussen (1994) model but failed to obtain convergence in the flash calculation (Ribeiro and Lage, 2008). The model in general assumes that the hydrate formation phenomena is a homogenous process rather than heterogamous which is absolutely unrealistic knowing that hydrate formation involves three different phases.

1.4.2.3 The model of Herri-Pic-Gruy-Cournil

In contradiction to Skovborg and Rasmussen (1994), Herri et al. (1999a) developed another kinetic model emphasizing on the necessity of including the population balance equations. In their study, the kinetics of methane hydrate formation was investigated with the aid of *in situ* measurements of the crystal size distributions with the light scattering technique. The technique used in their study allowed them to study the effect of additives on the induction delay as well as the quantity of hydrates formed. The limitations of the equipment used in their study include a minimum detectable particle diameter of 10 μm.

1.4.2.4 The model of Gnanendran and Amin

In contrast to the previous modeling efforts which concentrated on pure water-gas hydrate system, Gnanendran and Amin (2004) proposed a model for gas hydrate formation kinetics of a hydrate promoter-water-natural gas system in a semi batch stirred spray tank reactor. Their study aimed specifically at the storage of natural gas in the form of gas hydrates.

Other available models can be found in the summary of Ribeiro and Lage (2008).

1.5 Use of particle size analysis in modeling hydrate formation

The work of Sharma (1996) in Bishnoi laboratories marks the first attempt to obtain the second moment of hydrate particles distribution from actual particle size measurements and apply it in the Englezos et al. model (1987a) eliminating the need for the rest of the population balance equations needed to be solved in the model to determine the intrinsic rate constant for hydrate formation for ethane and methane gases. In their work, the second moment was obtained using an outside loop in which a Helium-Neon laser particle size analyzer was installed. Aside from measuring the hydrate particles distribution outside the reactor, the particle size analyzer used was only capable of measuring particles down to 5 μm.

The use of an *in situ* particle size analyser to determine the intrinsic kinetics of gas hydrates was reported by Clarke and Bishnoi (2004, 2005). In their study, carbon dioxide hydrates were formed in a semi-batch stirred tank reactor and the particle size distribution was measured *in situ* with a Focused Beam Reflectance Method (FBRM) probe. Then, the intrinsic rate constant of CO_2 hydrate formation was extracted by regression using a modified form of the heterogeneous kinetics model of Englezos et al. (1987a) and the experimental data. The probe used is capable of measuring particle chord lengths ranging from 0.5 μm and 1000 μm.

Bergeron and Servio (2008) determined the reaction rate constant for propane hydrate formation using a particle size analyzer capable of detecting particles with diameters as small as 0.6 nm. The data obtained were analyzed via their proposed kinetic model based on crystallization theory. However, they found that the model did not fit the experimental data properly when the actual (experimental) dissolution rate of propane at the vapor liquid interface is fed into the model. This lead them to solve the model simultaneously with two unknowns, the reaction rate constant and the theoretical dissolution rate of propane at the vapor liquid interface. The dissolution rate value that improved the model fitting of the experimental date was five times higher than the actual value. Moreover, the particles were measured outside the reactor.

1.6 Use of Raman Spectroscopy to Study Gas Hydrates

Raman spectroscopy (named after C. V. Raman) is a spectroscopic technique used to study vibrational, rotational, and other low-frequency modes in a system. The technique relies on inelastic scattering, or Raman scattering, of monochromatic light, usually from a laser in the visible, near infrared, or near ultraviolet range. The laser light interacts with phonons or other excitations in the system, resulting in the energy of the laser photons being shifted up or down. This shift in energy gives information about the phonon modes in the system.

Raman spectroscopy has been applied for gas hydrates structure identification, hydration number, and relative cage occupancies (Sum et al., 1997; Uchida et al., 1999; Subramanian et al., 2000; Wilson et al., 2002; and Schicks et al.,

2006). Raman guest spectra of gas hydrates have been reported for three known hydrate structures: structure I, structure II, and structure H.

1.7 Scope of this study

In all the sound studies of gas hydrate formation kinetics, hydrate formation has been recognized as a heterogeneous process wherein particle size distribution of the hydrate particles must be accounted for. Since no proper particle size measurements were available, Englezos et al. (1987a,b) had to make assumptions with regard to the particle size distribution during hydrate formation process when modelling particles growth.

In this study, actual particle size measurements were combined with Raman spectroscopy analysis to investigate the kinetics of hydrate formation from various natural gas hydrate formers. Experimental data on gas hydrates formation from methane, ethane, propane, and an equimolar ethane-propane mixture were collected with a modified apparatus that incorporates *in situ* particle size analyzer and Raman spectrometer. Since the experimental measurements were made on the particle sizes and their distribution, the need to make assumptions with regard to initial nuclei size and particle size distribution during hydrate growth was eliminated for modelling the experimental data. The working equations used by Englezos et al. (1987a) were suitably modified to incorporate the particle size measurement information in order to extract the intrinsic kinetic rate constant for hydrate growth by regressing the experimental data. The

intrinsic kinetic rate constant for hydrate formation of methane gas in structure I, ethane gas in structure I, and propane gas in structure II were determined. Then, an equimolar mixture of ethane and propane gases was used where the experimental data and the *a priori* determined rate constant for hydrate formation of propane in Structure II were used to extract the intrinsic rate constant of gas hydrate formation for ethane in structure II. Raman spectroscopy was used to identify the structure in which the gas hydrate former exists during the hydrate formation experiment to insure that the reported intrinsic rate constant of each gas hydrate former correspond to the right structure.

In Chapter 2, a review of the devolvement of the Englezos (1987a,b) kinetic model is presented. In Chapter 3, the experimental procedure and the apparatus used in this study is described in details. Chapter 4 shows the method used to determine the interfacial area. The use of the FBRM probe to study gas hydrates is discussed thoroughly in Chapter 5 followed by explanations of incorporating the measured data by the FBRM into the kinetic model in Chapter 6. Results and discussions are presented in Chapter 7 followed by conclusions and recommendations in Chapter 8.

CHAPTER TWO: KINETICS MODEL FOR HYDRATE FORMATION

2.1 Review of Englezos et al. Model (1987a)

The overall driving force for hydrate formation is the difference between the fugacity of the dissolved hydrate former gas and the three phase equilibrium fugacity of the hydrate former at the hydrate interface temperature which is the minimum fugacity at which hydrates can exist.

$$\Delta f = f - f_{eq} \tag{2.1}$$

f: is fugacity of the dissolved hydrate former gas either in the liquid film at the gas-liquid interface or in the bulk of the solution, MPa.

f_{eq}: is the three phase equilibrium fugacity of the hydrate former at the hydrate interface temperature, MPa.

As illustrated in Figure 2.1, each hydrate particle, which is assumed to be spherical, is surrounded by an adsorption "reaction" layer followed by a stagnant diffusion layer. Particles could be located either in the liquid film at the gas-liquid interface or in the bulk of the solution. The crystal growth rate is proposed to be a two step process as follow:

1. Diffusion of the dissolved gas from the bulk of the solution to the crystal-liquid interface through a laminar diffusion layer around the particle:

$$\left(\frac{dn}{dt}\right)_d = K_d A_P (f - f_s) \tag{2.2}$$

The subscript, d, denotes diffusion.

K_d : mass transfer coefficient, mol/(m^2.MPa.s)

A_P : interfacial surface area of a particle, m^2

2. Reaction at the interface of a particle, which is similar to an adsorption process (incorporation of the gas molecules into the hydrate lattice and the subsequent stabilization of the framework of the structured water):

$$\left(\frac{dn}{dt}\right)_r = K_r A_P (f_s - f_{eq}) \tag{2.3}$$

The subscript, r, denotes reaction. K_r has the same unit as that of K_d.

K_r : is the intrinsic rate constant for the hydrate formation.

Since, no accumulation is allowed in the diffusion layer around the particle, the two rates given by (Equations 2.2 and 2.3) are equal. Thus, for a particle:

$$\left(\frac{dn}{dt}\right)_P = \left(\frac{dn}{dt}\right)_r = \left(\frac{dn}{dt}\right)_d \tag{2.4}$$

The subscript, P, denotes particle.

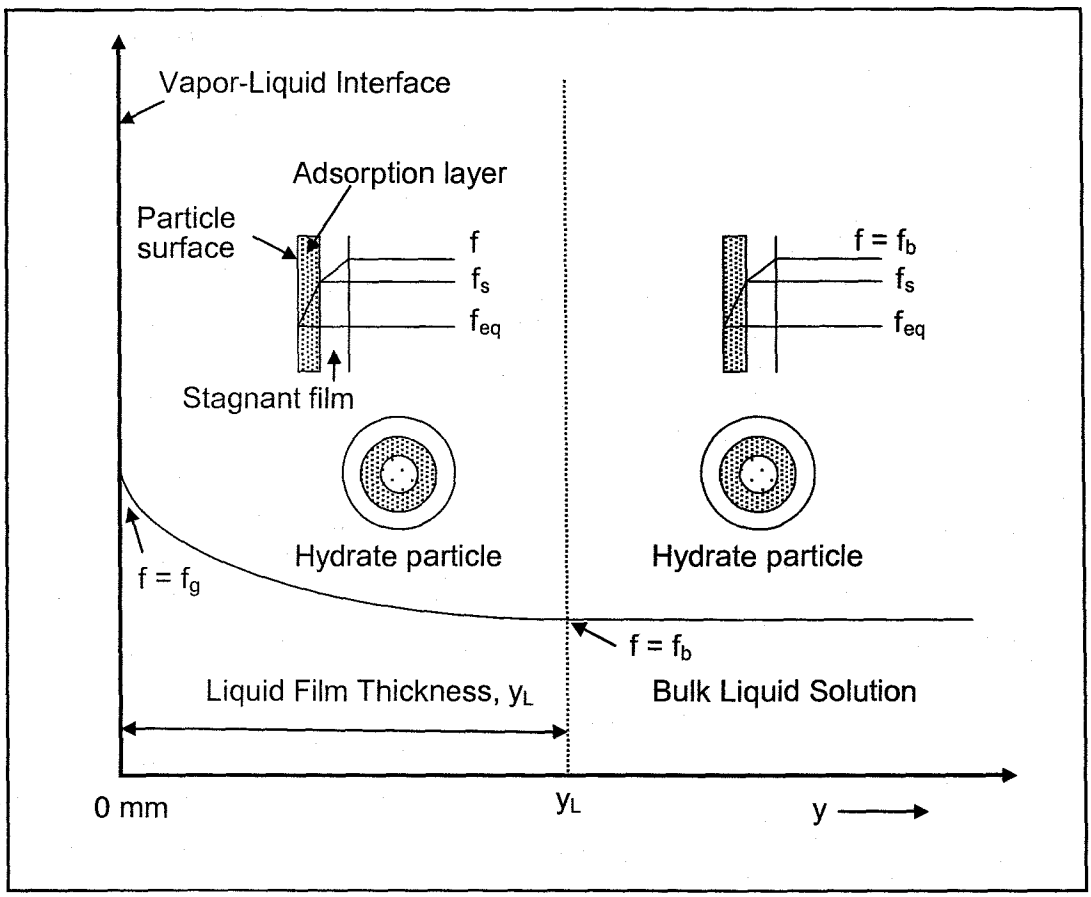

Figure 2.1: Schematic Representation of the Fugacity Profile of Gas in the Liquid and around a Particle (Dholabhai et al. 1993)

Now, let $\left(\frac{dn}{dt}\right)_P = R_P$ = moles of gas consumed per unit time in hydrate growth at the interface of a particle or the hydrate growth rate per particle.

$$R_P = K_d \cdot A_P \cdot (f - f_s) = K_r \cdot A_P \cdot (f_s - f_{eq}) \quad (2.5)$$

or:

$$\frac{R_P}{K_d A_P} = (f - f_s) \quad \text{and} \quad \frac{R_P}{K_r A_P} = (f_s - f_{eq})$$

Combining the two rates yields:

$$(f - f_s) + (f_s - f_{eq}) = \frac{R_P}{K_d \cdot A_P} + \frac{R_P}{K_r \cdot A_P} \quad (2.6)$$

Which can be simplified to:

$$(f - f_{eq}) = \frac{R_P}{A_P}\left[\frac{1}{K_d} + \frac{1}{K_r}\right] \quad (2.7)$$

Now, let $\frac{1}{K^*} = \left[\frac{1}{K_d} + \frac{1}{K_r}\right]$ (2.8)

where K^* is the combined rate constant, mole/(m^2.MPa.s), this leads to:

$$(f - f_{eq}) = \frac{R_P}{A_P}\left(\frac{1}{K^*}\right) \quad (2.9)$$

$$\therefore \left(\frac{dn}{dt}\right)_P = K^* \cdot A_P \cdot (f - f_{eq}) \quad (2.10)$$

where: $\left(\frac{dn}{dt}\right)_P$ is the rate of growth per hydrate particle, assumed in terms of moles of gas being converted into hydrate.

Global "Reaction" Rate

Integrating the rate per particle, $\left(\frac{dn}{dt}\right)_P$, for all particles:

$$R_y(t) = \int_0^\infty \left(\frac{dn}{dt}\right)_P \cdot \varphi(r,t)dr \qquad (2.11)$$

r : is the particle size, diameter, m.

$\varphi(r,t)dr$: is number of particles of size (*r*) to (*r+dr*) at time *t*, per unit volume of reaction mass, and $R_y(t)$ is the rate of hydrate growth per unit volume of reaction mass in units of moles of hydrate former.

Introducing the expression for, $\left(\frac{dn}{dt}\right)_P$

$$R_y(t) = \int_0^\infty K^* A_P (f - f_{eq}) \cdot \varphi(r,t)dr \qquad (2.12)$$

The area of a spherical particle is:

$$A_P = \pi \cdot r^2 \qquad (2.13)$$

Inserting this expression in the previous equation:

$$R_y(t) = \int_0^\infty \pi \cdot r^2 K^* (f - f_{eq}) \cdot \varphi(r,t)dr \qquad (2.14)$$

or: $$R_y(t) = \pi \cdot K^* (f - f_{eq}) \int_0^\infty r^2 \cdot \varphi(r,t)dr \qquad (2.15)$$

The definition of the second moment of PSD, μ_2 at any time, t, is:

$$\mu_2 = \int_0^\infty r^2 \cdot \varphi(r,t)\, dr \tag{2.16}$$

The dimension of μ_2, is m^2/m^3, which is per unit volume of the reaction mass.

$$\therefore R_y(t) = \pi \cdot K^* \cdot \mu_2 \cdot (f - f_{eq}) \tag{2.17}$$

Let $K = \pi \cdot K^* \mu_2$

$$\therefore R_y(t) = K \cdot (f - f_{eq}) \tag{2.18}$$

The dimension of $R_y(t)$ is (mole/m^3.s), which is per unit volume of the reaction mass.

2.2 Two film theory

The hydrate crystallization process in the liquid phase is a pseudo-first order irreversible reaction where water is present in excess amount. The two film theory is used to describe the absorption process of gas at the gas-liquid interface (Froment & Bischoff, 1979). When a gas phase is brought into contact with a liquid phase, the mass balance for the gas in a slice of thickness, *dy*, and unit cross sectional area in the liquid film assuming quasi-steady state (no accumulation of gas in the liquid film) is given by:

$$D\frac{d^2c}{dy^2} = R_y(t) \tag{2.18}$$

Substituting the value of $R_y(t)$ from Equation (2.18):

$$D\frac{d^2c}{dy^2} = K \cdot (f - f_{eq}) \tag{2.19}$$

D: is diffusivity of the gas in water, m^2/s.

c: concentration of gas in the liquid water, $mole/m^3$.

Assuming the number of moles of the water remains practically constant and the liquid solution is ideal, the concentration of the sparingly soluble gas in water is written in terms of its fugacity as:

$$c = c_{wo}\left(\frac{f}{H}\right) \tag{2.20}$$

c_{wo}: is the initial concentration of water molecules, $mole/m^3$.

H : Henry's constant, MPa, calculated from solubility experiments.

Substituting the expression for, *c*, in Equation (2.19) gives:

$$D\frac{d^2}{dy^2}\left(\frac{c_{wo}f}{H}\right) = K \cdot (f - f_{eq}) \tag{2.21}$$

$$\therefore D\frac{c_{wo}}{H}\frac{d^2f}{dy^2} = K\cdot(f - f_{eq}) \tag{2.22}$$

Let $Y = (f - f_{eq})$ (2.23)

and $D^* = \frac{D\cdot c_{wo}}{H}$ (2.24)

$$\therefore D^*\frac{d^2Y}{dy^2} = K\cdot Y \tag{2.25}$$

Equation (2.25) satisfies the following boundary conditions:

at $y = o,$ $Y = f_g - f_{eq}$ (2.26)

at $y = y_L,$ $Y = f_b - f_{eq}$ (2.27)

Rearranging Equation (2.25) gives:

$$\frac{d^2Y}{dy^2} - \frac{K}{D^*}\cdot Y = 0 \tag{2.28}$$

which is a second order homogenous differential equation that has the following general solution:

$$Y = C_1\cosh\left(y\cdot\sqrt{K/D^*}\right) + C_2 sinh\left(y\cdot\sqrt{K/D^*}\right) \tag{2.29}$$

To find the integration constants: C_1, and C_2, apply the boundary conditions as follow:

at $y = 0$ $Y = f_g - f_{eq}$

$$Y = C_1\cdot(1) + C_2\cdot(0) \tag{2.30}$$

$$Y = (f_g - f_{eq}) \cdot \cosh\left(\gamma \cdot \frac{y}{y_L}\right) + \frac{[(f_b - f_{eq}) - (f_g - f_{eq}) \cdot \cosh\gamma] \cdot sinh\left(\gamma \cdot \frac{y}{y_L}\right)}{sinh\gamma} \quad (2.39)$$

$$= \frac{(f_g - f_{eq}) \cdot \cosh\left(\gamma \cdot \frac{y}{y_L}\right) \cdot sinh\gamma + [(f_b - f_{eq}) - (f_g - f_{eq}) \cdot \cosh\gamma] sinh\left(\gamma \cdot \frac{y}{y_L}\right)}{sinh\gamma} \quad (2.40)$$

$$= \frac{(f_g - f_{eq}) \cdot \cosh\left(\gamma \cdot \frac{y}{y_L}\right) \cdot sinh\gamma + (f_b - f_{eq}) \cdot sinh\left(\gamma \cdot \frac{y}{y_L}\right) - (f_g - f_{eq}) \cdot \cosh\gamma \cdot sinh\left(\gamma \cdot \frac{y}{y_L}\right)}{sinh\gamma} \quad (2.41)$$

$$= \frac{(f_g - f_{eq}) \cdot \left[\cosh\left(\gamma \cdot \frac{y}{y_L}\right) \cdot sinh\gamma - \cosh\gamma \cdot sinh\left(\gamma \cdot \frac{y}{y_L}\right)\right] + (f_b - f_{eq}) \cdot sinh\left(\gamma \cdot \frac{y}{y_L}\right)}{sinh\gamma} \quad (2.42)$$

This is simplified from the following trigonometric definition:

$$\sinh(x - y) = [\sinh x \cdot \cosh y - \cosh x \cdot \sinh y] \quad (2.43)$$

where $x = \gamma$ and $y = \gamma \cdot \frac{y}{y_L}$ to give:

$$Y = \left[(f_g - f_{eq}) \cdot \sinh\left(\gamma - \gamma \cdot \frac{y}{y_L}\right) + (f_b - f_{eq}) \cdot sinh\left(\gamma \cdot \frac{y}{y_L}\right)\right] \cdot \frac{1}{sinh\gamma} \quad (2.44)$$

This will give the fugacity profile as:

$$f = f_{eq} + \left\{ (f_g - f_{eq}) \sinh\left[\gamma\left(1 - \frac{y}{y_L}\right)\right] + (f_b - f_{eq}) \sinh\left(\gamma \frac{y}{y_L}\right) \right\} \cdot \left(\frac{1}{\sinh\gamma}\right) \quad (2.45)$$

where: $$\gamma = y_L \cdot \sqrt{\left(\frac{\pi \cdot K^* \cdot \mu_2}{D^*}\right)} \quad (2.46)$$

and $$y_L = \frac{D \cdot a}{k_L \cdot a} \quad \text{or} \quad y_L = \frac{D}{k_L} \quad (2.47)$$

γ : Hatta number, which indicates how rapidly the reaction proceeds compared to the diffusion rate through the film, dimensionless.

y_L: film thickness, m.

k_L: liquid side mass transfer coefficient, m/s

a : gas-liquid interfacial area per unit of liquid volume, m^2/m^3.

It is worth noting that in deriving all of the above equations the gas phase resistance is assumed negligible since the partial pressure of water in the gas phase is very small.

The flux at the gas-liquid interface is obtained from Fick's Law as follow:

$$J_{y=0} = -D\left(\frac{dc}{dy}\right)_{y=0} = -D^*\left(\frac{df}{dy}\right)_{y=0} \qquad (2.48)$$

J: is the molar diffusion flux, $mole/m^2.s$

The gas transported into the liquid phase is either dissolved or converted to hydrate. The rate at which the gas is transported into the liquid phase is related to the flux at the interface by:

$$\left(\frac{dn}{dt}\right) = J_{y=0} \cdot A_{g-l} \qquad (2.49)$$

A_{g-l}: is the gas-liquid interfacial area, m^2 .

From Equation (2.45), taking the derivative of the fugacity with respect to the film thickness:

$$\frac{df}{dy} = \left\{ (f_g - f_{eq}) \cdot \cosh\left[\gamma\left(1 - \frac{y}{y_L}\right)\right] \cdot \left(\frac{-\gamma}{y_L}\right) + (f_b - f_{eq}) \cdot \cosh\left(\frac{\gamma \cdot y}{y_L}\right) \cdot \left(\frac{\gamma}{y_L}\right) \right\} \cdot \frac{1}{\sinh\gamma} \quad (2.50)$$

At $y = 0$:

$$\left(\frac{df}{dy}\right)_{y=0} = \left\{ (f_g - f_{eq}) \cdot \cosh\gamma \cdot \left(\frac{-\gamma}{y_L}\right) + (f_b - f_{eq}) \cdot \left(\frac{\gamma}{y_L}\right) \right\} \cdot \frac{1}{\sinh\gamma} \quad (2.51)$$

Rearranging:

$$\left(\frac{df}{dy}\right)_{y=0} = \frac{-\gamma}{y_L \cdot \sinh\gamma} \{ (f_g - f_{eq}) \cdot \cosh\gamma - (f_b - f_{eq}) \} \quad (2.52)$$

Now, substituting Equation (2.52) in Equation (2.48):

$$(J)_{y=0} = -D^* \cdot \left\{ \frac{-\gamma}{y_L \cdot \sinh\gamma} [(f_g - f_{eq}) \cdot \cosh\gamma - (f_b - f_{eq})] \right\} \quad (2.53)$$

$$\therefore (J)_{y=0} = \frac{D^* \cdot \gamma}{y_L \cdot \sinh\gamma} \{ (f_g - f_{eq}) \cdot \cosh\gamma - (f_b - f_{eq}) \} \quad (2.54)$$

Now, substituting Equation (2.54) in Equation (2.49) gives:

$$\frac{dn}{dt} = \frac{D^* \cdot \gamma}{y_L \cdot \sinh \gamma} \{(f_g - f_{eq}) \cdot \cosh \gamma - (f_b - f_{eq})\} \cdot A_{(g-l)} \quad (2.55)$$

Rearranging:

$$\frac{dn}{dt} = \frac{D^* \cdot \gamma \cdot A_{(g-l)}}{y_L \cdot \sinh \gamma} \{(f_g - f_{eq}) \cdot \cosh \gamma - (f_b - f_{eq})\} \quad (2.56)$$

Note that the units for the gas-liquid interfacial area, $A_{g\text{-}l}$, are m^2.

The initial conditions for this differential equation, n_o, is measured. It is the number of moles of gas that have been used to form the hydrate nuclei at the start of their growth (the turbidity point).

In order to determine the fugacity of the gas in the bulk of the liquid, f_b, as function of time, a mass balance in the bulk is done as follow:

$$Input\ Rate = Accumulation\ Rate + Reaction\ Rate$$

$$Reaction\ Rate = R_y(t) = \pi \cdot K^* \cdot \mu_2 \cdot (f_b - f_{eq}) \cdot V \quad (2.57)$$

$$Accumulation\ Rate = \frac{d}{dt}\left(\frac{c_{w0} \cdot f_b}{H}\right) \cdot V = \frac{c_{w0}}{H}\left(\frac{df_b}{dt}\right) \cdot V \quad (2.58)$$

$$Input\ Rate = (J)_{y=y_L} \cdot A_{(g-l)} = -D^* \cdot \left(\frac{df_b}{dy}\right)_{y=y_L} \cdot A_{(g-l)} \tag{2.59}$$

The derivative of the fugacity with respect to film thickness, at $y = y_L$, is obtained from Equation 2.50 as:

$$\left(\frac{df}{dy}\right)_{y=y_L} = \left\{(f_g - f_{eq}) \cdot \cosh\left(\gamma\left(1 - \frac{y_L}{y_L}\right)\right) \cdot \left(\frac{-\gamma}{y_L}\right) + (f_b - f_{eq}) \cdot \cosh\left(\gamma\frac{y_L}{y_L}\right) \cdot \left(\frac{\gamma}{y_L}\right)\right\} \cdot \frac{1}{\sinh\gamma} \tag{2.60}$$

$$\left(\frac{df}{dy}\right)_{y=y_L} = \left\{(f_g - f_{eq}) \cdot \left(\frac{-\gamma}{y_L}\right) + (f_b - f_{eq}) \cdot \cosh(\gamma) \cdot \left(\frac{\gamma}{y_L}\right)\right\} \cdot \frac{1}{\sinh\gamma} \tag{2.61}$$

which can be simplified to:

$$\left(\frac{df}{dy}\right)_{y=y_L} = \frac{-\gamma}{y_L \cdot \sinh\gamma}\{(f_g - f_{eq}) - (f_b - f_{eq}) \cdot \cosh(\gamma)\} \tag{2.62}$$

Inserting Equation (2.63) into equation (2.59) gives:

$$Input\ Rate = \frac{D^* \cdot \gamma \cdot A_{(g-l)}}{y_L \cdot \sinh\gamma}\{(f_g - f_{eq}) - (f_b - f_{eq}) \cdot \cosh(\gamma)\} \tag{2.63}$$

$$Accumulation\ Rate = Input\ Rate - Reaction\ Rate \tag{2.64}$$

Inserting the expressions for each term gives:

the turbidity point. Performing a mass balance in the bulk of the liquid phase for each gas to obtain the change in $f_{b,j}$ with respect to time gives:

$$\left(\frac{df_{b,j}}{dt}\right) = \frac{H_j \cdot D_j^* \cdot \gamma_j \cdot a}{c_{w0} \cdot y_L \cdot \sinh\gamma}\left\{\left(f_g - f_{eq}\right)_j - \left(f_b - f_{eq}\right)_j \cdot \cosh\gamma_j\right\} - \frac{\pi \cdot K_j^* \cdot H_j \cdot \mu_2}{c_{w0}}\left(f_b - f_{eq}\right)_j \tag{2.71}$$

At the turbidity point $f_{b,j} = f_{eq,j}$.

In addition to the mass balance equations, population balance equations are required to estimate μ_2. Again, more elaboration on this part is given in Chapter 6.

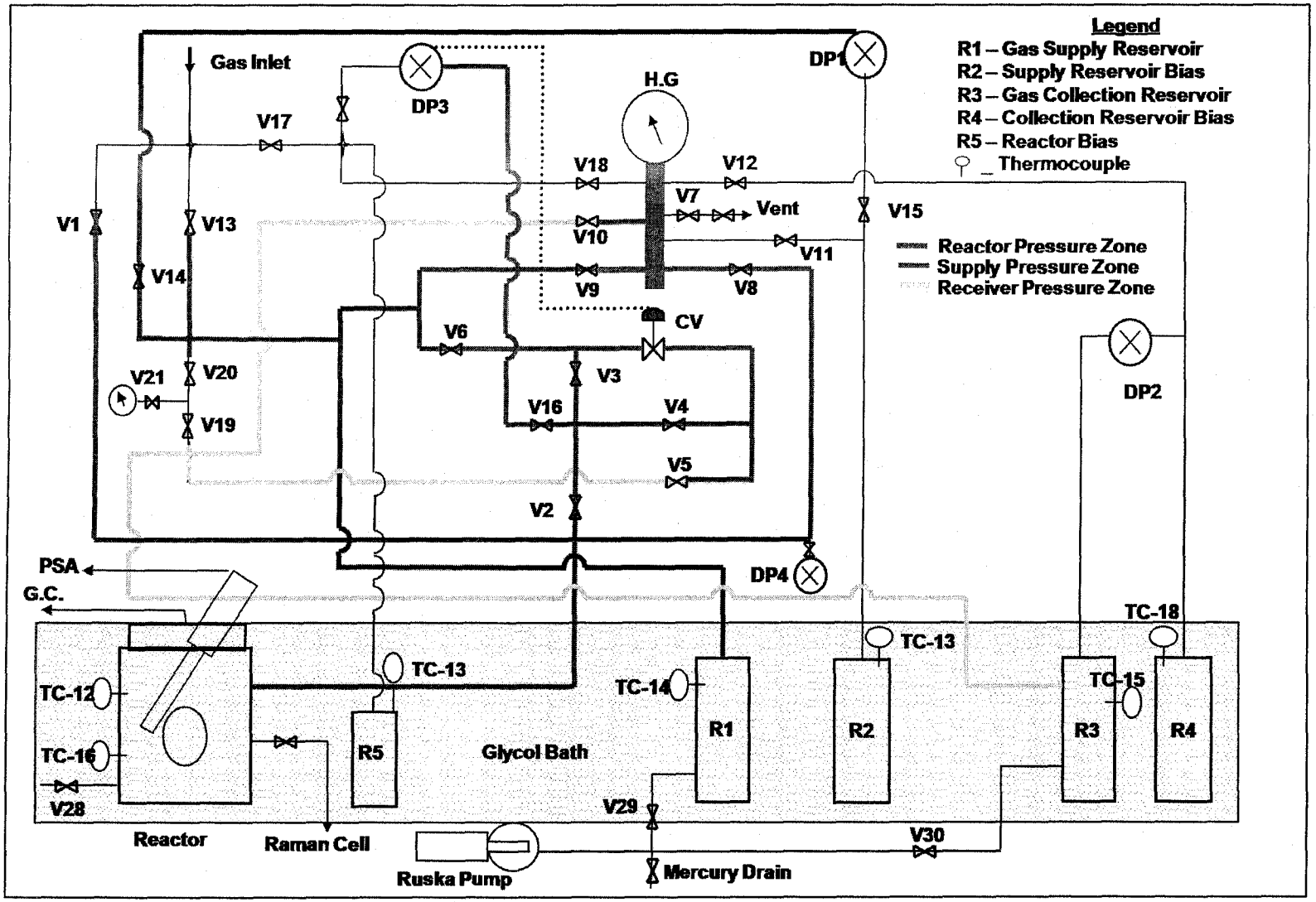

Figure 3.1: Schematic of the apparatus.

temperatures. The flange at the top of the reactor has provisions for a particle size analyzer probe and a mixer as shown in Figure 3.2.

3.1.1.1 Mixing system

The reactor is equipped with an Autoclave Engineers Magne Drive mixer inserted through the flange at the top of the reactor as shown in Figure 3.3. In addition to the bottom shaft impeller which agitates the solution, an additional impeller is added mid-way of the upper part of the shaft to agitate the gas phase of the reactor. Each impeller consists of six blades with dimensions of 13.5x9x1 mm. The agitation rate is controlled via Magnetic Hall Effect sensor by an electric driven motor capable of more than 1000 rpm.

3.1.1.2 Particle size probe

A Mettler-Toledo Lasentec® D600 focused beam reflectance measurement (FBRM) probe is inserted at an angle of 15° off of vertical as illustrated in Figure 3.4. Such orientation of the probe is required to improve the process of obtaining a representative particle size measurement of the hydrate sample. The FBRM probe in addition to the field unit and a data acquisition computer comprise Mettler-Toledo Lasentec® D600 FBRM system for particle size analysis. The field unit contains: laser diode and photo detectors, sensor assembly, counting circuits, laser scanner drive controller, and communication equipment. The field unit is integrated to a computer with version 6.0 build 16 Mettler-Toledo Lasentec® FBRM Control Interface software package. This package allows the

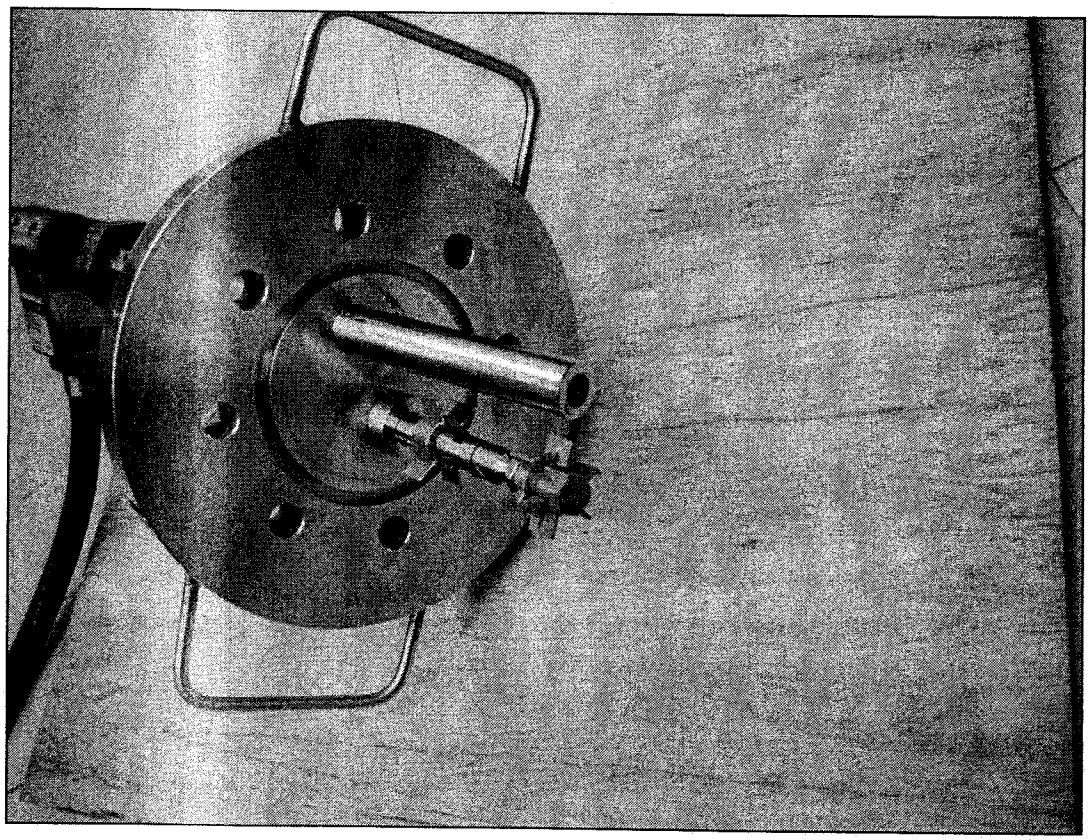

Figure 3.2: Reactor flange showing mixer and FBRM probe.

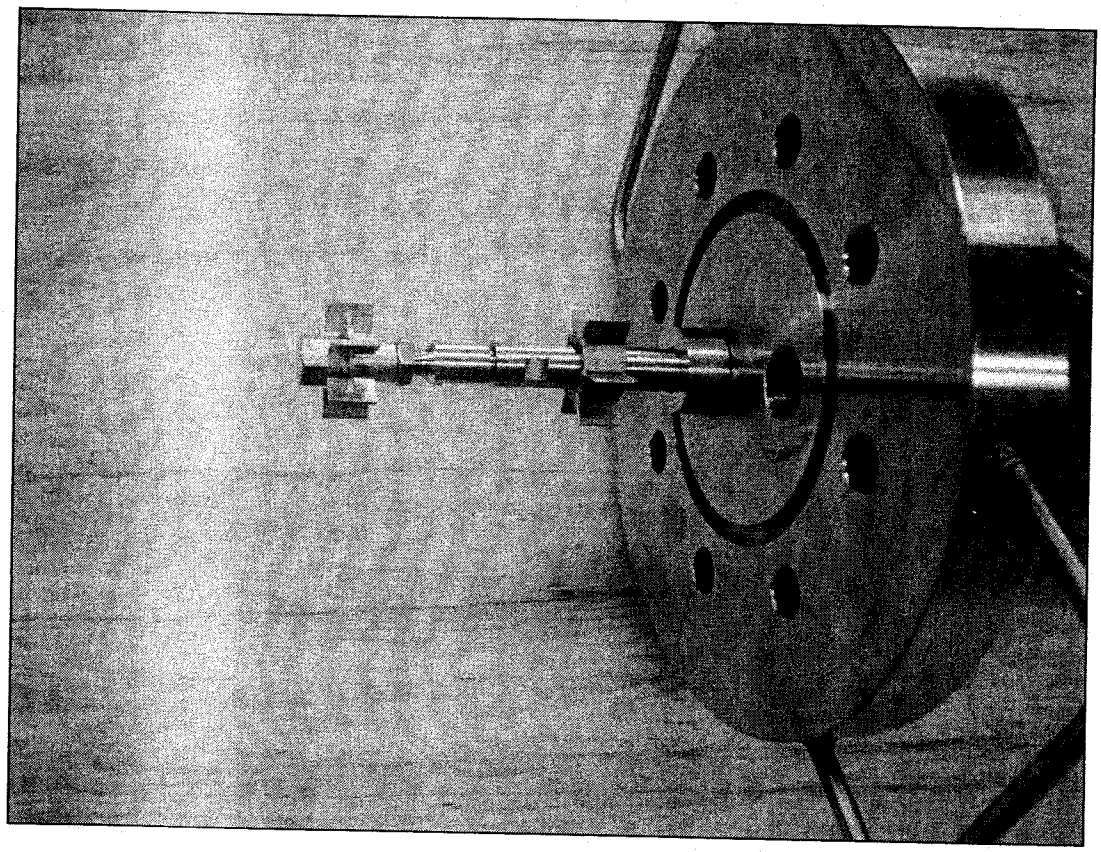

Figure 3.3: Side view of the mixer shaft.

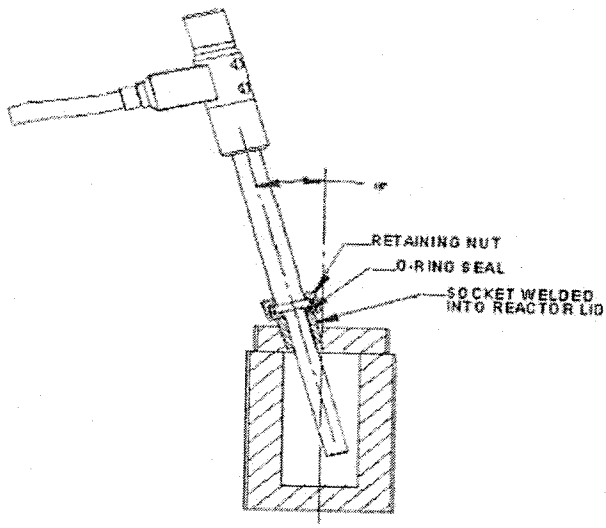

Figure 3.4: Placement and orientation of the PSA probe (www.mt.com\Mettler-Toledo Lasentec®).

user to configure and operate the Mettler-Toledo Lasentec® FBRM instrument, and simplifies data handling and analysis.

3.1.1.3 The Raman spectrometer and the sampling circuit

A flow line is connected to the bottom of the reactor to bring the hydrate slurry to a high pressure sampling cell. The sample is then returned to the reactor by a diaphragm Gilson 305 pump. The flow line connecting the reactor and the sampling cell is concentrically inserted in an insulated tubing which contains cooling fluid to control the temperature of the hydrate sample. The high pressure sampling cell is the same as that of Bishnoi and Clarke (2005) with slight modification to improve the temperature control of the hydrate slurry (see Figure 3.5). It mainly consists of a sapphire tube housed in an aluminum cell with provisions for cooling fluid to flow in and out of the cell. The sapphire tube wall thickness is 2.0 mm and its inside diameter is 5.0 mm. It is exposed to the Raman spectrometer, as seen in Figure 3.6, which is a Renishaw inVia Raman microscope equipped with a 1200 grooves/mm grating and a CCD detector. The excitation source is a 514nm Argon ion laser with a power output of 25 mW. During the acquisition of Raman spectra, the hydrate slurry is isolated and the pump is stopped.

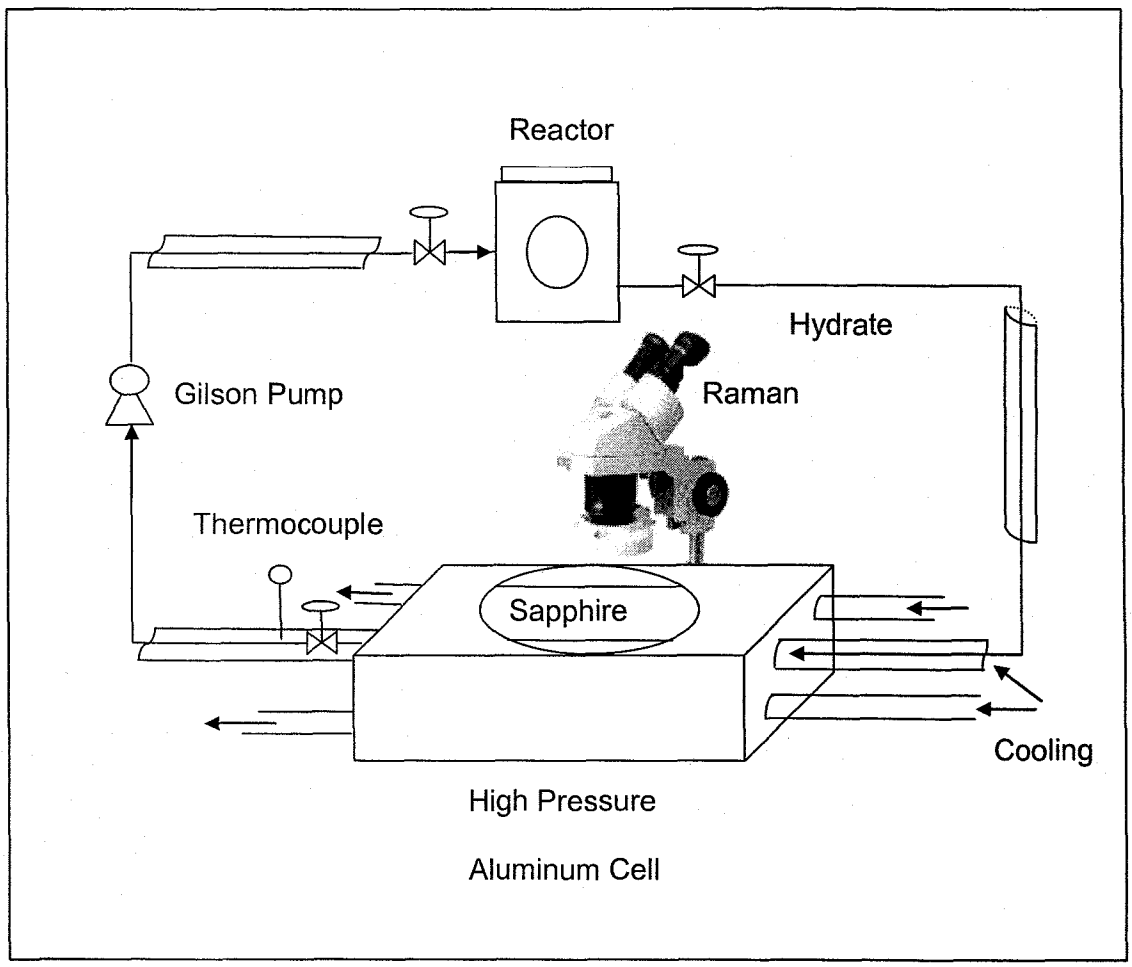

Figure 3.5: Raman spectroscopy sampling circuit.

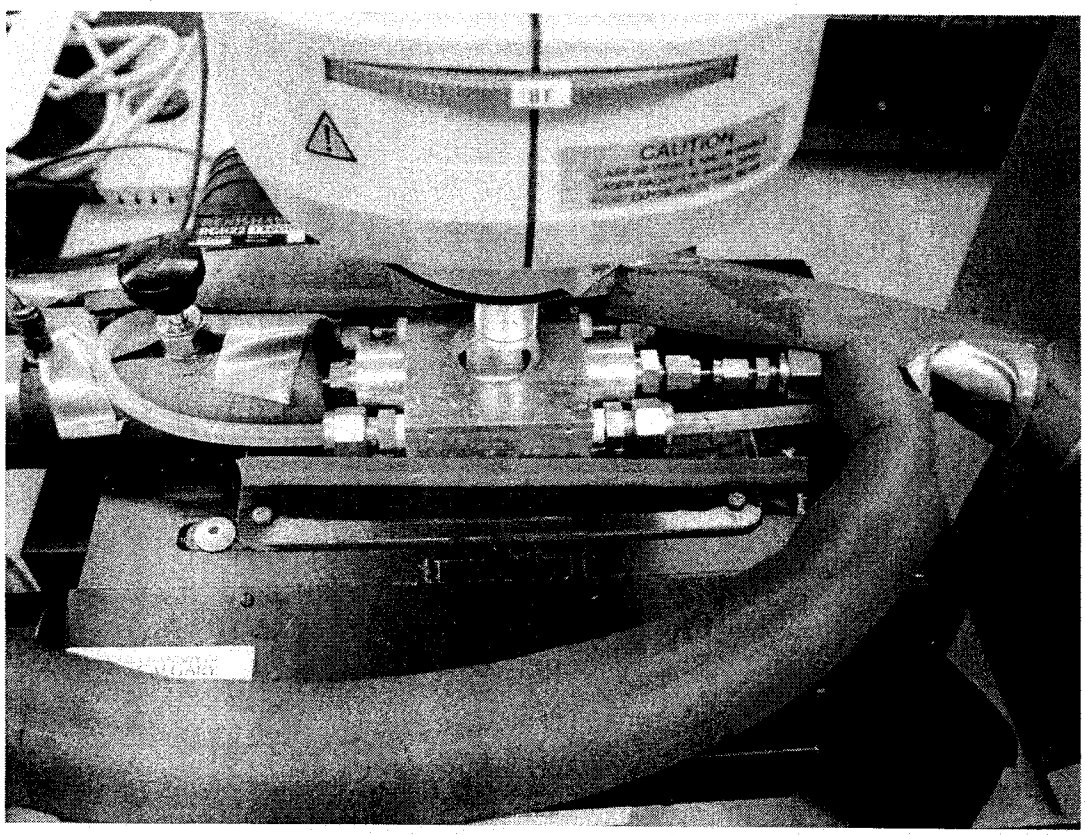

Figure 3.6: High pressure sampling cell under the Raman microscope.

3.1.2 Supply Reservoir

The supply reservoir is needed to supply the gas to the reactor during the gas consumption stage. The pressure in the reactor is held constant by controlling the flow of the gas from the supply reservoir. The supply reservoir is constructed from stainless steel 316. Its temperature is measured with a type-T thermocouple. It is connected to the higher side of the differential pressure transducer DP-1.

3.1.3 Collection Reservoir

The collection reservoir is needed only during the hydrates decomposition stage which is beyond the scope of this study. It is connected to pressure differential transducer DP-2, and its temperature is measured with type-T thermocouple. During the decomposition of gas hydrates, the released gas flow to the collection reservoir through the controller.

3.1.4 Bias Reservoirs

There are three bias reservoirs: reactor bias (R-5), supply bias (R-2), and collection bias (R-4). They are used for the differential pressure transducer (DP) cells to accurately measure the pressure in the reactor, supply and receiver reservoirs. The pressure in each bias reservoir remains constant during the course of the experiment and the pressure difference is measured with the designated differential pressure transducer. All of the bias reservoirs are constructed from stainless steel 316.

3.1.5 Cooling Systems

The temperature of the bath containing the reactor and the five reservoirs is controlled by circulating a mixture of water and ethylene glycol (50-50 by volume) to and from a refrigeration system that has a capacity of 170 litres. A level controller mounted in the refrigeration bath controls the operation of the two pumps circulating the cooling fluid between the refrigeration bath and the reactor bath. A side line from this system provides some of the cooling needed for the hydrate slurry line going into the Raman high pressure sampling cell. An additional cooling unit is used to provide the necessary cooling for the mixer system as well as the Raman high pressure sampling cell.

3.1.6 Thermocouples

To measure the temperature of the gas in the different reservoirs and in the reactor solution and gas phase type-T, copper-constantan thermocouples are used in the kinetics apparatus. These thermocouples are connected to the data acquisition system by shielded wires to reduce signal noise. The thermocouples are periodically calibrated against a precision thermometer by immersing them in a constant temperature bath. The accuracy of the temperature measurement is ± 0.1 K.

3.1.7 Pressure Measurements

There are two Heise gauges in the apparatus. One has a range of 0-250 bar while the other has a range of 0-5.0 bar. The higher range Hiese gauge is used

to measure the pressure in the bias reservoirs and the reactor while introducing the gas into the system. The maximum error of this gauge is ± 0.125 bar. The smaller range Hiese gauge is only used in low pressure experiments, mainly when performing the surface area experiments as will be subsequently explained. The actual pressures of the reactor and supply reservoir are measured by differential pressure transducers (DPs) connected to the data acquisition system by shielded wires. The reactor and its bias are connected to DP-3 cell while the supply and its bias are connected to DP-1 cell.

3.1.8 Reactor Pressure Controller

The pressure in the reactor is maintained constant during the experiment by allowing the makeup gas to flow from the supply reservoir, which is at a higher pressure, through a control valve. The pressure controller consists of a Yokogawa UT-320 digital proportional integral derivative (PID) controller and a fail to close valve. DP-3 reading is the input variable while the output is a current signal converted to a pneumatic signal to control the valve opening between the reactor and the supply reservoir. This digital controller has the capability of auto-tuning and fuzzy logic overshoot suppression.

3.1.9 Data Acquisition System

A National Instrument acquisition system is used for real time monitoring of the system pressures, temperatures, and control valve opening. The system consists of "Signal Conditioning eXtensions for Instrumentation" (SCXI-1000)

chassis, a computer interface NI-DAQ and a LabVIEW 7.0 software package. All the shielded wires from thermocouples, pressure transducers and the control valve are connected to the SCXI-1000 chassis. The LabVIEW software provides online monitoring of the real time system data (pressures, temperatures, and control valve opening) and save the data into an MS Excel file which can be accessed subsequently for data analysis. It also stores the pressure and temperature calibration files. Temperature and differential pressure values are calibrated against voltage readings. A precision thermometer was used for thermocouples calibration while a dead weight tester was used to calibrate the pressure transducers. The dead weight tester is set to give an accuracy of 10 PSI at 10,000 PSI indicated pressure which is 0.1 %. The followings are the formulas used in LabVIEW for calculating the pressure in the reactor and the supply respectively:

$$P_{Reactor} = P_{R5} - DP3 + P_{Atmospheric}$$

$$P_{Supply} = P_{R2} + DP1 + P_{Atmospheric}$$

Please note that P_{R5} *and* P_{R2} are the Heise gauge reading while filling the reservoirs, all pressure readings here are in bar.

3.1.10 Gas Chromatography

An SRI-8640 Gas Chromatograph (GC) model integrated to the Peak Simple II software was used to analyse the reactor gas phase when studying the kinetics of hydrates from gas mixtures. This gas chromatograph consists of a thermal

conductivity detector (TCD), and a Porapak Q column. The column of the GC was operated at 100° C. The gas chromatograph was calibrated using pure propane, pure ethane, and three different mixtures of both gases. Gas mixture samples were taken at gas dissolution saturation, during hydrate formation, and at the end of hydrate formation. To get a sample, a differential pressure was maintained between the reactor gas phase via the three way valve and the high pressure sampling chamber. That differential pressure was minimal so that it would not affect the gas consumption, and enough to get a reasonable reading in the GC. Helium gas was used to initially pressurize the sampling chamber to a pressure slightly lower than the reactor pressure. However, to maintain a reasonable material balance of the system content, several experiments were run separately and the gas chromatography analysis did not show a considerable change in the gas phase compositions from the initial gas phase sample.

3.2 Experimental Procedure

The first step after all necessary calibrations were established, was determining the volumes of the different sections in the apparatus. This step was done using the Ruska pump experiment described below.

3.2.1 Ruska Pump Experiment

The Ruska pump experiment was performed to determine the volume of each section of the equipment, namely, reactor and tubing, supply reservoir, and collection reservoir. The principle of the Ruska pump experiment is based on

measuring the subject volume by noticing the change in pressure and temperature of that section after injecting a known volume of mercury into it. Since the number of moles within the reservoir remains constant after mercury injection, pressures, volumes, and temperatures have the following relation:

$$\frac{P_1V_1}{z_1T_1}=\frac{P_2V_2}{z_2T_2}=\frac{P_2(V_1-\delta V)}{z_2T_2} \tag{3.1}$$

The subscripts 1 and 2 denote the equilibrium state before and after the injection of mercury into the reservoir respectively. The compressibility factors were calculated using the Trebble-Bishnoi equation of state (1987, 1988). The difference between V_1 and V_2 is the volume of mercury injected, and is denoted by δV in the above equation to yield:

$$V_2=\frac{\delta V}{\left(\frac{z_1P_2T_1}{z_2P_1T_2}-1\right)} \tag{3.2}$$

The experimental error in the measurement of the injected volume of mercury is less than 0.01 ml.

Each section of the apparatus is illustrated clearly by color coding in Figure 3.1. The apparatus is set up to have the mercury injected only into two reservoirs, namely: the supply and the collection, thus, the volume of the section that includes the reactor can be determined by including it with either sections during

the experiment and subtracting it later from the total volume. Here, it is included in the supply reservoir section during the first set of experiments, hence, the determined volume accounts for both the reactor section and the supply section. Then the supply section is isolated and its volume is determined.

To start the experiment, the system was filled with an inert gas, Helium, the initial temperature and pressure readings were recorded. Then, a 50.0 ml ±0.01 ml of mercury was injected into the supply/collection reservoirs, the change in pressure and temperature was recorded. Then an additional 50.0 ml ±0.01 ml of mercury was added, and the change in the temperature and pressure was recorded. This resulted in three similar values for the volume; the average was taken as the section volume which will be used in the calculations. A summary of the results of this experiment is tabulated in Table 3.1.

Apparatus Section	Volume, m^3
Reactor zone	0.000705
Supply reservoir zone	0.001057
Collection reservoir zone	0.001238

Table 3.1: Volumes of the different sections of the apparatus.

3.2.2 Preparation and Start Up

All reservoirs were purged with the experimental gas several times to ensure no gas from previous experiments is leftover. The reactor was then flushed several times with ultra pure water. The water used, in the present study, was first de-ionized through a purification system using (Millipore-Simplicity) model. This model produces ultra-pure water with a resistivity of 18.2 MΩ·cm at 25 ^{0}C. Then, the de-ionized water was distilled for further purification. The reactor was then charged with 280 ml of the ultra clean water. After the water reached thermal stability; at the desired operating temperature, the experimental gas was introduced slowly into the system. The reactor was filled to the desired experimental pressure, while supply reservoir was filled to a pressure roughly 2 bar higher than that of the reactor. The bias reservoirs were filled to pressures according to their span limit. Then, the data acquisition system was started, and given some time to get consistent readings, roughly 3 minutes, then, the controller was set to auto mode, and the stirrer was gradually increased from 0 to the desired stirring rate. Finally, the FBRM data acquisition was started. The data acquisition system records temperatures and pressures using LabView 7.0 software and the user interface allow different acquisition and averaging modes. In this work an interval of 10 seconds was chosen to log the data into the output data file.

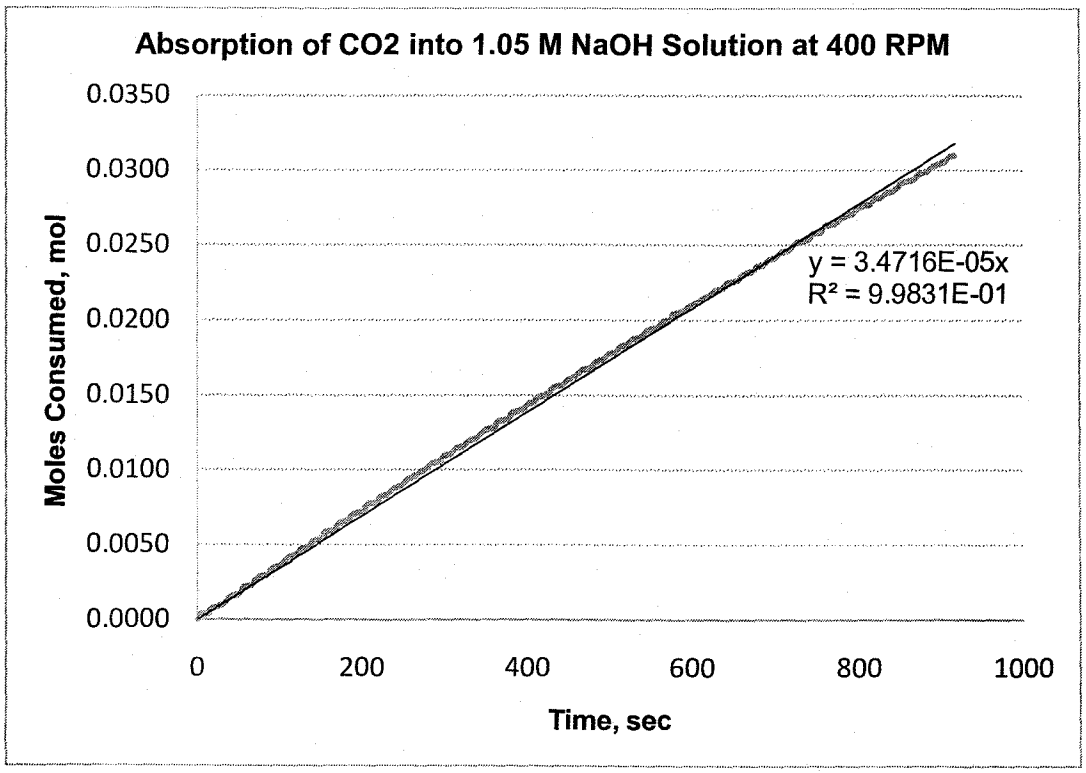

Figure 4.1: Gas consumption rate of CO_2 into 1.05 M NaOH solution at 400 RPM.

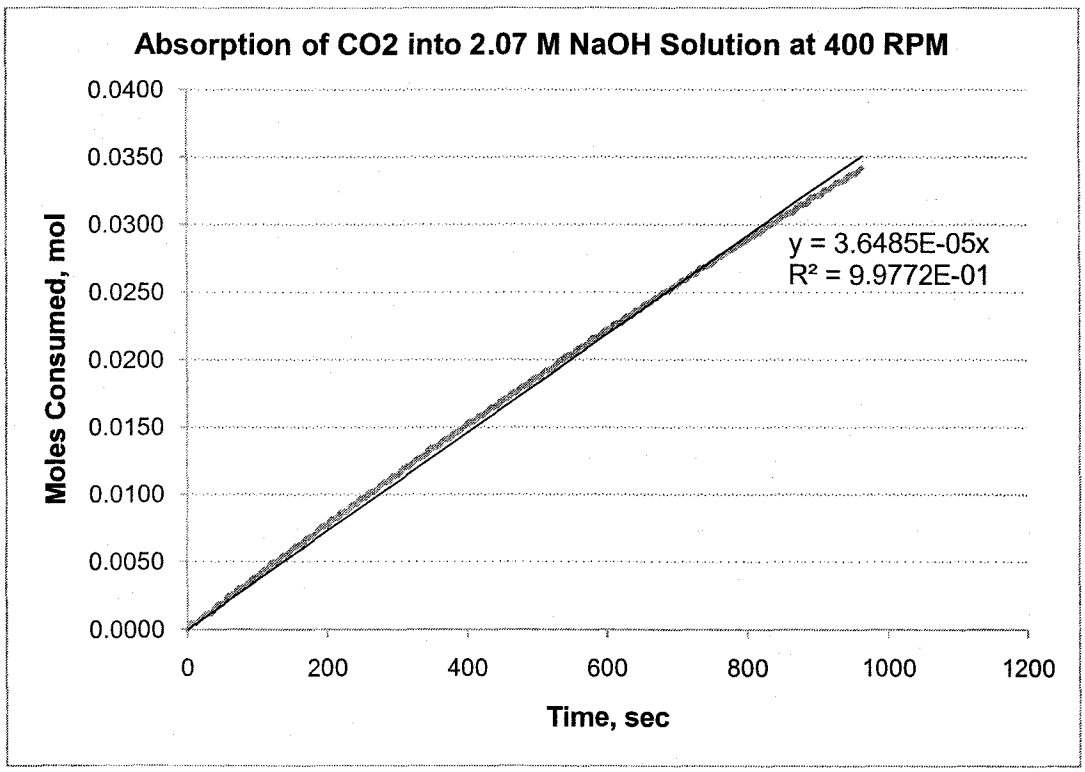

Figure 4.2: Gas consumption rate of CO_2 into 2.07 M NaOH solution at 400 RPM.

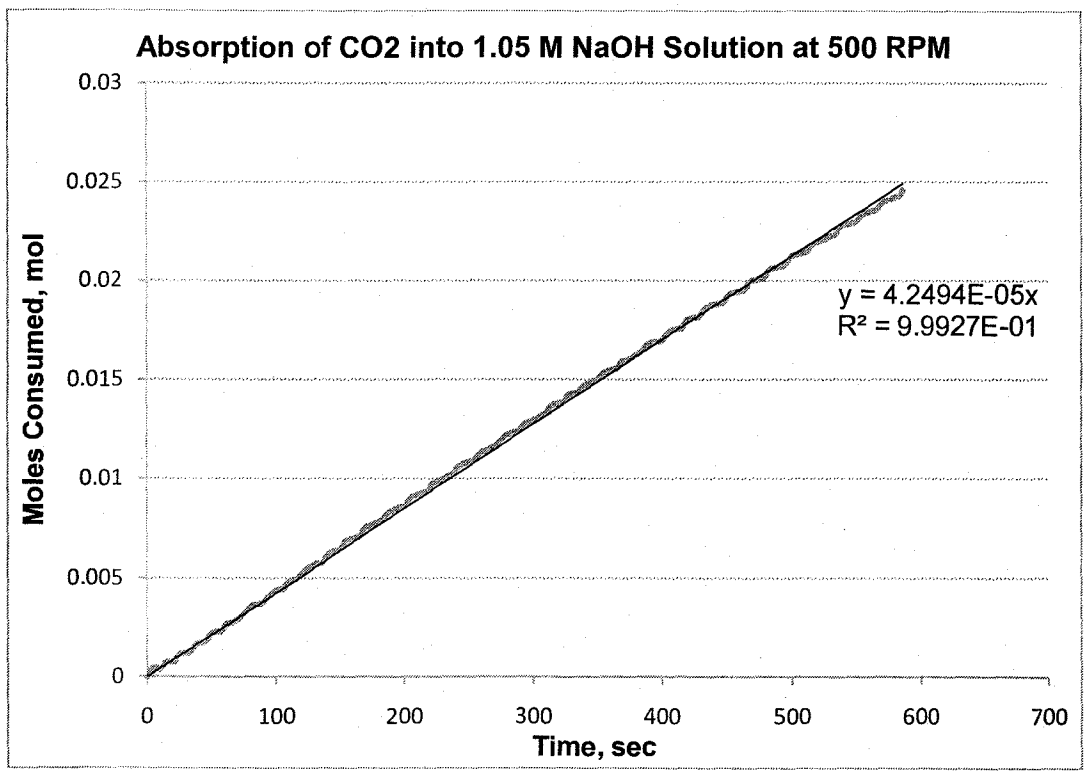

Figure 4.3: Gas consumption rate of CO_2 into 1.05 M NaOH solution at 500 RPM.

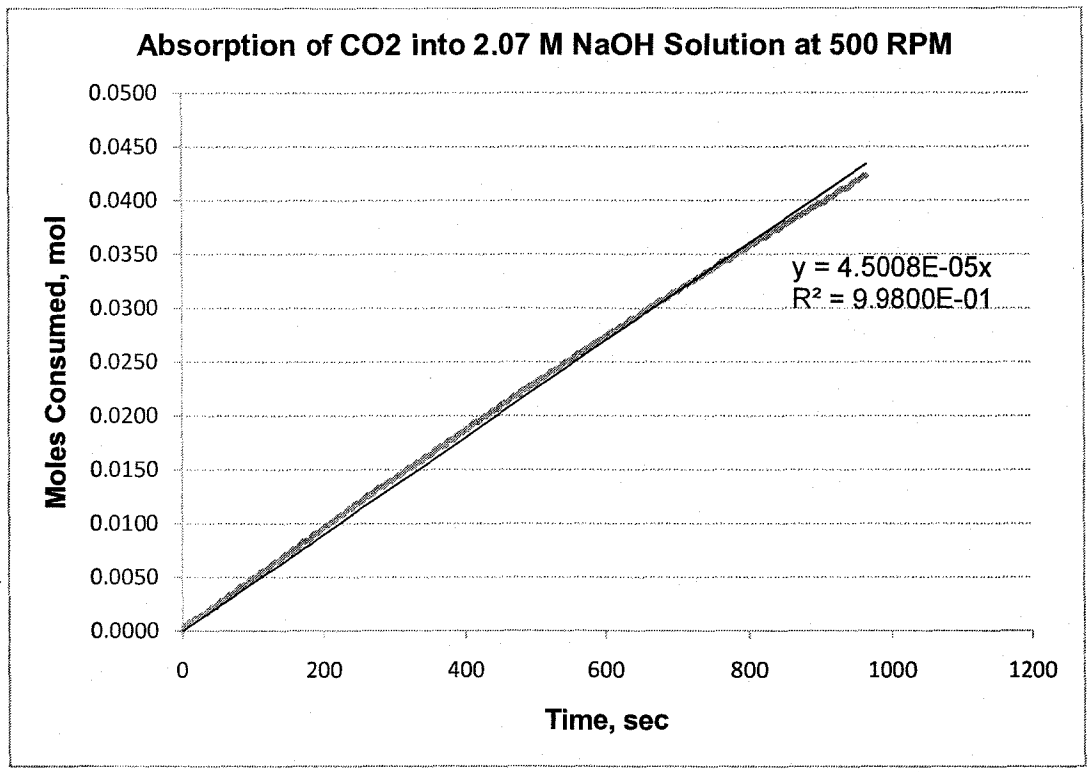

Figure 4.4: Gas consumption rate of CO_2 into 2.07 M NaOH solution at 500 RPM.

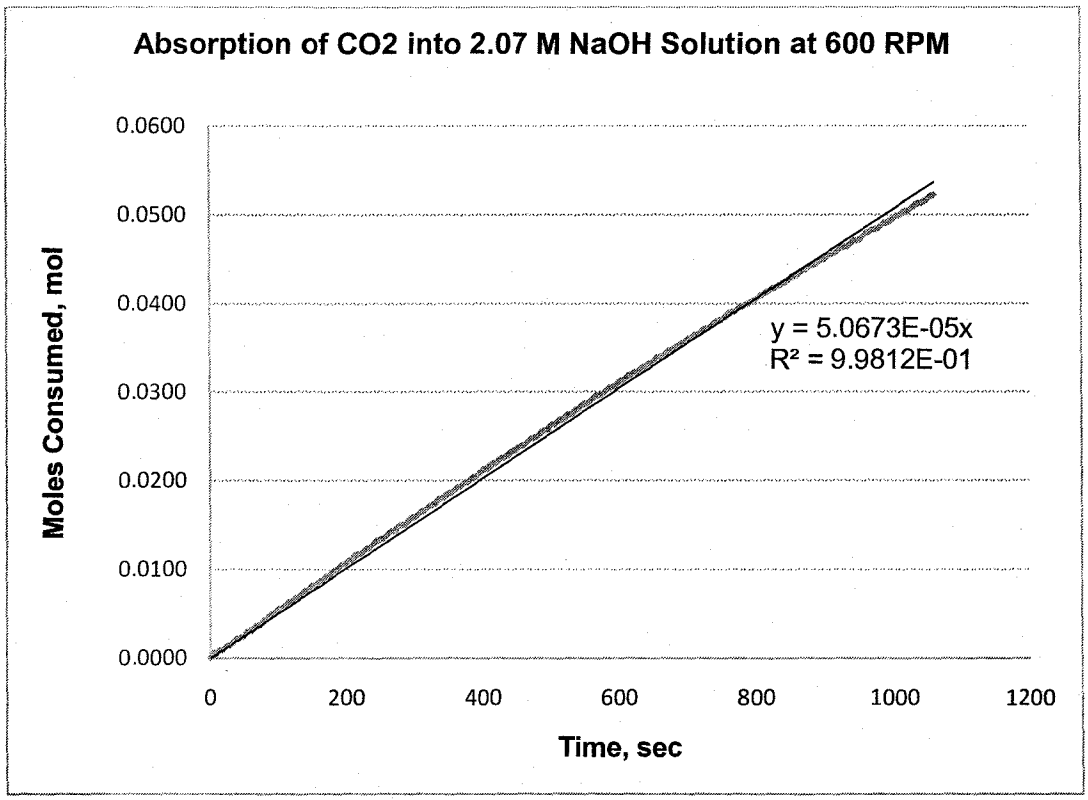

Figure 4.5: Gas consumption rate of CO_2 into 2.07 M NaOH solution at 600 RPM.

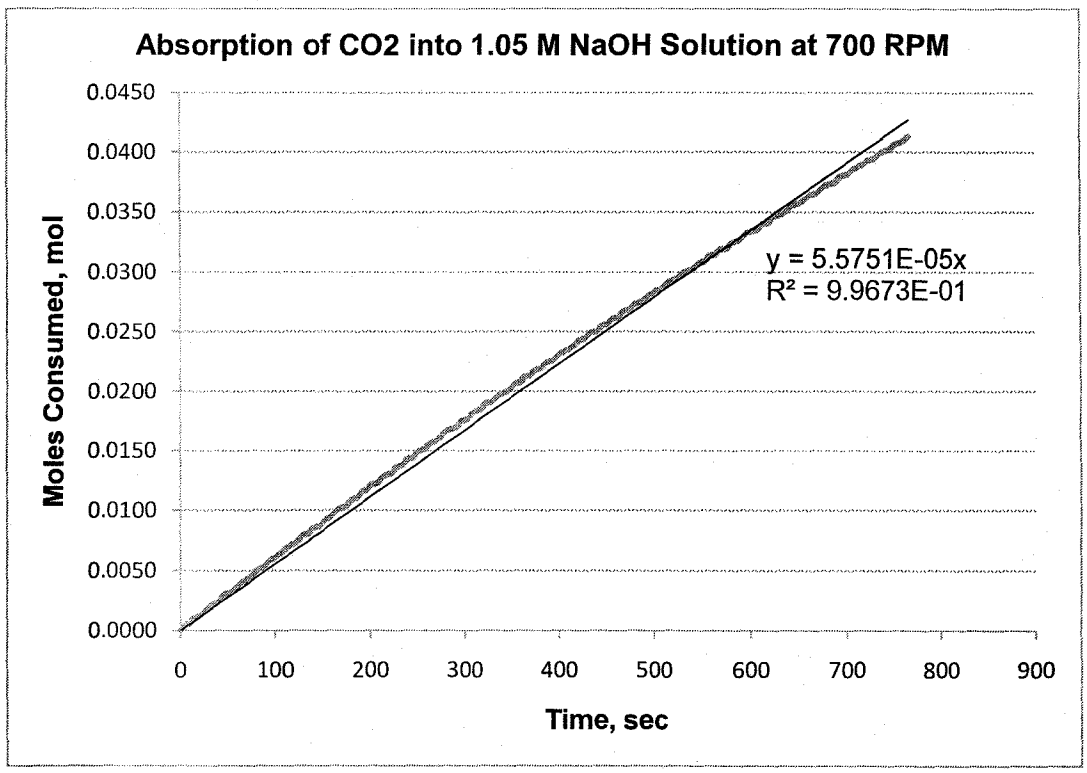

Figure 4.6: Gas consumption rate of CO_2 into 1.05 M NaOH solution at 700 RPM.

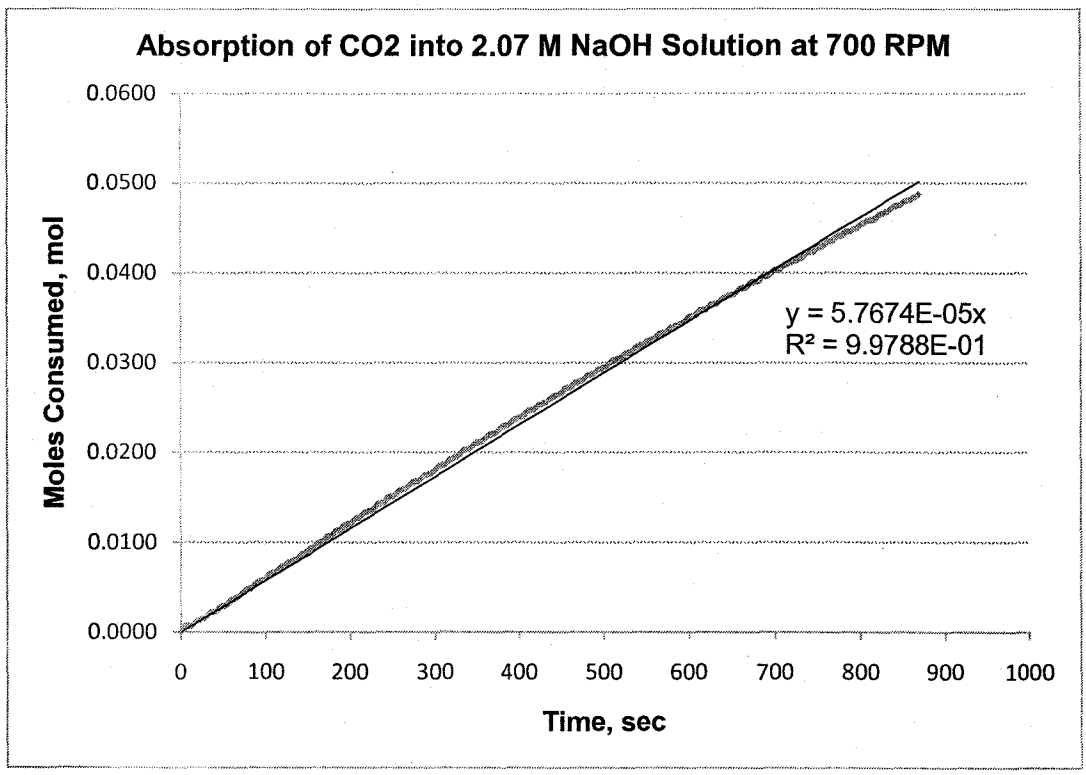

Figure 4.7: Gas consumption rate of CO_2 into 2.07 M NaOH solution at 700 RPM.

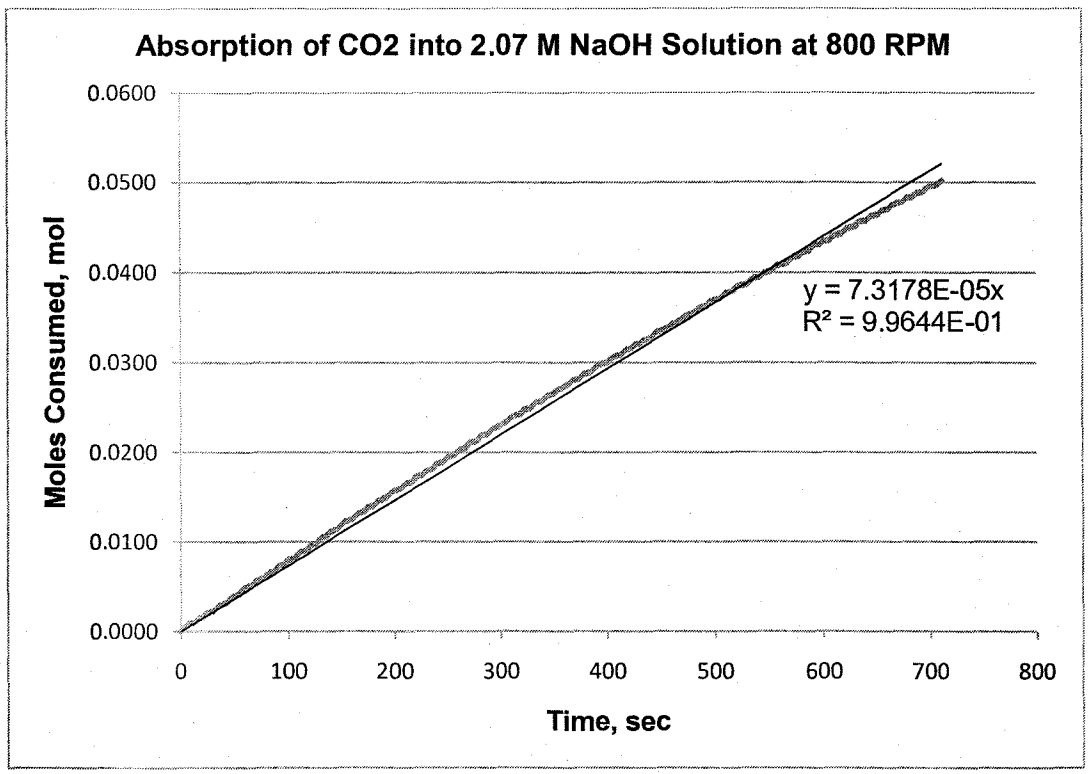

Figure 4.8: Gas consumption rate of CO_2 into 2.07 M NaOH solution at 800 RPM.

CHAPTER FIVE: PARTICLE SIZE MEASUREMENTS WITH FBRM PROBE

5.1 Terminology

The following terminology is presented as a brief sequential outline to the steps of FBRM measurements prior to data processing using FBRM CI software (Mettler-Toledo Lasentec® FBRM C1):

- **Chord Length** is a straight line between any two points on the edge of a particle, as illustrated in Figure 5.2, and sometimes is referred to as optical chord length.

- **Count** is a term used to describe the measure of a single chord. Each count represents a single chord of a given chord length in microns.

- **Channel** is a bin with a specific upper and lower limit in microns. Counts with a chord length between specific limits are put in a specific channel.

- **Primary Chord Length Distribution** is comprised of 1324 channels covering the range from 0 to 1024 μm on a linear scale. The FBRM hardware measures each optical chord length individually then stores the counts of equivalent chord lengths in the appropriate channel. The result is a count by chord length distribution called a primary chord length distribution. This is displayed as a number by micron distribution (number of counts by chord length in microns).

- **Measurement (or Record):** FBRM accumulates counts in a primary chord length distribution for an amount of time specified by the user. Once this time span is completed, the measurement is completed and the primary chord length distribution is passed from the FBRM hardware to the FBRM CI software. At this point, the FBRM hardware will start the next measurement. Once a measurement is saved to a file, it is referred to as a record. The record includes all measured data, as well as all instrument configuration information relating to this measurement.

- **Logarithmic Grouping** is one in which each channel width is progressively wider than the preceding channel width and where the distance between channel midpoints is proportionate to their logarithms. The log grouping provides high resolution on the small particle side of the distribution, while at the same time providing significantly lower resolution (channel averaging effect) on the larger particle side.

- **Linear Grouping** is one in which all channels have equal width. The distance between the channel midpoints is also equal. A linear grouping provides equal resolution throughout the distribution. For a linear channel group, each channel has an equal probability of a count being placed in it.

5.2 Principle of FBRM

The principle of the Mettler-Toledo Lasentec® FBRM is illustrated in Figure 5.1. An infrared laser, with a wavelength of 785 nm, housed in a cylindrical probe, rotates at high velocity propagating into the suspension through a sapphire window on the probe tip. When the beam hits a particle, it gets reflected and back propagates through the sapphire window. The optical signal travels through a fibre-optic cable to the field unit where it is then processed. The instrument gives a particle chord length distribution, which is a function of the true particle diameter distribution. The chord length is simply the distance between any two points on a particle's surface as illustrated in Figure 5.2. The chord length is given by the product of the beam velocity and the measured crossing time of the particle. Chord length counts are summed up in a finite number of chord length intervals, yielding a chord length distribution. The probe can measure particles down to a chord length of 0.5 μm.

5.3 Settings of FBRM to Study Gas Hydrates

The Mettler-Toledo Lasentec® FBRM method has the advantage of its ability to perform *in situ* particle size analysis in real time, without the need for sampling or dilution. It is also a non-destructive method where no change or damage to the measured particles in the system can be noticed. The instrument measures chord length distribution without assuming any particular shape of the particles

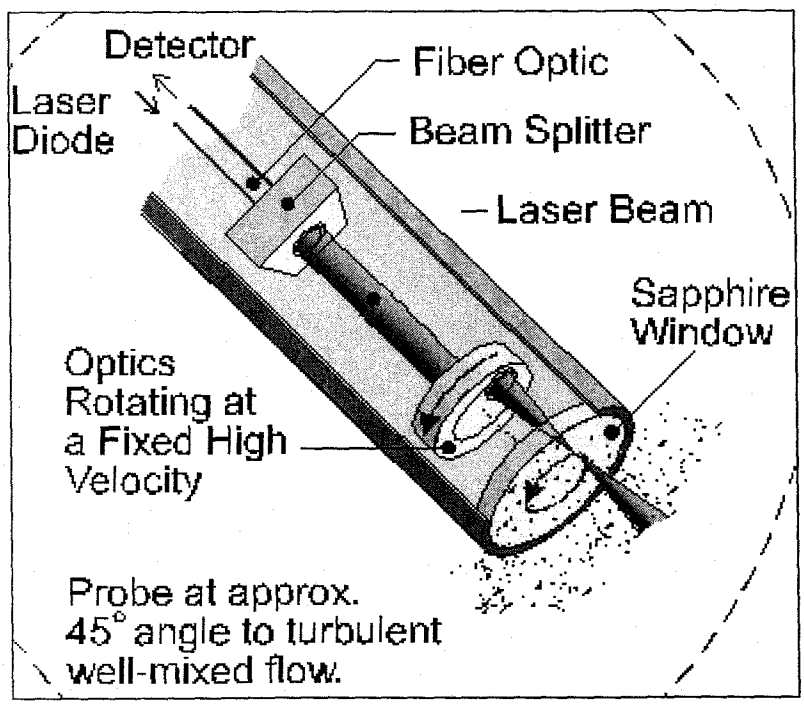

Figure 5.1: Enlarged view of the FBRM probe tip (www.mt.com\Mettler-Toledo Lasentec®).

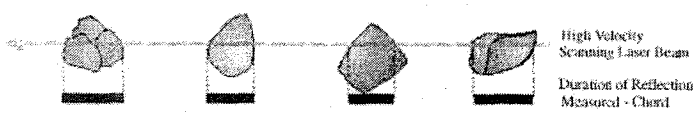

Figure 5.2: Chord length definition (www.mt.com\Mettler-Toledo Lasentec®).

giving the user the flexibility of choosing any shape and then converting the measured chord length to actual particle size utilizing any of the available conversion techniques to the desired particle shape.

Various factors like particles concentration in the sample, agitation rate, electronic settings of the probe (fine or coarse), and focal point position of the laser can affect the chord length distribution of gas hydrate particles in the hydrate sample. The hydrate particles concentration in the sample can be increased significantly at higher magnitude of the operating pressure which is avoided in this study for reasons pertaining to hydrate agglomeration and the high possibility of false turbidity point. Thus, the effect of hydrate particles concentration was not investigated in detail in the present study. The agitation rate was studied and reported in a different section where the optimum stirring rate of 700 rpm would be established. However, in the following sections brief descriptions pertaining to the effect of electronic settings and focal point positions on the chord length distribution of gas hydrate particles are given.

5.3.1 Electronic settings

Data processing of the FBRM detector response depends on both the signal strength and the signal slope. A schematic depiction of the internal signal processing of the FBRM is given in Figure 5.3 (Kail et. al. 2007). The filtering aspect of the backscattered light from a particle is crucial in this signal processing chain. The FBRM probe employed in this work has two different

signal filtering options, i.e., the "fine" and the "coarse" electronics. The difference between these two filter options lies in their cut-off frequency. As can be seen in Figure 5.3, once the laser beam hits the particle, a hypothetical noisy signal is detected (raw signal) caused by different transparencies or spot light reflections on the particle surface. This signal is filtered differently at fine or coarse settings. A triggered signal is then derived to give the measured chord lengths. With the fine electronics option, the filtered signal may fall below the threshold even though the laser still intersects the particle causing so called random chord splitting. The chances of detecting only one chord are higher using the coarse electronics setting. Although the depicted case in this graph favors the coarse over the fine setting, when measuring small particles in dense suspension, the coarse electronics may not be able to resolve single particles. The filtering is stronger using the fine electronics option which makes it favorable for most particle studies. In contrast, the coarse electronics option is required for aggregated particle studies (Heath et al., 2002).

During the early stages of this study, both settings of the FBRM electronics were tested. One conclusion drawn is that the use of fine electronics option is desirable when studying gas hydrates as it is believed that most of the particles in the initial stage of hydrates growth are in the lower side of the particle size distribution, i.e., below 15 μm. When using the coarse electronics setting, no chord lengths lower than approximately 15 μm were detected due to reasons explained above.

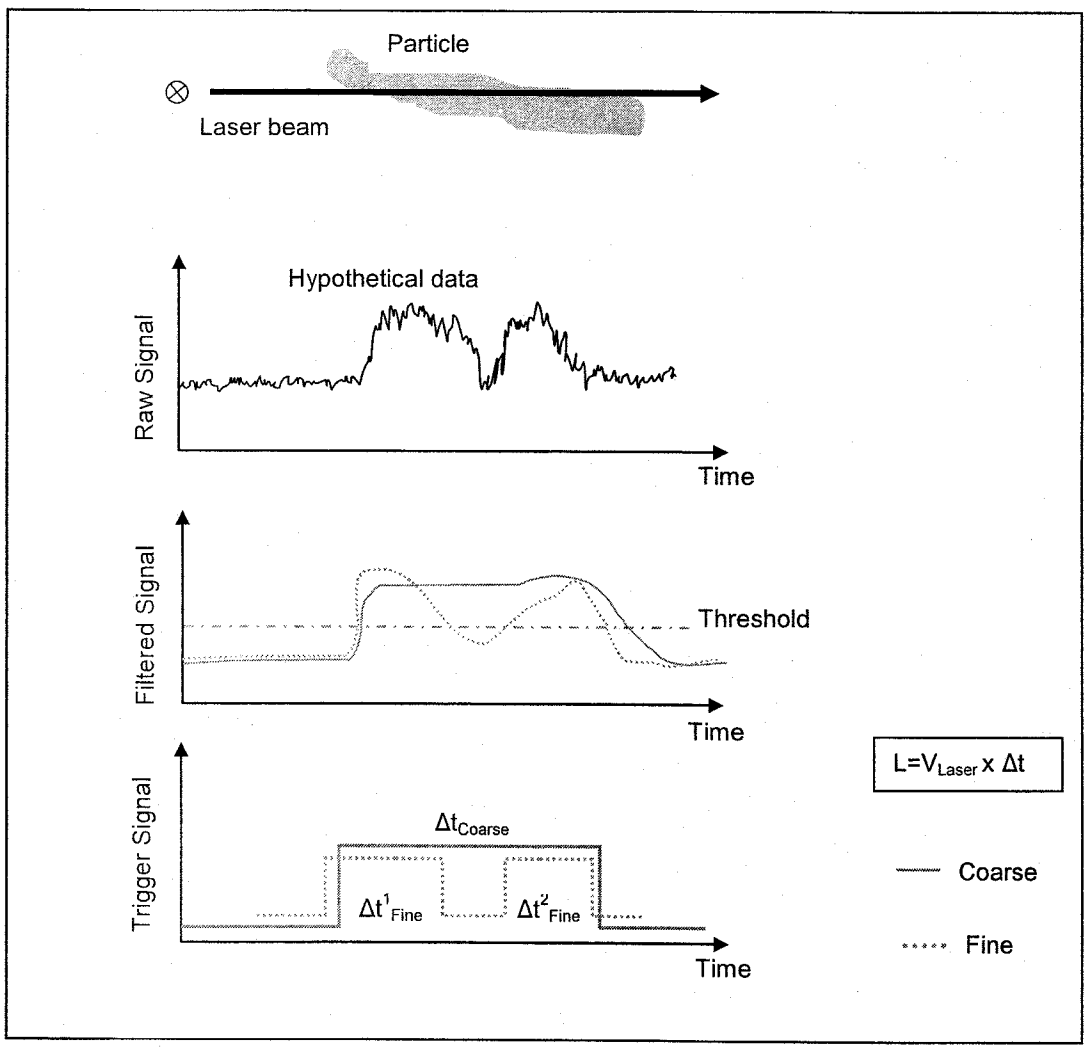

Figure 5.3: Main steps in signal processing chain for hypothetical data (Kail et. al., 2007).

5.3.2 Focal Point Position

The position of the focal point of the laser can be manually adjusted relative to the probe window. Hence, the viewing region can be moved further into the solution (+) or behind the probe window (-) as illustrated in Figure 5.4. The focal point can be set anywhere between -100 μm and +300 μm. The default manufacturer setting is at -20 μm.

According to the operation manual of the FBRM probe, the probe window is considered clean when it measures less than 300 counts per second submerged in distilled water, but for applications that generate less than 1,000 counts per second, much lower counts per second should be obtained for the probe window to be considered clean (Lasentec® D600 Hardware Manual, 2001). The presence of one particle in the viewing range of the probe results in 75 counts per second at the laser scanning speed of 2 m per second.

The growth of hydrate particles during kinetics experiments is indicated by a sudden rise in the number of counts of particles per second. Although the instant of hydrates growth can be detected easily by use of the FBRM probe, the increase in the number of counts per second is not high enough to eliminate the background noise effect (the initial counts of particles per second) on the total counts of particles. Subtraction of the background noise at the onset of hydrates growth is challenging due to oscillation of the counts between neighboring channels. Thus, it is recommended to start with the minimum possible number of counts per second.

During the initial experimental stage, it had been noticed that after any hydrate formation experiment, the background noise (the number of counts of particles per second in distilled water solution) differs from one run to another and rises to a high number in the majority of the cases. Adjustment of the focal point position of the FBRM probe was found to have a significant effect on the number of counts of particles per second. To study this effect, the "dirty" FBRM probe window (after arbitrary hydrate experiment) was utilized to produce different counts of particles per second in different mediums as shown in Figures 5.5 through 5.8. A close examination of these figures indicates that the further away the focal point position from the probe window, the lesser is the number of counts per second. That also shows that the probe window after the hydrate formation process has some fine particles adhering to it even after the decomposition process causing the higher number of counts when positioning the focal point closer to the probe window leading to the need of developing a procedure to clean it without removing the probe from the reactor as will be explained in a subsequent section.

The effect of focal point positioning on the number of counts per second during a hydrate formation experiment was also investigated. It is expected that during hydrate growth, the number of counts per second of smaller particles increases sharply at the early stage then decreases while the larger particles counts per second increases at a later stage. Figures 5.9, 5.10, 5.11, 5.12 show the effect of two different focal position (+10 μm and +300 μm) on the number of counts per

second of different particle size ranges. The conclusion drawn here is that a closer position to the window provides the expected trend of hydrate particles counts. This is in total agreement with what has been reported in the literature (Monnier et al.; 1996, and Law et al., 1997). Both groups observed substantial changes on the number of counts per second with focal position, suggesting that setting the position further into the solution (in the range 0.8 to 2 μm) gave better results for larger particles. However, Heath et al. (2002) suggested that the optimal performance was achieved when the focal point is set closer to the window. Larger particles may possess some difficulty entering the viewing region as the focal point is brought back towards or inside the window. On the other hand, a particle will appear larger when it is far from the focal point (Pons et al. 2006) due to broadening effect of the laser beam.

The manufacturer setting of the focal point as mentioned earlier is at -20 μm. The instrument is calibrated at this setting. A standard sample is provided with the instrument to verify the calibration. Changing the focal point position affects the output of the counts per second as illustrated in Figure 5.13. Higher counts per second are noticed at the +300 μm focal point position. It also affects the statistics of the distribution. Investigations proved that at the manufacturer setting (-20 μm) both the median particle size of the un-weighted distribution and

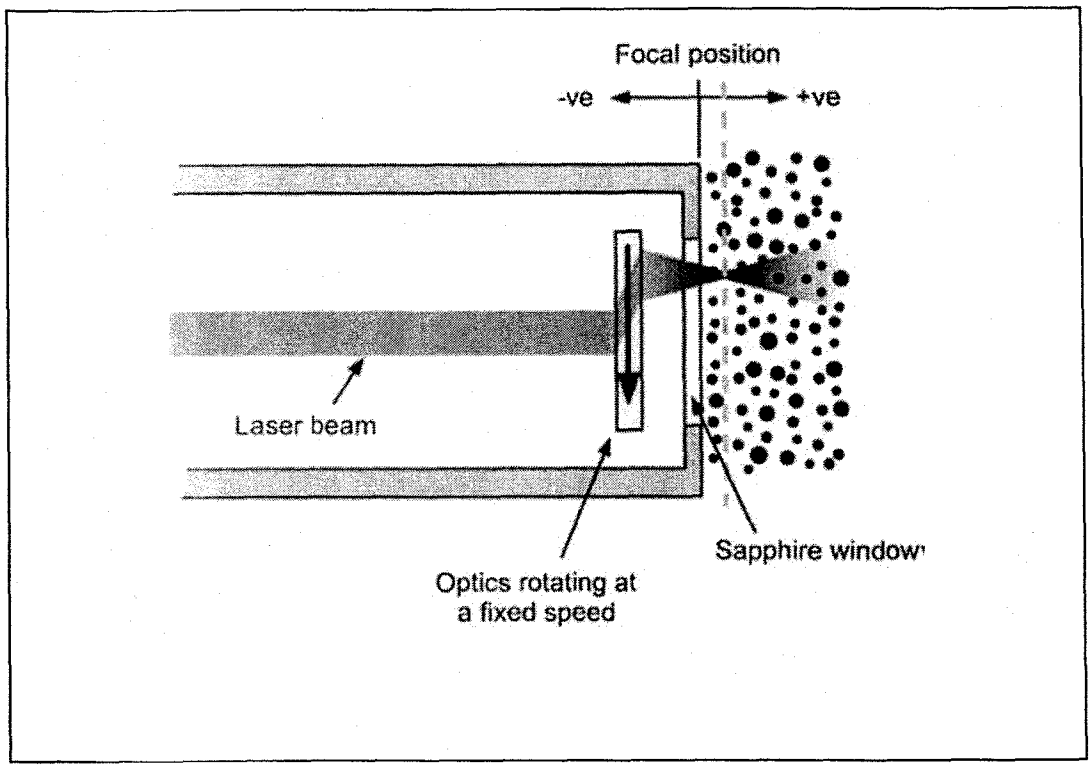

Figure 5.4: **Focal point positioning of the FBRM probe (Heath et al., 2002).**

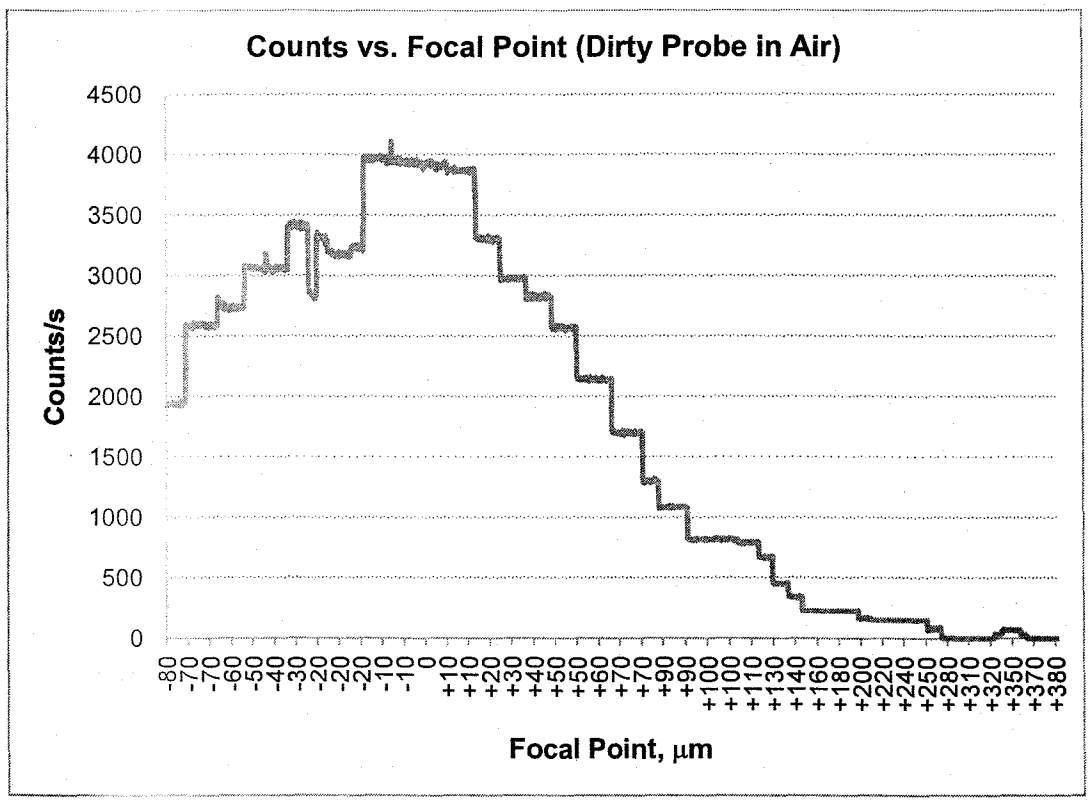

Figure 5.5: Effect of focal point position on the total number of counts/s while the probe window is exposed to air.

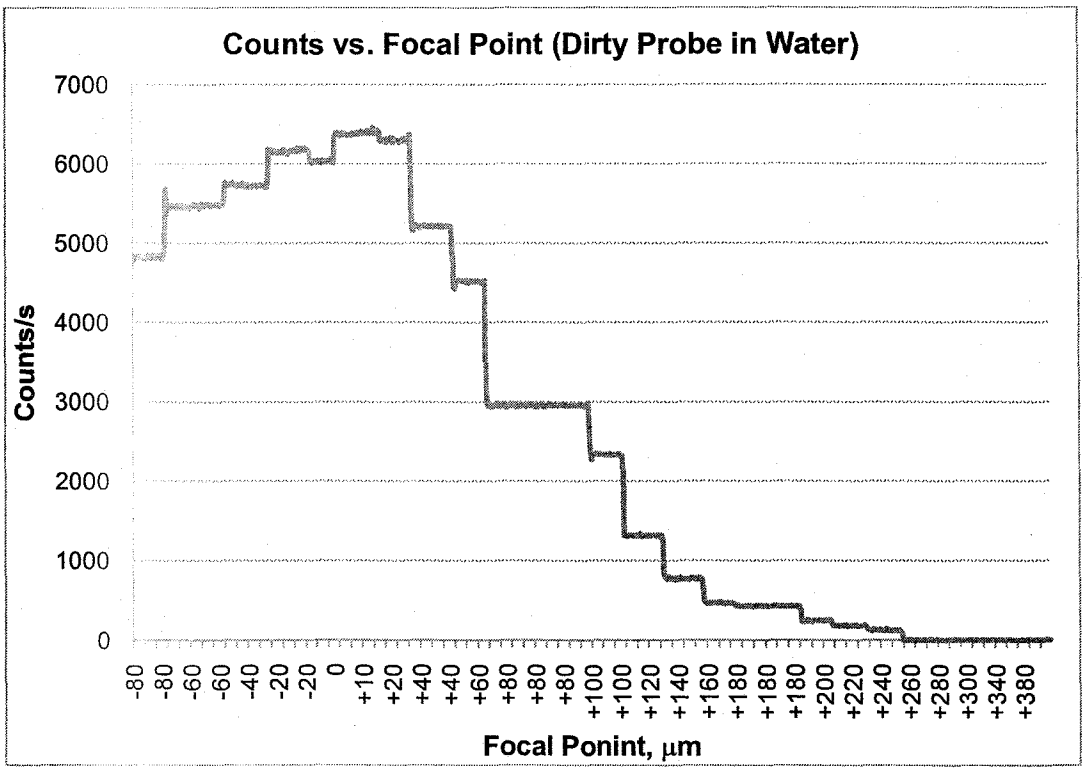

Figure 5.6: Effect of focal point position on the total number of counts/s while the probe window is immersed in distilled water.

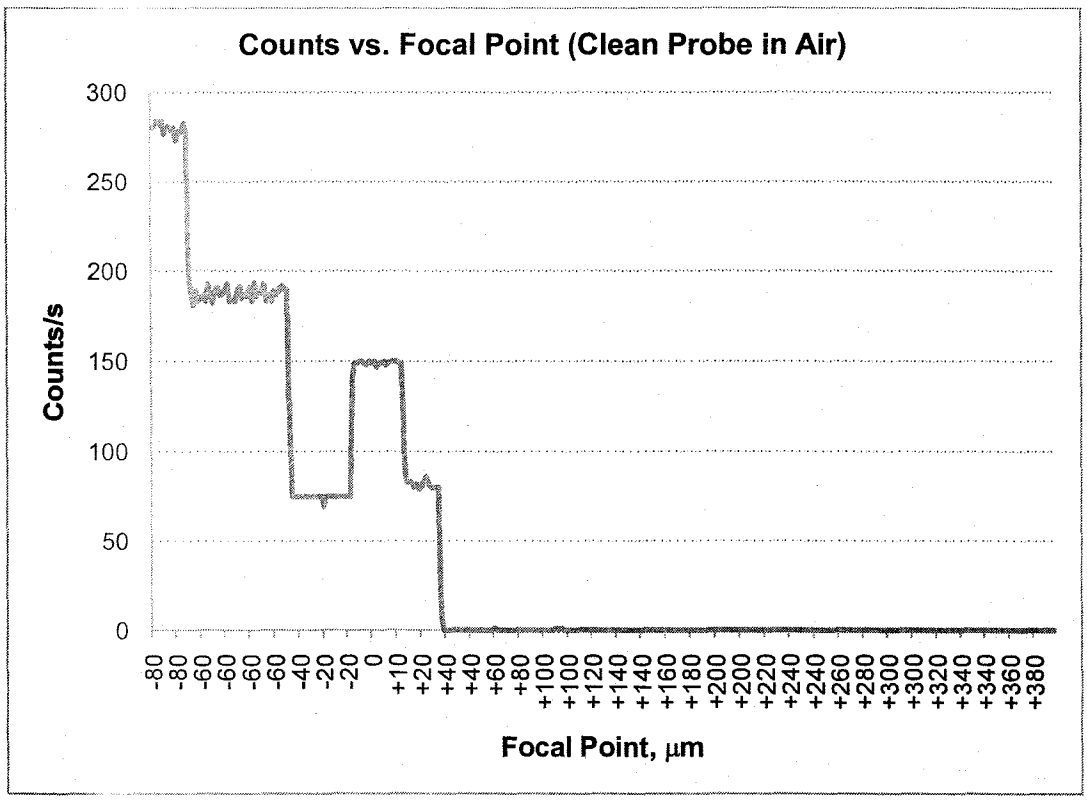

Figure 5.7: Effect of focal point position on the total number of counts/s of a clean probe window in air.

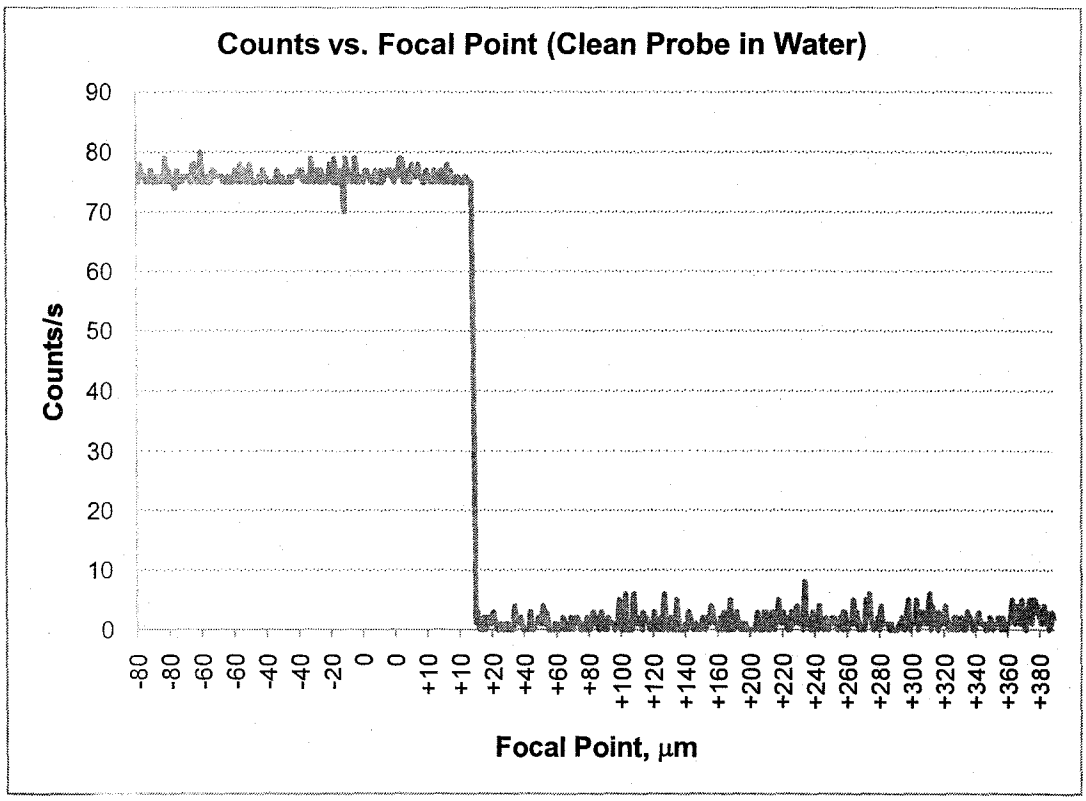

Figure 5.8: Effect of focal point position on the total number of counts/s of a clean probe window in distilled water.

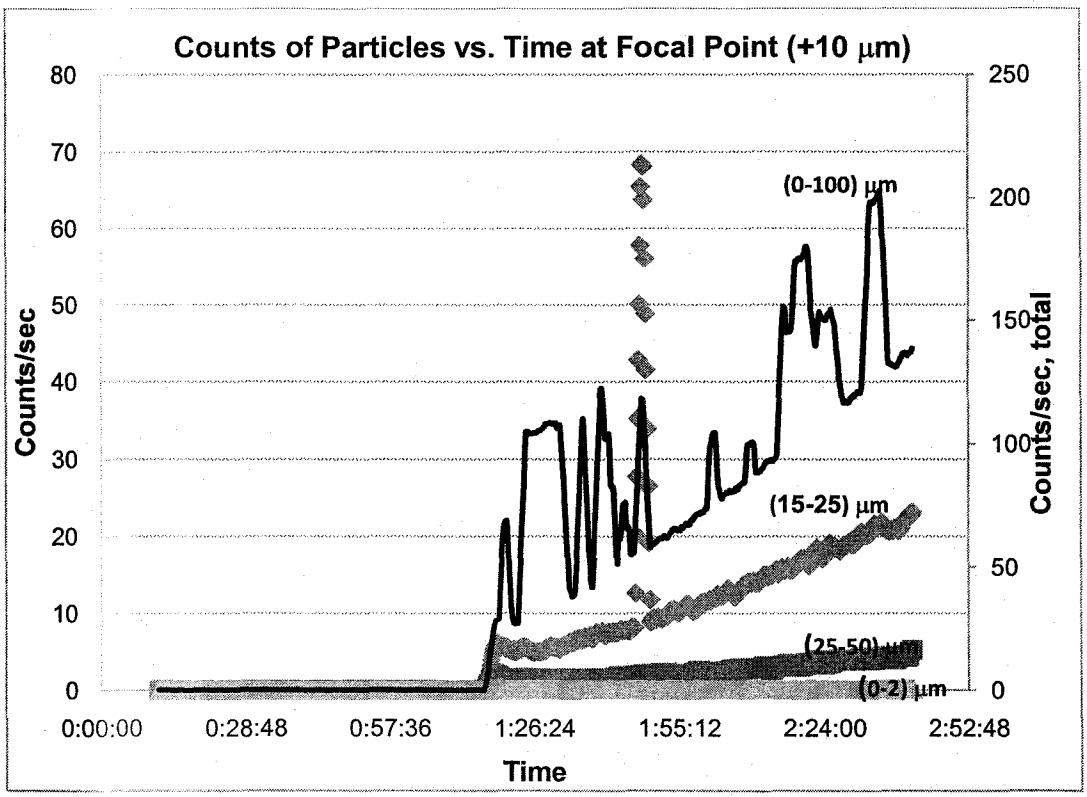

Figure 5.9: Large particles counts and total number of particles of hydrates at +10 μm focal point position.

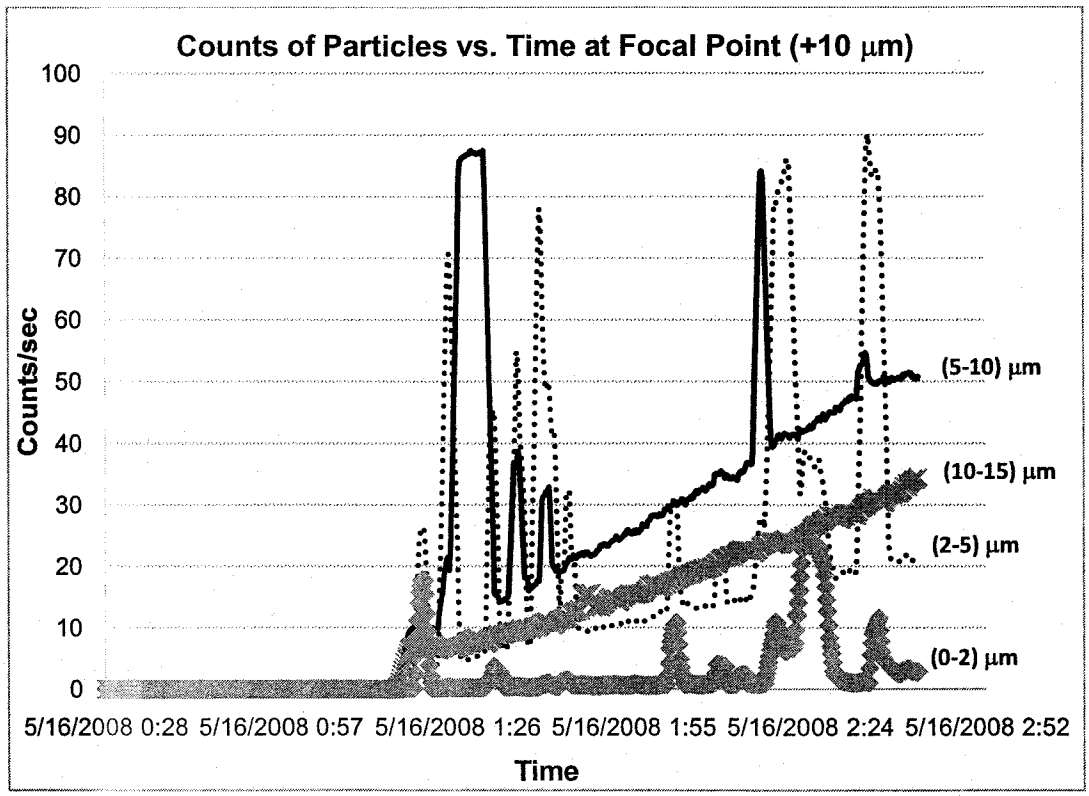

Figure 5.10: Small particles counts and total number of particles of hydrates at +10 μm focal point position.

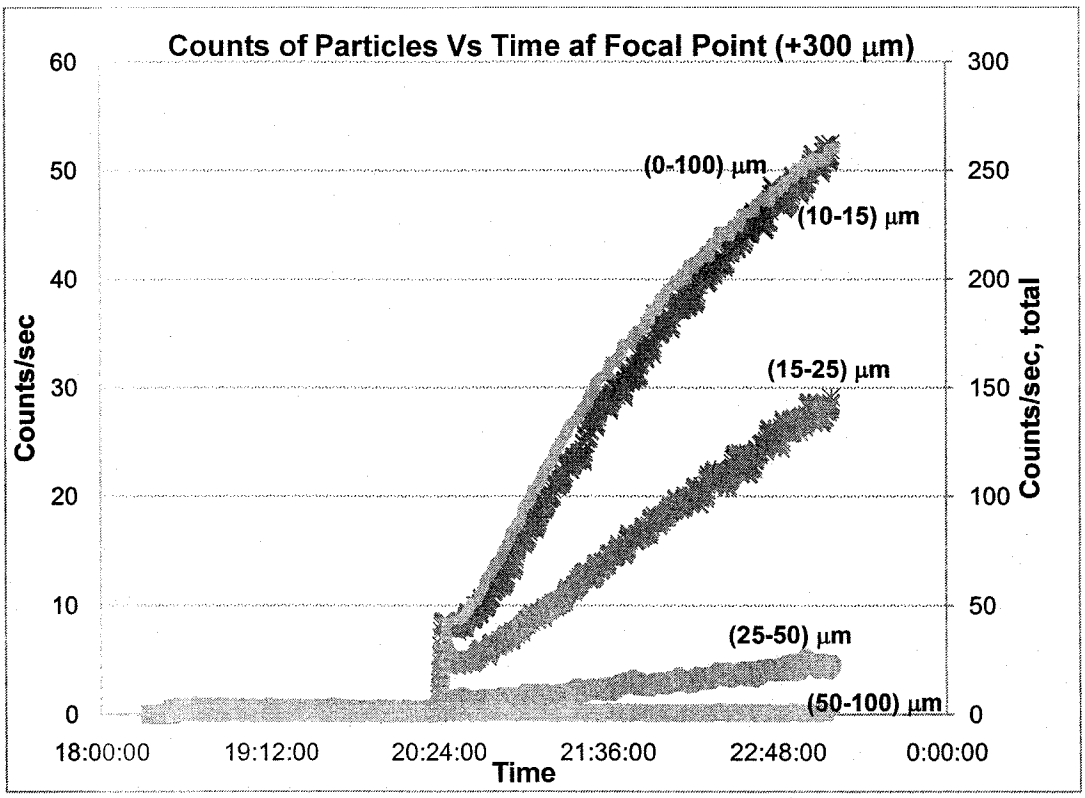

Figure 5.11: Large particles counts and total number of particles of hydrates at +300 μm focal point position.

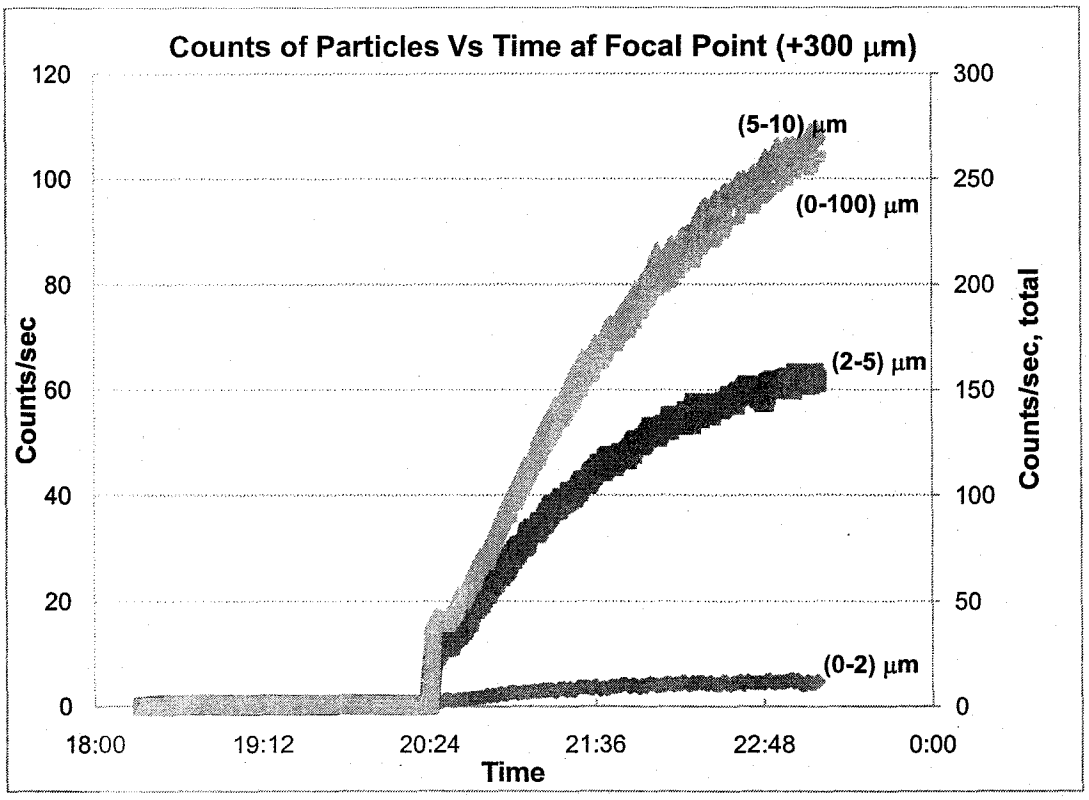

Figure 5.12: Small particles counts and total number of particles of hydrates at +300 μm focal point position.

the mean of the square weighted distribution are within the acceptable limit. In contrast, at the setting of (+300 μm) both statistics have values outside the acceptable limits. Shapes of the distribution of the particles in the standard sample are plotted against the manufacturers data at the two different settings in Figure 5.14 and Figure 5.15. Statistics at both settings and the manufacturer acceptable limits are summarized in Table 5.1.

In view of the above, the optimum focal point position is somewhere closer to the probe window yet external where hydrate particles are in the viewing region of the probe. Thus, the focal point is set at +10 μm for all of the hydrate experiments carried out in this study.

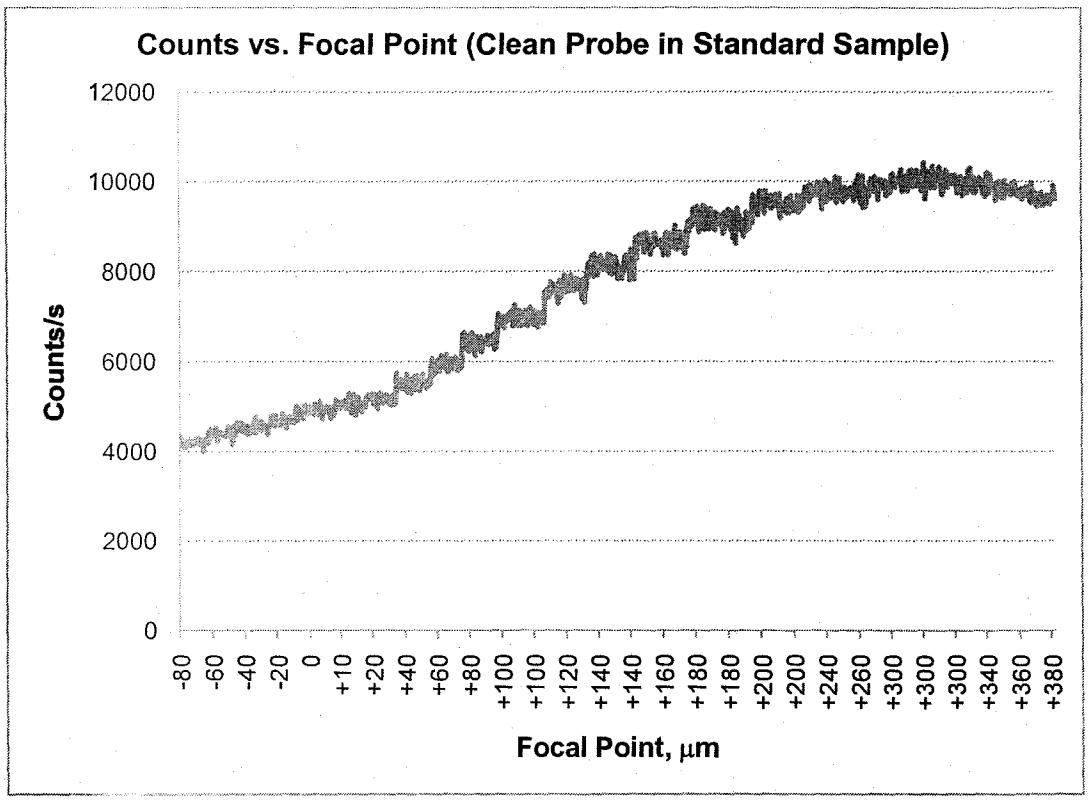

Figure 5.13: Effect of focal point positions on total number of counts of the standard sample particles.

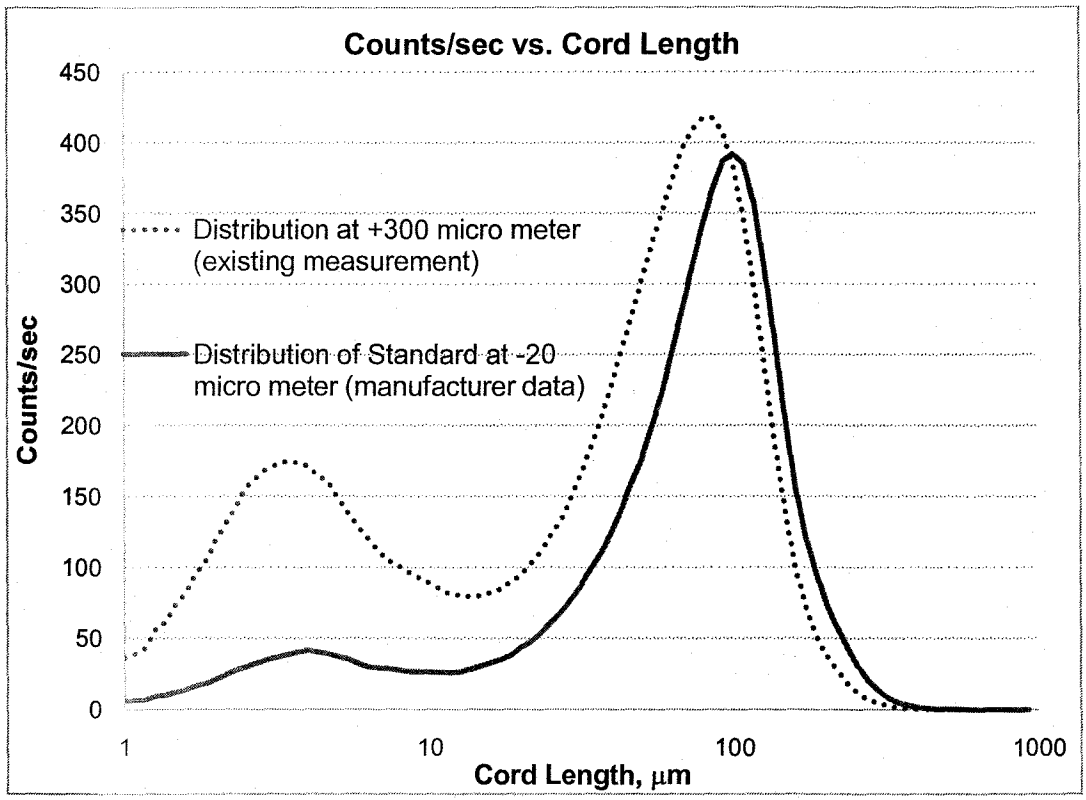

Figure 5.14: Distribution of standard sample at +300 μm and the reference manufacturer distribution at -20 μm.

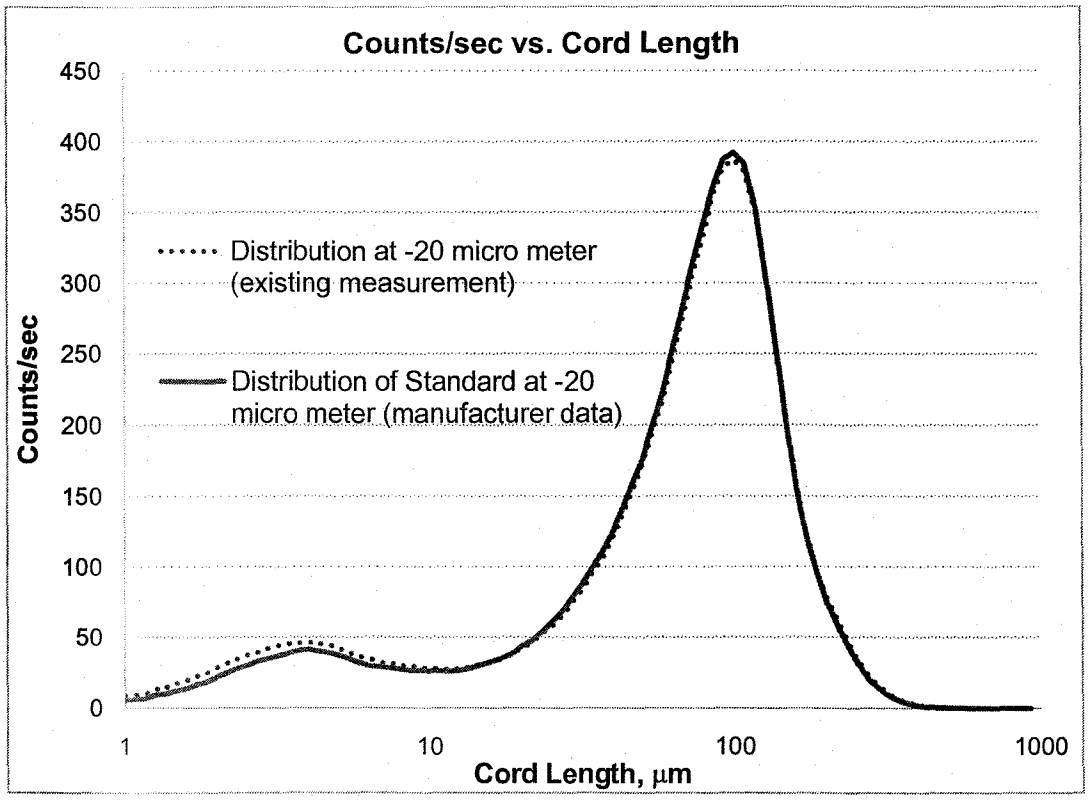

Figure 5.15: Distribution of standard sample at -20 μm and the reference manufacturer distribution at -20 μm.

Statistics	*%Diff. Manufacturer*	*%Diff. at -20 μm*	*%Diff. at +300 μm*
Median, No wt. (1-1000)	±2%	-1.02%	-44.9%
Mean, Sqr. wt. (1-1000)	±3%	-2.08%	-17%

Table 5.1: Statistics at both focal point settings and the manufacturer acceptable difference limits.

5.3.3 Data Collection from FBRM

The Mettler-Toledo Lasentec® FBRM measures and counts chord lengths over time. Therefore, the longer the measurement duration, the larger the sample population for describing the actual chord length population will be. However, that length should not be so long that the resolution of changes in the process over time is in jeopardy. A measurement duration of 10 seconds was found to be desirable in studying gas hydrates. The time averaging was set over 5 consecutive measurements.

5.4 A novel procedure to clean the FBRM probe window

As mentioned earlier, the background noise seems to have an effect on the total number of counts of hydrate particles at the beginning of the growth period. In the majority of experiments where the number of counts prior to hydrates formation is higher than 250 counts per second, a drop in the total number of hydrate particles is noticed at the onset of the hydrate formation, then, the number increases at a later stage. This lead to the conclusion that the high number of counts per second that appear as back ground noise in a clean water solution between hydrate formation experiments is not solely an instrument noise; rather, it is a combination of that and a remaining fine layer of very small gas bubbles left due to hydrates decomposition from a previous run. The probe can be removed from the reactor and cleaned as recommended by the manufacturer. Nonetheless, frequent removal and re-installations of the probe may not be desirable if an alternative procedure can be found. The high number

of counts after hydrate formation and decomposition experiments and the decrease in that number at the onset of a new hydrate growth experiment in the instances of high back ground noise triggered the idea that hydrate formation experiment can be set in a way to clean the probe window without the need to physically remove it. The principle here is simple; the way hydrates are decomposed in the solution affects the cleanness of the probe window. Moreover, it was found that decomposing the hydrate at a very slow rate by decreasing the pressure of the system very slowly while stirring until a clear solution (no bubbles or hydrate particles) is noticed reduces the back ground noise. Thus, after the necessary data of hydrate growth are obtained, the following procedure is adopted to minimize the back ground noise:

1. The stirring should be kept continuous at 700 rpm.
2. The system pressure should be lowered slowly by crack opening the bleed valve (V-7). Excess gas should be released at this point.
3. Continue lowering the system pressure to a point slightly below the three phase equilibrium pressure (H-L-V) at the experimental temperature.
4. Close V-7, and keep stirring.
5. Should the pressure rise above the three phase equilibrium, excess gas is released by slowly opening the bleed valve.
6. Once the solution is clear, the pressure should now be lowered slowly to release the soluble gas from the solution.
7. Now, the water can be flushed out, and fresh water can be introduced to the system.

5.5 Analysis of Chord Length Data from the FBRM Probe

Again, the focused beam reflectance method (FBRM) probe measures the total number of counts of particles per second. It does not make any estimate of the total number of particles per unit volume of the reaction mass. The chord length data generated by the FBRM probe can be reviewed and then exported to an Excel® sheet where further analysis is done. In this study, the linear channel grouping of chords between 0.5 μm and 100 μm was chosen. A Visual Basic code in Macro form is used to analyze the data exported into the Excel sheet. The following are the equations used in the code.

Let: $\bar{C}_i = \frac{average\ counts}{second}$, in the ith channel.

where, $\bar{L}_i$ = chord length, upper boundary of the channel, m

The zeroth moment of the chord length distribution can be calculated from:

$$\mu_0 = \sum_{i=0}^{100} \bar{C}_i \times (\bar{L}_i)^0 \quad (5.1)$$

The first moment of the chord length distribution can be calculated from:

$$\mu_1 = \sum_{i=0}^{100} \bar{C}_i \times (\bar{L}_i)^1 \quad (5.2)$$

The second moment of the chord length distribution can be calculated from:

$$\mu_2 = \sum_{i=0}^{100} \bar{C}_i \times (\bar{L}_i)^2 \quad (5.3)$$

The third moment of the chord length distribution can be calculated from:

$$\mu_3 = \sum_{i=0}^{100} \bar{C}_i \times (\bar{L}_i)^3 \quad (5.4)$$

Since the instrument gives a particle chord length distribution, which is a function of the true particle diameter distribution, a conversion method is needed to obtain the actual particle size. Many researchers have proposed methods to convert chord length distribution to actual particle size distribution (Heath et al., 2002; Hukkanen and Braatz, 2003; Wynn, 2003). For simplicity, it is assumed that the hydrate particles are spherical and the simple conversion method in which chord length can be divided by a factor of 0.791 to estimate the diameter is used (Nollet, 2004; Pons et al., 2006).

To calculate the volume of particles in a given reading, it is assumed that:

i. The particles are spherical, and
ii. The probe sees all the particles in the sampling volume.
iii. No gas bubbles in the readings.

At a given time, the volume of particles is simply the sum of the particles volumes.

Volume of a sphere with a diameter *D*, is given by:

$$V_H = \frac{\pi}{6} \times D^3 \tag{5.5}$$

Thus, the volume of the hydrate particles in the viewing region of the probe can be calculated from:

$$V_H = \frac{\pi}{6} \times \mu_3 \times \left(\frac{1}{0.791}\right)^3 \tag{5.6}$$

Thus, the second moment per unit volume of hydrate:

$$\left(\frac{\mu_2}{V_H}\right)_{Probe\ viewing\ region} = \frac{\mu_2 \times (\frac{1}{0.791})^2}{\frac{\pi}{6} \times \mu_3 \times (\frac{1}{0.791})^3} \quad (5.7)$$

Which can be simplified to:

$$\left(\frac{\mu_2}{V_H}\right)_{Probe\ viewing\ region} = \frac{\mu_2}{\frac{\pi}{6} \times \mu_3 \times (\frac{1}{0.791})} \quad (5.8)$$

Since this only accounts for the sampling volume which lies in the view region of the probe, a modification to the Englezos et al. (1987a,b) model is needed as will be discussed in details in the following chapter.

CHAPTER SIX: INCORPORATION OF THE PARTICLE SIZE DATA MEASUREMENTS IN THE ENGLEZOS ET AL. KENETICS MODEL

6.1 Population balance equations in the model

Solving Equations (2.56) and (2.67) of the Englezos et al. (1987a) model to extract the intrinsic rate constant for hydrate formation, K^*, requires estimation or determination of the second moment of the hydrate particle size distribution as a function of time. With no available particle size measurement tools in the apparatus used in the work of Englezos et al. (1987a) assumptions had to be made regarding the hydrate particle size distribution. In their work, the population balance equations were developed based on Kane et al. (1974) techniques for obtaining kinetics of secondary nucleation of a batch crystallizer. They made the following assumptions to estimate the second moment of the hydrate particles:

a) The initial particle size is the size of the thermodynamically stable nuclei.
b) The total number of nuclei (hydrate particles) is calculated assuming thermodynamically stable nuclei size and super saturation.
c) The number of hydrate particles remains constant as the number of the initially formed nuclei.

In this work, these assumptions are eliminated since the hydrate particle sizes are directly measured *in situ* using the FBRM probe.

6.2 Determination of the second moment of the particle size distribution from FBRM measurements

The FBRM probe only detects particles that come in the viewing region initiating the need to extrapolate that sampling volume to the total number of hydrate particles in the reaction mass (slurry). The sample that the probe can see is assumed to be a representative sample of the hydrate particles. The second moment of the particles per unit volume of the hydrate particles in the sample (in the viewing region of the probe) is calculated from equation 5.8. The second moment term that appears in the original model (Equations 2.56 and 2.77) represents the second moment of all the hydrate particles per unit volume of the hydrate-water slurry. That said, the term from equation 5.8 cannot be used directly in the model without the necessary adjustments.

The volume of hydrate particles in the total reacting mass can be found from the following correlation:

$$V_H = n_H \cdot \frac{M_H}{\rho_H} \tag{6.1}$$

Here: the density, ρ_H, is mass of hydrate (kg) per unit volume of hydrate (m^3), and the molecular weight of hydrate, M_H , is the mass (kg) of hydrate per mole of gas in the hydrate.

For simplicity, let the term in equation 5.8 which represents the second moment of the hydrates in the probe sampling volume equal to B.

$$B = \frac{\mu_2}{m^3} = \frac{\mu_2}{\frac{\pi}{6}\times\mu_3\times(\frac{1}{0.791})} \tag{6.2}$$

The denominator of the right hand side in the above relationship is the volume of the hydrate particles seen by the probe in measuring μ_2.

Now, the second moment of all hydrate particles in the solution per unit volume of the reacting mass can be found from:

$$\mu_{2Total} = \frac{B\times V_H}{V_{slurry}} \tag{6.3}$$

Inserting equation 6.1 into equation 6.3 yields:

$$\mu_{2Total} = \frac{B\times n_H\times M_H}{V_{Slurry}\times\rho_H} \tag{6.4}$$

The second moment term in the Englezos et al. Model (1987a) comes into the picture when finding the analytical solution of equation 2.8 as follow (Chapter 2):

$$f = f_{eq} + \left\{(f_g - f_{eq})\cdot\sinh\left[\gamma\left(1-\frac{y}{y_L}\right)\right] + (f_{gb} - f_{eq})\cdot\sinh\left(\gamma\frac{y}{y_L}\right)\right\}\cdot\left(\frac{1}{\sinh\gamma}\right) \tag{2.45}$$

where:

$$\gamma = y_L\cdot\sqrt{\left(\frac{\pi\cdot K^*\cdot\mu_2}{D^*}\right)} \tag{2.46}$$

Substituting the value of the total second moment from equation 6.4 into 2.46 yields:

$$\gamma = y_L\cdot\sqrt{\frac{\pi\cdot K^*\cdot B\times n_H\times M_H}{D^*\cdot V_{Slurry}\times\rho_H}} \tag{6.5}$$

This is substituted in the following equation (Equation 2.56):

$$\frac{dn}{dt} = \frac{D^* \cdot \gamma \cdot A_{(g-l)}}{y_L \cdot \sinh \gamma} \{(f_g - f_{eq}) \cdot \cosh \gamma - (f_b - f_{eq})\} \quad (2.56)$$

which is the first differential equation to be solved to obtain the intrinsic rate constant. The second moment term also appears in equation (2.67) as follow:

$$\left(\frac{df_b}{dt}\right) = \frac{H \cdot D^* \cdot \gamma \cdot a}{c_{w0} \cdot y_L \cdot \sinh \gamma} \{(f_g - f_{eq}) - (f_b - f_{eq}) \cosh \gamma\} - \frac{\pi \cdot K^* \cdot H \cdot \mu_2}{c_{w0}} (f_b - f_{eq}) \quad (2.67)$$

Inserting equation 6.4 into this equation yields:

$$\left(\frac{df_b}{dt}\right) = \frac{H \cdot D^* \cdot \gamma \cdot a}{c_{w0} \cdot y_L \cdot \sinh \gamma} \{(f_g - f_{eq}) - (f_b - f_{eq}) \cosh \gamma\} - \frac{\pi \cdot K^* \cdot H \cdot B \cdot n_H \cdot M_H}{c_{w0} \cdot V_{slurry} \cdot \rho_H} (f_b - f_{eq}) \quad (6.6)$$

which is the second differential equation to be solved simultaneously with the previous one (Equation 2.56) to obtain the intrinsic rate constant for hydrate formation. The definition of γ is given in Equation 6.5.

6.3 Extension to account for gas hydrates formed from binary gas mixtures

The final sets of equations that describe the kinetics of hydrate formation from gas binary mixtures, for $j = 1,2$,are:

$$\gamma_j = y_L \cdot \sqrt{\frac{\pi \cdot K_j^* \cdot B \cdot n_H \cdot M_{H_{mixture}}}{D^* \cdot V_{Slurry} \cdot \rho_{H_{mixture}}}} \quad (6.7)$$

$$\left(\frac{dn_{H,j}}{dt}\right) = \frac{D^*_j \cdot \gamma_j \cdot A_{(g-l)}}{y_L \cdot \sinh \gamma_j} \left\{(f_g - f_{eq})_j \cosh \gamma_j - (f_b - f_{eq})_j\right\} \quad (6.8)$$

$$\left(\frac{df_{b,j}}{dt}\right) = \frac{H_j \cdot D_j^* \cdot \gamma_j \cdot a}{c_{w0} \cdot y_L \cdot \sinh \gamma} \left\{(f_g - f_{eq})_j - (f_b - f_{eq})_j \cosh \gamma_j\right\} - \frac{\pi \cdot K_j^* \cdot H_j \cdot B \cdot n_H \cdot M_H}{c_{w0} \cdot V_{slurry} \cdot \rho_H} (f_b - f_{eq})_j \quad (6.9)$$

M_H and ρ_H are the molecular weight of the gas hydrate mixture and density of the hydrate mixture respectively.

6.4 Determination of Model Parameters

A summary of all of the parameters needed to solve the two differential equations describing the kinetics of gas hydrates (Equations 2.56 and 6.6, for single gas, Equations 6.8 and 6.9, for gas mixtures) for the only unknown adjustable parameter in the Model, the intrinsic reaction rate constant, K^*, is provided in Table 6.1. Included in the table is the method of computation or the source of each parameter.

6.4.1 Parameters from solubility experiments

The solubility experiments of the different gases at different isotherms were performed to determine the apparent dissolution rate constant, k_La, and Henry's constant, H. For the solubility experiments, the rate of physical absorption of a gas in an agitated liquid is given (Danckwerts, 1970) by:

$$\frac{dn}{dt} = k_L A_{(g-l)}(c^* - c) \qquad (6.10)$$

This equation is derived from the two film mass transfer theory with the following assumptions:

1) the gas film resistance is negligible;
2) there is no accumulation in the liquid film;

3) mass transfer occurs through the liquid film in the direction normal to the interface; and

4) the gas liquid interface is at equilibrium.

where c is the concentration of the gas in the liquid, k_L is the liquid mass transfer coefficient, $A_{(g-l)}$ is the gas-liquid interfacial area and c^* is the equilibrium concentration of the gas in the liquid phase. Assuming the liquid volume remains unchanged, Equation (6.10) may be written as:

$$\frac{dn}{dt} = k_L A_{(g-l)} \left(\frac{n^*-n}{V}\right) = k_L a(n^* - n) \tag{6.11}$$

The above equation can be integrated with respect to time to give:

$$n = n^* - [n^* - n_0][exp(-k_L at)] \tag{6.12}$$

where n_0 is the number of moles of gas dissolved at $t=0$ and n^* is the moles of gas dissolved at equilibrium. In the solubility experiments, the moles of gas consumed at any time $\boldsymbol{t}$ is measured online (using Equation 3.4) thus, the quantities n^* and $k_L a$ can be estimated from the least-squares analysis. The parameters k_L and a cannot be determined simultaneously because they are completely correlated. Henry's constant, H, is calculated from:

$$H = \frac{f_{eq}}{x^*} \tag{6.13}$$

where

$$x^* = \frac{n^*}{n^*+n_{w0}} \tag{6.14}$$

n_{w0} is the initial number of moles of water, which is assumed to remain constant.

Parameter	Method/source
f_g, f_{eq}	Calculated from Trebble-Bishnoi EOS (1987, 1988)
$k_L a$	Determined from solubility experiments.
H	Determined from solubility experiments.
$A_{(g-l)}$	Determined from surface area experiments.
D	Calculated from Wilke and Chang correlation
M_H	Calculated using the method of Clarke and Bishnoi (2001a)
ρ_H	Calculated using a correlation from Sloan (1997).

Table 6.1: Model parameters and their source or computation method.

6.4.2 Molecular mass and Density of Gas Hydrates

The molar mass and density of hydrate depend upon the degree of filling of each cavity by each individual component of the gas mixture forming hydrate. If the fractional occupancy of each cavity by each component of the gas mixture is known, both the molar mass and the density of the hydrate can be determined. From the statistical model of van der Waals and Platteeuw (1959), the equilibrium fractional occupancy of each cavity can be calculated. According to their model, the ratio of the number of molecules of species *k* in cavity *i* to the number of water molecules is given by:

$$\frac{N_{k,i}}{N_w} = y_{k,i} v_i \tag{6.15}$$

where:

$$y_{k,i} = \frac{C_{ki} f_k}{1 + C_{ki} f_k} \tag{6.16}$$

The fugacity, f_k, is the fugacity of the hydrate former at equilibrium, and calculated using the Trebble-Bishnoi equation of state (1987, 1988). The term, C_{ki}, is the Langmuir constant found by using an intermolecular potential function. The Kihara potential is traditionally used with gas hydrates. In equation 6.15, v_i is the number of type "*i*" cavities in unit cell.

Molecular Mass:

Once the fractional occupancy and the number of water molecules in a unit cell are determined, the molar mass can be written as (Clarke and Bishnoi, 2001):

$$M = N_w\left[M_w + \sum_k M_k\left(\sum_i \frac{N_{k,i}}{N_w}\right)\right] \tag{6.17}$$

Density:

Knowing the values for the fractional filling of each cavity, the hydrate density can be calculated based upon a unit cell volume. The hydrate density, based upon a single unit cell, can be written as (Sloan, 1997):

$$\rho = \frac{N_W / N_A M_W + \sum_{k=1}^{C}\sum_{i=1}^{N} y_{k,i} v_i M_k}{V_{cell}} \tag{6.18}$$

6.5 Determination of the K^*

The gas consumption curve for each gas at each isobaric-isothermal conditions during the growth period is the part that is modelled to determine the combined rate constant for hydrate formation, K^*. This combined rate constant is only referred to as intrinsic once the heat and mass transfer resistances around the hydrate particles have been eliminated. From the temperature and pressure measurements, the moles of gas remaining in the gas phase are calculated using the Trebble-Bishnoi equation of state (1987, 1988). At any time *t*, the number of moles of the gas that have been consumed is the difference between the number of moles of the gas that were initially present minus the number of moles of the gas present at time *t*, or:

$$n_H(t) + n_L(t) = n(0) - n(t) \tag{6.19}$$

where $n_H(t)$ is the number of moles of the gas in the hydrate phase at time *t*, $n_L(t)$ is the number of moles of the gas absorbed into the liquid phase, n_0 is the number of moles of the gas initially present in the gas phase (reactor and supply reservoir) before the start of the stirring, and $n(t)$ is the number of moles of the gas in the gas phase (reactor and supply reservoir) at time *t*. Prior to hydrate formation, $n_H(t)$ is zero, thus, all the gas consumed is in the liquid phase. After the turbidity time, the moles of the hydrate former that have gone into the liquid phase, $n_L(t)$, are determined from the measured value of Henry's constant and the three-phase equilibrium fugacity, calculated from the Trebble-Bishnoi equation of state (1987, 1988).

The following least-squares objective function was used to determine the combined rate constant for hydrate formation, K^*:

$$S_{LS} = \sum_{i=1}^{N} \left(n_{exp} - n_{calc}\right)_i^2 \tag{6.20}$$

where the total number of experimental points for each run is (N), the number of moles of hydrate former in the hydrate phase from the experimental data is n_{exp}, and the predicted number of moles of hydrate former in the hydrate phase by the model is n_{calc}. The only unknown parameter in the model is K*, which is the combined rate constant of hydrate formation. The ordinary differential equations

were solved using MatLab® 2008a, with the function ODE15s(), which is an implicit, varying order, solver for stiff differential equations. The optimisation of K^* value is carried out with MatLab® using the fminsearch() function. The second moment as a function of time is supplied into the Model by curve fitting the experimental data from FBRM with MatLab®, using the built-in cubic spline function, spline().

CHAPTER SEVEN: RESULTS AND DISCUSSION

7.1 Optimum Stirring Rate Experiments

In order to determine the intrinsic rate constant of hydrate formation using the kinetic model, the experiments are to be carried under an optimum stirring rate. This optimum stirring rate is defined as the stirring rate at which the heat and mass transfer resistances around the hydrate particles are eliminated and the process of removal of the hydrate particles from the gas-liquid interface into the bulk of solution is satisfactory. Mathematically, at this optimum stirring rate the mass transfer coefficient around the hydrate particle, K_d, in Equation 2.8, is much greater than the intrinsic rate constant for hydrate particle growth reaction, K_r, thus, $K^* \approx K_r$.

A set of experiments were performed using ethane gas at an isothermal-isobaric conditions with the pre-determined surface areas at different stirring rates ranging from 500 to 800 rpm. At each stirring rate, the combined rate constant, K^*, was determined using the procedure described in Section 6.5. The values obtained are plotted in Figure 7.1. The trend shows that at a stirring rate of 700 rpm or greater, the kinetic parameter is no longer affected by further increase in the stirring rate which implies that the mass and heat transfer resistances around the hydrate particles have been eliminated. Therefore, all subsequent solubility and hydrate experiments are carried out at this stirring rate of 700 rpm. At this stirring rate, the value of K^* is equal to the intrinsic rate constant of hydrate formation, K_r.

This stirring rate is much higher than that used by Englezos et al. (1987a) and Clarke and Bishnoi (2005) in their studies because the current apparatus is modified to incorporate the new stirring system. Unlike the previous apparatus used for the kinetics studies the current apparatus does not have any baffle system, thus, the higher optimum stirring rate is justifiable.

7.2 Experiments conducted to extract the intrinsic rate constant for hydrate formation

Gas hydrates formation experiments are conducted at four different isothermal-isobaric conditions for ethane gas, three different isothermal-isobaric conditions for methane gas, three different isothermal-isobaric conditions for propane gas, and at one isothermal-isobaric condition for the equimolar ethane-propane mixture. In general all experiments are conducted between 274 and 282K. The three phase (gas-liquid-hydrate) pressure-temperature equilibrium curve and the dew point pressure-temperature curve determine the suitable operating conditions for each experiment where it is desirable to form hydrate in the region above the three phase equilibrium curve and below the dew point to avoid any gas condensation.

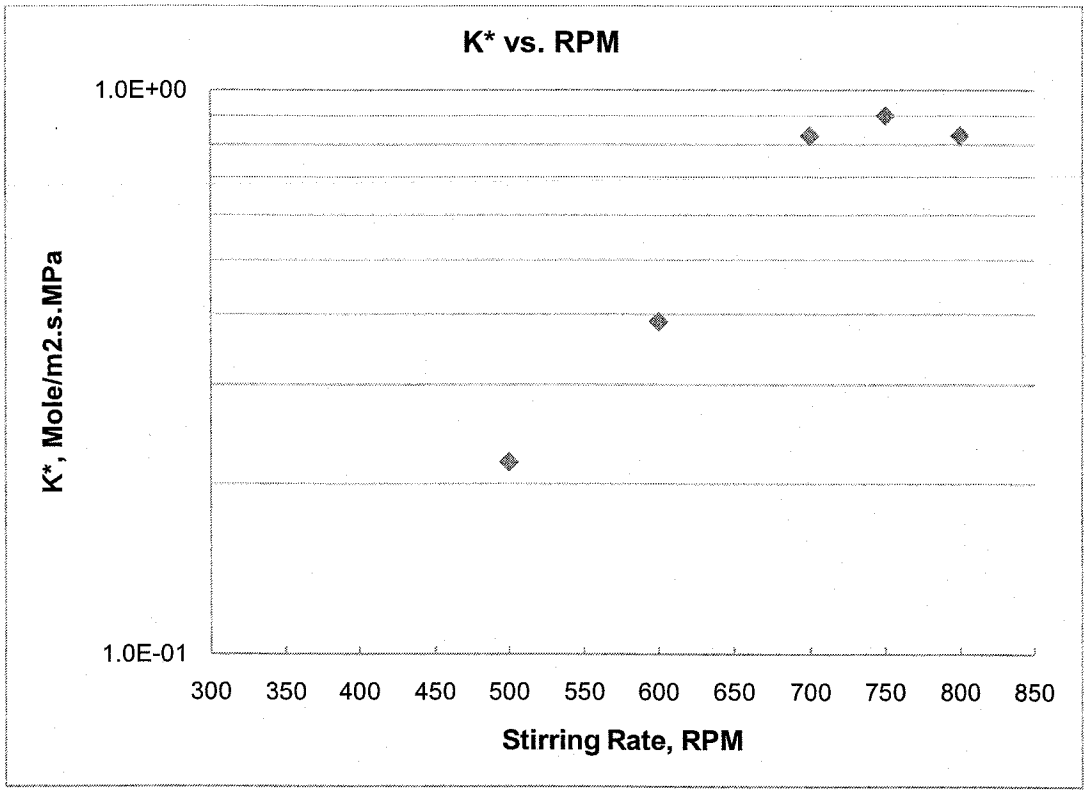

Figure 7.1: Effect of stirring rate on the combined rate constant, *K, of ethane hydrate formation at 276 K and 1.18 MPa.**

7.3 Solubility Experiments

At each isotherm, separate solubility experiments preceded gas hydrate formation experiments to determine the apparent dissolution rate, $k_L a$, and Henry's constant for each gas. The experimental data from the solubility experiments are modelled as explained in Section 6.4.1. Experimental data for ethane, methane, and propane gases are shown in Appendix C.

7.4 Results of hydrate formation experiments

The gas consumption curves for all the gases at the different isotherms in hydrate formation experiments are shown in Appendix D. The trend in all of them is as follow, a sharp increase in the gas consumption is noticed at the beginning of the run. Then it reaches *a plateau* where supersaturation takes place, this region of the curve is also referred to as the nucleation period. Once the induction time ends, the hydrate formation step takes place where a sharp increase in the gas consumption can be seen, this is the growth period of the hydrate particles.

As mentioned earlier, the FBRM probe was used to obtain data on the particle size distribution during each of the hydrate formation experiments. Data obtained by the probe are chord lengths of the hydrate particles. As an illustration, the data obtained during one of the experiments of methane hydrate formation are shown in Appendix E. These figures represent the cord length distribution of hydrate particles at the turbidity point, about 5 and 10 minutes after the turbidity point. It is noted that the scale of the y-axis is different in these

plots. It can be seen from the three different sampling intervals of the chord length distribution shown in these figures that as the hydrate particles grow the number of counts of chords in the next size chords increases. The data for all the experiments that were carried out exhibit the same behaviour as that shown in the figures in Appendix E.

7.4.1 Intrinsic rate constant for ethane hydrate formation in Structure I

Experiments for ethane gas hydrate formation were carried out at temperatures ranging from 274 to 282 K and pressures ranging from 0.99 to 1.6 MPa to determine the intrinsic rate constant of ethane hydrate formation at each isotherm. The results are shown in Figures 7.2 through 7.5. In these figures, the points are the experimental data points and the solid lines are the computed values from the Model. The predicted values by the model seem to fit the experimental data well. The regressed intrinsic rate constants for each isotherm are tabulated in Table 7.1. These values are four orders of magnitude higher than those reported by Englezos et al. (1987a) without removing the inconsistency resulting from representing the particle size by its radius rather than its diameter (see Table 7.2). This implies that the measured surface area of all hydrate particles is less than what was estimated by Englezos et al. (1987a). For the sake of comparison, one run of ethane gas hydrate formation at 274 K, was analysed following the same procedure that was used by Englezos et al. (1987a) without incorporating the actual particle size measurements carried out herein. The intrinsic rate constant thus obtained is close to the value obtained by

Englezos et al. (1987a) shown in Table 7.2. The fit of the experimental data is shown in Figure 7.6. This finding leads to the conclusion that the kinetic growth rate model (Equation 2.10) represents the intrinsic hydrate growth phenomenon well. Thus, the rate constants obtained in the present study are true intrinsic rate constants which are independent of the hydrodynamics and geometry of the equipment.

It is worth noting that the intrinsic rate constants of ethane hydrate formation determined herein have the same order of magnitude as of those determined in the work of Sharma (1996) which are given in Table 7.3. The intrinsic rate constants determined in the current study are, however, slightly higher than those reported by Sharma (1996). The measured surface area by Sharma (1996) are likely larger because the particle size measurements by Sharma (1996) were conducted outside the reactor in a sampling loop where breakage of particles could possibly occur. Hence, the higher values of the intrinsic rate constants obtained in the present study are justifiable.

The intrinsic rate constants determined in this work using particle size analyzer do not show a strong dependence on the temperature within the temperature range specified.

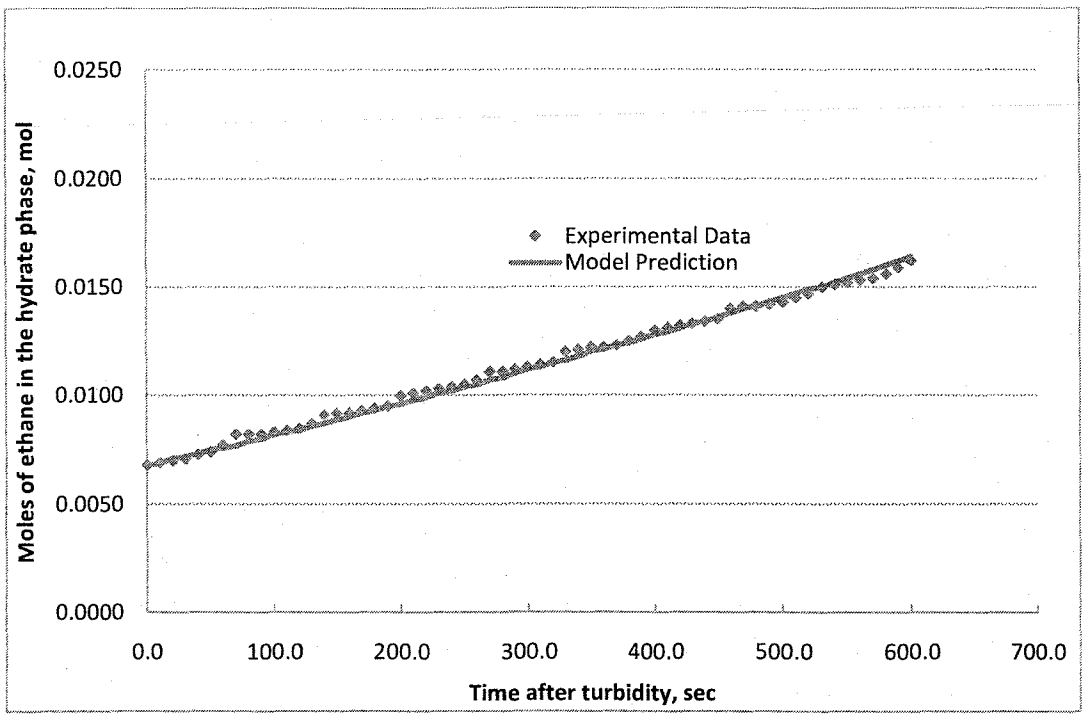

Figure 7.2: Number of moles of ethane in the hydrate phase during hydrate formation at 274 K and 0.99 MPa.

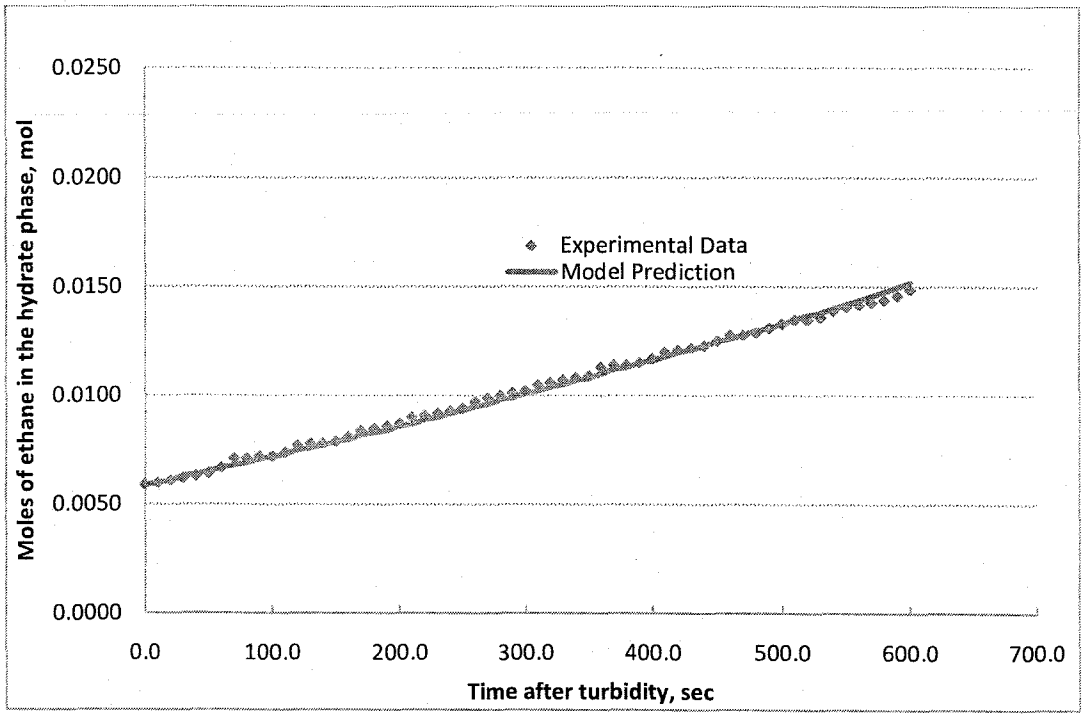

Figure 7.3: Number of moles of ethane in the hydrate phase during hydrate formation at 276 K and 1.08 MPa.

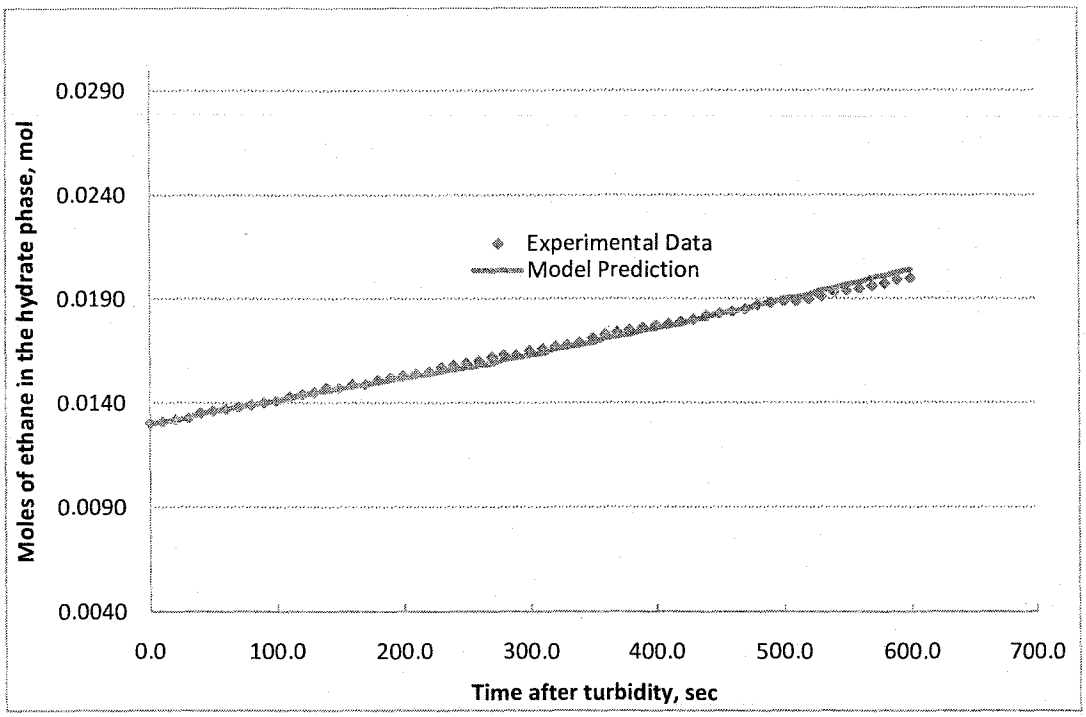

Figure 7.4: Number of moles of ethane in the hydrate phase during hydrate formation at 279 K and 1.34 MPa.

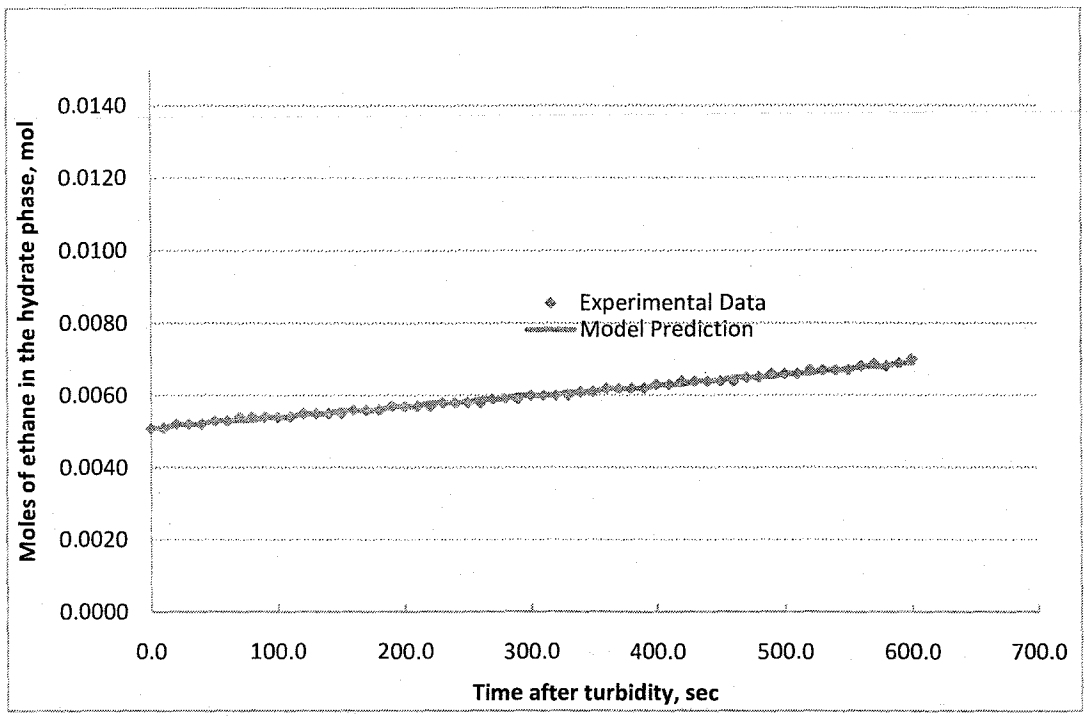

Figure 7.5: Number of moles of ethane in the hydrate phase during hydrate formation 282 K and 1.59 MPa.

Temperature, K	K^*, mol/(m^2.MPa.s)
274	0.9987
276	1.071
279	0.7944
282	0.9467

Table 7.1: Intrinsic rate constant of ethane hydrate formation in structure I determined in this work using PSA,$(K^* \approx K_r)$.

Temperature, *K*	K* , mol/(m^2.MPa.s)
274	0.12×10^{-4}
276	0.11×10^{-4}
279	0.13×10^{-4}
282	0.14×10^{-4}

Table 7.2: Intrinsic rate constant of ethane hydrate formation in structure I from Englezos et al. (1987a).

Temperature, K	K^* , mol/(m^2.MPa.s)
274	0.21
276	0.17
279	0.24

Table 7.3: Intrinsic rate constant of ethane hydrate formation in structure I determined by Sharma (1996).

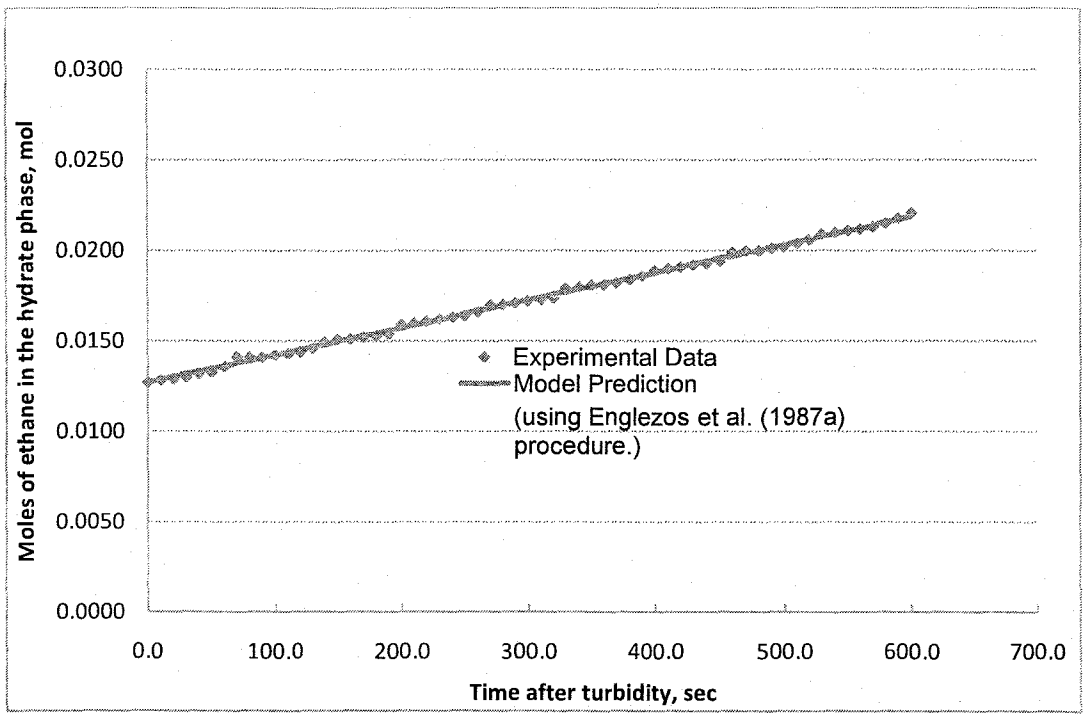

Figure 7.6: Number of moles of ethane in the hydrate phase during hydrate formation at 274 K and 0.99 MPa.

7.4.2 Intrinsic rate constant for methane hydrate formation in Structure I

Ultra pure methane gas (99.97 mol%) was used to perform hydrate formation experiments at temperatures ranging from 276 to 282 K and pressures ranging from 3.2 MPa to 7.3 MPa to determine the intrinsic rate constant of methane hydrate formation at each temperature. The predicted values by the model matched the experimental data well as illustrated in Figures 7.7 through 7.9. The regressed intrinsic rate constants for each temperature are given in Table 7.4. The intrinsic rate constants for methane hydrate formation determined by Englezos et al. without particle size measurements are shown in Table 7.5 and those by Sharma (1996) with particle size measurements are shown in Table 7.6. The determined rate constants from this study compare favourably with those reported by Sharma (1996).

Again, one methane hydrate run was analysed following the same procedure that was used by Englezos et al. (1987a) without incorporating the actual particle size measurements carried out herein, and the same intrinsic rate constant was reproduced. Thus, the rate constants obtained in the present study are true intrinsic rate constants which are independent of the hydrodynamics and geometry of the equipment. The model prediction and the experimental data for this part are depicted in Figure 7.10.

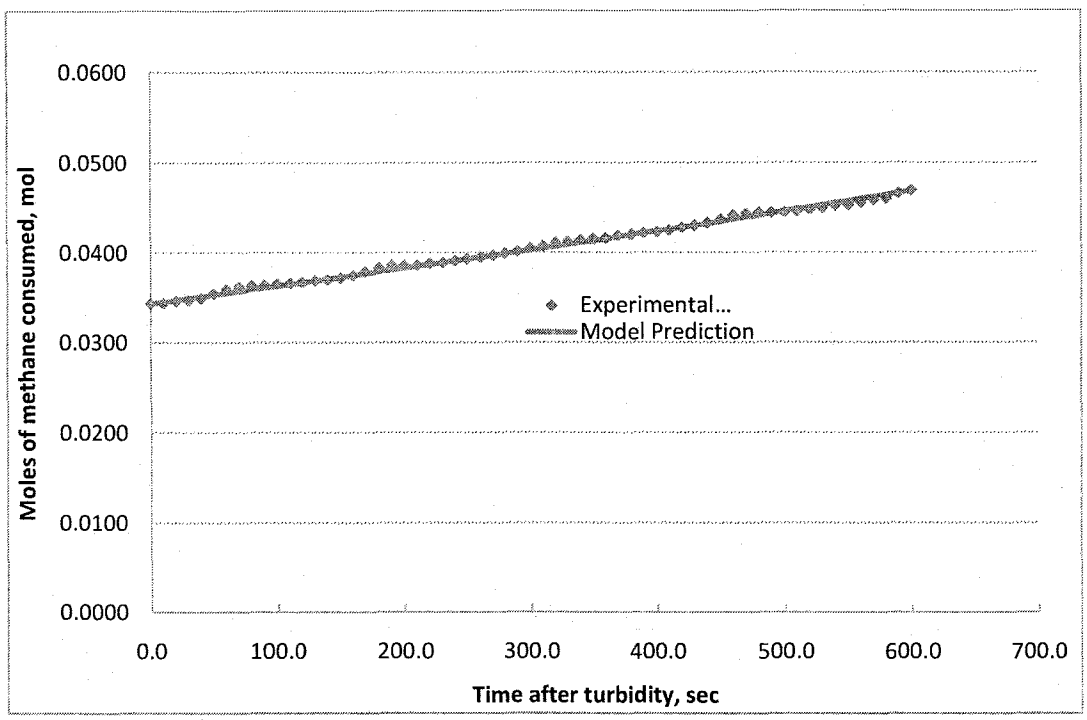

Figure 7.7: Number of moles of methane in the hydrate phase during hydrate formation at 276 K and 4.65 MPa.

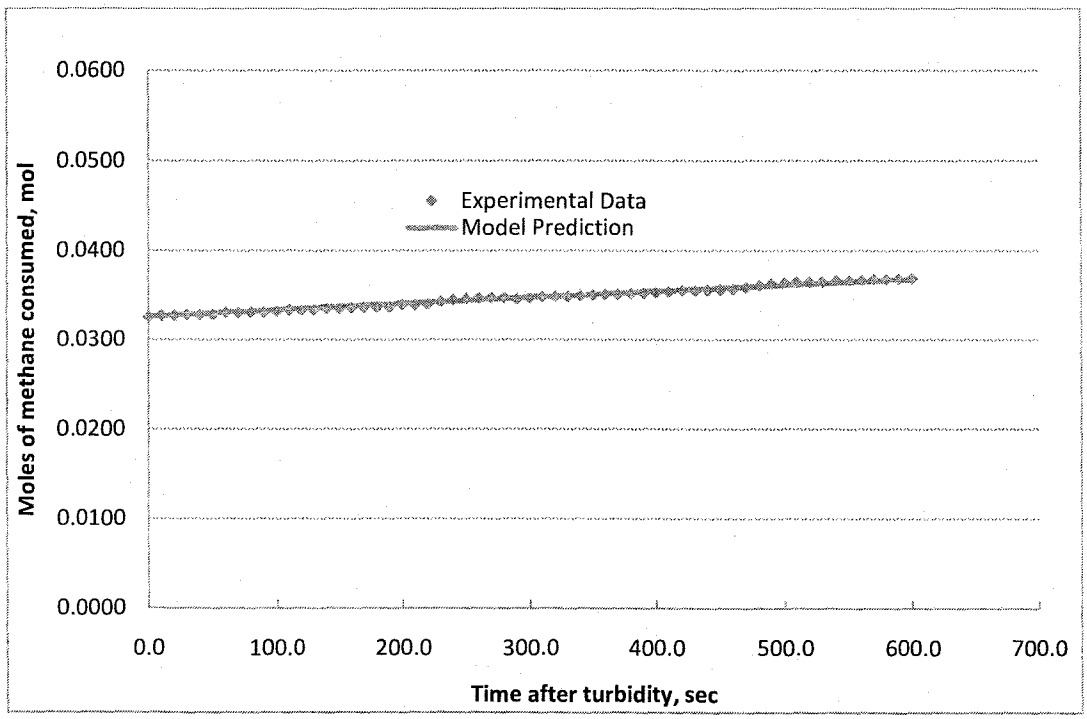

Figure 7.8: Number of moles of methane in the hydrate phase during hydrate formation at 279K and 5.16 MPa.

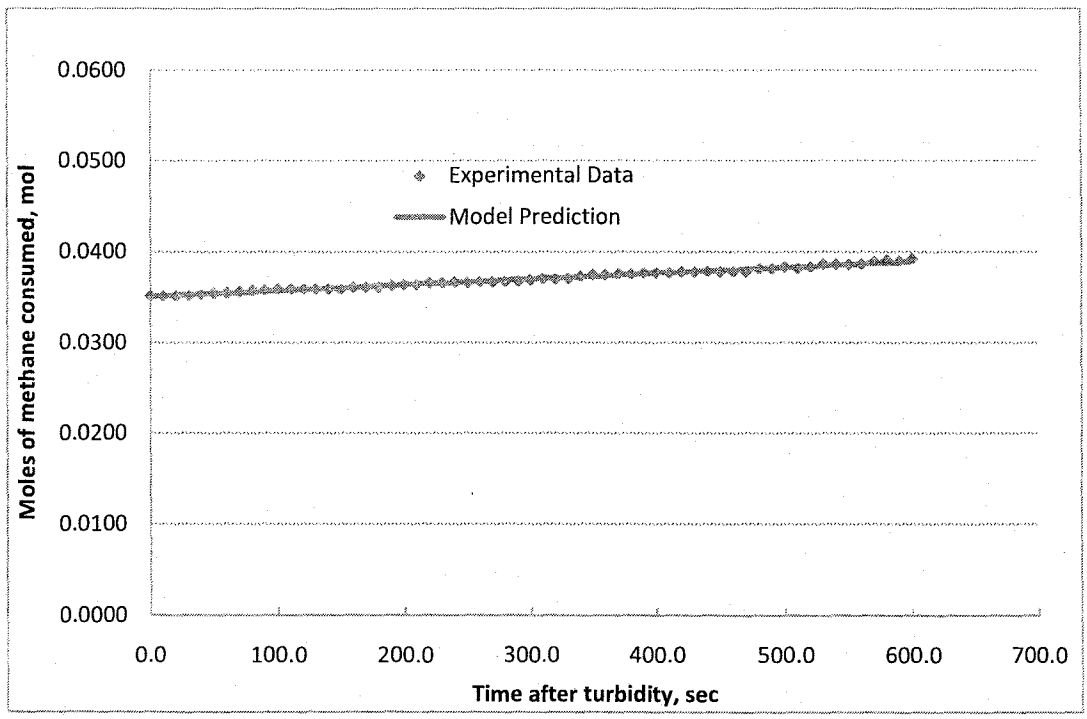

Figure 7.9: Number of moles of methane in the hydrate phase during hydrate formation at 282 K and 7.25 MPa.

Temperature, *K*	K* , mol/(m^2.MPa.s)
276	0.0654
279	0.0812
282	0.0603

Table 7.4: Intrinsic rate constant of methane hydrate formation in structure I determined in this work using PSA,$(K^* \approx K_r)$.

Temperature, K	K^* , mol/(m^2.MPa.s)
274	0.65×10^{-5}
276	0.55×10^{-5}
279	0.57×10^{-5}
282	0.58×10^{-5}

Table 7.5: Intrinsic rate constant of methane hydrate formation in structure I from Englezos et al. (1987a).

Temperature, K	K^* , mol/(m^2.MPa.s)
274	0.06
276	0.10
278	0.18

Table 7.6: Intrinsic rate constant of methane hydrate formation in structure I determined by Sharma (1996).

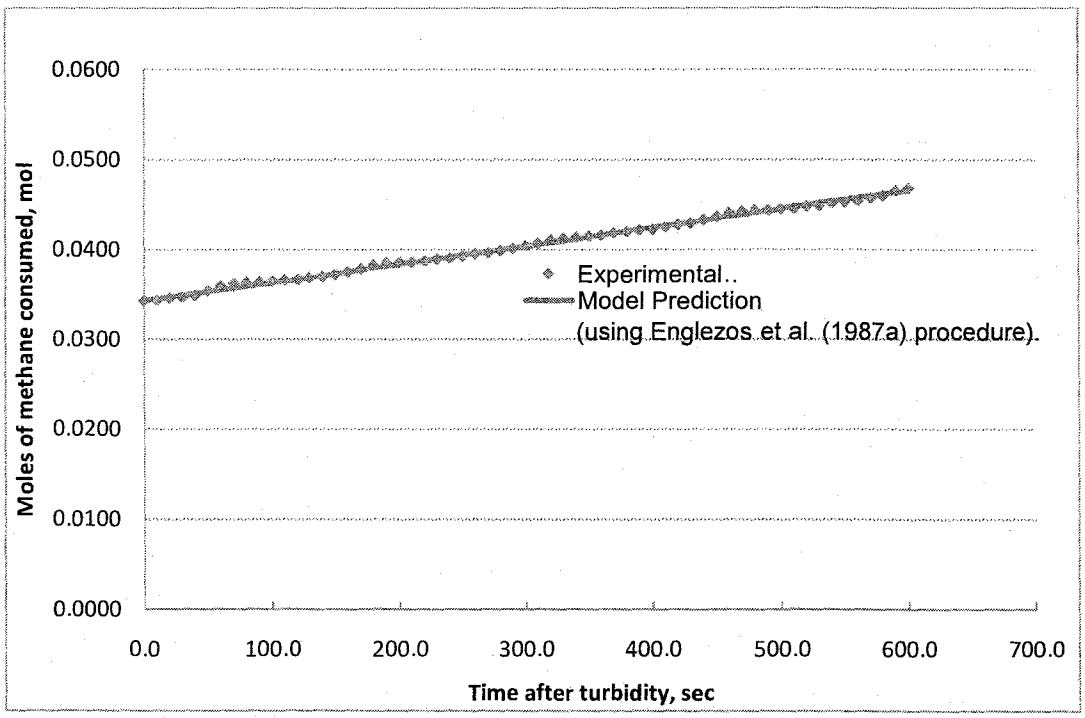

Figure 7.10: Number of moles of methane in the hydrate phase during hydrate formation at 276 K and 4.6 MPa.

7.4.3 Intrinsic rate constant for propane hydrate formation in Structure II

Experiments for propane (99.5 purity) gas hydrate formation were carried out at temperatures ranging from 274 to 276 K and pressures ranging from 0.39 to 0.43 MPa to determine the intrinsic rate constant of propane hydrate formation at each temperature. The results are shown in Figures 7.11 through 7.13. In these figures, the points are the experimental data points and the solid lines are the computed values from the Model. The predicted values by the model fit the experimental data well. The regressed intrinsic rate constants for each temperature are tabulated in Table 7.7.

The intrinsic rate constants for propane also do not show a strong dependence on temperature. It is worth noting that the value of the intrinsic rate constant of propane hydrate formation (structure II) is approximately half that of the ethane hydrate formation (structure I).

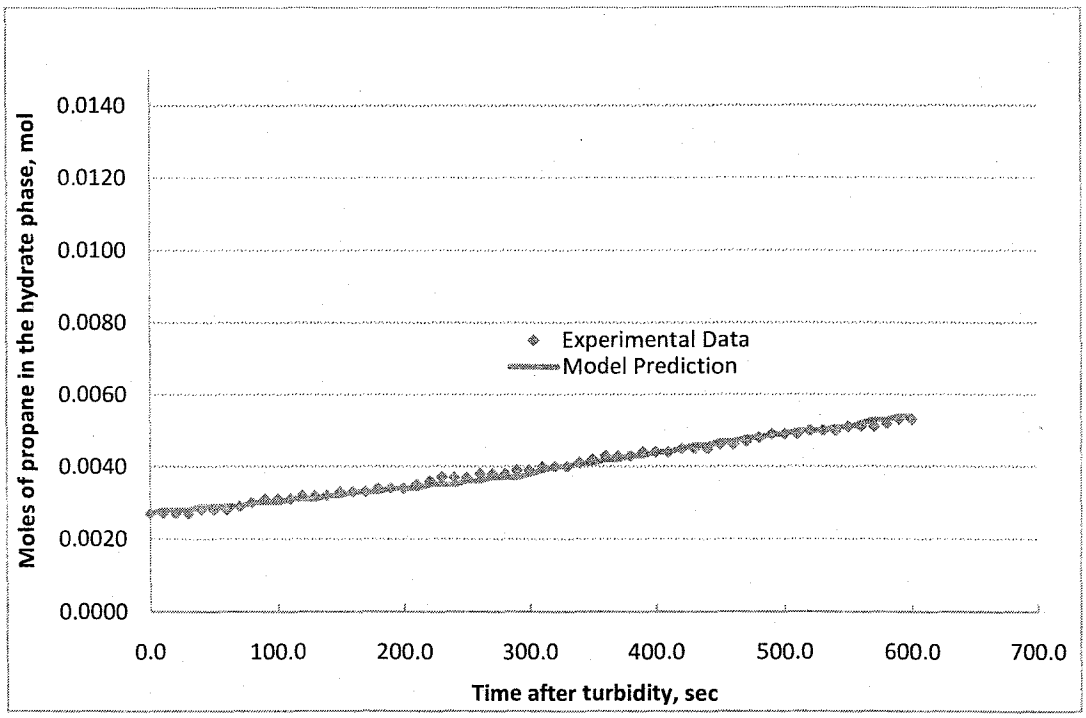

Figure 7.11: Number of moles of propane in the hydrate phase during hydrate formation 274 K and 0.39 MPa.

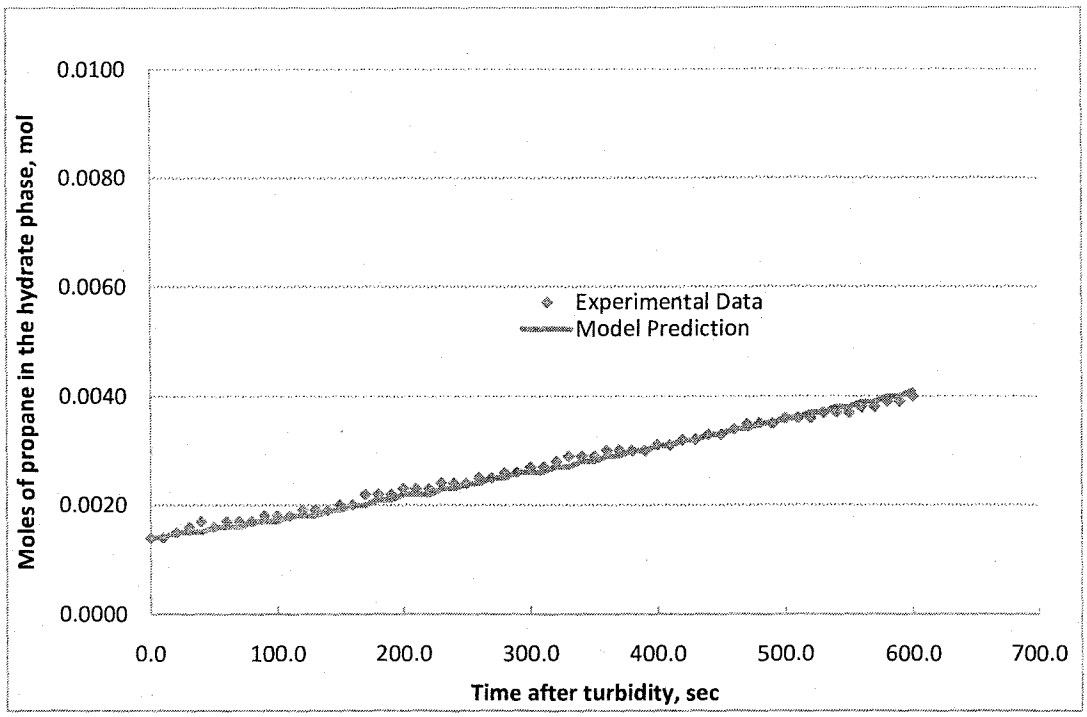

Figure 7.12: Number of moles of propane in the hydrate phase during hydrate formation 275 K and 0.43 MPa.

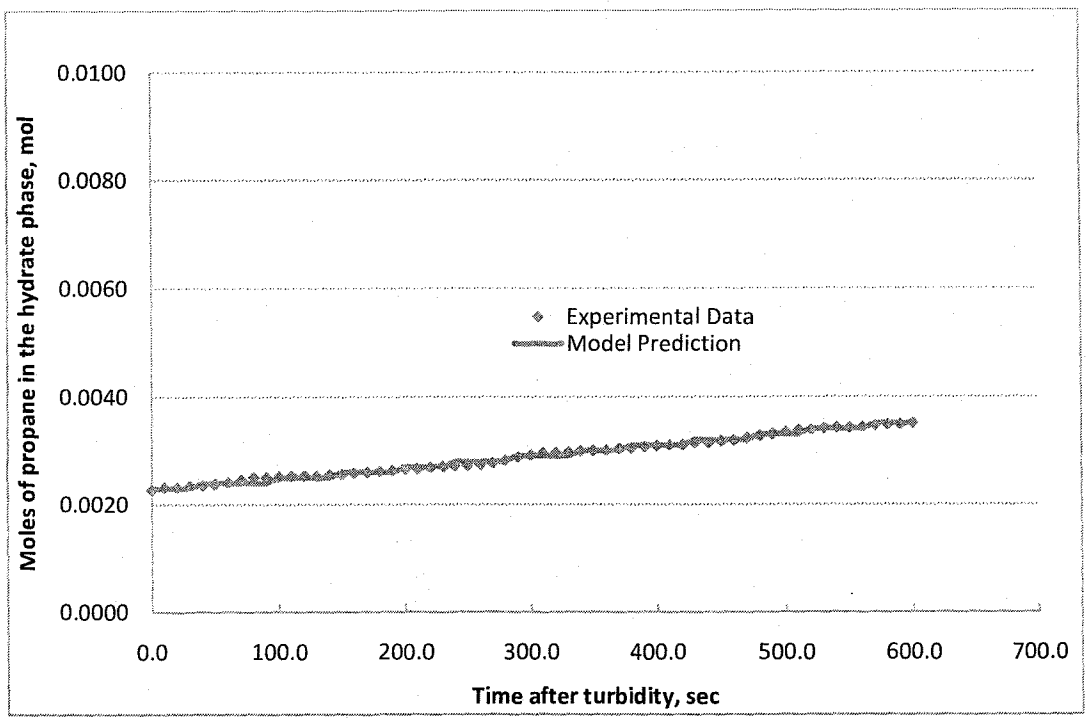

Figure 7.13: Number of moles of propane in the hydrate phase during hydrate formation 276 K and 0.42 MPa.

Temperature, K	K* , mol/(m^2.MPa.s)
274	0.4611
275	0.5195
276	0.4207

Table 7.7: Intrinsic rate constant of propane hydrate formation determined in this work using PSA,($K^* \approx K_r$).

7.4.4 Intrinsic rate constant for ethane hydrate formation in Structure II

The binary hydrate mixture of ethane and propane can be a structure I hydrate, a structure II hydrate, or both. The structure identity is a function of temperature, pressure, and composition of the mixture (Sloan and Koh, 2007). The phase equilibrium diagram of binary gas mixtures of ethane and propane in contact with excess water is shown in Figure 7.14. At a temperature of 274 K, when the mole fraction of ethane in the system is zero, i.e., only propane gas is present, structure II hydrate forms at approximately 2 bar, but, at 1.0 mole fraction of ethane structure I hydrate forms at approximately 5 bar. In between, at 0.73 mole fraction ethane, a quadruple point exists in which both incipient hydrate structures are in equilibrium with vapor and aqueous phases at approximately 8 bar.

To determine the intrinsic rate constant of ethane in structure II, an equimolar composition of ethane and propane gas mixture was used. The experimental data along with the known intrinsic rate constant of propane hydrate formation, determined *a priori*, were modelled by the model described earlier in Section 6.3 to extract the only unknown parameter in the Model which is the intrinsic rate constant of ethane hydrate formation in structure II.

The gas phase compositions were analyzed using gas chromatography. Gas samples were taken at the beginning of the experiment, at the supersaturation period, and at the end of the hydrate growth period. The analysis did not show a

significant change in the gas phase composition. This is likely due to the low solubilities and similar diffusivities of ethane and propane gases in water. The gas phase analysis is depicted in Figure 7.15.

The intrinsic rate constant for ethane hydrate formation in structure II hydrate was found to be 0.0137 mol/(m^2.MPa.s) which is more than one order of magnitude smaller than that in structure I hydrate. Also, this intrinsic rate constant is about one order of magnitude smaller than that of propane hydrate formation. In structure II hydrate, both gases, ethane and propane, occupy the large cages ($5^{12}6^4$). The thermodynamic occupancy is 0.9758 and 0.02303 for propane and ethane respectively (MEGHA software). It is worth noting that the ratio of the two intrinsic rate constants for both gases (propane and ethane) in structure II hydrate is similar to that of the cage occupancies of both guest molecules. The experimental mole consumption of the gas and the predicted values are illustrated in Figure 7.16.

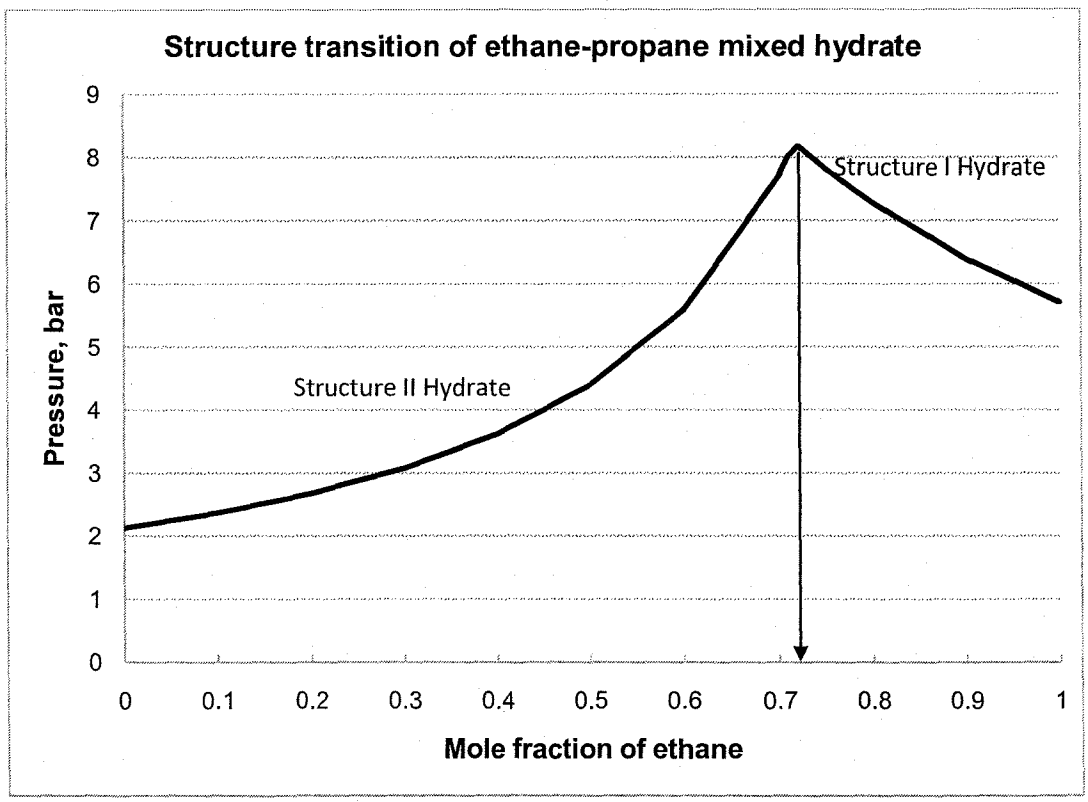

Figure 7.14: P-x diagram for ethane + propane + water system at 274 K (MEGHA Prediction).

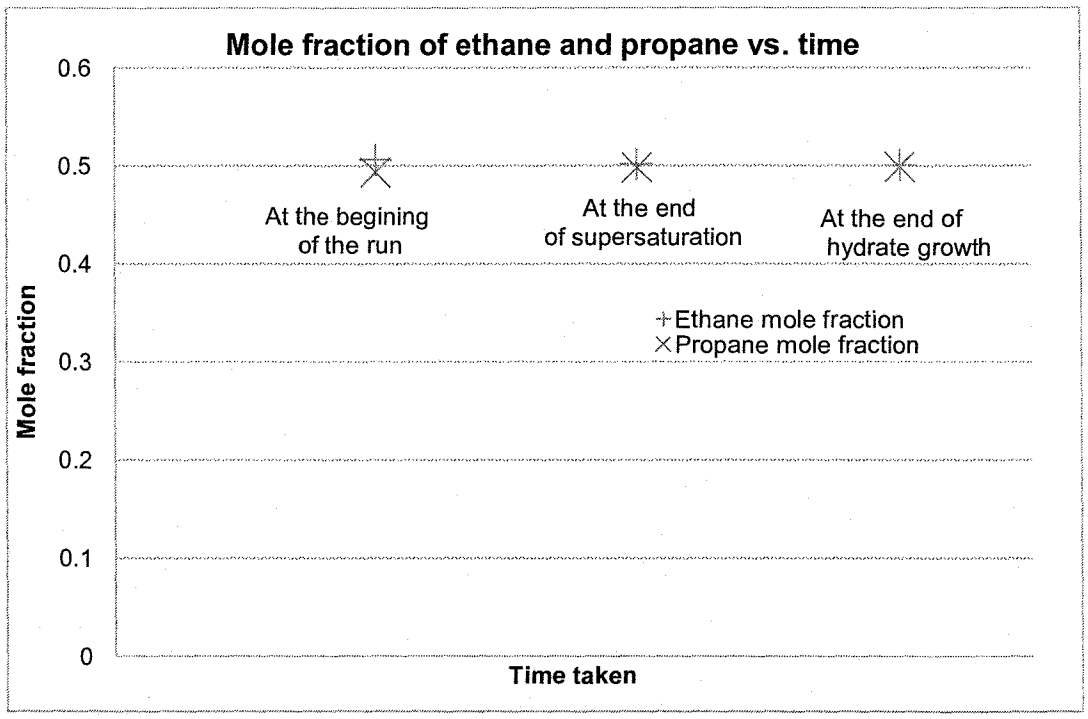

Figure 7.15: Compositions of propane and ethane in the gas phase of the reactor.

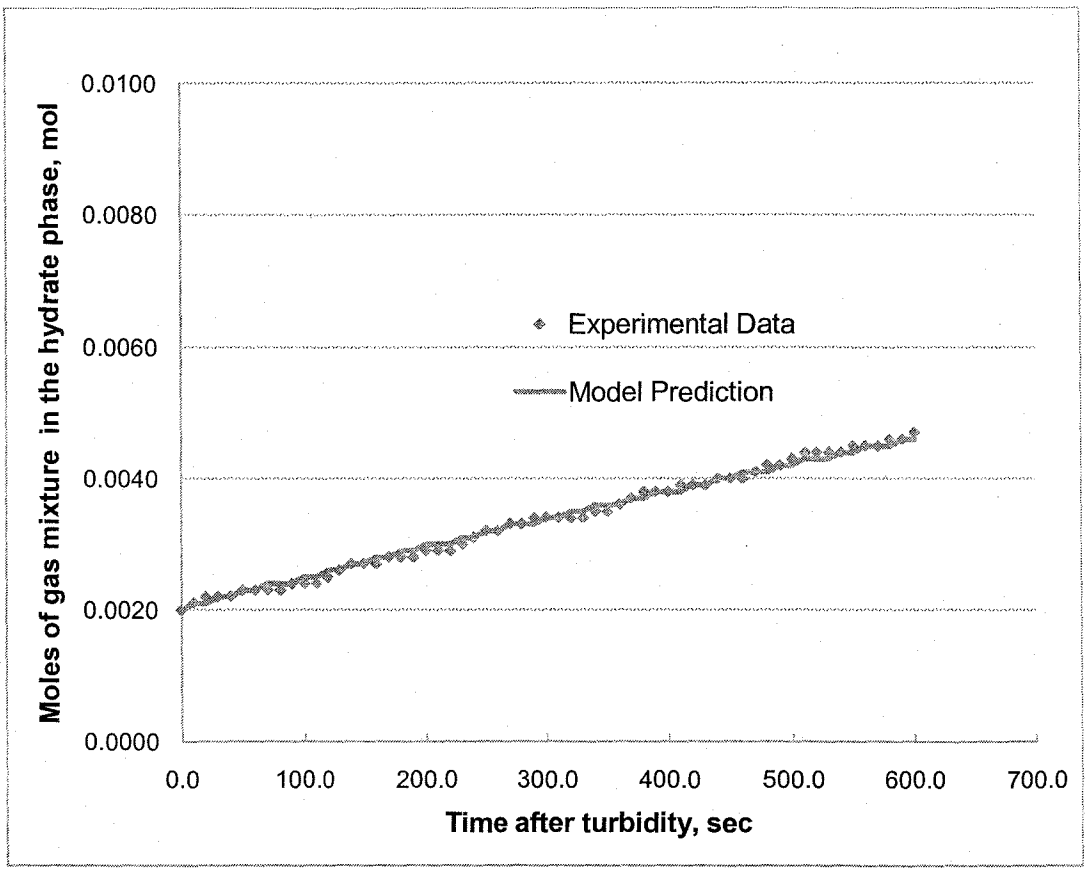

Figure 7.16: Number of moles of gas in the hydrate phase during hydrate formation of 50 % C_2H_6 and 50 % C_3H_8 at 274 K and 0.35 MPa.

7.4.5 Raman Spectroscopy Analysis

For each gas hydrate former, once the gas hydrate slurry in the reactor has formed to a sufficient solids concentration and the necessary data for the kinetics study has been taken, a sample is brought into the sapphire sampling cell by opening the inlet valve and starting the circulation pump. The microscope is then focused with a 5x objective lens on a single hydrate particle. Then, the acquisition of Raman spectra is commenced. A total of 20 acquisitions per sample with cosmic ray removal provided a satisfactory reproduction of the available Raman spectra reported in the literature data summarized in Table 7.8.

7.4.5.1 Results from single gas hydrate formers

Pure ethane hydrate has intense peaks in two different regions of the Raman spectrum (Herzberg, 1951). Figures 7.17 and 7.18 show the peaks measured in this study. The first peak at 1001 wavenumber corresponds to the C-C stretch in the large cage of structure I hydrate, while the latter two peaks at 2891 and 2946 wavenumbers correspond to the C-H stretches in the large cage of structure I hydrate. The current measured values match the reported literature values very well.

Pure methane gas in structure I hydrate has two distinctive peaks at 2905 and 2915 wavenumbers. The first peak, at 2905, corresponds to the C-H vibration mode of methane molecules in the large cavity of structure I hydrate. The second peak, at 2915, corresponds to the C-H vibration mode of methane

molecules in the small cavity of the structure I hydrate. The measured values in this study (see Figure 7.19) compare favourably with the values reported in the literature.

Pure propane hydrate in structure II has one distinguished Raman peak at 878 wavenumber corresponding to the C-C stretch in the large cage. The measured peak in this study is depicted in Figure 7.20. The measured value matches the reported value very well.

7.4.5.2 Results from equimolar ethane propane hydrate mixture

Difference in frequencies of bands of ethane in the C-C regions between structure I and structure II hydrates is much higher than that in the C-H regions. The differences are 8 and 4 cm^{-1} for the C-C and C-H stretches respectively. Thus, the shift in the C-C region is enough evidence for the presence of ethane in structure II hydrate in the presence of propane. Figure 7.21 shows the measured spectra of gas hydrate formed from the equimolar ethane-propane mixture in this work. The first peak at 878 wavenumber corresponds to the C-C stretch of propane in the large cage of structure II hydrate, while the second peak at 993 wavenumber corresponds to the C-C stretch of ethane in the large cage of structure II hydrate. This provides evidence that the determined intrinsic rate constant of ethane hydrate formation using this mixture at the experimental conditions corresponds to structure II hydrate.

Component	Vibrational mode	Cage type	Wavenumber (cm^{-1})
			Hydrate
C_2H_6	v3 sym C-C stretch	sI large	1001
	v3 sym C-C stretch	sII large	993
	v1+2v11 C-H stretch	sI large	2891
	v1+2v11 C-H stretch	sI large	2946
	v1+2v11 C-H stretch	sII large	2887
	v1+2v11 C-H stretch	sII large	2942
C_3H_8	v8 sym C-C stretch	sII large	878
CH_4	v3 sym C-H stretch	sI large	2905
	v3 sym C-H stretch	sI small	2915

Table 7.8: Raman wavenumbers of Subramanian (2000) as reported by Sloan and Koh (2007).

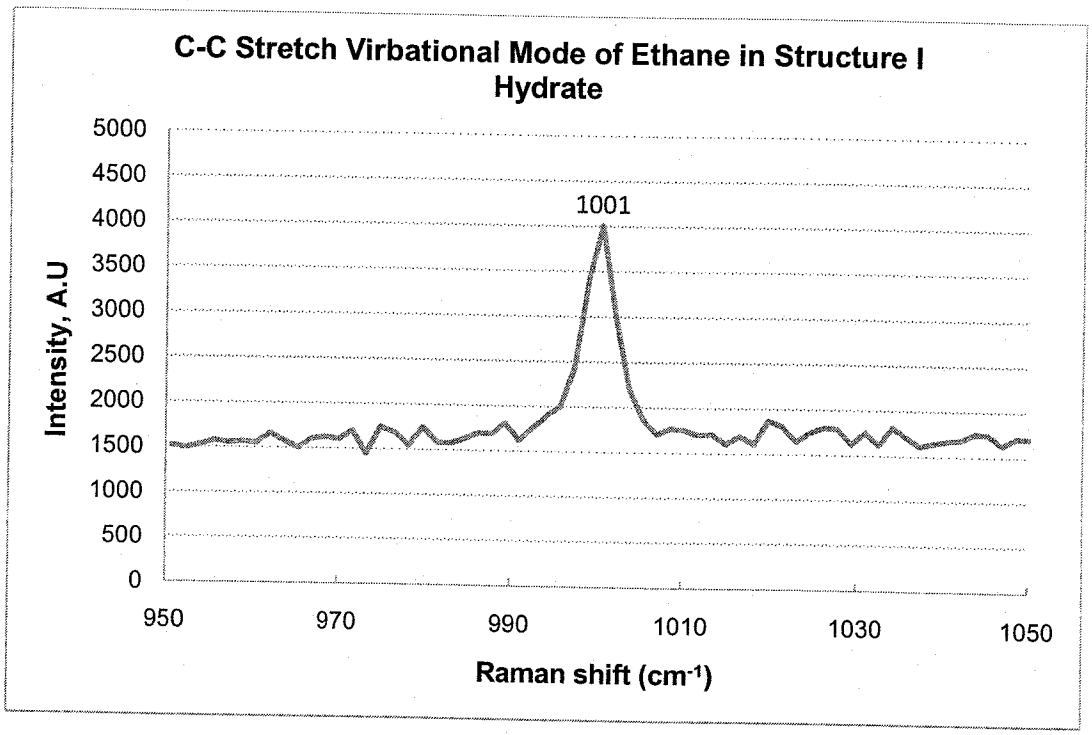

Figure 7.17: Raman spectra for structure I ethane hydrate, C-C stretch region obtained in this work.

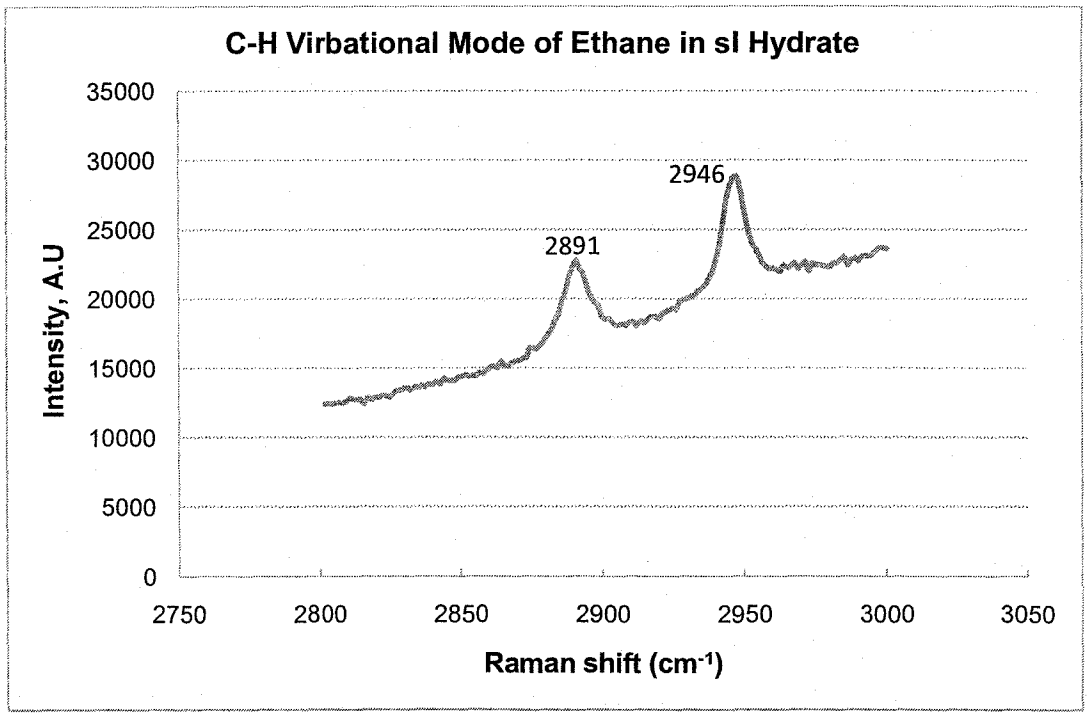

Figure 7.18: Raman spectra for structure I ethane hydrate, C-H vibration region obtained in this work.

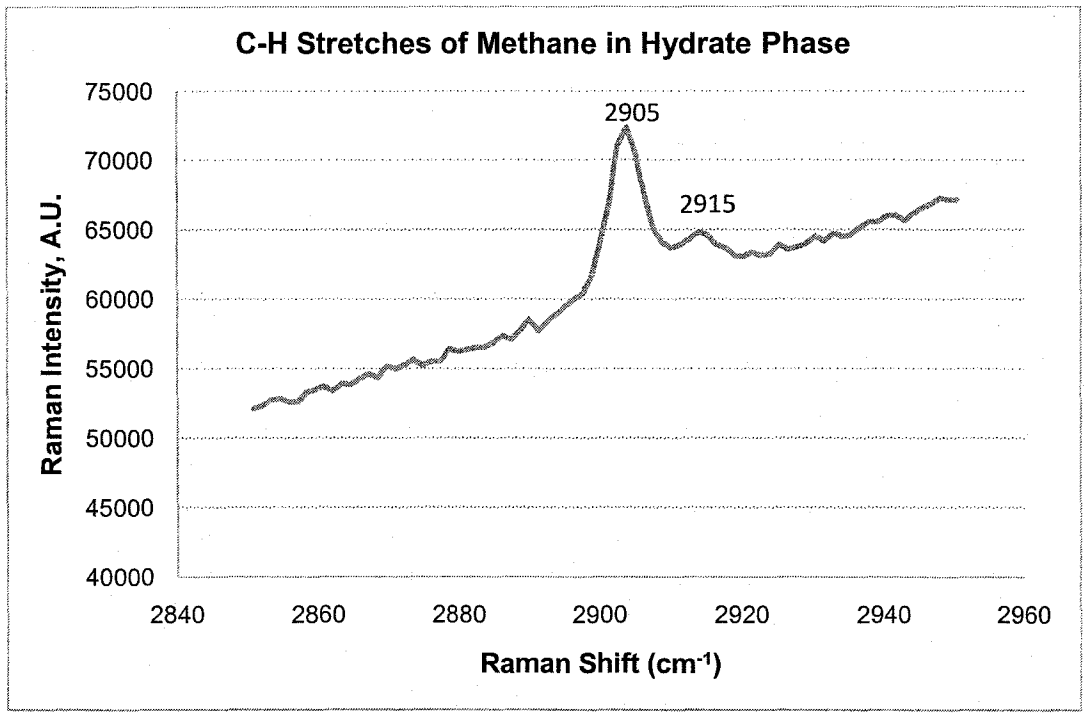

Figure 7.19: Raman spectra for structure I methane hydrate, C-H stretch vibration region obtained in this work.

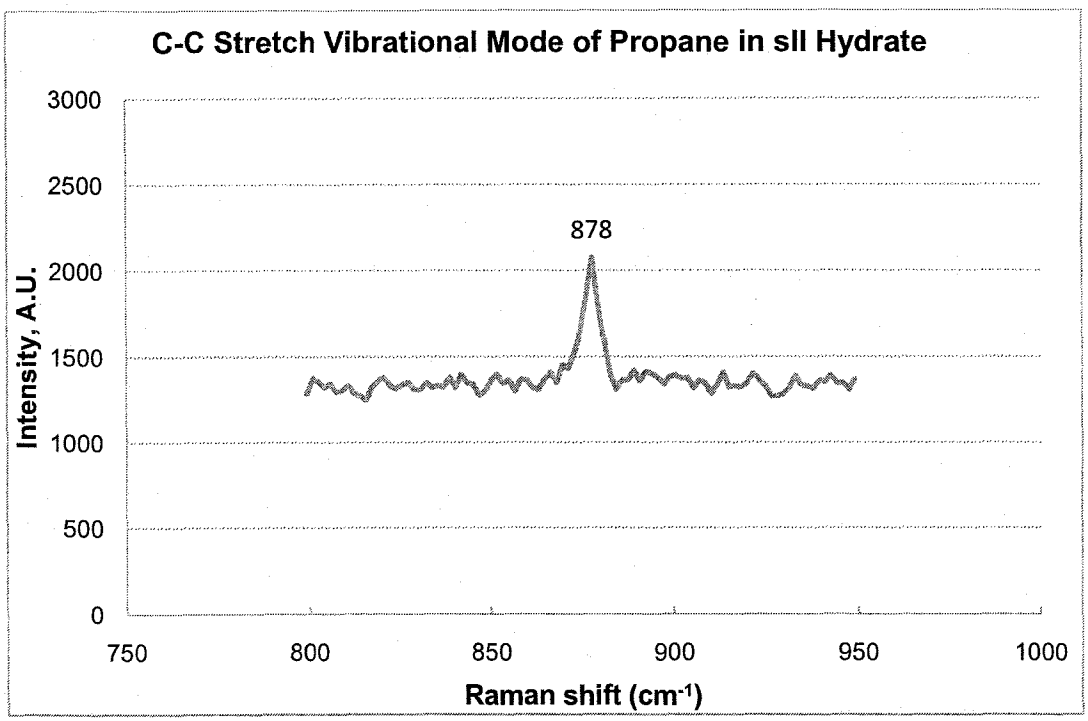

Figure 7.20: Raman spectra for structure II propane hydrate, C-C stretch vibration region obtained in this work.

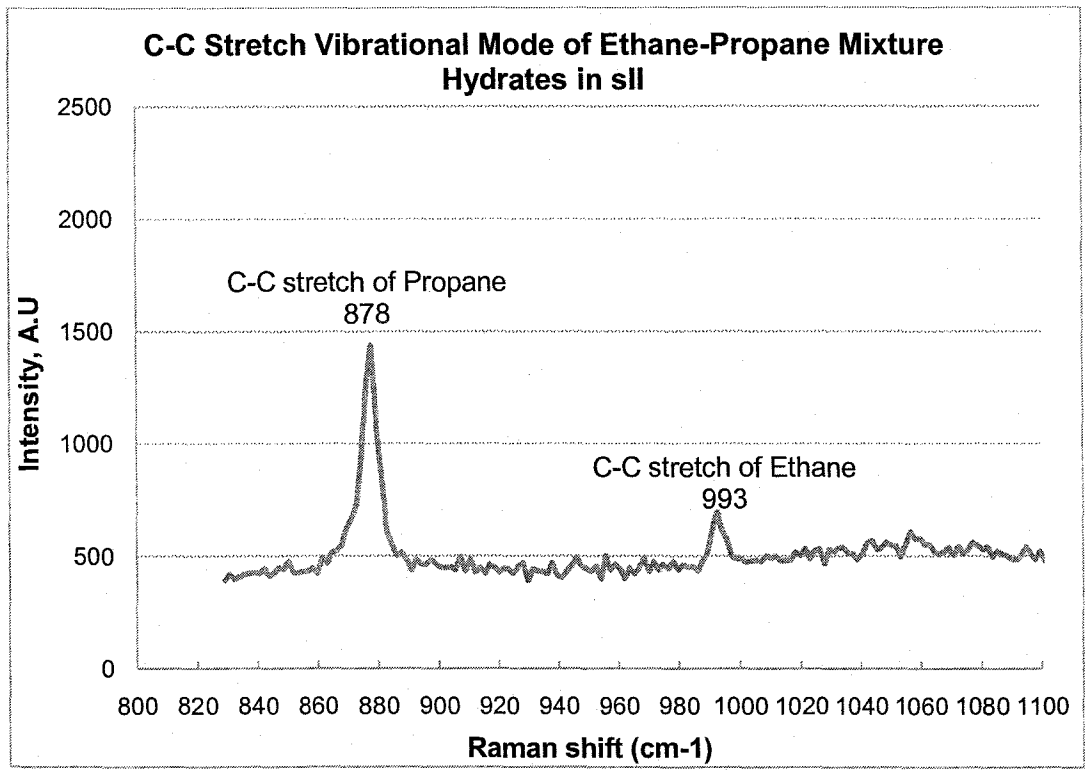

Figure 7.21: Raman spectra for structure II ethane-propane mixture hydrate, C-C stretch vibration region obtained in this work.

CHAPTER EIGHT: CONCLUSIONS AND RECOMMENDATIONS

8.1 Conclusions

Actual particle size measurements of the hydrate particles during the growth period were made during hydrate formation of ethane, methane, propane, and an equimolar mixture of ethane and propane using an *in situ* particle size analyser. The kinetic model was modified to incorporate the measured second moment of particles, and the intrinsic rate constants of hydrate formation for the following were determined:

- ethane gas in structure I hydrate.
- methane gas in structure I hydrate.
- propane gas in structure II hydrate, and
- ethane gas in structure II hydrate.

Based on the observations and findings from this study, the following conclusions are drawn:

1) The newly determined intrinsic rate constants indicate the necessity of including the actual particle size measurements in modelling the gas hydrate growth period. The actual measurements differ significantly from the previously estimated values based on the assumption of thermodynamically stable critical nuclei sizes.
2) The kinetic model successfully captures the intrinsic nature of the hydrate growth phenomenon. Therefore, the determined intrinsic rate constants obtained in this study can be used in designing processes involving

hydrate formation once they are coupled with heat and mass transfer balances.

3) The intrinsic rate constant of ethane hydrate formation in structure II hydrate is significantly smaller than that of ethane hydrate formation in structure I hydrate.
4) In the presence of propane, the intrinsic rate constants of hydrate formation of ethane and propane in structure II hydrate are proportional to the occupancy ratio of both gases in the large cage of that structure.
5) Use of FBRM particle size analyzer to study hydrate formation is not a straightforward procedure. A novel procedure was developed to measure hydrate particle sizes using the FBRM probe.
6) The FBRM probe can precisely detect system changes such as hydrate formation and provide further insight into the process.
7) The successful integration of Raman spectroscopy with the hydrate formation apparatus ensures that the reported intrinsic rate constants of hydrate formation for the subject gases belong to the exact hydrate structure reported.

8.2 Recommendations

1) The procedure developed in this study to use the FBRM probe to obtain satisfactory particle size measurements of hydrate particles is recommended for future studies.

2) The intrinsic rate constant is dependent on the hydrate structure. Thus, different hydrate mixtures should be studied to determine the intrinsic rate constants of different gases in different structures.
3) The FBRM probe should be coupled with the PVM (particle video microscope) probe provided by the same manufacturer to further investigate the shape of the hydrate particles during the growth period. The PVM probe is capable of providing digital image analysis of the hydrate particles in the suspension.

REFERENCES

Alotaibi, F., Clarke, M., Bishnoi, P.R., "Determination of the intrinsic kinetics of formation and decomposition of gas hydrates from mixtures of CO_2 and N_2 using an *in situ* particle size analyzer", Proceedings of the 5th International Conference on Gas Hydrates, Trondheim, Norway, June 12-16, 2005.

Alotaibi, F.D., "Decomposition Kinetics of N_2 and CO_2 Hydrates", MSc. Thesis, 2006.

Bergeron, S., Servio, P., "Reaction rate constant of propane hydrate formation", Fluid Phase Equilibria, 265, pp. 30–36, 2008.

Bischoff, K.B., Froment, G.F., "Chemical Reactor Design", pp. 31&313, Wiley, New York, 1979.

Bishnoi, P.R., Clarke, M. A. "Design of a high-pressure optical sampling cell for the application of Raman microscopy in gas hydrate formation and decomposition kinetics", Proceedings of the 5th International Conference on Gas Hydrates, Trondheim, Norway, June 12-16, 2005.

Bishnoi, P. R., Jeje, A. A., Kalogerakis, N. and Saeger, R., "The kinetics of formation and decomposition from mixtures of natural gas components-experimental data and development of generalized predictive rate expressions", Annual Report to Energy Mines and Resources, Ottawa, Canada, 1985.

Bishnoi, P.R., Kalogerakis, N., Jeje, A.A., Dholabhai, P.D., Englezos, P., "The kinetics of formation and decomposition of hydrates from mixtures of natural gas components", Final Report to Energy Mines and Resources, Ottawa, Canada, 1986.

Bishnoi, P.R., Gupta, A.K., Englezos, P. and Kalogerakis, N., "Multiphase equilibrium flash calculations for systems containing gas hydrates", Fluid Phase Equilibria, 53, pp. 97–104, 1989.

Bollavram, P., Devarakonda, S., Selim, M.S., Sloan, E.D, "Growth Kinetics of Single Crystal sII Hydrates: Elimination of Mass Transfer Effects", Proceedings of the 3rd International Conference on Gas Hydrates, Salt Lake City, Utah, July 18-22, 533-543, 2000.

Clarke, M.A, Pooladi-Darvish, M., Bishnoi, P.R., "A Method to Predict Equlibrium Conditions of Gas Hydrate Formation in Porous Media", Ind. Eng. Chem. Res, 38, 2485-2493, 1999.

Clarke, M.A., Bishnoi, P.R., "Determination of the Intrinsic Rate of Ethane Gas Hydrate Decomposition", Chemical Engineering Science, 55, 4869-4883, 2000.

Clarke, M.A., "Determination of the Intrinsic Rate of Gas Hydrate Decomposition Using Particle Size Analysis", Annals New York Academy of Sciences, 912, 556-563, 2000.

Clarke, M.A., Bishnoi, P.R., "Determination of the Intrinsic Kinetics of Gas Hydrate Decomposition using Particle Size Analysis", Proceedings of the 3rd International Conference on gas Hydrates, Salt Lake City, Utah, July 18-22, 556-563, 2000.

Clarke, M.A., "Determination of the Intrinsic Kinetics of Gas Hydrate Decomposition by Particle Size Analysis", PhD Thesis, University of Calgary, 2001.

Clarke, M.A., Bishnoi, P.R., "Measuring and Modeling the Rate of Decomposition of Gas Hydrates formed from Mixtures of Methane and Ethane", Chemical Engineering Science, 56, 4715-4724, 2001.

Clarke, M.A., Bishnoi, P.R., "Development of an Implicit Least Squares Optimization Scheme for the Determination of Kihara Potential Parameters using Gas Hydrate Equilibrium Data", Fluid Phase Equilibria, 211, 51-60, 2003.

Clarke M.A., Bishnoi, P.R, "Determination of the Intrinsic Kinetics of Gas Hydrate Decomposition using Particle Size Analysis", presented at the 3rd International Conference on Gas Hydrate. Salt Lake City, Utah. July 18-22, 2003.

Clarke, M.A., Bishnoi, P.R., "Determination of the Intrinsic Rate Constant and Activation Energy of CO2 Gas Hydrate Decomposition using *In Situ* Particle Size Analysis", Chemical Engineering Science, 59, 2983-2993, 2004.

Clarke, M.A, Bishnoi, P.R., "Determination of the Intrinsic Kinetics of CO2 Gas Hydrate Formation using *in situ* Particle Size Analysis", Chemical Engineering Science, 60, 695-709, 2005.

Claussen, W.F., "A Second Water Structure for Inert Gas Hydrates", Journal of Chemical Physics,19,1452-1432, 1951.

Danckwerts, P.V., "Gas Liquid Reactions", McGraw-Hill, New York, 1970.

Danckwerts, P.V., Sharma, M.M., "The absorption of carbon dioxide into solutions of alkalis and amines with some notes on hydrogen sulphide and carbonyl sulphide", Transactions of the Institution of Chemical Engineers and the Chemical Engineer 244, 522–528, 1966.

Dholabhai, P.D., Kalogerakis, N., Bishnoi, P.R., "Kinetics of Methane Hydrate Formation in Aqueous Mixed Electrolyte Solutions", Can. J. Chem. Eng., 71, 68-74, 1993.

Englezos, P., Bishnoi, P.R., "Prediction of gas Hydrate Formation Conditions in Aqueous Electrolyte Solutions", AIChE Journal, 34, 1718-1727, 1988.

Englezos, P., Kalogerakis, N.E, Dholabhai, P., Bishnoi, P.R., "Kinetics of Methane and Ethane Hydrate Formation", Chemical Engineering Science, 42, 2647–2658, 1987a.

Englezos, P., Kalogerakis, N.E., Dholabhai, P.D., Bishnoi, P.R., "Kinetics of Gas Hydrate Formation from Mixtures of Methane and Ethane", Chemical Engineering Science 42, 2659–2666, 1987b.

Glew, D.N., Hagget, M.L., "Kinetics of formation of ethylene oxide hydrate", Part I: experimental method and congruent solutions, Canadian Journal of Chemistry 46, 3857–3865, 1968a.

Glew, D.N., Hagget, M.L., "Kinetics of formation of ethylene oxide hydrate", Part II: incongruent solutions and discussion, Canadian Journal of Chemistry 46, 3867–3877, 1968b.

Gnanendran, N., Amin, R., "Modeling hydrate formation kinetics of a hydrate promoter–water–natural gas system in a semi-batch spray reactor", Chemical Engineering Science 59, 3849–3863, 2004.

Gudmundsson, J., Borrehaug, A., "Frozen Hydrate for Transport of Natural Gas", Proceedings of the 2nd Int. Conf. on Natural Gas Hydrates, Toulouse, France, June 2-6, Guillon, O., Ed., INP ENGISC, 983-986, 1996.

Hamme, R.C., Emerson, S.R., "The Solubility of Neon, Nitrogen, and Argon in Distilled Water and Seawater", Deep Sea Research I, 51, 1517-1528, 2004.

Hayduk. W., Laudie, H., "Prediction of diffusion coefficients for nonelectrolytes in dilute aqueous solutions", A.Z.CbE. J. 20, 611-615, 1974.

Heath, A.R., Fawell, P.D, Bahri, P.A., Swift, J.D., "Estimating Average Particle Size by Focused Beam Reflectance Measurement (FBRM)", Part. Syst. Char., 19, 84-95, 2002.

Herri, J.M., Gruy, F., Pic, J.S., Cournil, M., Cingotti, B., Sinquin, A., "Interest of *in situ* turbidimetry for the characterization of methane hydrate crystallization: application to the study of kinetic inhibitors", Chemical Engineering Science, 54, 1849–1858, 1999a.

Herri, J.M., Pic, J.S., Gruy, F., Cournil, M., "Methane hydrate crystallization mechanism from *in situ* particle sizing", A.I.Ch.E. Journal 45, 590–602, 1999b.

Hirai, H., Tanaka, H., Kawamura K., Yamamoto Y., Yagi, T., "Structural Changes in gas Hydrates and Existence of Filed Ice Structure of Methane Hydrate above 40 GPa", J. Phy. Chem. Solids., 65, 1555, 2004.

Holder, G.D., Corbin, G., Papadopoulos, K.D, "Thermodynamic and Molecular Properties of Gas Hydrates from Mixtures Containing Methane, Argon and Krypton", Ind. and Eng. Chem, 19,282, 1980.

Hukkanen, E.J., Braatz, R.D., "Measurement of particle size distribution in suspension polymerization using *in situ* laser backscattering", Sensors and Actuators B, 96, 451-459, 2003.

Jeffery, G.A, McMulan, R.K., "The Clathrate Hydrates", Progress in Inorganic Chemistry, 8, 45-51, 1967.

John, V.T., Papadopoulos, K.D., Holder, G.D., "A generalized model for predicting equilibrium conditions for gas hydrates", A.I.Ch.E. Journal, 3, 252–259,1985.

Juvekar, V.A., Sharma, M.M., "Chemical Methods for the Determination of Liquid Side Mass Transfer Coefficient and Effective Interfacial Area in Gas Liquid Contactors", Chemical Engineering Science, 28, 813-844, 1973.

Kane, S.G., Evans, T.W., Brian, P.L.T., Sarofim, A.F., "Determination of the kinetics of secondary nucleation in batch crystallizers", A.I.Ch.E. J. 20, 855-862, 1974.

Kail, N., Briesen, H., Marquardt, W., "Advanced geometrical modeling of focused beam reflectance measurements (FBRM)", Part. Part. Syst. Char. 24, 184–192, 2007.

Kim, H.C., Bishnoi, P.R., Heidemann, R.A., Rizvi, S.S.H., "Kinetics of Methane Hydrate Decomposition", Chem. Eng. Sci., 42, 1645-1653, 1987.

Koh, C.A, Sloan, E.D., "Natural Gas Hydrates: Recent Advances and Challenges in Energy and Environmental Applications", AIChE, 53, 1636-1643, 2007.

Lekvam, K., Ruoff, P., "A reaction kinetics mechanism for methane hydrate formation in liquid water", Journal of the American Chemical Society 115, 8565–8570, 1993.

Loveday, J.S., Nelmes, R.J., Gutharie, M., Klug, D.D., Tse, J.S., "Transition From Cage Clathrate to Filled Ice: The Structure of Methane Hydarates III", Phys. Rev. Lett., 87, 2001.

Makogan, Y.F., "Hydrates of Natural Gas", Translated from Russian by W.J. Cieslesicz, PennWell Books, Tulsa, Oklahoma, 1981.

Malegaonkar, M.B., Dholabhai, P.D., Bishnoi, P.R., "Kinetics of carbon dioxide and methane hydrate formation", Canadian Journal of Chemical Engineering 75, 1090–1099, 1997.

"MATLAB" R2008a, The MathWorks Inc., Cochituate Place, 24 Prime Park Way, Natick, Mass. 01760, USA.

"MEGHA", Megha Technologies Inc., Calgary, Canada.

Mehta, A.P., "Structure H Hydrate Phase Equilibria", PhD Thesis, Colorado School of Mines, 1996.

MettlerToledo Lasentec, "FBRM D-600 Hardware Manual", 2002.

Muller-Bongartz, B., Wideman, T.R., Sloan, E.D., Proc. of Second International Offshore and Polar Engineering Conference, pp 628, 1992.

Mullin, J., "Crystallization", 3rd Edition, Butterworth-Heinemann, Oxford, U.K., 1993.

Natarajan, V., Bishnoi, P.R., "Formation and Decomposition of Gas Hydrates", Fluid Phase Equilibria, 117, 168-177, 1996.

Nijsing, R.A.T.O., Hendriksz, R.M., Kramers, H., "Absorption of CO2 in jets and falling films of electrolyte solutions with and without chemical reaction", Chemical Engineering Science, 10, 88–104, 1959.

Nixon, M.F., Grozic, J.L.H., "Submarine Slope Failure Due to Gas Hydrate Dissociation: a Preliminary Quantification", Can. Geotech. J., 44, 314-325, 2007.

Ng, H.J., Robinson, D.B., "The Measurement and Prediction of Hydrate Formation in Liquid Hydrocarbon-Water Systems", Industrial & Engineering Chemistry Fundamentals, 15(4), 293, 1976.

Nollet, L.M.L., "Handbook of Food Analysis: Methods and Instruments in Applied Food Analysis", 2nd Edition, 3, pp 1819, 2004.

Olsen, M.B., Majumdar, A., Bishnoi, P.R., "Experimental Studies on Hydrate Equilibrium Carbon-Dioxide and Its Systems", Int. J. of The Soc. of Mat. Eng. for Resources", 7(1), 17-23, 1999.

O'Sullivan, T.D., Smith, N.O., "The Solubility and Partial Molar Volume of Nitrogen and Methane in Water and in Aqueous Sodium Chloride from 50 to 125° and100 to 600 Atm.", The Journal of Physical Chemistry, 74(7), 1460-1465, 1970.

Pangborn, J.B., Barduhn, A.J., "The kinetics of methyl bromide hydrate formation", Desalination 8, 35–68, 1970.

Parent, J.S., Bishnoi, P.R., "Investigation into the nucleation behavior of methane gas hydrates", Chemical Engineering Communications 144, 51–64, 1996.

Parent, J.D., "Equilibrium Compositions and Enthalpy Changes for the Reactions of Carbon Oxygen and Steam", Inst. Gas Technol. Res. Bull., 1, 1948.

Parrish, W.R., Prausnitz, J.M., "Dissociation Pressures of Gas Hydrates formed by Gas Mixtures", Industrial Engineering Chemical Process Design Development, 11(1), 26, 1972.

Pons, M., Milferstedt, K., Morgenroth, E., "Modeling of chord length distributions", Chemical Engineering Science, 61, 3962-3973, 2006.

Renishaw, "inVia Raman microscope operation manual", Spectroscopy Products Division, Old Town, Wotton-under-Edge, Gloucestershire GL12 7DW, United Kingdom, 2003.

Riberio, C.P., Lage, P.L.C, "Review: Modeling of hydrate formation kinetics: State-of-the-art and future directions", Chemical Engineering Science 63 2007–2034, 2008.

Ripmeester, J.A., Ratcliffe, C.I., Tse, J.S., "The Nuclear Magnetic Resonance of 129Xe Trapped in Clathrates and Some Other Solids", J. Chem. Soc. Farad. Trans., 84, 3731-3737, 1988.

Ripmeester, J.A., Tse, J.S., Ratcliffe, C.I, Powell, B.M., "A New Clathrate Hydrate Structure", Nature, 325, 135-136,1987.

Rogers, R.E., Zhong, Y., "Feasibility of Storing Natural Gas in Hydrates Commercially", Proceedings of the 3rd Int. Conf. on Gas Hydrates, Salt Lake City, Utah, July 21-24, 843-850, 1999.

Schicks, J.M., Naumann, R., Erzinger, J., Hester, K.C., Koh, C.A., Sloan, E.D., "Phase transitions in mixed gas hydrates: experimental observations versus calculated data", J Phys Chem B,110:11468–11474, 2006.

Seo, Y., Lee, H., "Structure and Guest Distribution of the Mixed Carbon Dioxide and Nitrogen Hydrates as Revealed by X-ray Diffraction and ^{13}C NMR Spectroscopy". Journal of Phys. Chem., 108, 530-534, 2004.

Sharma, M.M., "Perspectives in Gas-Liquid Reactions", Chemical Engineering Science, 38, 21-28, 1983.

Sharma, M.M., Danckwerts, P.V., "Chemical methods for measuring interfacial areas and mass transfer coefficients in two fluid systems", British Chemical Engineering, 15, 522–528, 1970.

Sharma, S., "Gas Hydrate Particle Size Measurements", MSc. Thesis, University of Calgary, 1996.

Shindo, Y., Fujioka, Y., Yanagisawa, Y., Hakuta, T., Komiyama, H., "Formation and stability of CO_2 Hydrate, Direct Ocean Disposal of Carbon Dioxide, eds. Handa, N. & Ohsumi, T., Tokyo, Terraqub, pp. 217-231, 1993.

Skovborg, P., Rasmussen, P., "A mass transport limited model for the growth of methane and ethane gas hydrates", Chemical Engineering Science 49, 1131–1143, 1994.

Sloan, E. D., Koh, C.A, "Clathrate Hydrates of Natural Gases, 3rd Edition", New York: Marcell Dekker, Inc., 2007.

Sloan, E.D., "A changing hydrate paradigm—from apprehension to avoidance to risk management", Fluid Phase Equilibria 228–229, 67–74, 2005.

Sloan, E.D., "Natural Gas Hydrates", SPE Technology Today Series, JPT, December, 1991.

Sloan, E.D., Proc. of 69th Annual Gas Processors Convention, Phoenix, 8, 1990.

Sloan, E. D., Fleyfel, F., "A Molecular Mechanism for Gas Hydrate Nucleation from Ice", AIChE J., 637, 1281, 1991.

Sloan, E. D., "Clathrate Hydrates of Natural Gases", New York: Marcell Dekker, Inc., 1998.

Sridharan K., Sharma, M.M., "New Systems and Methods for the Measurements of Effective Interfacial Area and Mass Transfer Coefficients in Gas-Liquid Contactors", Chemical Engineering Science, 31, 767-774, 1976.

Stewart, P.B., Munjal, P., "Solubility of Carbon Dioxide in Pure Water, Synthetic Seawater, and Synthetic Seawater Concentrates at -5° to 25° C. and 10 to 45 atm. Pressure", Journal of Chemical and Engineering Data, 15(1), 1970.

Subramanian S, Kini, R.A., Dec, S.F., Sloan, E.D., "Evidence of structure II hydrate formation from methane plus ethane mixtures", Chemical Engineering Science 55:1981–1999, 2000.

Sum, A.K., Burruss, R.C., Sloan, E.D., "Measurement of clathrate hydrates via Raman spectroscopy", J Phys Chem B,101:7371–7377, 1997.

Suess, E., Bohrmann, G., Greinert, J., Lausch, E., "Flammable Ice", Scientific American, 281(5), 76-83, 1999.

Takaoki, T., Iwasaki, T., Katoh, T., Takashi, A., Kiyoshi, H., "Use of Hydrate Pellets for Natural Gas Transportation", Proceedings of the 4th Inter. Conf. on Gas Hydrates, Yokohama, Japan, May 17-20, 406, 2002.

Trebble, M.A., Bishnoi, P.R., "Development of a New Four-Parameter Equation of State", Fluid Phase Equilibria, 35, 1-17, 1987.

Trebble, M.A., Bishnoi, P.R., "Extension of the Trebble-Bishnoi Equation of State to Mixtures", Fluid Phase Equilibria, 40, 1-19, 1988.

Udachin, K.A., Ripmeester, J.A., "A Complex Clathrate Hydrate Structure Showing Bimodal Guest Hydration", Nature, 397, 420-423, 1999.

Udachin, K.A., Enright G.D., Ratcliffe, C.I., Ripmeester, J.A., "Structure, Stoichiometry, and Morphology of Bromine Hydrate", J. Am. Chem. Int. Ed., 119, 1997.

Udachin, K.A., Ratcliffe, C.I., Ripmeester, J.A., "A Dense and Efficient Clathrate Hydrate Structure with Unusual Cages", Angew. Chem. Int. Ed., 40, 2001.

van der Waals, J.H., Platteeuw, J.C., "Clathrate Solutions", Adv. Chem. Phys., 2(1), 1-45, 1959.

von Stackelberg, M., Muller, H.R., "Feste Gas Hydrate II", Zeitungen Elektrochem., 58, 25-36, 1954.

Vysniauskas, A., Bishnoi, P.R., "Kinetics of ethane hydrate formation", Chemical Engineering Science 40, 299–303, 1985.

Vysniauskas, A., Bishnoi, P.R., "A Kinetic Study of Methane Hydrate Formation", Chemical Engineering Science, 38, 1061, 1983.

Wilke, C.R., Chang, P., "Correlation of diffusion coefficients in dilute solutions", A.I.Ch.E. Journal 1, 244, 1955.

Wilson, L.D., Tulk, C.A., Ripmeester, J.A., "Instrumental techniques for the investigation of methane hydrates: cross-calibrating NMR and Raman spectroscopic data", Paper presented at 4th International Conference on Gas Hydrates, May 19–23, Yokohama, Japan, 2002.

Worlitschek, J., Mazzotti, M., "Choice of the focal point position using Lasentec FBRM", Part. Part. Syst. Charact. 20,12–17, 2003.

Wynn, E.J.W., "Relationship between particle-size and chord-length distributions in focused beam reflectance measurement: stability of direct inversion and weighting, Powder Technol. 133,125–133, 2003.

APPENDICES

Appendix A: Three phase equlibrium "MEGHA" predictions.

Appendix B: Calculation of Henry's Constant for Surface Area.

Appendix C: Solubiltiy Data.

Appendix D: Hydrate Formation Experiments.

Appendix E: Chord Length Distributions.

APPENDIX A: THREE PHASE EQULIBRIUM "MEGHA" PREDICTIONS.

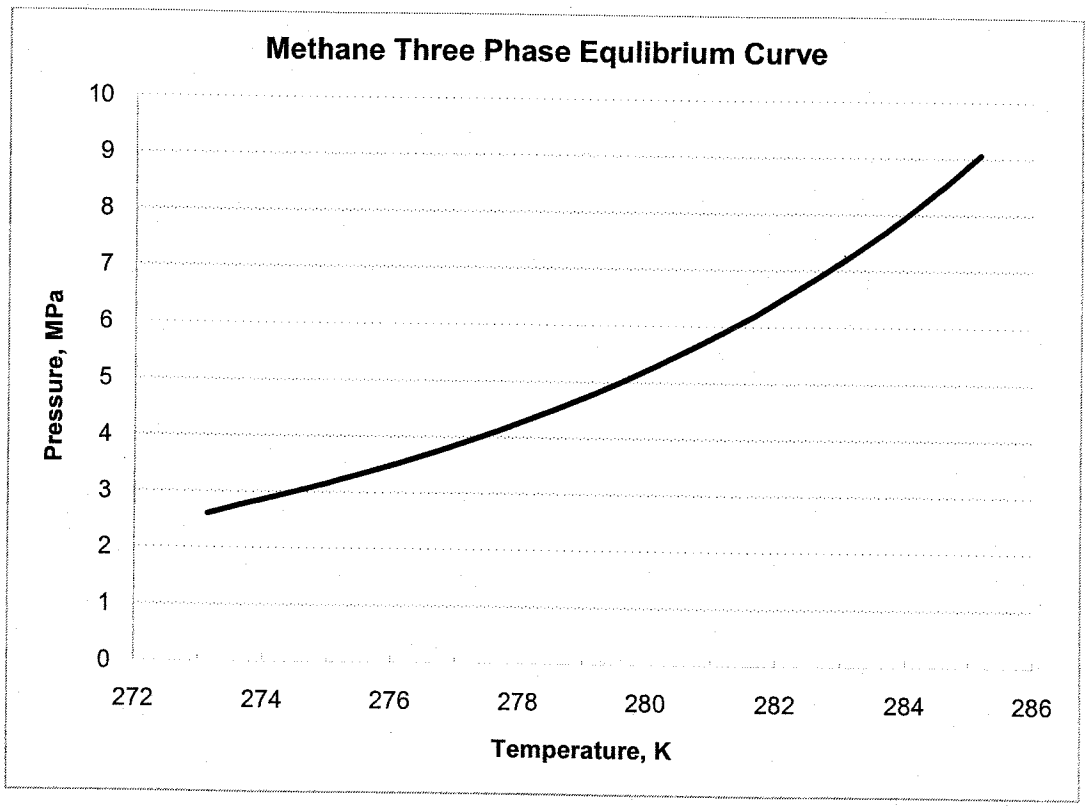
Methane Three Phase Equlibrium Curve
Pressure, MPa
10
9
8
7
6
5
4
3
2
1
0
272
274
276
278
280
282
284
286
Temperature, K

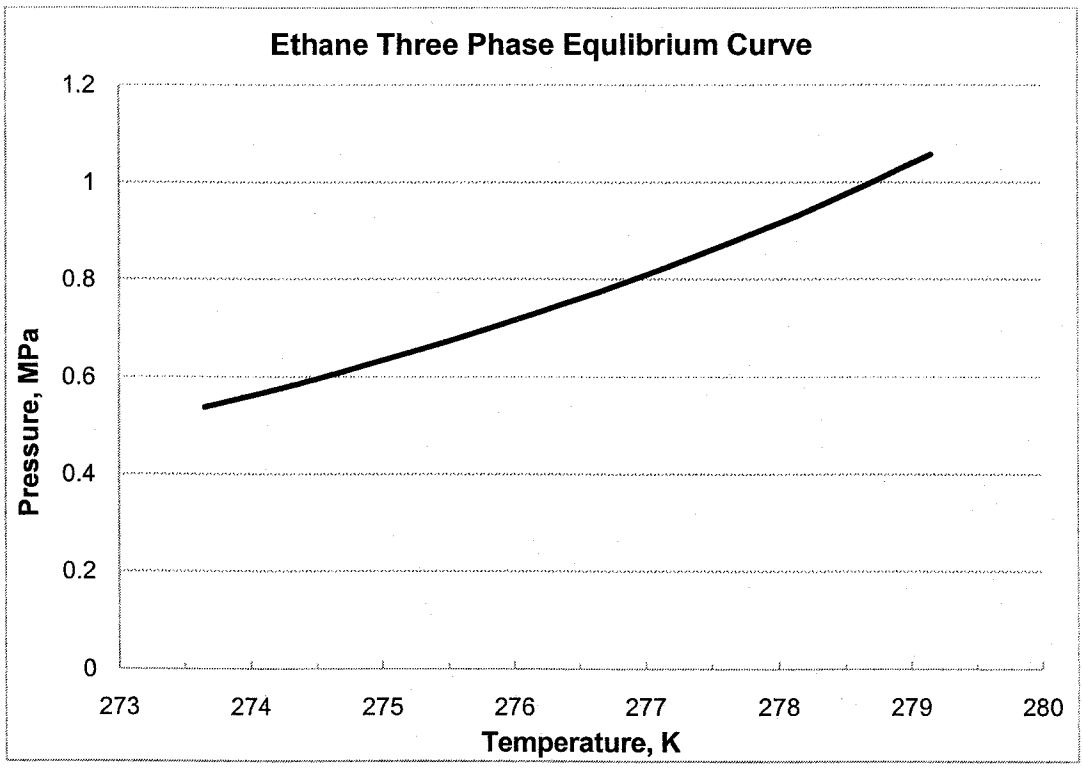
Ethane Three Phase Equlibrium Curve
1.2
1
0.8
0.6
0.4
0.2
0
Pressure, MPa
273
274
275
276
277
278
279
280
Temperature, K

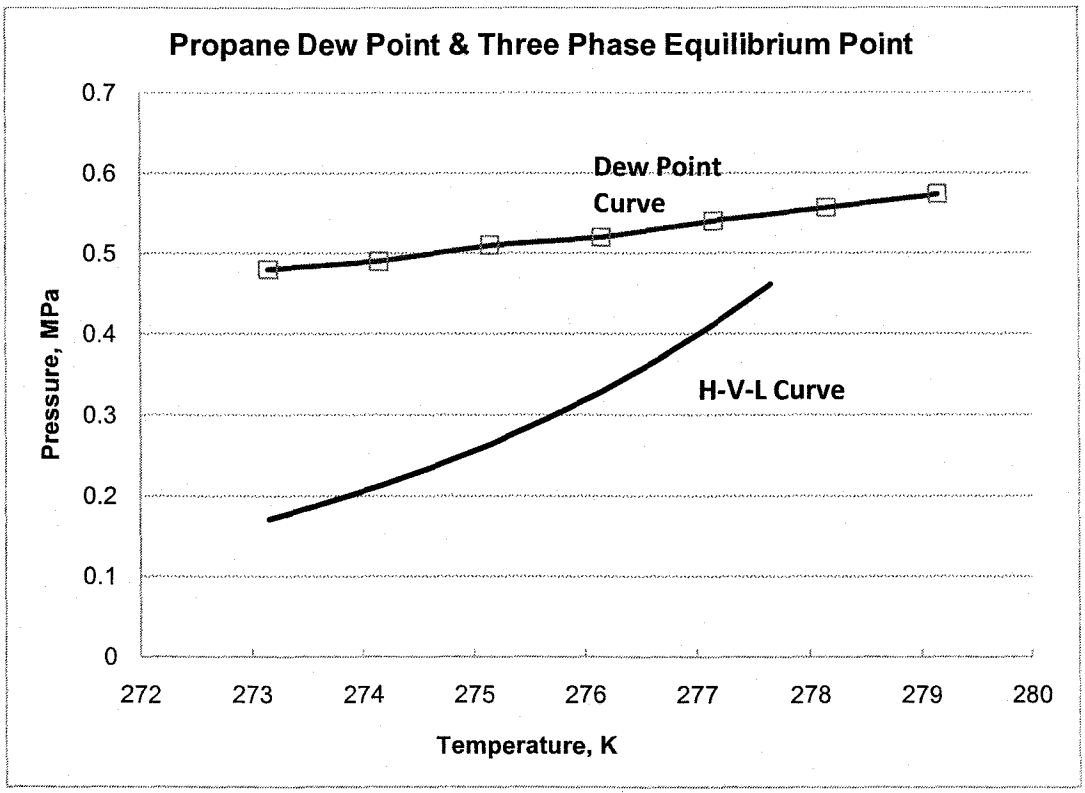
Propane Dew Point & Three Phase Equilibrium Point
Pressure, MPa
0.7
0.6
0.5
0.4
0.3
0.2
0.1
0
Dew Point Curve
H-V-L Curve
272
273
274
275
276
277
278
279
280
Temperature, K

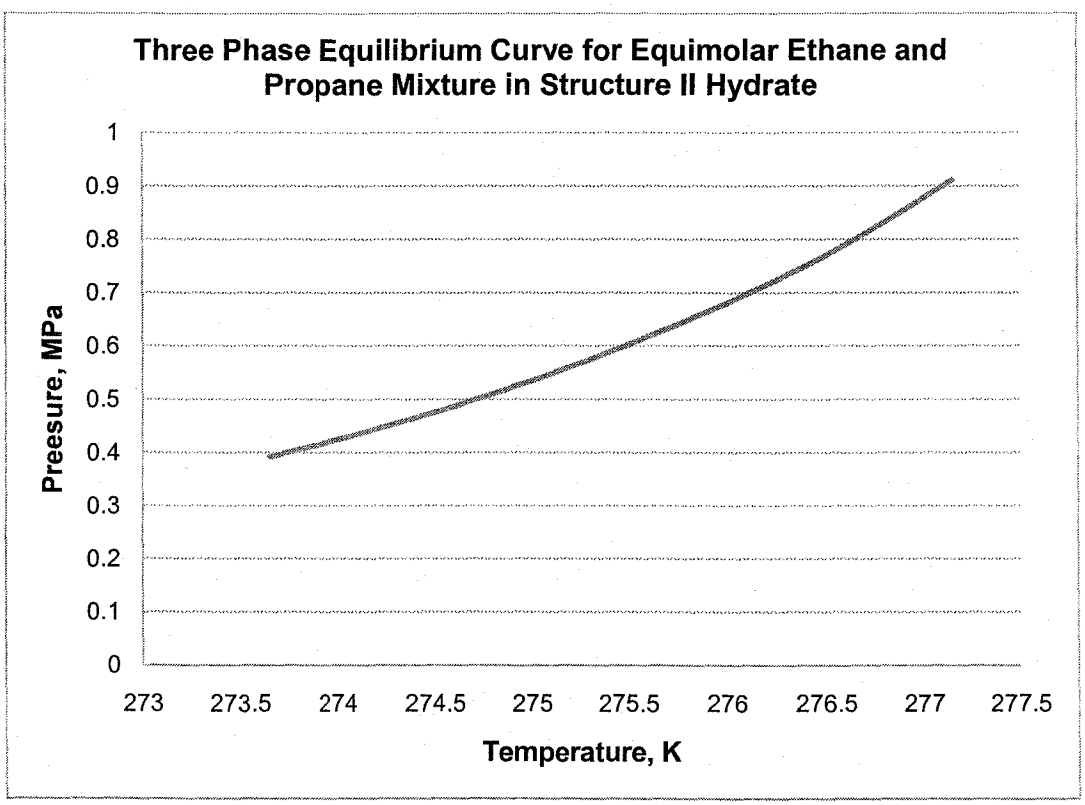
Three Phase Equilibrium Curve for Equimolar Ethane and Propane Mixture in Structure II Hydrate
Preesure, MPa
1
0.9
0.8
0.7
0.6
0.5
0.4
0.3
0.2
0.1
0
273
273.5
274
274.5
275
275.5
276
276.5
277
277.5
Temperature, K

APPENDIX B: CALCULATION OF HENRY'S CONSTANT FOR SURFACE AREA EXPERIMENTS.

From Danckwerts (1966), where temperature, *T*, is in K and Henry's constant, *H*, is in (mole/L.atm):

$$\log_{10} H = \frac{1140}{T} - 5.30$$

$$\log_{10} H = \frac{1140}{273.15 + 22} - 5.30$$

$$H = 0.0365 \frac{mole}{L \cdot atm}$$

This is the Henry's constant for CO_2 absorption in water. To account for the ionic strength in the NaOH solution:

$$\log_{10}\left(\frac{H}{H_w}\right) = -K_s \cdot I$$

$$K_s = (i_+)_{Na^+} + (i_-)_{OH^-} = (0.094) + 0.061) - 0.014$$

$$K_s = 0.141 \frac{L}{g \cdot ion}$$

Henry's constant for 1.05 M NaOH solution is:

$$\log_{10}\left(\frac{H}{0.0365}\right) = -0.141 \frac{L}{g \cdot ion} \times 1.05 \frac{g \cdot ion}{L}$$

$$\left(\frac{H}{0.0365}\right) = 10^{-0.14805}$$

$$H = 0.02596 \frac{mole}{L \cdot atm}$$

$$H = 25.96 \frac{mole}{m^3 \cdot atm}$$

Henry's constant for 1.05 M NaOH solution is:

$$\log_{10}\left(\frac{H}{0.0365}\right) = -0.141 \frac{L}{g \cdot ion} \times 2.07 \frac{g \cdot ion}{L}$$

$$\left(\frac{H}{0.0365}\right) = 10^{-0.29187}$$

$$H = 0.01864 \frac{mole}{L \cdot atm}$$

$$H = 18.64 \frac{mole}{m^3 \cdot atm}$$

APPENDIX C: SOLUBILITY DATA FOR ETHANE, METHANE, AND PROPANE

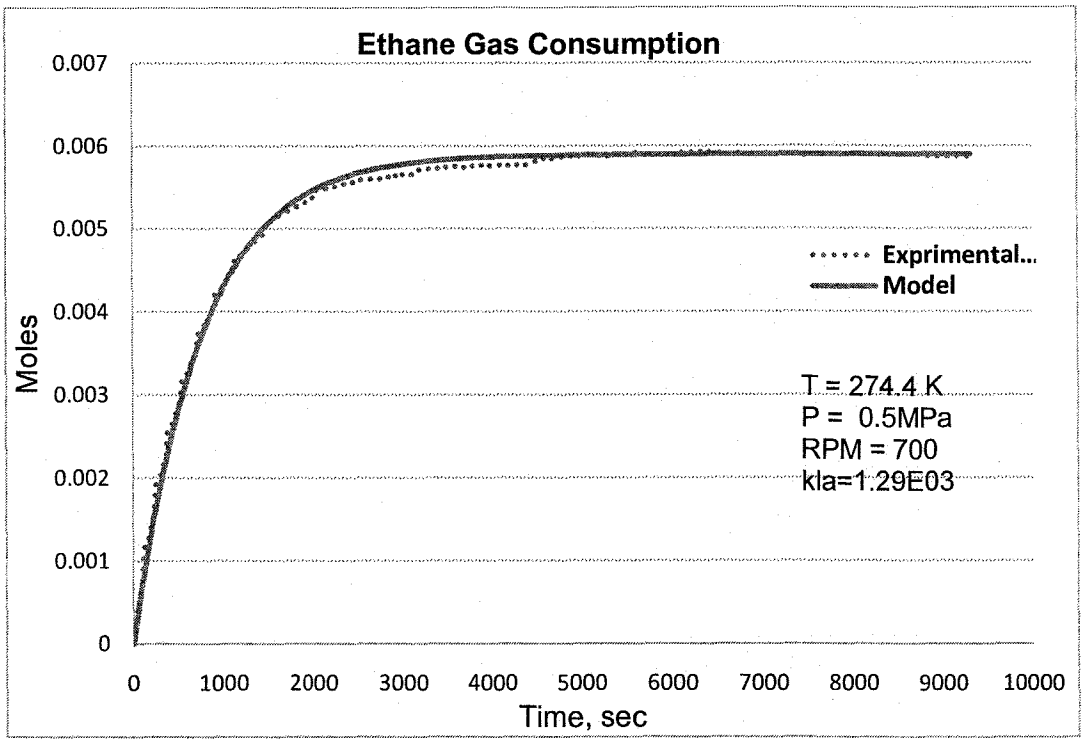
Ethane Gas Consumption
0.007
0.006
0.005
0.004
0.003
0.002
0.001
0
Moles
0
1000
2000
3000
4000
5000
6000
7000
8000
9000
10000
Time, sec
Exprimental...
Model
T = 274.4 K
P = 0.5MPa
RPM = 700
kla=1.29E03

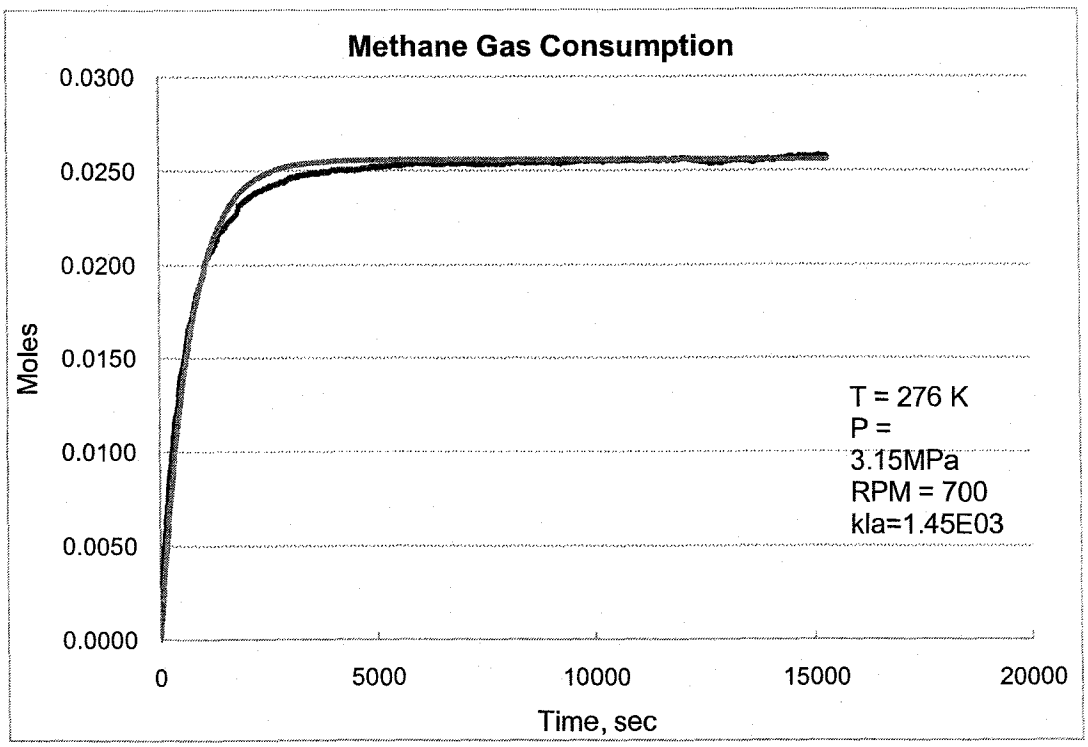
Methane Gas Consumption
0.0300
0.0250
0.0200
0.0150
0.0100
0.0050
0.0000
Moles
0
5000
10000
15000
20000
Time, sec
T = 276 K
P =
3.15MPa
RPM = 700
kla=1.45E03

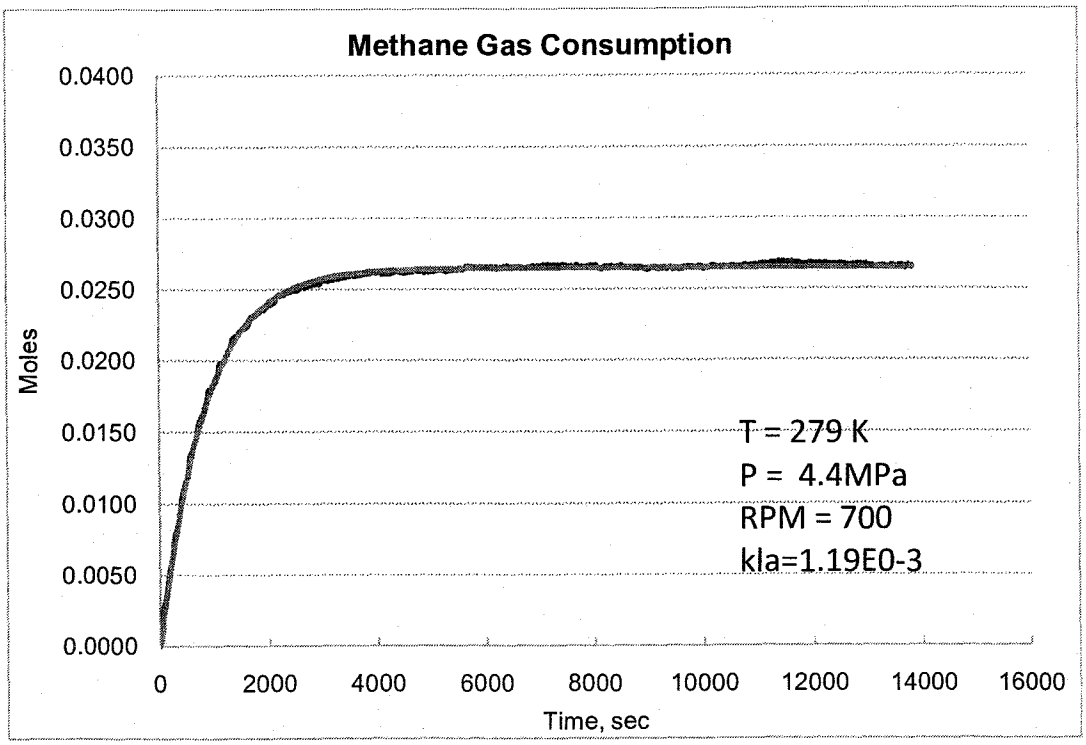
Methane Gas Consumption
Moles
0.0400
0.0350
0.0300
0.0250
0.0200
0.0150
0.0100
0.0050
0.0000
0
2000
4000
6000
8000
10000
12000
14000
16000
Time, sec
T = 279 K
P = 4.4MPa
RPM = 700
kla=1.19E0-3

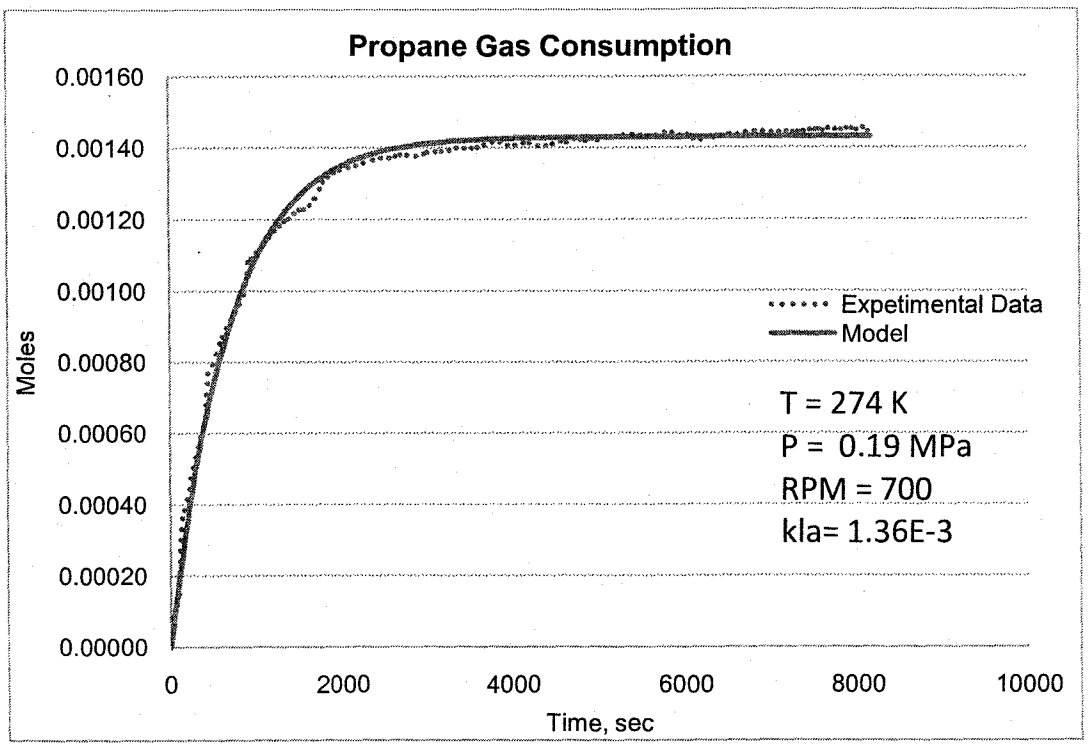
Propane Gas Consumption
0.00160
0.00140
0.00120
0.00100
0.00080
0.00060
0.00040
0.00020
0.00000
Moles
0
2000
4000
6000
8000
10000
Time, sec
Expetimental Data
Model
T = 274 K
P = 0.19 MPa
RPM = 700
kla= 1.36E-3

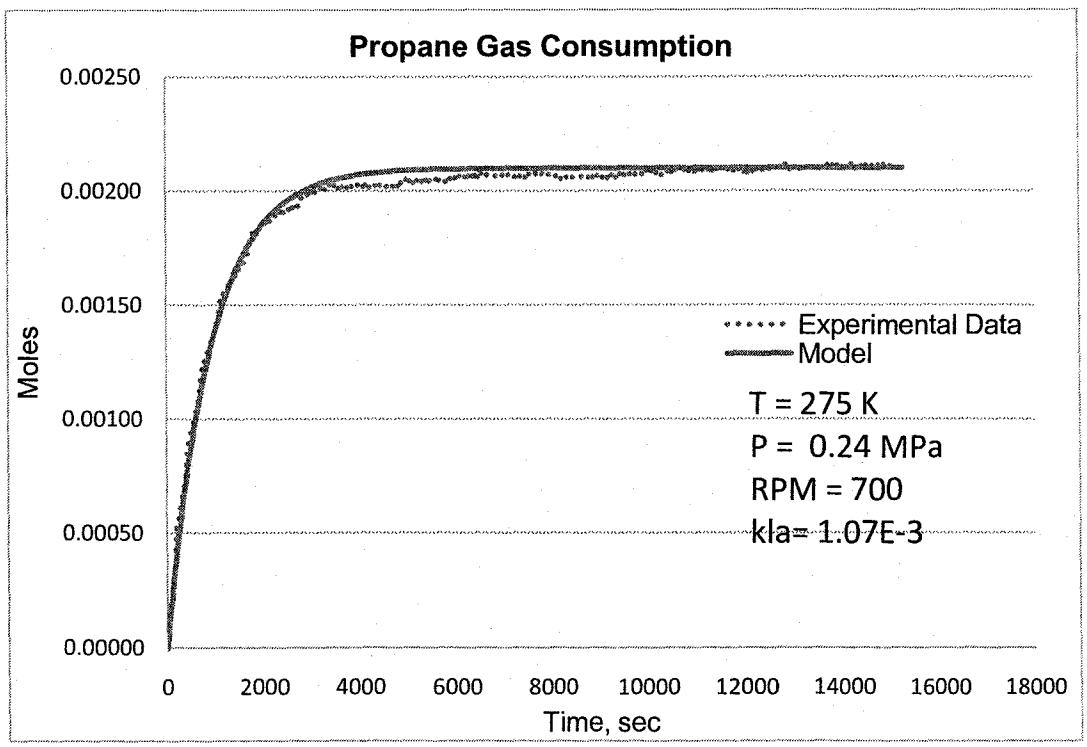
Propane Gas Consumption
0.00250
0.00200
0.00150
0.00100
0.00050
0.00000
Moles
0
2000
4000
6000
8000
10000
12000
14000
16000
18000
Time, sec
Experimental Data
Model
T = 275 K
P = 0.24 MPa
RPM = 700
kla= 1.07E-3

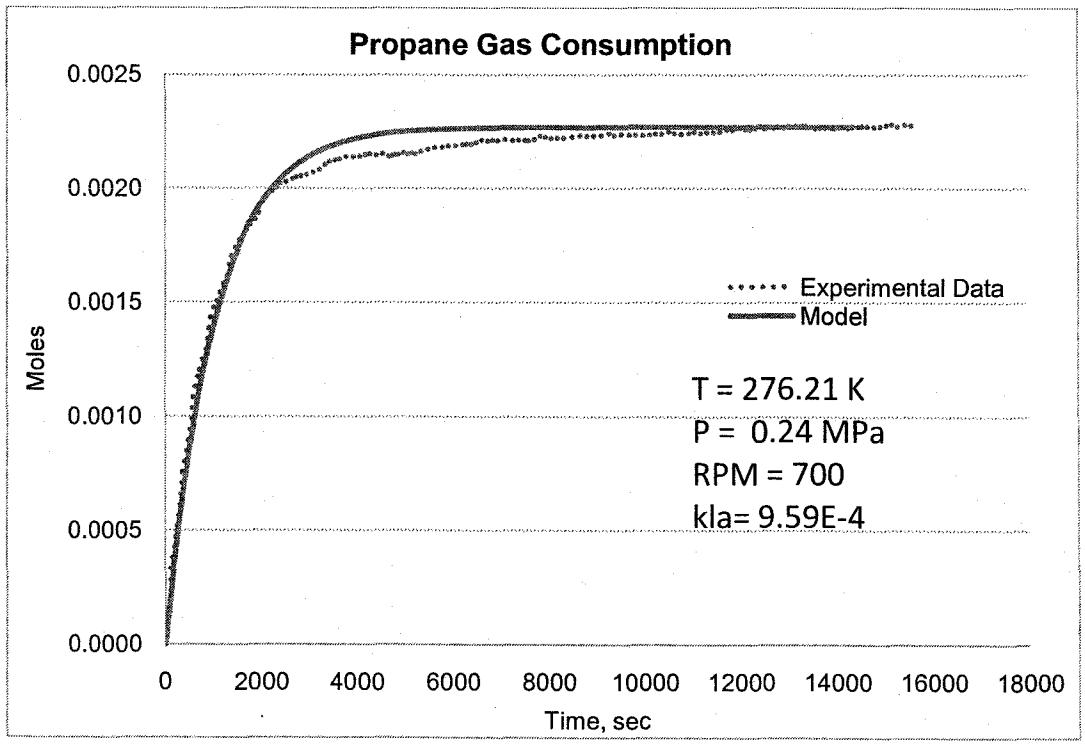
Propane Gas Consumption
0.0025
0.0020
0.0015
0.0010
0.0005
0.0000
Moles
0
2000
4000
6000
8000
10000
12000
14000
16000
18000
Time, sec
Experimental Data
Model
T = 276.21 K
P = 0.24 MPa
RPM = 700
kla= 9.59E-4

APPENDIX D: HYDRATE FORMATION EXPERIMENTS GAS CONSUMPTIONS CURVES

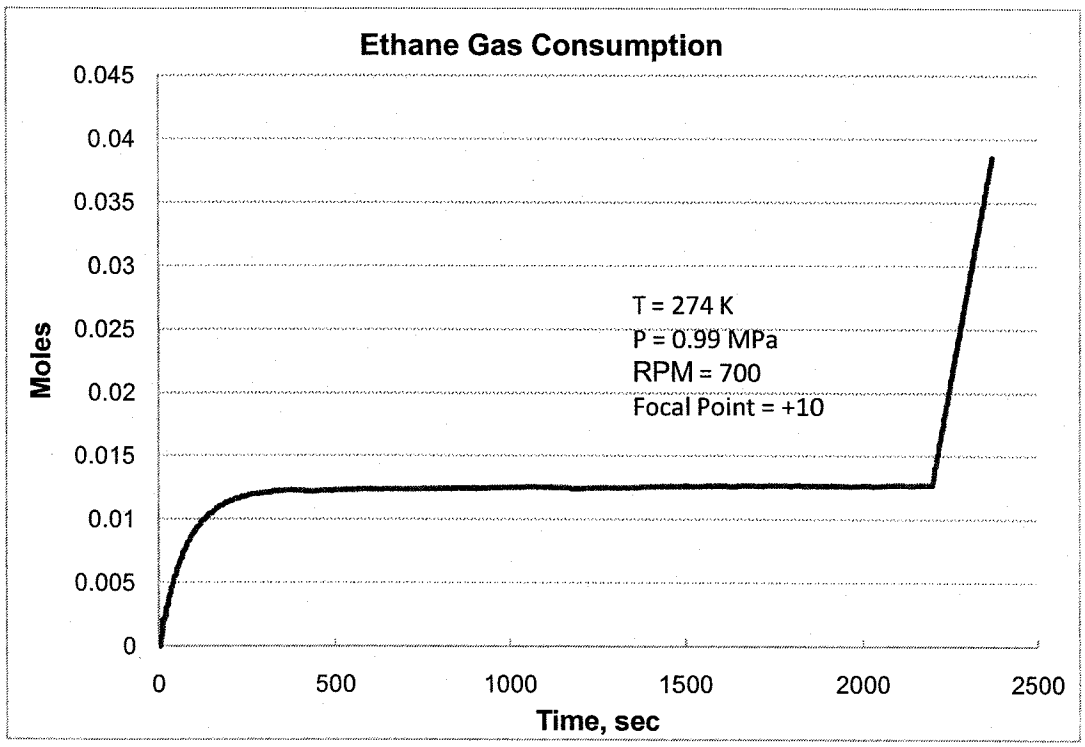
Ethane Gas Consumption
Moles
0.045
0.04
0.035
0.03
0.025
0.02
0.015
0.01
0.005
0
T = 274 K
P = 0.99 MPa
RPM = 700
Focal Point = +10
0
500
1000
1500
2000
2500
Time, sec

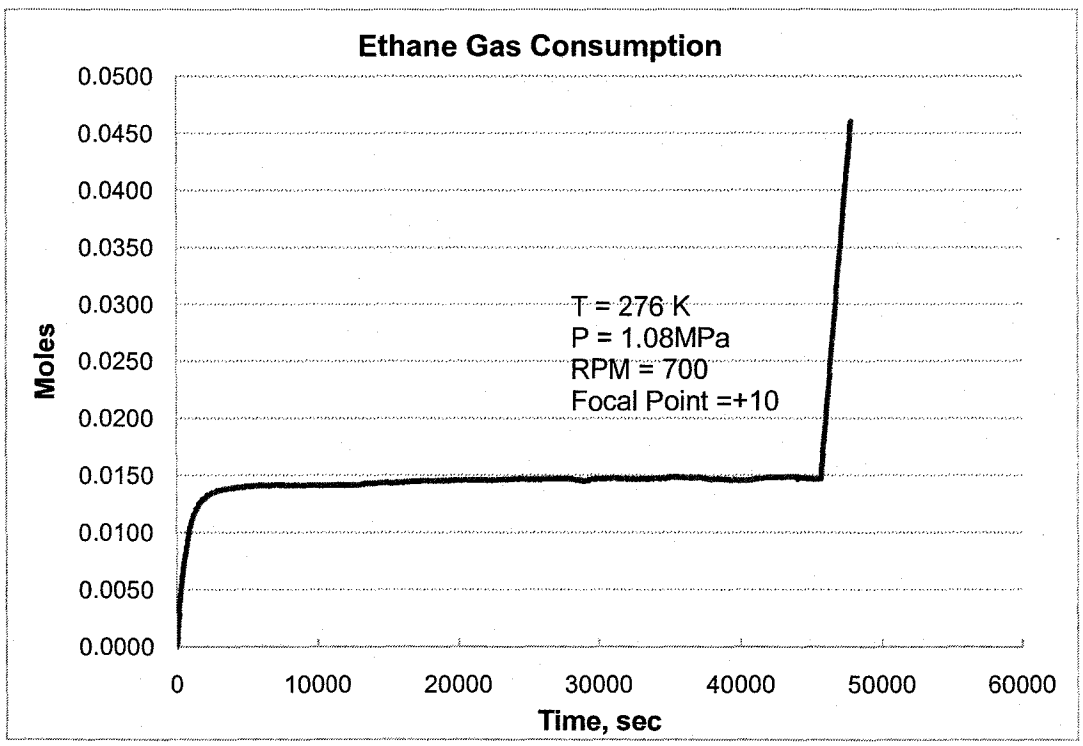
Ethane Gas Consumption
Moles
0.0500
0.0450
0.0400
0.0350
0.0300
0.0250
0.0200
0.0150
0.0100
0.0050
0.0000
T = 276 K
P = 1.08MPa
RPM = 700
Focal Point =+10
0
10000
20000
30000
40000
50000
60000
Time, sec

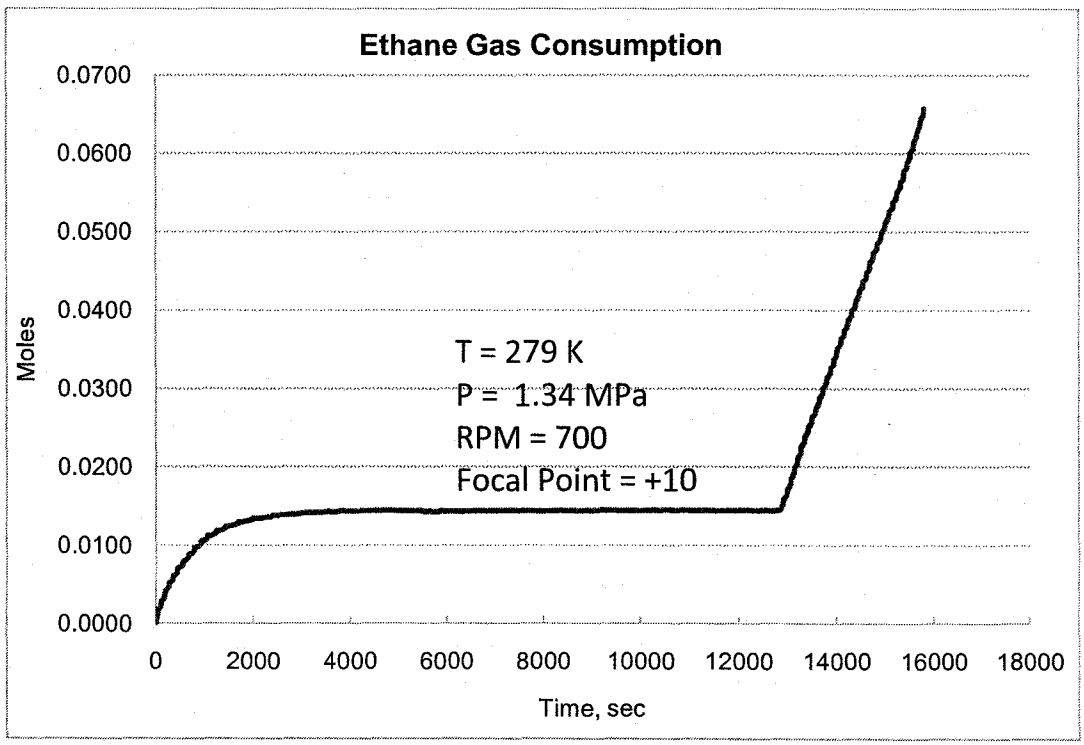
Ethane Gas Consumption
Moles
0.0700
0.0600
0.0500
0.0400
0.0300
0.0200
0.0100
0.0000
T = 279 K
P = 1.34 MPa
RPM = 700
Focal Point = +10
0
2000
4000
6000
8000
10000
12000
14000
16000
18000
Time, sec

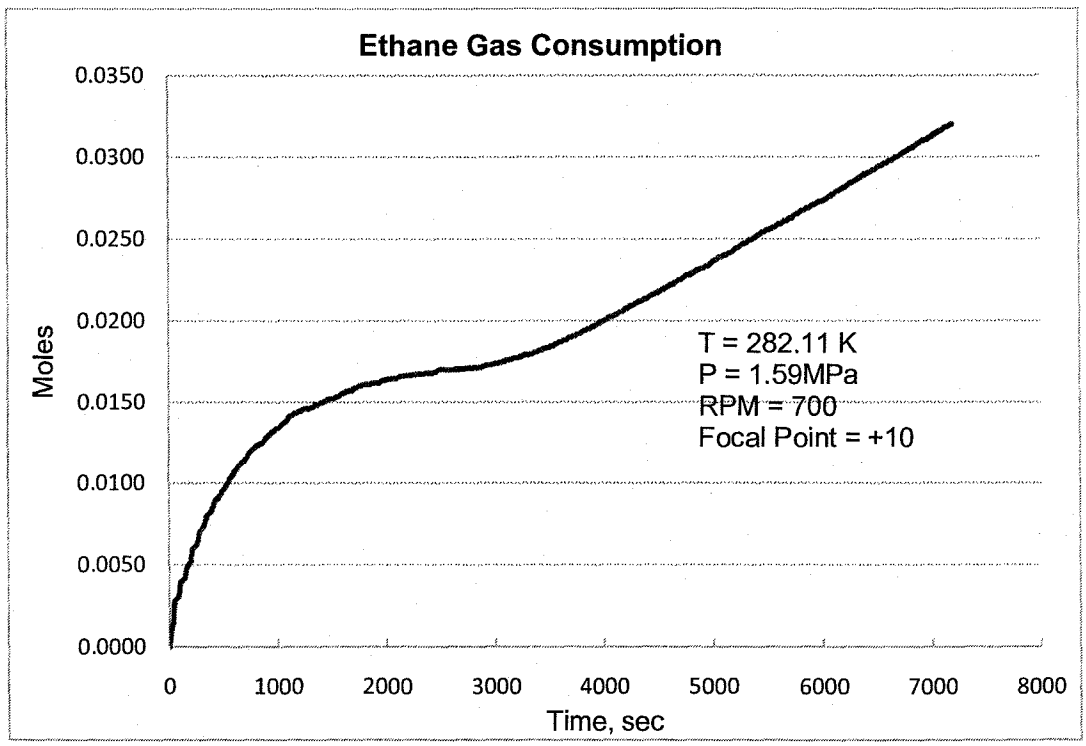
Ethane Gas Consumption
0.0350
0.0300
0.0250
0.0200
0.0150
0.0100
0.0050
0.0000
Moles
T = 282.11 K
P = 1.59MPa
RPM = 700
Focal Point = +10
0
1000
2000
3000
4000
5000
6000
7000
8000
Time, sec

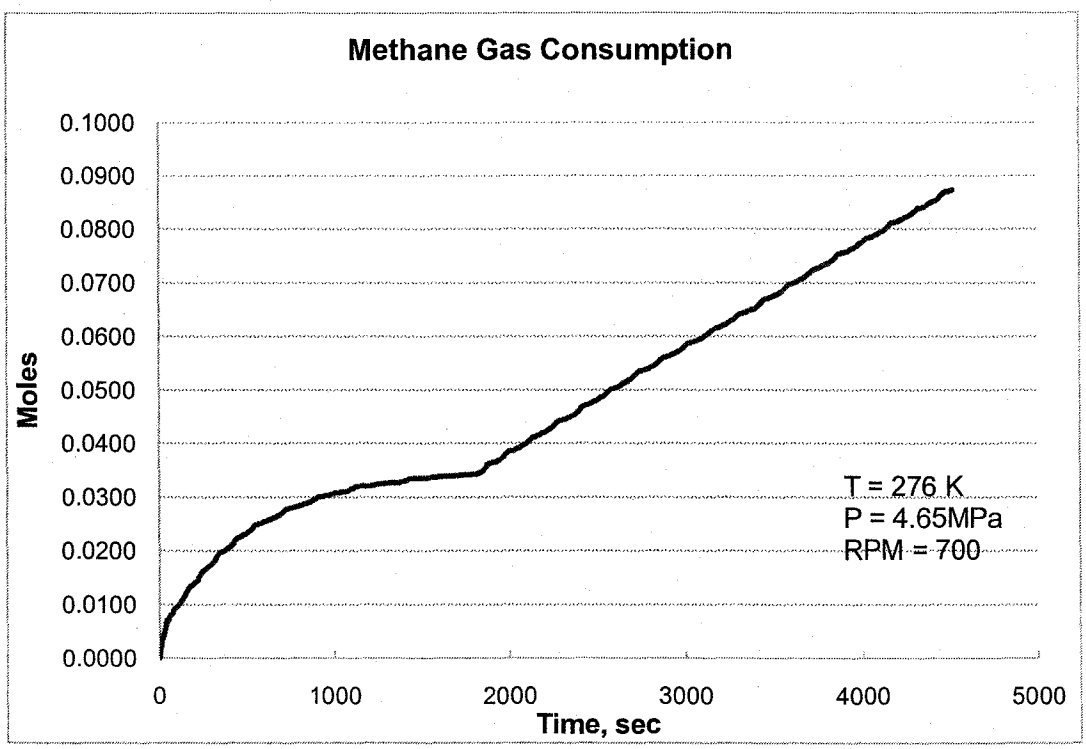
Methane Gas Consumption
Moles
0.1000
0.0900
0.0800
0.0700
0.0600
0.0500
0.0400
0.0300
0.0200
0.0100
0.0000
0
1000
2000
3000
4000
5000
Time, sec
T = 276 K
P = 4.65MPa
RPM = 700

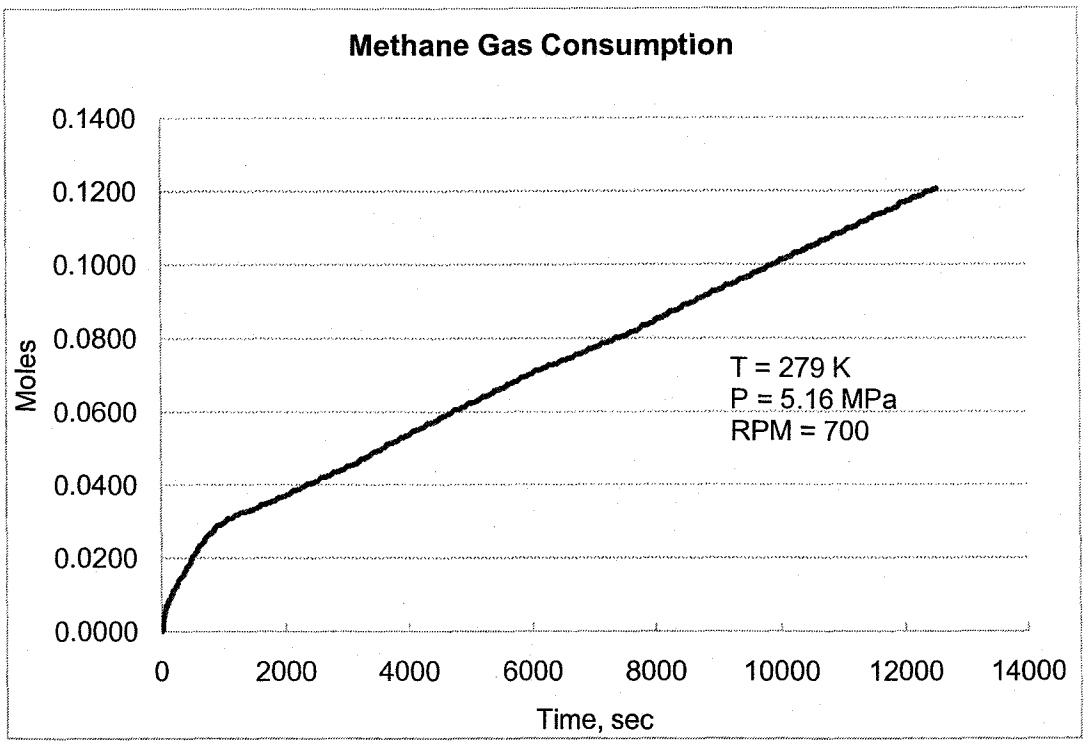
Methane Gas Consumption
0.1400
0.1200
0.1000
0.0800
0.0600
0.0400
0.0200
0.0000
Moles
T = 279 K
P = 5.16 MPa
RPM = 700
0
2000
4000
6000
8000
10000
12000
14000
Time, sec

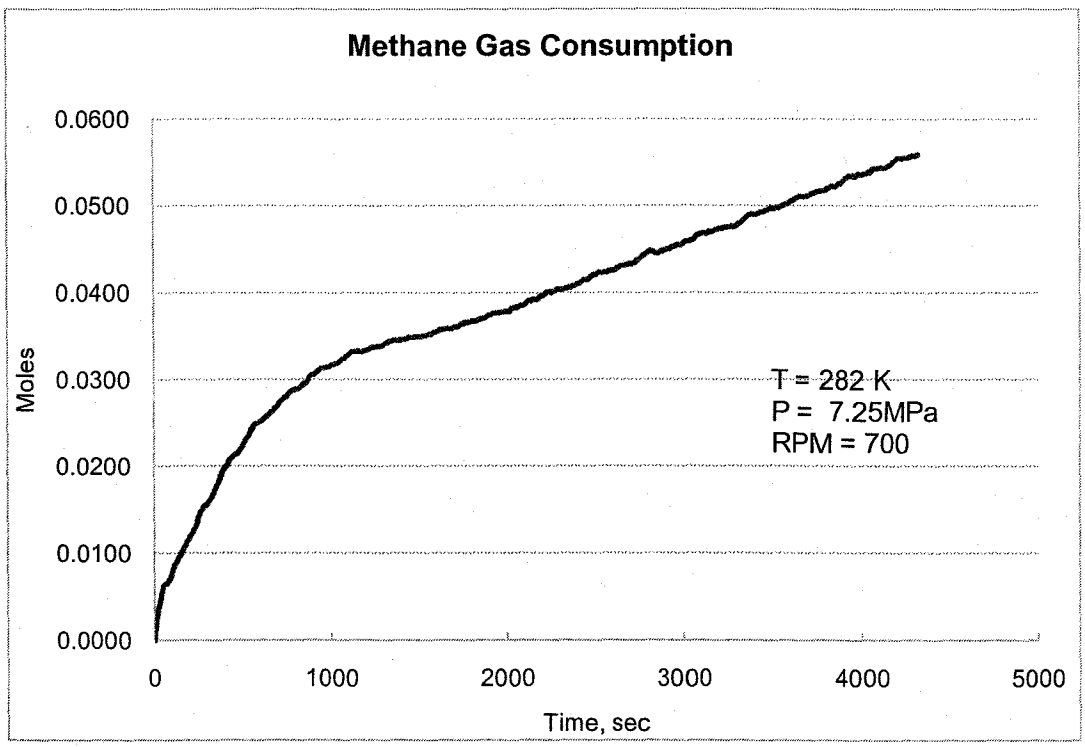
Methane Gas Consumption
Moles
0.0600
0.0500
0.0400
0.0300
0.0200
0.0100
0.0000
0
1000
2000
3000
4000
5000
Time, sec
T = 282 K
P = 7.25MPa
RPM = 700

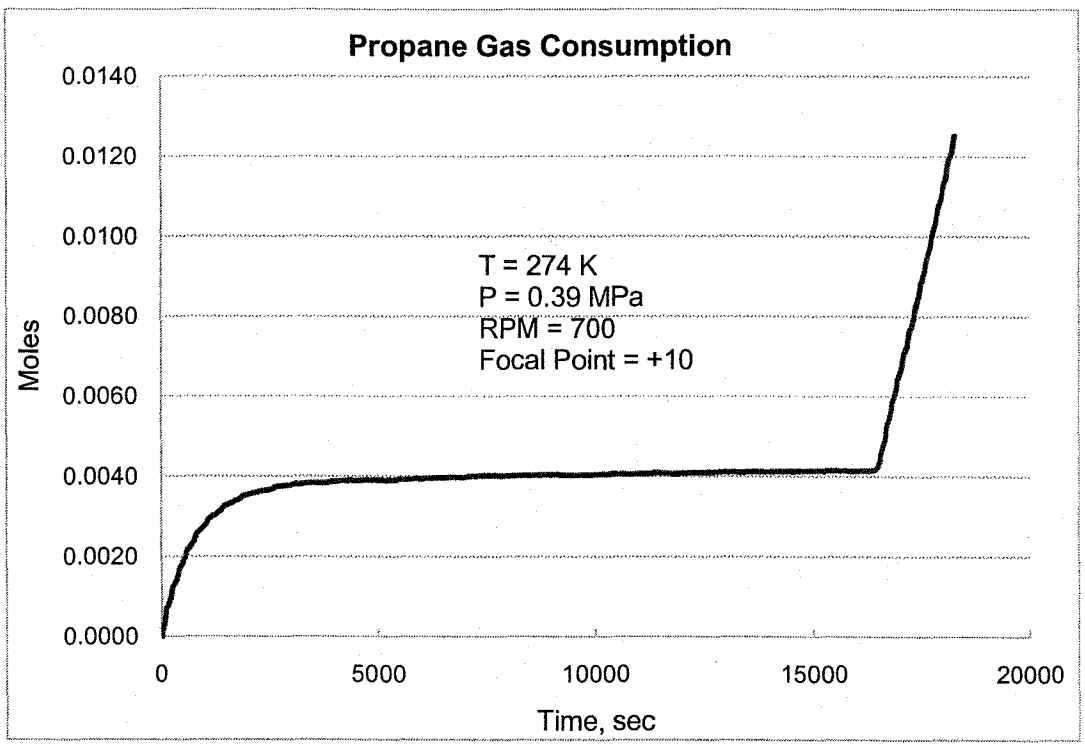
Propane Gas Consumption
0.0140
0.0120
0.0100
0.0080
0.0060
0.0040
0.0020
0.0000
Moles
T = 274 K
P = 0.39 MPa
RPM = 700
Focal Point = +10
0
5000
10000
15000
20000
Time, sec

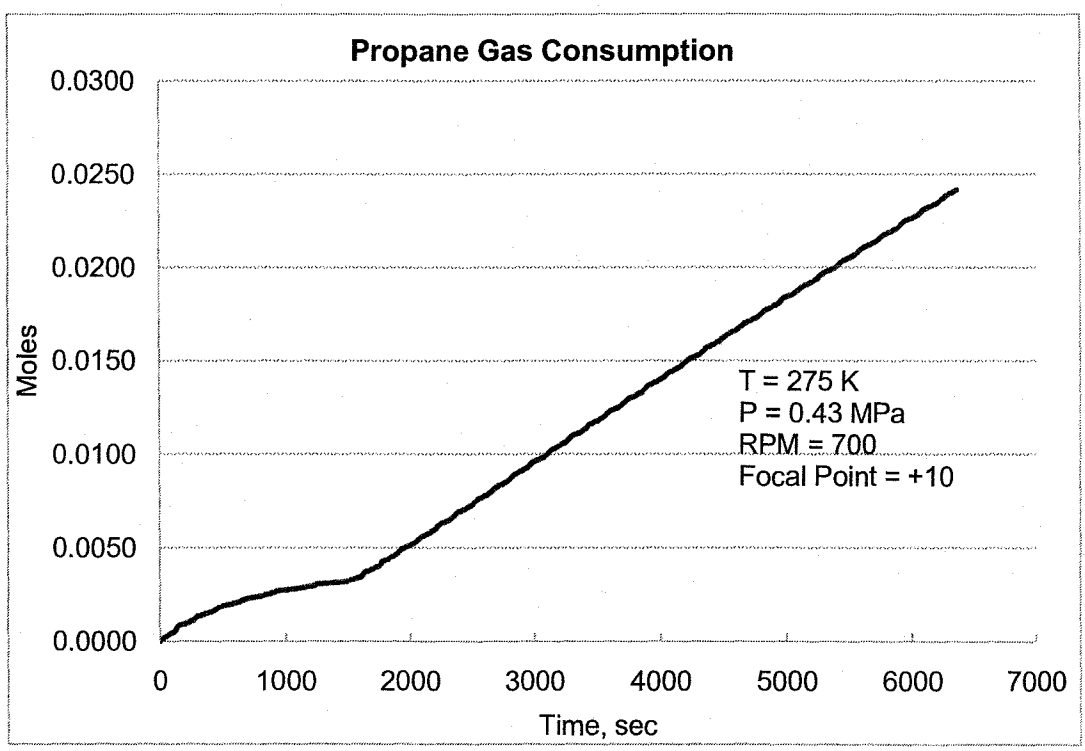
Propane Gas Consumption
0.0300
0.0250
0.0200
0.0150
0.0100
0.0050
0.0000
Moles
T = 275 K
P = 0.43 MPa
RPM = 700
Focal Point = +10
0
1000
2000
3000
4000
5000
6000
7000
Time, sec

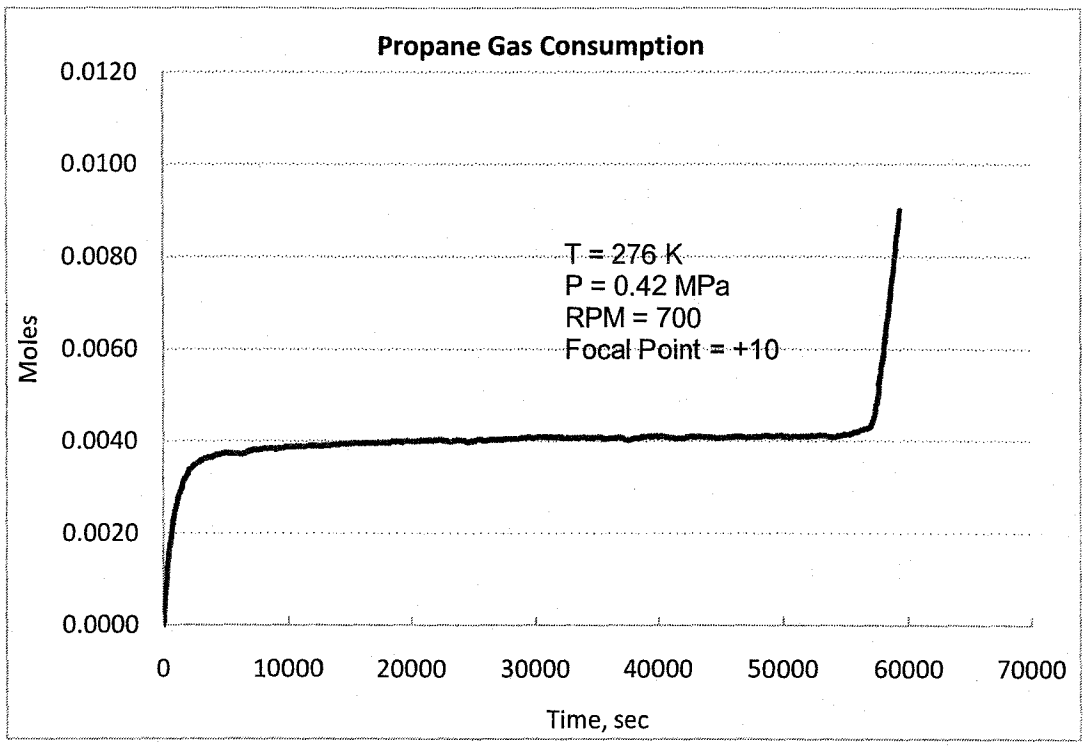
Propane Gas Consumption
0.0120
0.0100
0.0080
0.0060
0.0040
0.0020
0.0000
Moles
T = 276 K
P = 0.42 MPa
RPM = 700
Focal Point = +10
0
10000
20000
30000
40000
50000
60000
70000
Time, sec

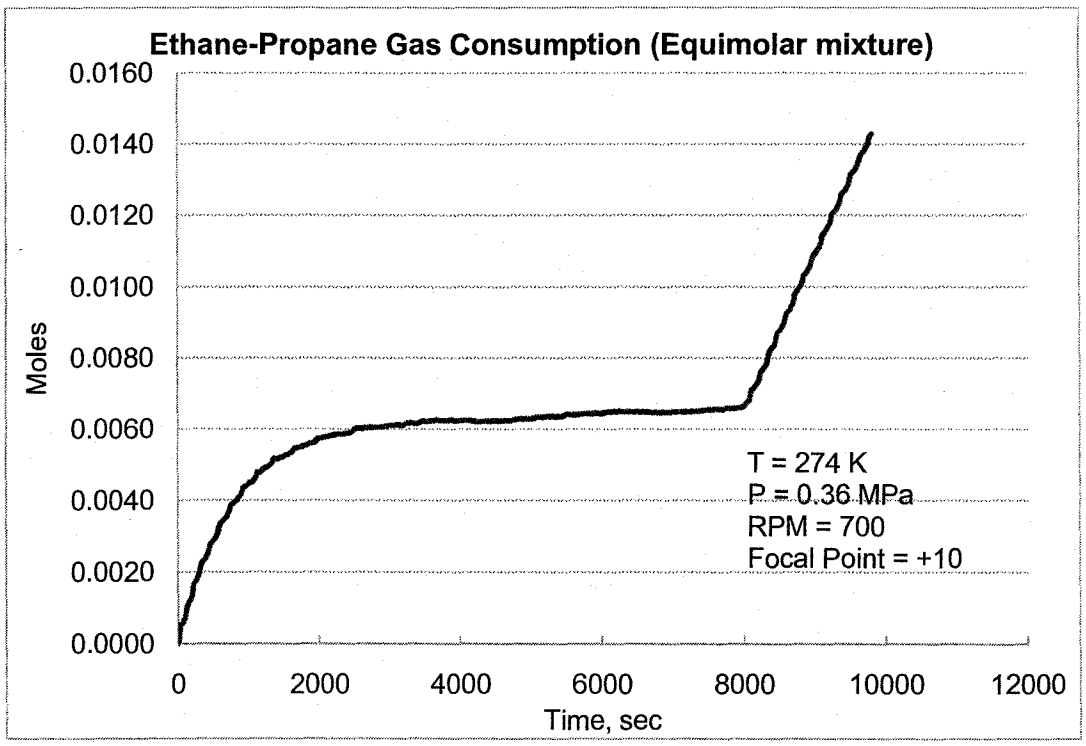
Ethane-Propane Gas Consumption (Equimolar mixture)
Moles
0.0160
0.0140
0.0120
0.0100
0.0080
0.0060
0.0040
0.0020
0.0000
0
2000
4000
6000
8000
10000
12000
Time, sec
T = 274 K
P = 0.36 MPa
RPM = 700
Focal Point = +10

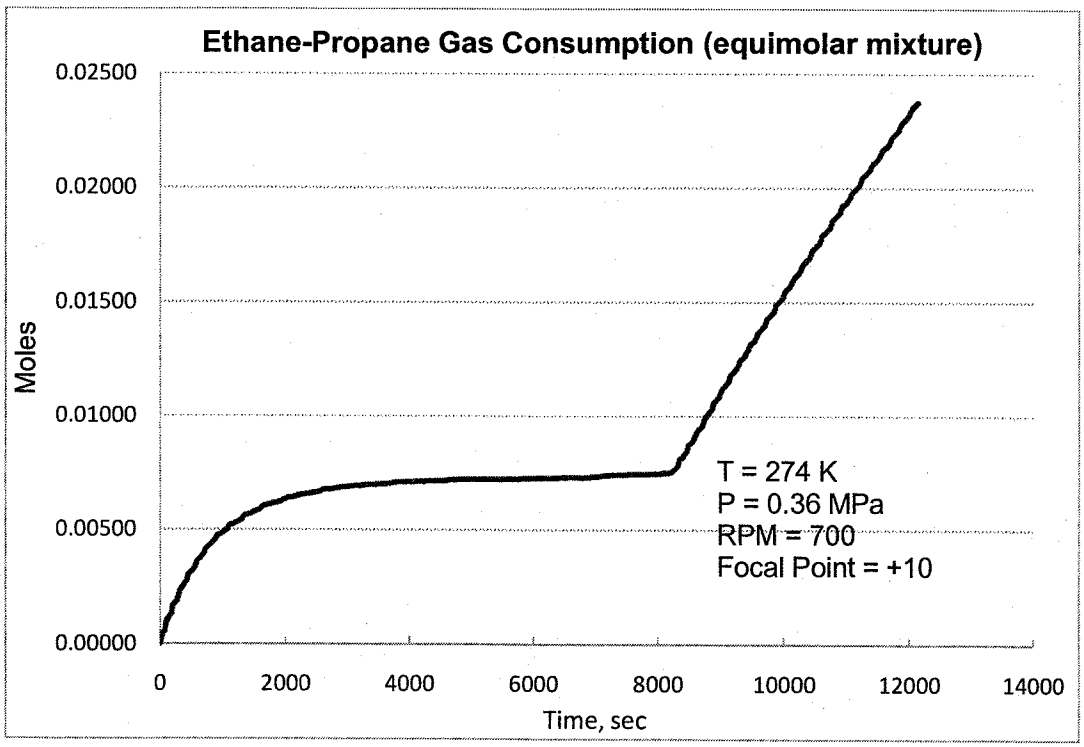
Ethane-Propane Gas Consumption (equimolar mixture)
0.02500
0.02000
0.01500
0.01000
0.00500
0.00000
Moles
0
2000
4000
6000
8000
10000
12000
14000
Time, sec
T = 274 K
P = 0.36 MPa
RPM = 700
Focal Point = +10

APPENDIX E: CHORD LENGTH DISTRIBUTIONS

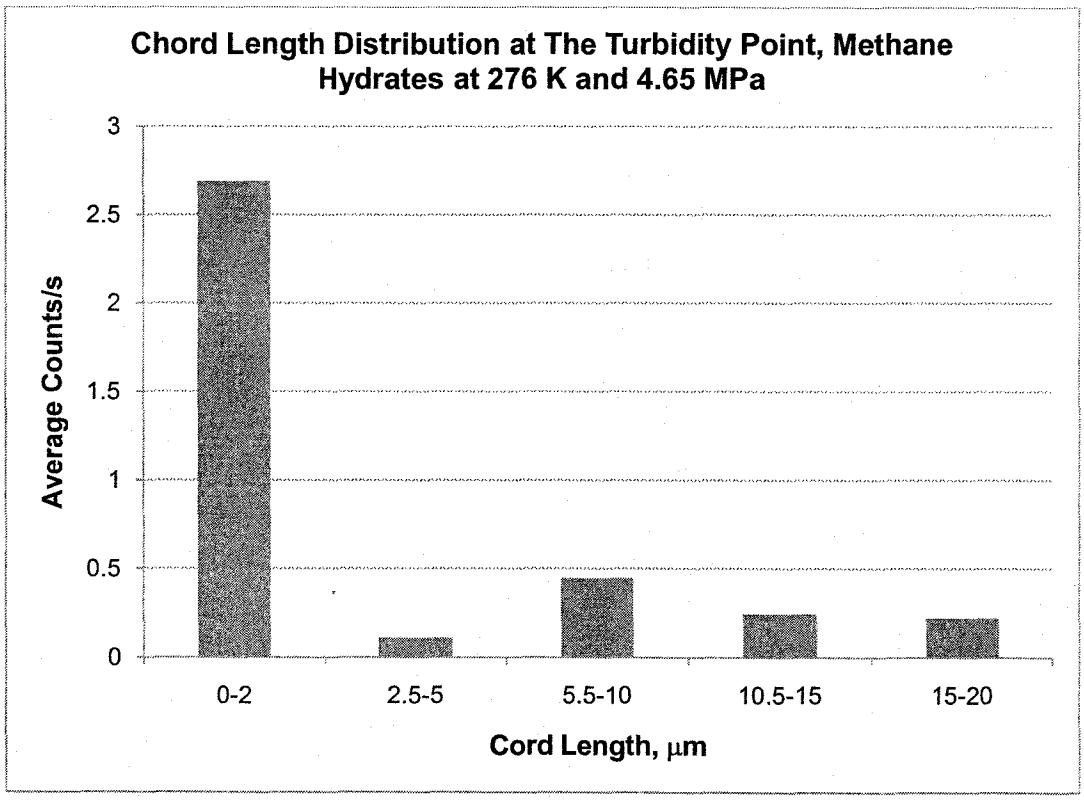
Chord Length Distribution at The Turbidity Point, Methane Hydrates at 276 K and 4.65 MPa
Average Counts/s
3
2.5
2
1.5
1
0.5
0
0-2
2.5-5
5.5-10
10.5-15
15-20
Cord Length, μm

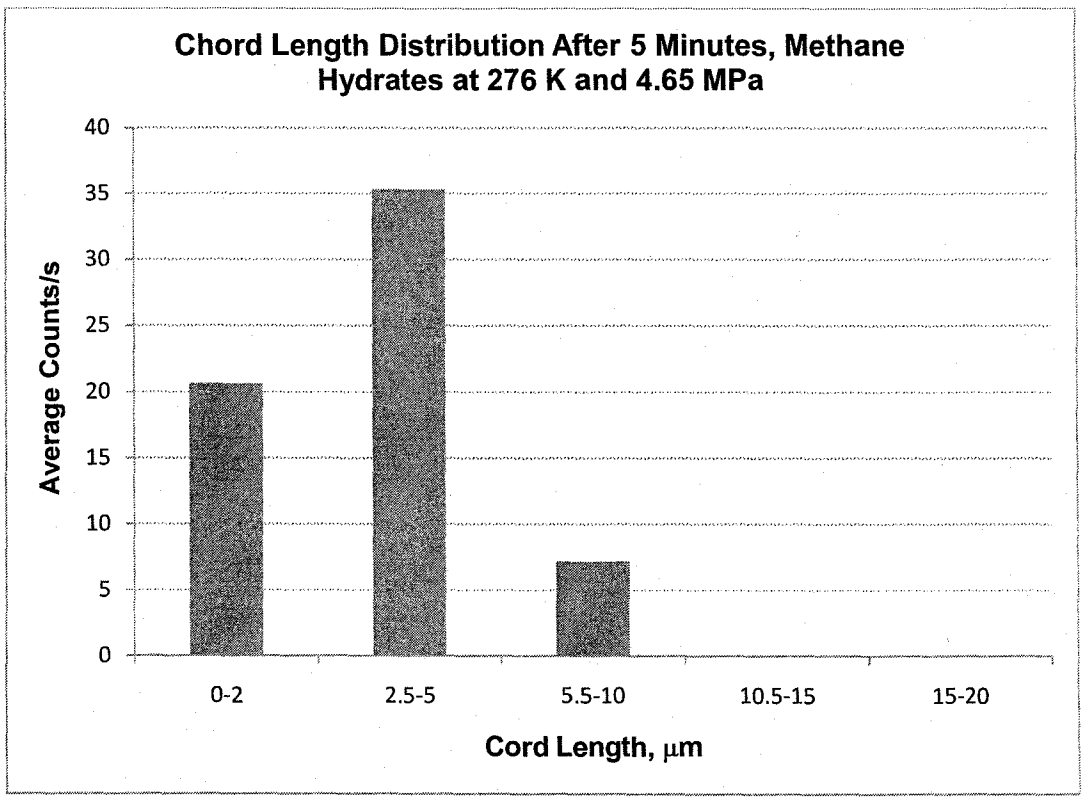
Chord Length Distribution After 5 Minutes, Methane Hydrates at 276 K and 4.65 MPa
Average Counts/s
40
35
30
25
20
15
10
5
0
0-2
2.5-5
5.5-10
10.5-15
15-20
Cord Length, μm

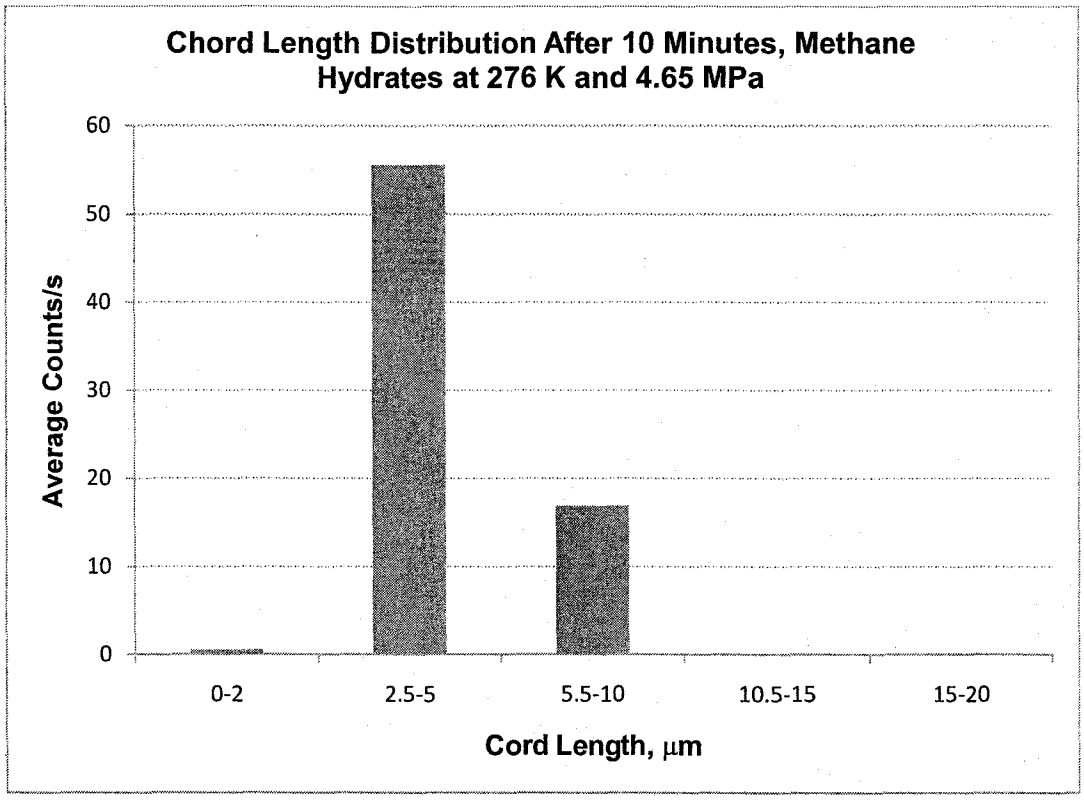
Chord Length Distribution After 10 Minutes, Methane Hydrates at 276 K and 4.65 MPa
Average Counts/s
60
50
40
30
20
10
0
0-2
2.5-5
5.5-10
10.5-15
15-20
Cord Length, μm

Appendix B: Report on Formation and Decomposition of CO_2 Hydrate in Porous Media

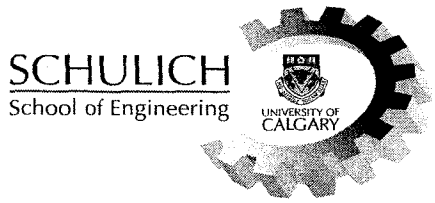

Formation and Dissociation of CO_2 Hydrates in Porous Media

Interim Report on Research Progress

Graduate Student
Chee Wee SIA

Supervisors
Brij B. Maini and P.R. Bishnoi
Department of Chemical and Petroleum Engineering
University of Calgary

CHAPTER 1

INTRODUCTION

Background

Gas hydrate is a crystalline solid that consists of low molecular weight gas molecules trapped in the cages formed by hydrogen bonded water molecules. Due to this tight structure, hydrate is capable to hold a large volume of gas in a small space. A unit volume of hydrate can release up to 180 unit volumes of gas at standard conditions. The high concentration of natural gas in hydrate formation and the large number of exploration discoveries position this source of energy on a par with bitumen and heavy-oil [Collet & Kuskra, 1998]. Using the most state-of-the-art method of prediction, Klauda and Sandler (2005) estimated that the in-situ methane hydrates resource is more than 4.4×10^{16} m^3 (STP) which would make the world's in-situ methane gas hydrate deposits surpass the recoverable conventional methane by at least two orders of magnitude [Sloan & Koh, 2008]. Figure 1.1 shows the three-phase CH_4 hydrate-equilibrium curve. Area above the curve is the hydrate stability zone. The stability zone of hydrate structure is in the low temperature and high pressures region. In natural environment this conditions can be found in shallow depth deep ocean floor and beneath the permafrost site.

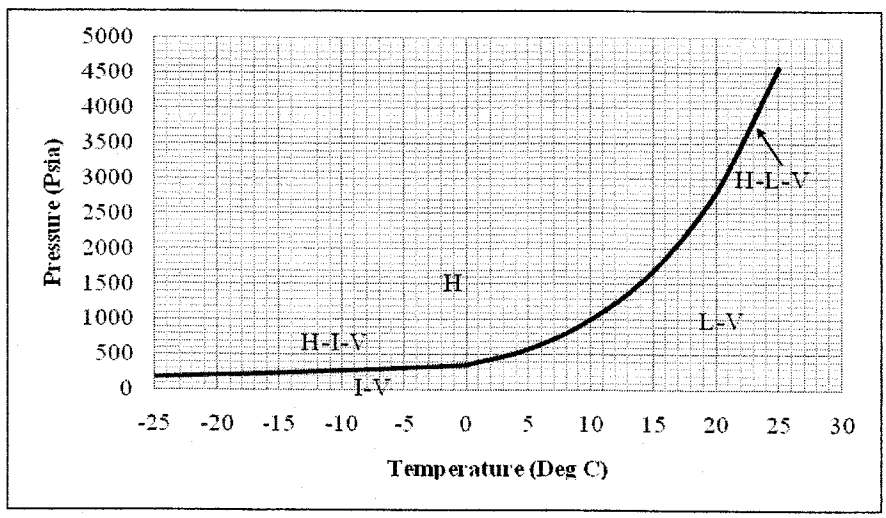

Figure 1.1: Three-phase equilibrium curve for CH_4-H_2O system

Various techniques have been proposed to recover gas from hydrate deposits. However, only three recovery techniques appear to be viable *i.e.* thermal stimulations, depressurization and inhibitors injection.

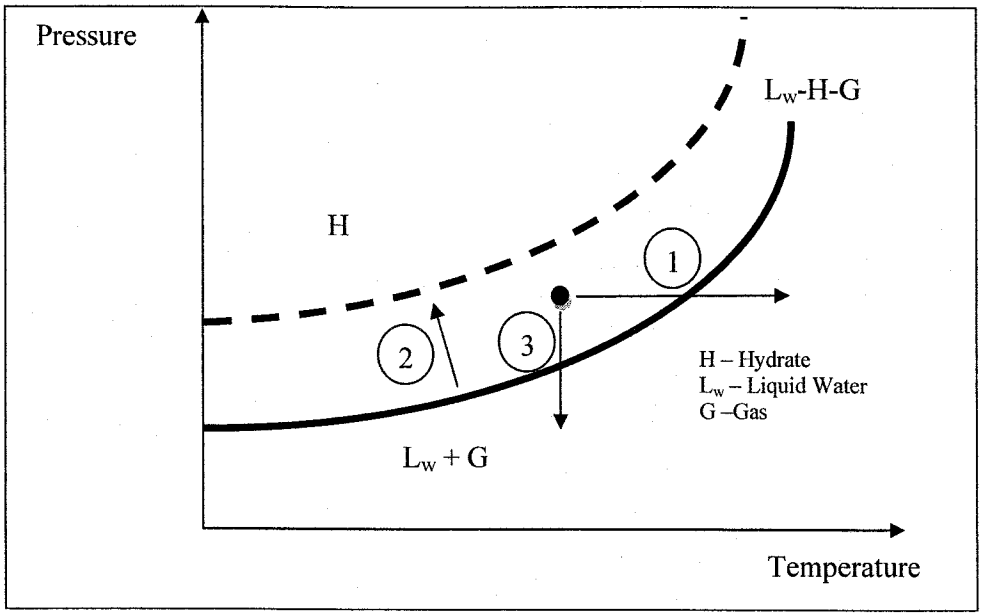

Figure 1.2: Common methods of production and the effects on the hydrate stability. (1) Thermal Stimulation, (2) Inhibitor Injection and (3) Depressurization

Thermal stimulations are the techniques where heat is introduced into the reservoir causing the destabilization of hydrate. When heat is brought into the system, it increases the temperature. To dissociate the hydrates using thermal stimulation, it is expected that the heat input is high enough to force the system to cross the thermodynamic-equilibrium curve boundary. This method is highly energy intensive and a substantial part of the injected energy may be lost to the underlying and overburden formations. In inhibitors injection, a chemical inhibitor is injected into the reservoir which shifts the thermodynamic-equilibrium curve to higher pressure and leads to dissociation of gas hydrates. From experience, this method has not proven to be very successful due to the limited transmissibility of the inhibitor. The effects only can be seen in the vicinity of the

wellbore. Depressurization method appears to be the most cost-effective technique of recovery. This technique is executed by lowering the pressure of the fluids that are in contact with hydrate by production. This then pushes the hydrate out of its stability region and result in dissociation.

A number of dissociation models to predict the production rate of gas hydrates from dissociation have been reported. Table 1.1 shows a summary of the dissociation model developed since 1982.

Table 1.1: Summary of Hydrate Dissociation Model Since 1982
[modified from Sloan & Koh, 2008]

	Heat Transfer		Fluid Flow		Kinetics	Solution Model
Model	Conduction	Convection	Gas	Water		
Holder & Angert (1982)	X		X			Numerical
Burshears *et al.* (1986)	X		X	X		Numerical
Jamaludin *et al.* (1989)	X				X	Numerical
Selim & Sloan (1989)	X	X	X			Analytical
Yousif & Sloan (1991)			X	X	X	Numerical
Makogon (1997)	X	X	X	X		Analytical
Tsypkin (2000)	X	X	X	X		Analytical
Masuda *et al.* (2002)	X	X	X	X		Numerical
Moridis *et al.* (2002)	X	X	X	X	X	Numerical
Hong *et al.* (2003)	X	X	X	X	X	Analytical
Hong & Pooladi-Darvish (2005)	X	X	X	X	X	Numerical
Nazridoust & Ahmadi (2007)	X	X	X	X		Numerical
Ahmadi *et al.* (2007)	X	X	X	X	X	Numerical

Khairkhah *et al.* (1999) suggested that for a fair prediction of gas production from hydrate dissociation, one should at least consider heat transfer, fluid flow and intrinsic kinetics. An early attempt that covers all these mechanisms was conducted by Hong *et al.* (2003) where from their analytical model, the heat transfer and kinetic of dissociation were shown to be the two most dominant mechanisms. Fluid flow effects were visible only when the permeability of the reservoir system was very low.

Pooladi-Darvish (2004) mentioned that one of the most important unknowns in modelling hydrate dissociation in reservoirs is the rock permeability in the presence of hydrates. So far, permeability models based on experimental results have not been incorporated in any simulation package. Large uncertainty still exists regarding the value of physical properties of hydrates in porous media and this leads to unreliable modelling of reservoir behaviour.

Waite *et al.* (2002) used von Herzen and Maxwell's needle probe method to measure thermal conductivity in four porous mixtures of quartz sand and methane gas hydrate. The pore pressure was set to be constant. The study discovered that the thermal conductivity decreased with increasing temperature and increased with increasing methane pore pressure. At constant pore volume, the largest thermal conductivity was in the mixture containing 33% hydrate rather than in hydrate-free sand.

Kneafsey *et al.* (2007) listed down information needed for reliable prediction of feasibility of producing natural gas from hydrate. That includes the hydrate configuration within the porous medium, the permeability and relative permeability saturation relationship. The arrangement of hydrate within the porous medium is thought to affect the thermal conductivity and the relative permeability.

Khairkhah *et al.* (1999) proposed that the controlling mechanisms of fluid flow, intrinsic kinetics and heat transfer should be integrated into the decomposition model. For this purpose, several reasonable simplifying assumptions have to be made which may degrade the prediction of the process performance. The past studies [Hong *et al.*, 2003, Hong & Pooladi-Darvish, 2005] have shown that gas production rate is highly related to the permeability of the hydrate layer. Spangenberg (2001) developed a model that relates the content of gas hydrate and its electrical properties in porous sediment. This model developed two different equations using the Kozeny grain model as the basis and concluded that the permeability is not a function of the saturation of hydrates alone, but

the formation behaviour of the hydrate in porous media strongly affects the magnitude of the permeability.

Kumar *et al.* (2010) performed an experimental study to determine the permeability of porous media in the presence of hydrate using silica glass beads as the matrix. The results obtained revealed that for less than 35% initial water saturations used to form hydrates, the hydrate tends to form on the grain surfaces. As the initial water saturation increased, the results indicate a pore-filling tendency of hydrate formation. Waite *et al.* (2004) suggested that the methane hydrate cements unconsolidated sediment when forming in systems containing an abundant gas phase.

Tohidi *et al.* (2001) presented their work on visual observation of gas hydrate formation and dissociation in synthetic porous media by means of glass micromodels. The study was conducted by forming hydrates using tetrahydrofuran, from free methane gas and from dissolved carbon dioxide. They concluded that the clathrates form within the centre of the pores spaces rather than on grain surfaces. The cementation of grains only occurred in the sections of small grain sizes. However, they did not perform the visual investigation when the gas is not the limiting factor. Hence, it is not universally accepted that the hydrates formation behaviour is pore-filling.

Kleinberg *et al.* (2005) used acoustic well log to explore the micro-pore-scale hydrate growth behaviour. They concluded that the hydrates occur as a matrix pore-filling material rather than coating on the sediment of the grain. Murray *et al.* (2006) studied the growth habit of hydrates in marine sediment using the Archie resistivity method and nuclear magnetic resonance responses. This study found that the hydrates are predominantly grown in the pore spaces and not coating the grains and the grains of the sediment remain liquid-water wet.

The preceding review of literature shows that the debate regarding the gas hydrate formation habits are still on going. This issue remains controversial. The formation habit of gas hydrate in porous media affects some of the important parameters that are required

to investigate the practicability of gas hydrate formation and decomposition in porous media.

Problem Statement

The information regarding the permeability and the knowledge of hydrate configuration within porous medium are essential for reliable prediction of the feasibility of producing natural gas from hydrates. The relative permeability, thermal conductivity and the kinetics of a rock containing hydrate is dependent on the hydrate content, the formation habit of the hydrate and the physical properties of the porous medium. The random arrangement of sand grains and variations in the size and shape of grains are the major contributors to the distribution of pore sizes that exist in the rock. This also decreases the deterministic nature of surface area of hydrates formed in the porous medium. The question is whether or not the permeability, thermal conductivity and the hydrate specific surface area of a porous medium in the presence of hydrate can be predicted from the knowledge of the properties of the porous medium and the hydrate saturation.

This research was developed to respond to the abovementioned problems. A series of work that comprises experimental work, modelling, and verification of the findings and application of the models are included. The experimental study was conducted to generate some useful permeability, thermal data and the gas production profile.

The objectives and the scope of study are discussed in Chapter 3.

CHAPTER 2
LITERATURE REVIEW

The Feasibility Investigations of Gas Production from Hydrate

Since early 1980's, even before the intrinsic kinetics model of hydrate dissociation was introduced, there was some work done to model the gas production from hydrate dissociation. However, the assumption of thermodynamic equilibrium involved in such work makes it unreliable.

One of the first models that incorporated kinetics was model developed by Jamaluddin *et al.* (1989). The investigation using this numerical model suggested that by changing the system pressure, one can move the heat transfer rate controlling regime to the regime where both heat transfer and intrinsic kinetics become dominants regime. The dissociation rate is very sensitive to the system pressure, activation energy values and the surface roughness.

Selim & Sloan, (1990) proposed an analytical model that explains the hydrate dissociation under thermal stimulation. The study discovered that the hydrate dissociation rate is a strong function of the thermal properties and the porosity of the porous medium. However, this model does not take into account the kinetics.

Yousif *et al.* (1991) conducted experimental and theoretical investigation of methane hydrate dissociation using fully hydrate saturated Barea sandstone samples. The investigation took into account the kinetics of dissociation coupled with the multi-phase flow equation, and these equations were solved numerically. The satisfactory match between the mathematical model and the experimental data showed that an appreciable amount of water is simultaneously produced with gas. This also showed that kinetics is one of the mechanisms that must be considered in gas production prediction from hydrate dissociation.

One of the attempts that incorporated all these mechanisms was the study conducted by Hong *et al.* (2003). The sensitivity analyses that were carried out using the proposed analytical model suggested that the Class 1 hydrate deposit has a huge potential. The study also discovered that the multi-phase flow is the limiting factor if the reservoir has low permeability. The importance of the kinetics and heat transfer is time dependent, where the former is more important at the early time of dissociation and the later is at the late time. The study also suggest that the surface roughness factor, $\psi = \frac{A_h}{\phi A_{geo}}$ is important to the heat transfer and the kinetics of intrinsic dissociation mechanisms (A_{geo} is the geometry surface area of the medium).

Kumar *et al.* (2010) conducted the first experimental study to investigate the permeability in the presence of hydrate and learned that the formation habit of gas hydrate in porous media is saturation dependent. The hypothesis was proposed based on the comparison between the experimental data and Kozeny grain permeability model. The numerical model that included kinetics of dissociation, heat transfer and fluid flow was developed. The conclusion according to Kumar (2005) based on the history match shows that kinetics was one of the dominant mechanisms in the dissociation process and should not be neglected.

Important Rate Controlling Mechanisms

Fluid flow

In the mass balance, the fluid flow mechanism is governed by the Darcy's equation. The major parameter that affects this equation is the permeability in the presence of hydrate.

$$\rho_f \vec{u}_f = -\frac{\rho_f k_{eff,f}}{\mu_f} \nabla P_f \qquad [2.1]$$

Where,

ρ_f = fluid density

$\vec{u}_f$ = Darcy velocity of the fluid

$k_{eff,f} = k(S_h)k_{rf}$ = effective permeability of the fluid in the presence of hydrate

P_f = pressure of the fluid

The internal rock structure such as pore shape and connectivity of the pore network influence the Archie's saturation exponent. The model proposed by Spangenberg (2001) coupled with the Kozeny grain permeability models indicated that the permeability at the certain saturation is affected by the formation habit (Kleinberg *et al.*, 2003).

Nazridoust & Ahmadi (2007) investigated the methane hydrate dissociation in sandstone core numerically. The model incorporated Kim-Bishnoi kinetic model. The results produced from this study were compared to the published experimental data. This study confirmed that gas hydrate dissociation and gas generation are sensitive to the porosity and relative permeability of the porous medium.

Kinetics

Clarke-Kim-Bishnoi model defines the kinetics of dissociation of gas hydrate as:

$$-\frac{dn_g}{dt} = K_d A_h (f_{eq} - f_g) \qquad [2.2]$$

Where,

$\frac{dn_g}{dt}$ = gas production rate from the dissociation [mol/s]

$K_d = K_\circ \exp\left[-\frac{E}{RT_{sur}}\right]$ = dissociation rate constant

A_h = Dissociating hydrate surface area

$(f_{eq} - f_g)$ = fugacities difference (fugacity at equilibrium minus fugacity of the gas)

The model shows that the kinetics is driven by the difference of fugacities, $f_{eq} - f_g$.

Ahmadi *et al.* (2007) studied the natural gas production from dissociation of methane hydrate in a confined reservoir by a depressurization well, numerically. This study

evaluated the temperature, pressure, gas mass flow and heat flux profile during the period of dissociation. The study emphasized the importance of the inclusion of kinetic of dissociation; it affects the time-evolution of the dissociation fronts.

The most promising type of hydrate deposit is the one with underlain free gas (Moridis *et al.*, 2007). This is the condition where the system is gas rich.

The preceding review of literature confirms the idea proposed by Khairkhah *et al.* (1999) that a practical feasibility investigation of the gas production from natural hydrate reservoir requires the inclusion of fluid flow, kinetics and heat transfer as the controlling mechanism.

Heat transfer

Waite *et al.* (2002) used von Herzen and Maxwell's needle probe method to measure the thermal conductivity of porous mixture of quartz sand methane gas hydrate and observed that the presence of hydrate facilitated heat transfer between highly conductive quartz grains and raised the overall thermal conductivity relative to a gas filled quartz sand sample.

As of today, there is still no reported experimental study regarding the thermal conductivity versus hydrate saturation in porous media.

Gas Hydrate Formation Habits

Kneafsey *et al.* (2007) opined on the required information for reliable feasibility prediction of producing gas from hydrates should include the arrangement of hydrate within porous medium. The formation habit may affect the thermal conductivity, and relative permeability of the porous medium containing hydrate. Murray *et al.* (2006) cited the work done by Helgerud, 2001. He listed the possible formation habits of gas hydrate in porous media. These include

- hydrate cements the grain at the grain contacts
- hydrate cements the grain uniformly

- hydrate fills the pores and partially supports the grains
- hydrate fills the pores with negligible interaction with the grains

Tohidi *et al.* (2001) conducted visual investigations of gas-hydrate formation and dissociation in porous media using glass micromodels. The visual investigations discovered that hydrates formed within the centre of pore spaces and the cementation only happened in the areas of small grain size. Thin layer of water encapsulated the grains.

The investigation of the formation habit in the deep sea environment was conducted by Kleinberg *et al.* (2003), by comparing the relative permeability to water using NMR correlation and the existing permeability models. The experimental value seems to agree with the pore filling Kozeny grain model value. This suggests that the methane hydrate in deep sea environment is primarily pore-filling and not grain-coating. The gaseous methane was found to occupy the largest pore spaces.

Waite *et al.* (2004) used a rock physics model to investigate the formation habit of gas hydrate in pore space in partially water saturated Ottawa sand. The study discovered that methane hydrate cements unconsolidated sediment when forming in systems containing an abundant gas phase. Winters *et al.* (2004) investigate the natural and laboratory-formed methane hydrate using physical properties and rock physics models. The authors believe that the formation habit of gas hydrate is determined by the location of water molecules that are available to form hydrate. By comparing the measured shear strength and acoustic velocity of three different samples, they concluded that the natural gas hydrate formed in natural environment (sample from Mallik 2L-38 well) does not cement sediment grains. The hydrate formed in Ottawa sands appeared to cement sediment grains.

Kleinberg & Griffin (2005) used the nuclear magnetic resonance (NMR) measurements that were made on the subsurface permafrost environment to study the water distribution and to predict the hydraulic permeability of the sediment. By taking advantage of the

sensitivity of NMR to water distribution, they discovered that the water was encapsulating the grains which suggest that in the permafrost environment ice formed in the interior of the pore.

The study on the marine and arctic environment conducted by Murray *et al.* (2006) was based on the computed value with density-magnetic resonance technique and the acoustic compressional velocities, the results suggest that hydrate formation habit is mainly in the pore space. The study is consistent with the discovery by Kleinberg & Griffin (2005).

The methane hydrate formation and dissociation in a partially saturated sand sample was studied by Kneafsey *et al.* (2007). They wanted to observe the changes happening due to hydrate formation and dissociation for the evaluation of hydrate dissociation kinetics in porous media.

Schultheiss & Holland (2008) presented their work at the 2008 offshore Technology Conference held in Houston, Texas and made a bold conclusion:

> "Gas hydrate-bearing pressure cores subjected to X-ray tomographic reconstructions provide compelling evidence that gas hydrate morphology in many natural sediment environments is particularly complex and impossible to replicate in the laboratory."

Worthington (2008) stressed the importance of knowing the formation habit, because a hydrate-supported structure will not produce as well as a framework-supported structure due to pore collapse with dissociation.

Kumar *et al.* (2010) studied the formation and dissociation of carbon dioxide hydrate in the synthetic porous medium. In their study, they compared the measured permeability with theoretical values derived using Kozeny grain permeability model. They concluded that the formation habit of gas hydrate is saturation dependent. Hydrate saturation below 35%, hydrate is grain-coating and vice versa.

Heat transfer in Porous Media containing Hydrate

Revil (2000) presented a theoretical model for the prediction of the thermal conductivity of unconsolidated sediments. The model employed the effective medium approach to relate the effective thermal conductivity of the isotropic mixtures of grains saturated by pore fluid, porosity and the thermal conductivities of the grains and the pore fluid.

$$\kappa = \frac{\kappa_f}{f} = \left[f\Theta + \frac{1}{2}(1-\Theta)\left(1-\Theta+\sqrt{(1-\Theta)^2+4f\Theta}\right)\right] \qquad [2.3]$$

Where, κ = effective thermal conductivity of the porous medium

κ_f = thermal conductivity of fluid in the pores

$f = \phi^{\frac{m}{1-m}}$

$\Theta = \frac{\kappa_s}{\kappa_f}$ = dimensionless conductivity ratio

κ_s = thermal conductivity of grain matrix

Waite *et al.* (2006) used the needle probe thermal conductivity data to estimate the thermal diffusivity and specific heat of tetrahydrofuran hydrate and Ih ice. The specific heat can be calculated from the combined thermal conductivity and diffusivity.

Waite *et al.* (2007) however compared the effect of pore space methane hydrate, relative to water on the bulk thermal properties of the sediment and discovered that the small difference between the water thermal conductivity and methane hydrate thermal conductivity is too insignificant to provide a sensitive measure of hydrate content in water saturated systems. They used the needle probe technique in their study. They also discovered that thermal conductivity, thermal diffusivity and the specific heat of sI methane do not vary much with temperature and pressure. However, the system understudy is not gas rich.

CHAPTER 3
RESEARCH OBJECTIVES & SCOPES

From the review of literature regarding the methods of prediction of gas hydrate production, class 1G hydrate deposit appears to be the most promising type of hydrate deposits. Technically, the dissociation of the gas hydrate in this type of hydrate deposits can be easily induced due to the fact that the hydrate stability zone is located at the base of the reservoir. A slight disturbance on the thermodynamics properties of the system promotes dissociation.

Research Objectives and Scopes

The feasibility investigation of the gas hydrate production requires proven models for reliable prediction. Cost effective investigations of the mechanisms involved can be conducted in the laboratory. The controversial matter regarding the formation habit needs to be taken into account. The main objective of this work is to provide an experimentally validated method of estimating the petrophysical properties that are required in the existing simulators.

1. The first part of this study is to develop the experimentally validated grain coating permeability model that considers the grain size distribution. This model will be used to relate the hydrate saturation and properties of porous media with Masuda permeability reduction exponent.

   Background: Until today, only one laboratory study regarding the permeability variation in the presence of hydrate was reported (Kumar *et al.*, 2010). The permeabilities at different hydrate saturation were measured and used to predict the permeability reduction exponent of Masuda's permeability model.

   Scope: In the current study, similar experiments were conducted using a sand pack with different properties. The data obtained from the current experimental study and from Kumar *et al.* (2010) are used to develop the grain coating permeability model.

Masuda permeability reduction exponent will be explained in term of the properties of the porous medium where the hydrates are formed.

Proposed Execution method: The Revil-Glover-Pezzard-Zamora permeability model is used as the basis of the formulation. The average diameter from the log normal grain size distribution is used to determine the effective mean diameter of porous media.

$$D_{eff} = \exp\left(\frac{1}{3}\left(\langle \ln v \rangle - \ln\tfrac{\pi}{6}\right) + \frac{1}{18}\sigma^2_{\ln v}\right) \qquad [3.1]$$

Where,

D_{eff} = effective mean diameter

$\langle \ln v \rangle$ = log mean of the grain size

$\sigma_{\ln v}$ = standard deviation of the grain size distribution

The effective porosity in the presence of hydrate will be evaluated accordingly and the cementation exponents will be derived from the comparison of the existing study (Glover and Walker, 2009) with the existing correlations (Attia, 2005 and Salem, 1993) to account for the tortuosity.

The model will be compared with the measured values.

Deliverables: Permeability model in the presence of hydrate for grain coating formation habit and Masuda permeability reduction exponent in term of physical properties of porous media.

2. The second part of the work concerns the model to predict the thermal conductivity of the porous medium containing hydrate with excess gas and to evaluate the sensitivity of thermal conductivity with hydrate saturation.

Background: Heat transfer, one of the important rate controlling mechanisms employs thermal conductivity as one of the important inputs. As discussed in the previous section, it was discovered that the thermal conductivity of methane hydrate does not vary much with the temperature and pressure (Waite *et al.*, (2007). So far, there is no experimentally validated model to relate the effective thermal conductivity of porous medium containing hydrate (gas rich system) with the hydrate saturation.

Execution method: The current experimental study does not provide sufficient information for thermal conductivity evaluation. The preliminary analysis shows that the kinetics is too dominant. A simple experiment involving unsteady state heat transfer will be designed.

$$\frac{1}{r}\frac{\partial}{\partial r}\left(r\frac{\partial T}{\partial r}\right)+\frac{1}{r^2}\frac{\partial}{\partial \phi}\left(\frac{\partial T}{\partial \phi}\right)+\frac{\partial}{\partial z}\left(\frac{\partial T}{\partial z}\right)=\frac{\rho C_p}{k}\frac{dT}{dt} \qquad [3.2]$$

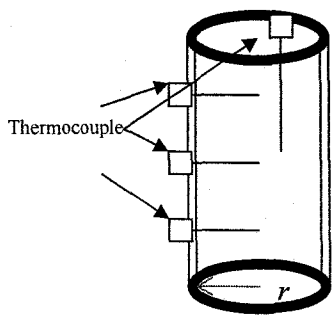

Figure 3.1: Brief proposed setup for heat conduction experiment

Initial and Boundary conditions:

$$T(r,\phi,z,0)=T_{ini}$$

$$\left.\frac{\partial T(r,t)}{\partial r}\right|_{r=0}=0 \text{ and } \frac{\partial T(L/2,t)}{\partial z}=0 \text{ and } \frac{\partial T(\phi,t)}{\partial \phi}=0$$

The experiment is to obtain the relationship between the heat diffusivity with hydrate saturation (for excess gas system). Hydrate formed in the porous medium system, at

known hydrate saturation and excess gas. During the heat transfer experiment the hydrate containing sand-pack will be transferred to a stirred bath maintained at a lower temperature.

The theoretical model introduced by Revil (2000) will be used as the basis. By taking into account the formation habit and the saturation of the hydrate in the porous medium, the thermal conductivity of porous medium in the presence of hydrate is to be formulated. The formulation will take into account the grain size distribution.

Deliverables: model to predict the thermal conductivity of the porous medium containing hydrate with excess gas.

3. The third part of the study is to relate the specific surface area of hydrate with grain properties (formation habit: grain coating).

   Background: The Kim-Bishnoi kinetic model (1987) was developed to describe the kinetics of hydrate dissociation. The dissociation was driven by the fugacities difference where it can be represented by the difference in pressure. Other terms in the model are the dissociation constant and specific surface area of the dissociating hydrate, which were well investigated by Clarke and Bishnoi (Clarke & Bishnoi, 2000 and Clarke & Bishnoi, 2001). The surface area of hydrate per unit volume of dissociating hydrate in porous media is one of the parameters that was not well investigated due to the unknown distribution and the shape of hydrate in porous media (Hong *et al*, 2003 and Jamaluddin *et al.*, 1989).

   Proposed Method of Execution: According to the numerical studies conducted by Kumar (2005) and some preliminary assessment of the current experimental result, the kinetics of dissociation is dominant throughout the dissociation process. The specific surface area can then be investigated by taking into account the grain size distribution, and reasonable assumptions. The grain size distribution is assumed to be in accordance with Gaussian log-normal distribution. It is also assumed that the gas

hydrate formation habit is grain coating, with uniform thickness, the specific surface area of the dissociating hydrate can be quantified. The result is to be validated using the data obtained from the experimental study.

Deliverables: A method to relate the effective specific surface area of the dissociating hydrate, hydrate saturation and grain size distribution for grain coating formation habit.

4. To fourth part of the study is to propose
    a. the permeability model in the presence of hydrate; pore filling formation habit
    b. the model to predict the thermal conductivity of the porous medium containing hydrate with excess gas; pore filling formation habit
    c. the method to obtain the effective specific surface area of the dissociating hydrate for pore filling formation habit

Background: A number of papers in the literature opined on the subject matter regarding the formation habit of gas hydrate in porous media. The hydrates formed in the natural environment and the hydrates formed in the laboratory have different formation habits. To results from the laboratory study need to be adjusted accordingly to account for difference in formation habit.

Proposed Method of Execution: The abovementioned objectives will be executed by using the same approach as grain coating formation habit. Since the current study does not have any experimental data about the hydrate formed in the natural environment, except for the known formation habit, the only way to validate the model is by inductive deduction.

CHAPTER 5
EXPERIMENTAL STUDY & DISCUSSION

The experimental setup used in this study is the same as the one used by Kumar *et al.* (2010).

Samples

Carbon dioxide hydrate is used for the study. The porous medium is packed in a windowed cell (Jerguson Cell). The types of sand used for this study are rounded silica sands, supplied by AGSCO .

Properties of porous medium:

- The grain size distributions of the samples were measured using a particle size analyzer.
- The sand grain density, ρ_{grain} was determined using Le-Chatelier Flask.
- The porosity, ϕ was determined from the ratio of volume of sand grains to volume of the cell.
- Absolute permeability, k_{abs} was experimentally determined using Darcy's Law for gas flow. 99.9% purity dry carbon dioxide gas is used to form hydrates.

Hydrate Formation System

The hydrate formation system was located in a temperature controlled environment. For this study, a temperature above freezing point was set. Table 4.1 shows the summary of the properties of the system.

Table 4.1: Properties of the system

Fluids	Carbon Dioxide and Water
System Temperature (° C)	3.9
Minimum pressure to form CO_2 hydrate at the given temperature	211 psia
Medium	Porous medium with known particle size distribution

Bulk Volume (cm^3)	86.1
Water Saturations (%)	30 – 67

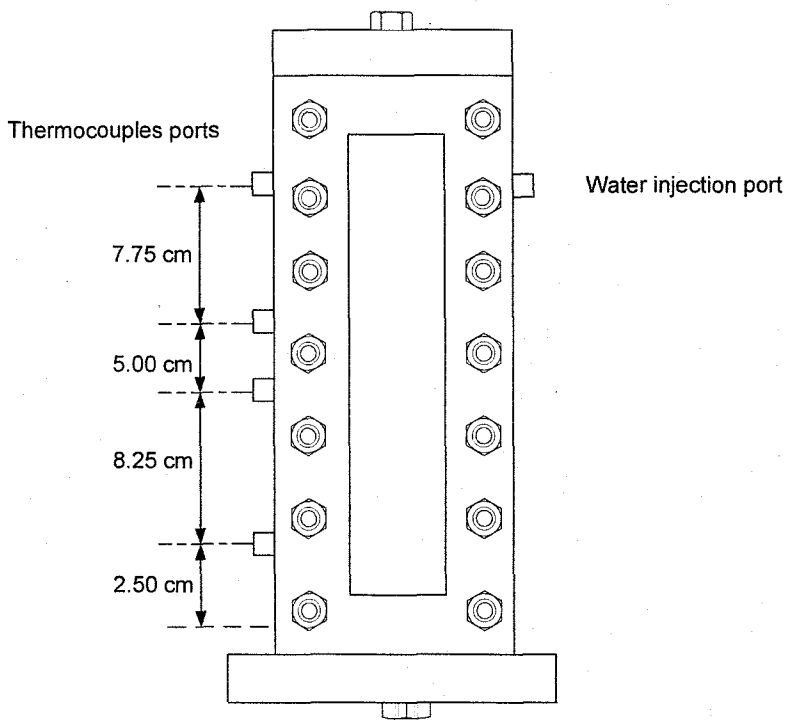

Figure 5.1: Position of thermocouples on the Jerguson Cell

The inlet pressure and the pressure difference between the outlet and the inlet of the system were measured using the calibrated pressure transducers. Pressure transducer 1 (PT1) has the capability to measure pressure up to 800 psi. Pressure transducers 2 and 3 (PT2 and PT3) are the differential pressure transducers which measure the pressure difference up to 50 psig and 250 inches of H_2O respectively. PT1 and PT2 were calibrated using a Dead Weight Tester.

Mass Flow meter was used to measure the flow rate of supplied gas in standard liters per minute. To quantify the amount of gas consumed during formation, a totalizer was used.

The outputs of the mass flow meter, thermocouples and the pressure transducers were recorded using a data acquisition system.

A back pressure regulator was used to control the outlet pressure. A bubble meter, which was located downstream of the back pressure regulator, was used to measure the produced gas flow rate.

The liquid bath containing 10% weight ethylene glycol and 90% weight of water was maintained at the desired temperature by the cooling unit. This anti-freeze solution composition could hold the bath in liquid state to as low as -10° C.

Table 4.2: Parameters Measured in this Study

	Task	Parameters	Notes
1	Properties of the Packing Measurements	Absolute Permeability	Measured using flow of gas
2		Grain size distribution	Measured using Particle size analyzer
3		Grain Density	Measured using Le-Chatelier Flask
6	Hydrate Formation investigation	Water Saturation	To be varied (30 – 67%)
7		Temperature	4 degree C, controlled by the bath temperature
8		Pressure	Dependent on the system temperature
9		Gas Consumed	Recorded in standard litres
10	Permeability Measurement	Outlet Pressure	Set by the back pressure regulator
11		Pressure difference	Measured using Pressure transducers 2 & 3
12		Inlet Pressure	Measured using Pressure transducer 1 against atmospheric pressure
13		Gas Flow Rate	Measured using Mass flow meter and corrected to the system pressure
14	Hydrate Dissociation Investigation	Initial Pressure in the system	$P_{in} - \frac{\Delta P}{2}$
15		Outlet Pressure	$P_{in} - \Delta P \approx P_{BPR}$ *pressure*
16		Gas produced	Collected in gas production unit, the cross-sectional area of the cylinder = 60 cm^2
17		Temperature	Dissociation Temperature recorded by thermocouples

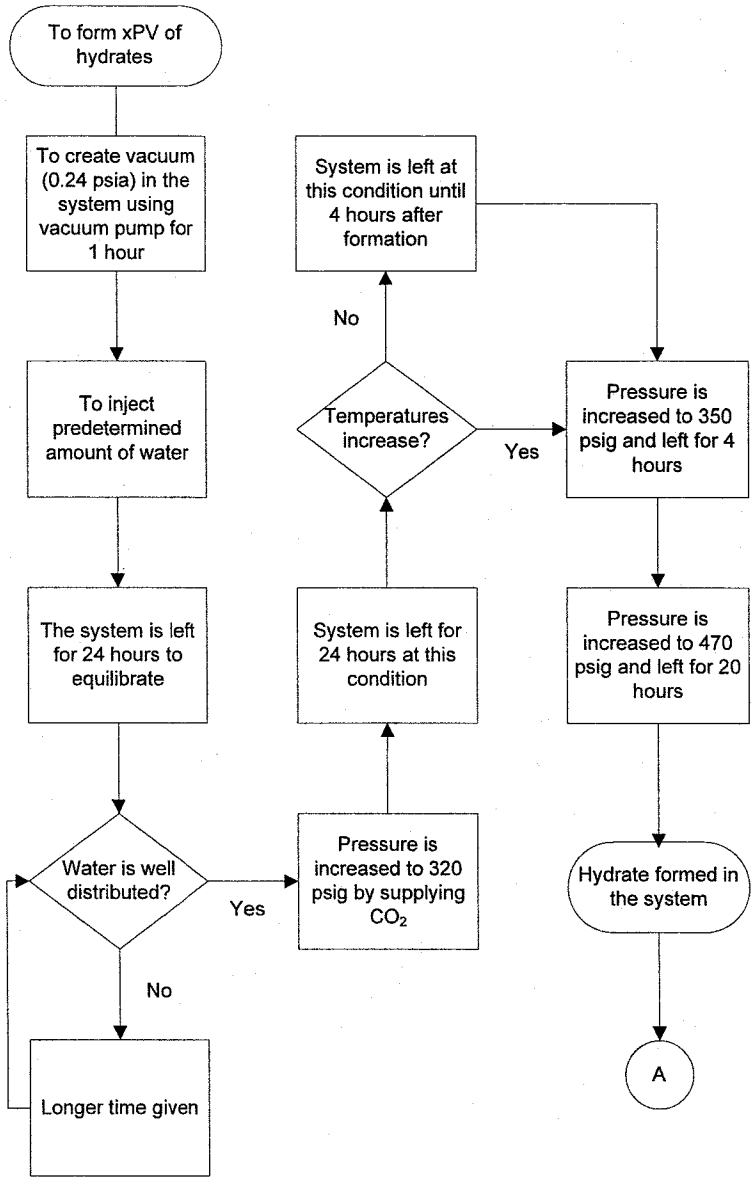

Figure 5.2: Formation of Hydrates

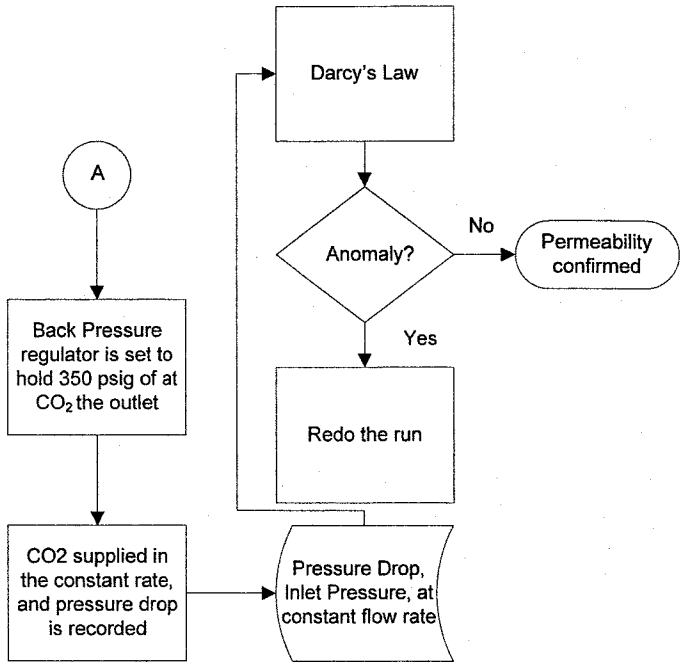

Figure 5.3: Permeability Determination

Figure 5.3 shows the flow on how the hydrate dissociation experiment is conducted.

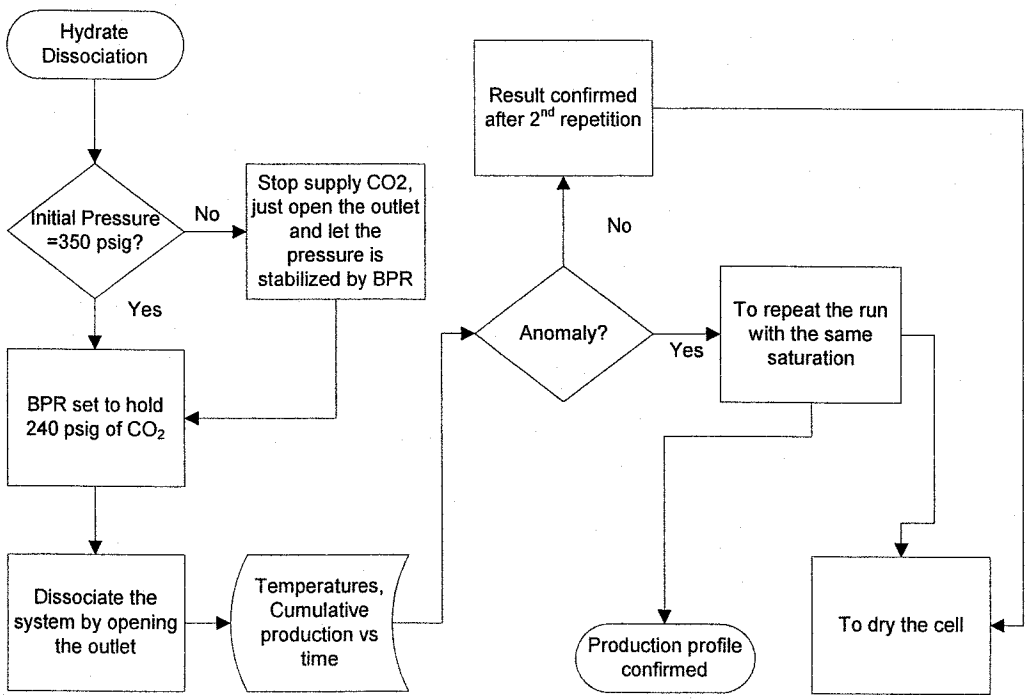

Figure 5.4: Hydrate Dissociation Investigation

Experimental Results

Some of the experimental results obtained from the laboratory work are presented in this section. This section is divided into five parts.

Part A: Hydrate Formation

Part B: Permeability and the repeatability

Part C: Existing models versus experimental results

Part D: The dissociation of hydrates and cumulative gas production

Part E: Temperature profile during dissociation

The biggest challenge in this experimental study was to obtain uniformly distributed hydrate in the system. The uniformly distributed hydrate gave consistent and repeatable results.

Part A: Hydrate Formation

Hydrate formation is exothermic in nature.

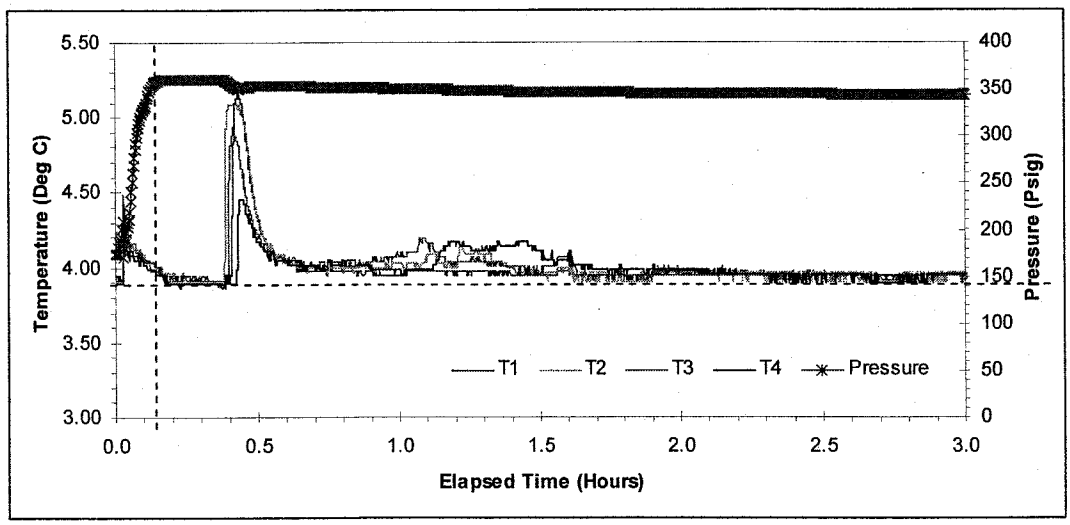

Figure 5.5: Temperature and Pressure versus Elapsed time during formation of hydrate (S_{wi} = 45%)

In this experimental study, temperatures at the designated locations were recorded. When the pressure of the cell was increased above the hydrate formation pressure, and hydrate was expected to form.

Figure 5.5 and figure 5.6 are the examples used to show the formation characteristics. The samples have different initial water saturations, 45% and 60% respectively. Based on the temperatures recorded by the thermocouples and gas inflow recorded by the mass flow meter these two samples are compared.

Referring to Figure 5.5, when the pressure was increased to 350 psi, the start of the hydrate growth only can be witnessed after 14 minutes. The continuous supply of CO_2 gas maintained the pressure above the hydrate formation pressure. The peak temperature recorded by each of the thermocouple was different. Even the initiation periods of hydrate formation at the specified location was different.

Random smaller peaks of temperature can be observed there after. No general order can be observed. After 2.5 hours no obvious new peaks recorded.

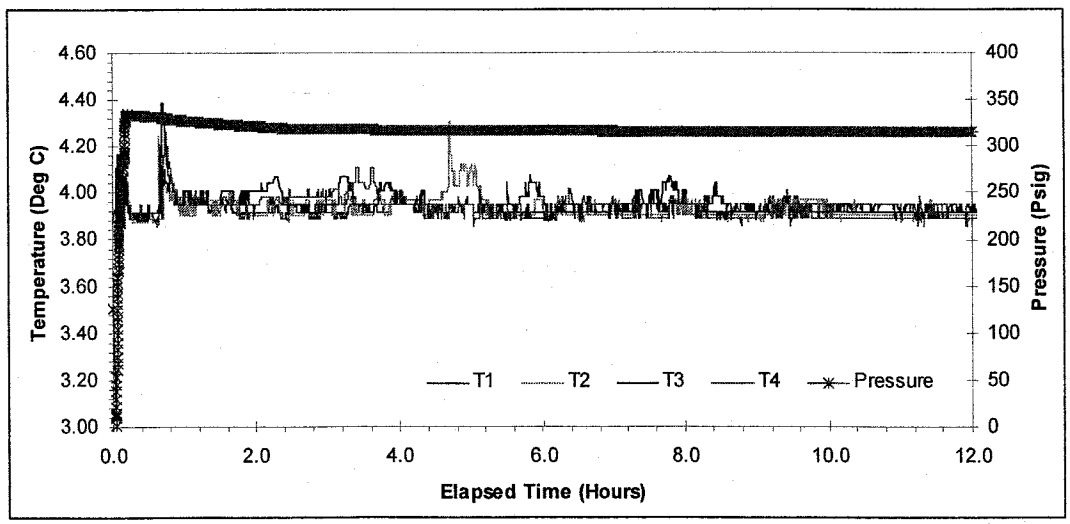

Figure 5.6: Temperature and Pressure versus Elapsed time during formation of hydrate (S_{wi} = 62%)

Figure 5.6 shows the graph of temperature and pressure versus elapsed time during hydrate formation for sample with 60% initial water saturation. More random peaks can be observed. Similar to Figure 5.5, no general temperature patterns can be observed.

Based on these two figures, the hydrate formation temperature profile cannot be used as the indicator to tell how well distributed the hydrate in the porous medium. The random peaks of temperature can be observed in all the samples.

Part B: Permeability and the repeatability

Permeability of the porous medium in the presence of hydrate was measured by varying the flow rate against pressure. Not much information regarding this aspect is published.

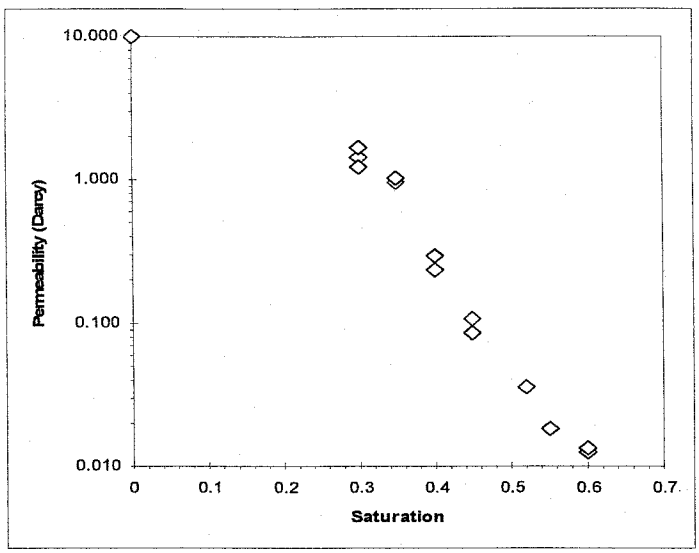

Figure 5.7: Graph of Permeability versus initial water saturation

Figure 5.7 shows the graph of permeability of the porous medium in the presence of hydrate versus the initial water saturation forming the hydrate. The investigation was conducted for the saturation varying from 30% to 62%. The absolute permeability of the porous medium is 10 Darcy. With 30% hydrate formed in the system, the permeability dropped below 2 Darcy, and the porous medium is almost impermeable when the hydrate saturation is above 60%. Each of the run was repeated twice, and the results are

repeatable. The repeatability is not an issue if the distribution of water in the porous medium is uniform.

Kumar *et al.* (2010) conducted similar study but using bigger grain size medium. The trend observed in his work is almost similar.

Part C: Existing models versus experimental results

Kleinberg *et al.* (2003) elaborated the existing permeability models to study the formation habit of gas hydrate formed in the sample formed in natural environment. In the current study, the models are compared with the measured permeability.

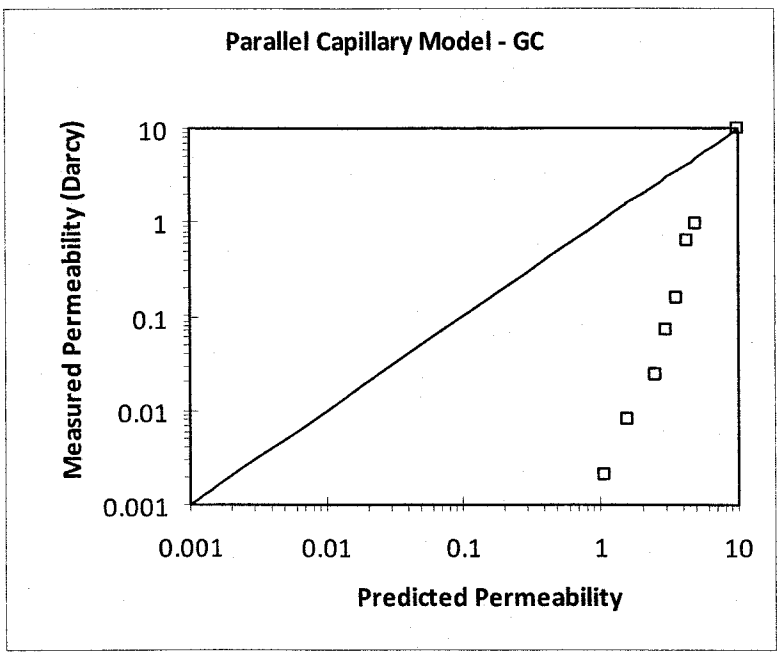

Figure 5.8: Measured permeability versus predicted permeability using parallel capillary model (grain coating)

Figure 5.8 is the graph of measured permeability versus predicted permeability using parallel capillary model for grain coating formation habit. From the comparison, it is obvious that either the capillary permeability model is not a good model for permeability prediction or the hydrate formed in the system under study is not grain coating. Based on

the published results by Kleinberg *et al.* (2003) and Kumar *et al.*, (2010) the performance of this model is questionable. This is due to the omission of the tortuosity and the control of pore throats on permeability.

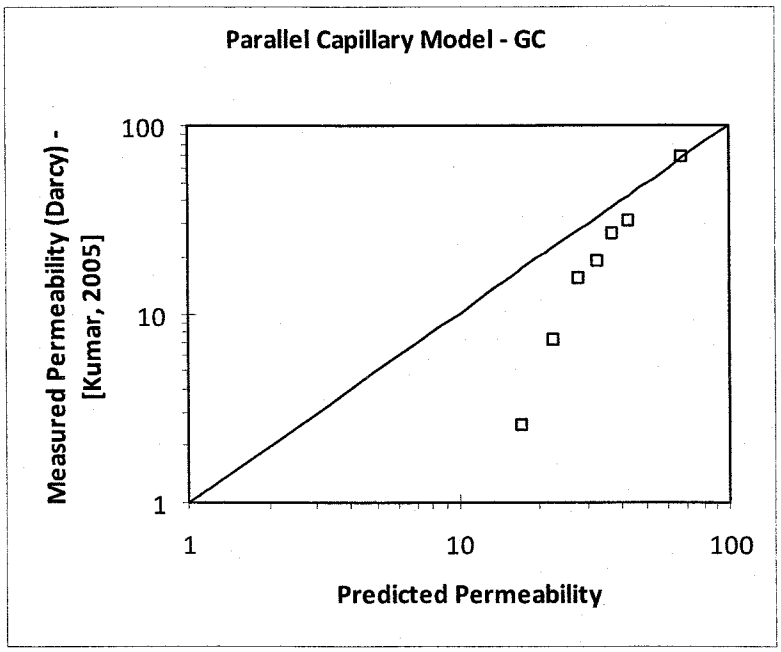

Figure 5.9: Measured permeability versus predicted permeability using parallel capillary model (grain coating) (measured by Kumar *et al.*, 2010)

Kozeny Grain model, does take into account the tortuosity. However, it is kept constant *i.e.* the tortuosity does not vary with the hydrate saturation. The predicted permeability using this model is compared to the measured permeability from the current study. Even though the permeability measured by Kumar *et al.* (2010) agrees with this model to certain extend, the measured permeability in the current study differ from the predicted permeability by an order of magnitude.

Figure 5.10 and Figure 5.11 are the graphs of measured permeability versus predicted permeability using Kozeny grain model for grain coating and pore filling formation habit respectively.

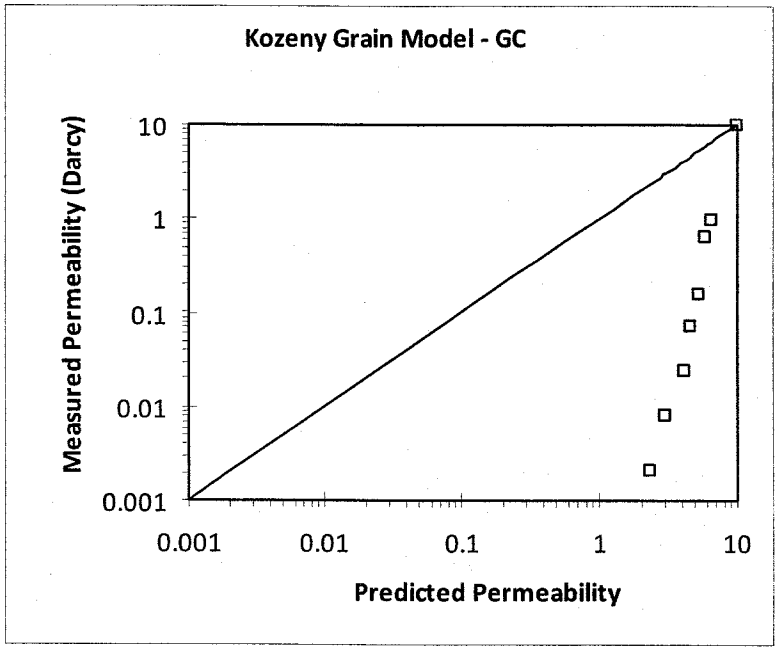

Figure 5.10: Graph of measured permeability versus predicted permeability using Kozeny Grain Model (Grain coating)

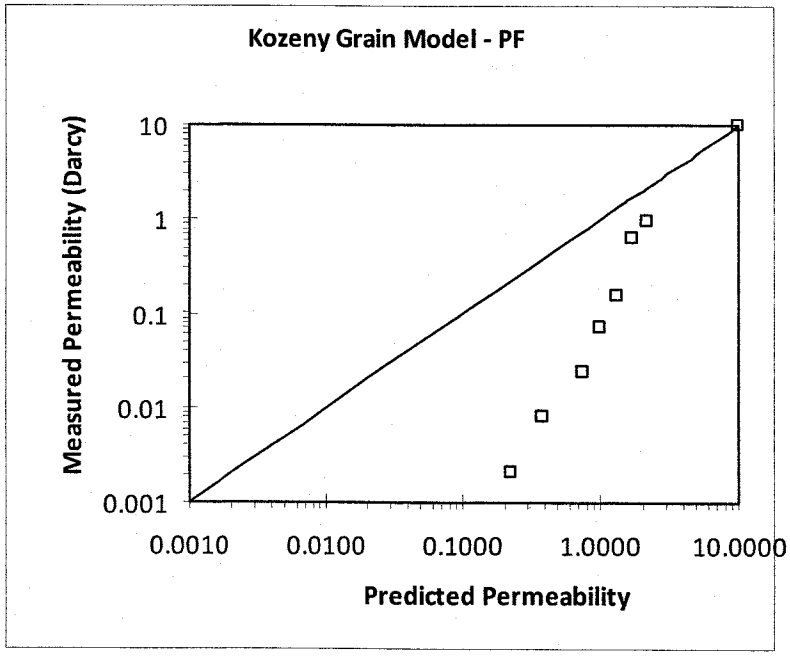

Figure 5.11: Graph of measured permeability versus predicted permeability using Kozeny Grain Model (Pore Filling)

From the comparison, neither the grain coating nor the pore filling model describes the observed behaviour.

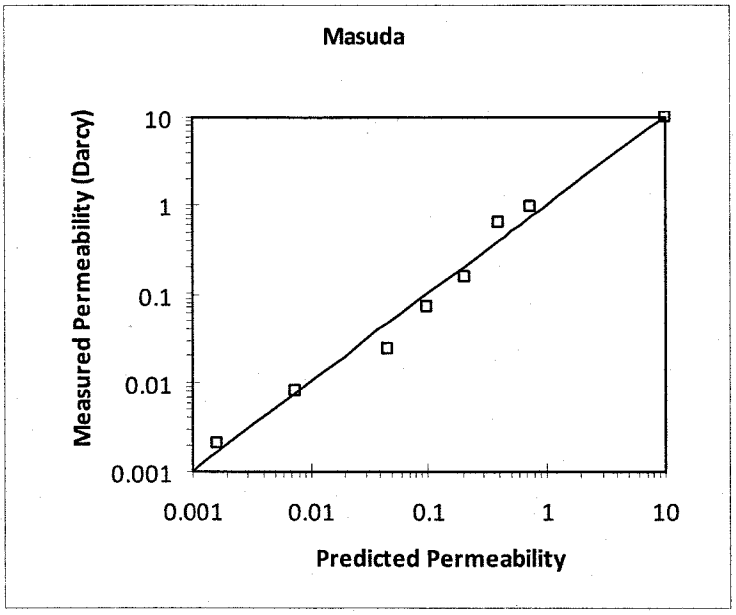

Figure 5.12: Graph of measured permeability versus predicted permeability using University of Tokyo Model

Figure 5.12 shows the graph of measured permeability versus predicted permeability using University of Tokyo model. By varying the Masuda permeability reduction exponent value, N, a very good match is achieved when $N = 9$.

As described by Kleinberg *et al.* (2003) this model is very versatile, but cannot explain the formation habit of the gas hydrate in porous media. We believe that the permeability reduction exponent can be related to the properties of the porous media. However, further investigation is required before any firm conclusion can be made.

Part D: The dissociation of hydrates and cumulative gas production

In the experimental study, the gas was collected during dissociation by lowering the output pressure below the hydrate formation pressure.

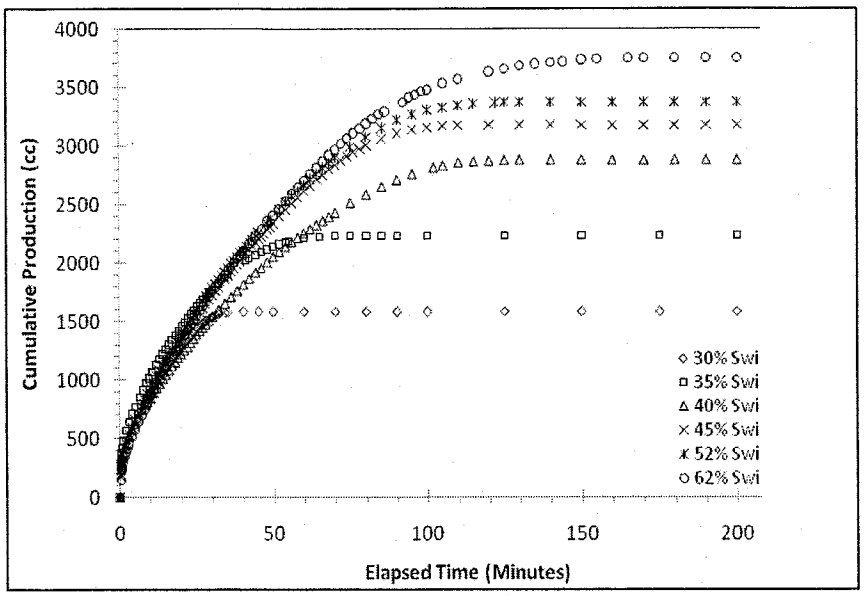

Figure 5.12: Graph of Cumulative Gas Production during Hydrate dissociation

Figure 5.12 is the graph of cumulative gas production from hydrate dissociation for different initial hydrate saturation. Higher the initial hydrate saturation produces more gas during dissociation. The outlet pressure was set around 200 - 250 psi for all the run. The rate of gas production for all the run at the early time of dissociation is almost the same.

It is planned that at the later stage of this research work, this piece of information will be used for history matching. The investigation conducted by Kumar (2005) shows that the kinetics are dominant all the way.

Part E: Temperature Profile during Dissociation

Dissociation of gas hydrate is endothermic in nature. Figure 5.13 and Figure 5.14 shows the graph of the temperature recorded by the designated thermocouples during dissociation of gas hydrate for two repeatable runs (S_h = 35% and S_h = 62%).

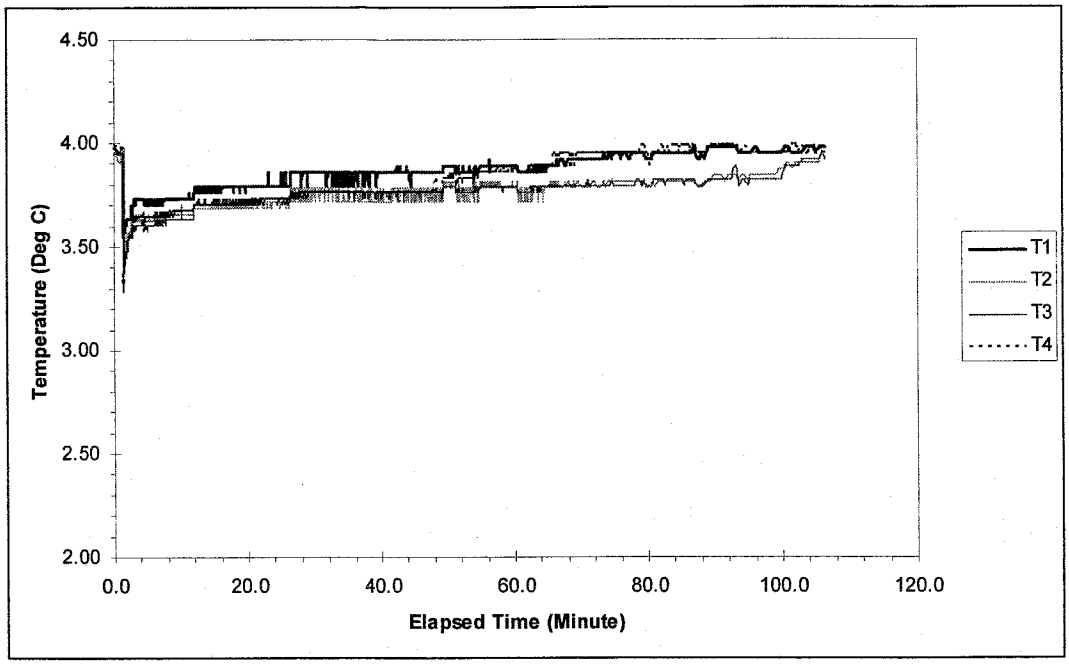

Figure 5.13: Graph of Temperature versus Elapsed Time during dissociation of Gas Hydrate (S_h = 35%)

Prior to dissociation, the pressure in the cell for the system described by Figure 5.13 is 366 psi. When the outlet of the back pressure regulator was set to 208 psi, the temperature in the cell dropped to 3.3 degree Celsius from 3.9 degree Celsius immediately. Within tens of seconds, the temperature rises by couple of degrees and by the end of the production, the temperature reached 3.9 degree Celsius.

Figure 5.14 is the temperature recorded during dissociation of gas hydrate with initial hydrate saturation of 62%. The initial pressure in the cell was 336 psi before the system was depressurised to 259 psi. The temperature dropped during the dissociation is not as big as the one shown in Figure 5.13 because of the depressurization pressure is significantly lower. The temperature distribution in the cell is almost uniform throughout until t = 90 minutes.

The thermocouple 1 and thermocouple 4 for both runs recorded higher temperature due to the fact that these thermocouples are located next to the top and bottom walls.

The effect of heat transfer will be investigated in detail at a later stage of the study.

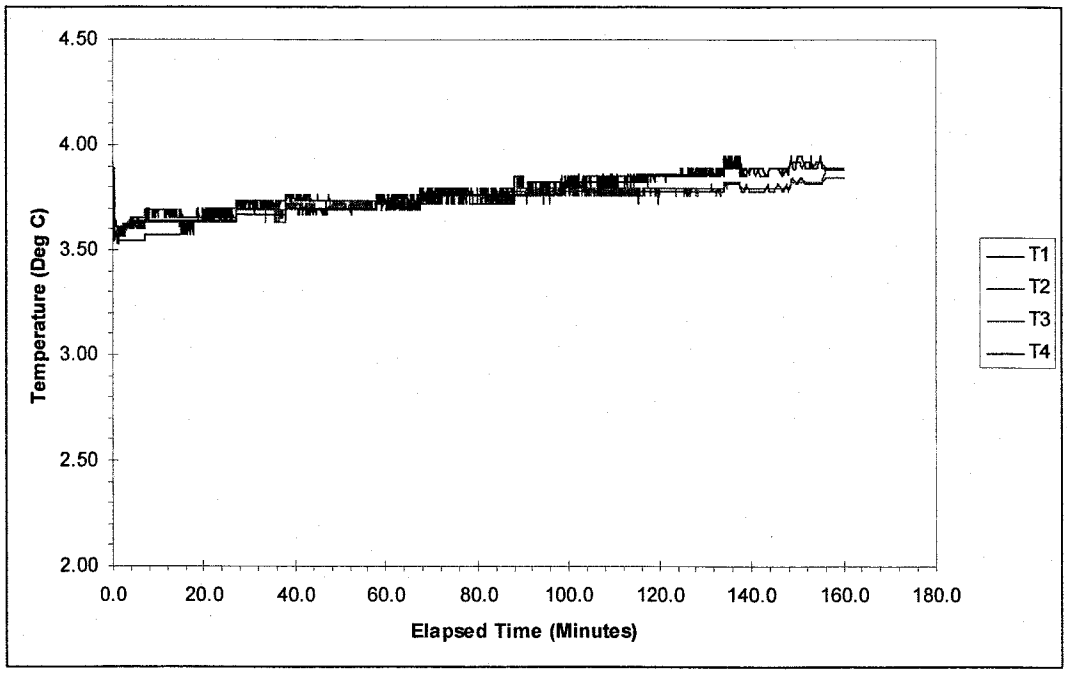

Figure 5.14: Graph of Temperature versus Elapsed Time during dissociation of Gas Hydrate (S_h = 62%)

CHAPTER 6
CONCLUSION

From the literature review and the experimental study the following conclusions can be made:

i. The temperature profiles during hydrate formation cannot be used as the indicator to show how well-distributed the hydrate formed in porous media. The random peaks of temperatures in the sample and even at different saturation are different were observed shows that hydrate formation is highly stochastic.

ii. The temperature profile during hydrate dissociation can be used as the indicator to show how well-distributed hydrate formed in porous medium qualitatively. The temperature drop during dissociation is dependent on the depressurization pressure, and uniform temperature profiles are obtainable if the hydrate is evenly distributed.

iii. The existing permeability models cannot determine the formation habit of gas hydrate of the system under study. The tortuosity is important parameter that needs to be incorporated to have more realistic representation. (For grain coating formation habit)

iv. The University of Tokyo model can match the measured values well but the relationship between the system and the Masuda permeability exponent is not well-understood. The author speculated that the exponent has relationship with the formation habit and the properties of the porous medium. The relationship between the exponent, formation habit and the physical properties of the porous medium will be investigated (if there is any).

v. The history match of production profile and temperature variation in the dissociation of gas hydrate conducted by Kumar (2005) shows that the kinetics is dominant, and the preliminary investigation from the current study has the same outcome. This will be used to investigate the surface area of the dissociating hydrate in relation with the properties of the porous medium.

vi. The thermal conductivity of porous medium in the presence of hydrate is not well-studied. Since the dissociation of gas hydrate in our system is dominated by the kinetics, the variation of thermal conductivity, and hydrate saturation cannot be investigated. The author proposes to conduct experiments to determine the thermal diffusivity of the porous medium containing hydrate.

References:

1. Ahmadi, G., Ji, C., and Smith, D.H., "Natural Gas Production from Hydrate Dissociation: An Axisymmetric Model", Journal of Petroleum Science and Engineering, 58, 245 – 258, (2007).
2. Attia, M.A., "Effects of Petrophysical Rock Properties on Tortuosity Factor", Journal of Petroleum Science and Engineering, 48, 185 – 198, (2005).
3. Clarke, M., and Bishnoi, P.R., "Determination of the Intrinsic Rate of Ethane Gas Hydrate Decomposition", Chemical Engineering Science, 55, 4869 – 4883, (2000).
4. Clarke, M., and Bishnoi, P.R., 'Measuring and Modelling the Rate of Decomposition of Gas Hydrates Formed from Mixtures of Methane and Ethane" Chemical Engineering Science, 56, 4715 – 4724, (2001).
5. Collett, T.S., "Well log Evaluation of Gas Hydrate Saturation" Transactions SPWLA 39th Annual Logging Symposium, 26 – 29 May, Houston Texas, Society of Petrophysicists and Well Log Analysts, MM1 – MM14, (1998a).
6. Collett, T.S., " Well Log Characterization of Sediment Porosities in Gas-Hydrate-Bearing Reservoirs", Society of Petroleum Engineers, SPE Paper 49298, 765 – 776, (1998b).
7. Hong, H., Pooladi-Darvish, M., and Bishnoi, P.R., "Analytical Modelling of Gas Production From Hydrates in Porous Media", Journal of Canadian Petroleum Techology, 42(11), 45 – 56, (2003).
8. Hong, H., and Pooladi-Darvish, M., "A Numerical Study on Gas Production from Formations Containing Gas Hydrate" Paper CIPC 2003 – 60 presented at the 2003 CIPC Conference, Calgary, (2003).
9. Jamaluddin, A.K.M., Kalogerakis, N., Bishnoi, P.R., "Modelling of Decomposition of a Synthetic Core of Methane Gas Hydrate by Coupling Intrinsic Kinetics with Heat Transfer Rates", Canadian Journal of Chemical Engineering, 67, 948 – 954, (1989).
10. Khairkhah, D., Pooladi-Darvish, M. Bishnoi, P.R., Collet, T.S., and Dallimore, S.R., "Production Potential of the Mallik Field Reservoir", Scientific Results from JAPEX/JNOC/GSC Mallik 2L-38 Gas Hydrate Research Well, Mackenzie Delta, Northwest Territories, Canada, (ed) Dallimore, S.R., Uchida, T., and Collet, T.S., Geological Survey of Canada, Bulletin 544, 377 – 390, (1999).

11. Kleinberg, R.L., Flaum, C., Griffin, D.D., Brewer, P.G., Malby, G.E., Peltzer, E.T., and Yesinowski, J.P., "Deep sea NMR: Methane Hydrate Growth Habit in Porous Media and its Application to Hydraulic Permeability, Deposit Accumulation, and Submarine Slope Stability" Journal of Geophysical Research, 108(B10), 2508, doi:10.1029/2003JB002389, (2003).
12. Kleinberg, R.L., and Griffin, D.D., "NMR Measurements of Permafrost Unfrozen Water Assay, Pore-scale Distribution of Ice and Hydraulic Permeability of Sediments" Cold Regions Science and Technology, 42, 63 -77, (2005)
13. Kneafsey, T.J., Tomutsa, L., Moridis, G.J., Seol, Y., Freifeld, B.M., Taylor, C.E., and Gupta, A., "Methane Hydrate Formation and Dissociation in a Partially saturated Core-Scale Sand Sample", Journal of Petroleum Science and Engineering, 56, 108 – 126, (2007).
14. Kumar, A., Maini, B.B., Bishnoi, P.R., Clarke, M., Zatsepina, O., Srinivasan, S., "Experimental Determination of Permeability in the Presence of Hydrates and Its Effect on the Dissociation Characteristics of Gas Hydrates in Porous Media" Journal of Petroleum Science and Engineering, 70, 114 – 122, (2010).
15. Moridis, G.J., Kneafsey, T. and Pruess, K., "Depressurization – Induced Gas Production from Class 1 Hydrate Deposits", SPE Reservoir Evaluation & Engineering, 10, 458 – 481, (2007).
16. Murray, D.R., Kleinberg, R.L., Sinha, B.K., Fukuhara, M., Osawa, O., Endo, T., and Namikawa, T., "Saturation, Acoustic Properties, Growth habit, and State of Stress of a Gas Hydrate Reservoir from Well Logs", Petrophysics, 47(2) 129 – 137, (2006).
17. Nazridoust, K., and Ahmadi, G., "Computational Modelling of Methane Hydrate Dissociation in a Sandstone Core", Chemical Engineering Science, 62, 6155 – 6177, (2007).
18. Pooladi-Darvish, M., "Gas Production From Hydrate Reservoirs and Its Modeling", Journal of Petroleum Technology, 56(6), 65 – 71, (2004).
19. Revil, A., "Thermal Conductivity of Unconsolidated Sediments with Geophysical Applications", Journal of Geophysical Research, 105(B7), 16749 – 16768, (2000).
20. Salem, H.S., "Derivation of the Cementation Factor (Archie's Exponents) and the Kozeny-Carman Constant from Well Log Data and Dependence on Lithology and

Other Physical Parameters", Society of Petroleum Engineers, SPE Paper 26309, (1993).

21. Schultheiss, P.J., and Holland, M.E., "Borehole Pressure and Laboratory Pressure Core Analysis for Gas Hydrate Investigations", Offshore Technology Conference, Houston, Texas, U.S.A., 5 – 8 May 2008, (2008).
22. Selim, M.S., and Sloan, E.D., "Hydrate Dissociation in Sediment", SPE Reservoir Engineering, 5(2), 245 – 251, (1990).
23. Spangenberg, E., "Modeling of the Influence of Gas Hydrate Content on the Electrical Properties of Porous Sediment", Journal of Geophysical Research, 106(B4), 6535 – 6548, (2001).
24. Tohidi, B., Anderson, R., Clennel, M.B., Burgass, R.W., and Bikerdab, A.B., "Visual Observation of Gas-Hydrate Formation and Dissociation in Synthetic Porous Media by Means of Glass Micromodels", Geology, 29(9), 867 – 870, (2001).
25. Waite, W.F., deMartin, B.J., Kirby, S.H., Pinkston, J., and Ruppel, C.D., "Thermal Conductivity Measurement in Porous Mixtures of Methane Hydrate and Quartz Sand", Geophysical Research Letters, 29(4), 82(1) – 82(4), (2002).
26. Waite, W.F., Gilbert, L.Y., Winters, W.J., and Mason, D.H., "Estimating Thermal Diffusivity and Specific Heat from Needle Probe Thermal Conductivity Data", Review of Scientific Instruments, 77, 044904, (2006).
27. Waite, W.F., Stern, L.A., Kirby, S.H., Winters, W.J., and Mason, D.H., "Simultaneous Determination of Thermal Conductivity, thermal Diffusivity and Specific Heat in sI Methane Hydrate", Geophysical Journal International, 169, 767 – 774, (2007).
28. Waite, W.F., Winters, W.J., and Mason, D.H., "Methane Hydrate Formation in Partially Water – Saturated Ottawa Sand", American Mineralogist, 89, 1202 – 1207, (2004).
29. Winters, W.J., Pecher, I.A., Waite, W.F., and Mason, D.H., "Physical Properties and Rock Physics Models of Sediment containing Natural and Laboratory-Formed Methane Gas Hydrate", American Mineralogist, 89, 1221 – 1227, (2004).

30. Worthington, P.F., "Petrophysical Evaluation of Gas Hydrate Formations" International Petroleum Technology Conference held in Kuala Lumpur, Malaysia, 3 – 5 December 2008, (2008).
31. Yousif, M.H., Abass, H.H., Selim, M.S., Sloan, E.D., "Experimental and Theoretical Investigation of Methane-Gas-Hydrate Dissociation in Porous Media", SPE Reservoir Engineering, 6(1), 69 – 76, (1991).

Appendix C: Report on Replacement of CH4 with CO2 in Methane Hydrate Deposits

SEQUESTRATION OF CO_2 BY REPLACEMENT OF CH_4 BY CO_2 IN HYDRATE DEPOSITS

Ph.D. Student

Carlos Alberto Giraldo Sierra

Supervisors: Dr. Matthew Clarke & Dr. Brij Maini

DEPARTMENT OF CHEMICAL AND PETROLEUM ENGINEERING

CALGARY, ALBERTA

JANUARY, 2010

Table of Contents

List of Tables

List of Figures and Illustrations

List of Symbols

Symbol	Definition
A_{dec}	Surface area of hydrates per unit volume m^{-1}
A_{SH}	Specific surface area of hydrate particle m^{-1}
E	Activation Energy (J/mol)
f_e	Fugacity at equilibrium (Pa)
f	Fugacity of the gas
H	Molar enthalpy (J/mol)
H_d	Heat of decomposition (J/mol)
H_f	Heat of formation (J/mol)
H_R	Heat of Reaction (J/mol)
k_d	Decomposition rate constant (mol/m^2 Pa s)
k_d^0	Intrinsic decomposition rate constant (mol/m^2 Pa s)
n	Number of moles
P_e	Equilibrium Pressure (Pa)
P	Pressure (Pa)
Q	Rate of heat transfer (J/s)
r	Rate of production/consumption (mol/s)
R	Universal gas constant (8.314 J/mol K)
S	saturation
t	Time (s)
T	Temperature (K)
u	Velocity (m/s)
U	molar internal energy (J/mol)
V	Volume of the porous media (m^3)
x	Position in the cell (m)
y	Molar gas composition

Greek Letters

Symbol	Definition
φ	Fugacity coefficient
Φ_f	Porosity
ρ	Density (mol/m^3)

Chapter One: INTRODUCTION

1.1 General Aspects

Presently, the society is facing serious problems concerning the increasing demand of energy, of which more than 80% is supplied by fossil fuels. However, the combustion of these fuels is a major source of greenhouse gases (CO_2, NO_x), which are widely accepted as a cause of global warming. This fact has led to international meetings such as the Kyoto Protocol (1997) and the United Nations Climate Change Conferences in Bali (2007) and Copenhagen (2009), where more than 100 nations (including Canada) agreed to reduce their greenhouse gas atmospheric discharges.

Although the ideal solution would be non-carbon energy resources, it is widely believed that the fossil fuels will continue to play a major role in meeting the energy demand in the foreseeable future. The expectation is that natural gas, given its significantly lower carbon footprint, will displace some growth in the use of oil and coal. However, the world emissions of carbon dioxide are expected to increase from 24 billion metric tons in 2001 to 39 billion metric tons in 2025; as result, the global temperature will continue increasing.

This fact has created a global concern over climate change which has stimulated considerable research in methods to curb or sequester the CO_2 emissions. As such, the capture and long term storage of CO_2 in subsurface formations has emerged as a prominent strategy for mitigating greenhouse gas emissions. It is in this context that naturally-occurring Gas Hydrates, which are crystalline inclusions of water and low molecular weight gases (primarily methane) that form at appropriate conditions of temperature and pressure, offer excellent opportunities not only for sequestering the industrially produced CO_2, but also as a source of natural gas. The volume of methane locked in hydrate deposits in Canada was estimated (Majorowicz, 2001) to be between 10^{12} and 10^{14} m^3 @ STP, which is comparable to the 1.95×10^{12} m^3 @ STP of proved

world reserves of natural gas from conventional sources (Energy Information Administration form the US government (2009).

Considering all these facts, the Department of Chemical & Petroleum Engineering at the University of Calgary has been investigating the recovery of natural gas from hydrate deposits and sequestration of CO_2 in the form of hydrates (Hong, 2003; Kumar 2005). However, these studies have treated the gas recovery and CO_2 sequestration as separate stand-alone processes. On the other hand, an intriguing idea is to combine methane recovery from gas hydrates with CO_2 sequestration (Oghaki, 1996). In this scheme, when CO_2 contacts the CH_4-hydrate at certain conditions of temperature and pressure, a replacement reaction occurs (the methane molecule is freed and CO_2 is trapped) in the hydrate structure. This idea offers twin advantages: reducing CO_2 emissions and assisting gas hydrate exploitation, thus overcoming economical impediments of CO_2 sequestration and methane hydrate dissociation while keeping the stability of the subsurface structure and producing no water whatsoever.

Despite of the potential benefits of this procedure, currently only scarce data are available on CH_4-CO_2 replacement in porous media (Jadhawar, 2005; Yang, 2008). Thus, in order to develop this technology as a plausible and cost-effective option for producing methane and abating the atmospheric CO_2 concentration, it is necessary to have relevant experimental and theoretical information about the kinetics of exchange in porous media. Thus, the main purpose of this research is to obtain experimental and theoretical information on the intrinsic kinetics of formation/decomposition of the CH_4 and CO_2 hydrates as well as evaluate the effect of two variables on methane recovery and CO_2 sequestration in porous media. The results of this work will help in assessing the viability of this technology at the industrial level.

1.2 Objectives

Conventionally, studies on gas hydrates are focused on the recovery of natural gas using traditional methods such as thermal stimulation, depressurization and inhibitor

injection. Likewise, much research has been done in the industrial field in order to avoid gas hydrate formation in the gas and hydrocarbon processing facilities, as consequence of the enormous economical losses caused by their presence in the pipelines, valves and equipment. However, little research has been done on the replacement of the methane molecule in the hydrate structure with CO_2 although this method offers excellent possibilities not only as an additional energy source to increase the diversified energy portfolio that Canada has, but also as a mean to store the industrially produced CO_2 as clathrate hydrate in the subsurface geologic formations.

In order to assess the feasibility of this technology industrially it is necessary to have reliable data about the kinetics of exchange in porous media, effect of pressure, temperature, CO_2 injection flow rate, porosity, type of porous medium among many others. Currently, very little information is available in the literature. Considering the large number of factors that need to be addressed to understand this phenomenon, the objectives of the present research are to:

- Determinate the intrinsic rate constants of dissociation/formation of CO_2 and CO_2/CH_4 mixtures as well as the dissociation of CH_4 in bulk water.
- Evaluate the effect of temperature and CO_2 injection flow rate on methane recovery and CO_2 sequestration in porous media.
- Develop a model to represent the exchange reaction in the porous media.
- Validate the model with the data obtained from the experiments.

The product of this research will provide additional data set that will contribute to further studies on the industrially feasibility of this method.

Chapter Two: LITERATURE REVIEW

2.1 Gas Hydrates

Gas clathrates (commonly called gas hydrates) are a group of nonstochiometric, icelike crystalline solids made up of a combination of water and suitable sized guest molecules under conditions of high pressure and low temperature. In these systems water molecules form a hydrogen-bonded lattice with large interstitial cavities, which generally encage small gas molecules such as methane, ethane, propane, carbon dioxide, nitrogen etc. Gas hydrates have the potential for significant impact on world energy and the environment. In general, the importance of gas hydrate studies can be summarized as follows.

2.1.1 Potential Applications of Gas Hydrates

Although studies have historically focused on gas hydrates as troublemakers, due to the plugging of natural gas pipelines and interfering with natural gas processing and, transportation, gas hydrates have also a potential for commercial applications.

Natural occurring gas hydrates located in the permafrost or under the ocean floor constitutes a potential energy source due to their high capacity to store large amounts of gas. Conservative estimates suggest that the gas content in the hydrates is around $20*10^{15}m^3$ (Collett et al., 1998). Due to this fact, the production of natural gas from these hydrates zones have become of great interest for the hydrocarbon industry. Researchers have proposed several methods for recovering the gas such as thermal stimulation, depressurization and solvent injection.

Another important application of gas hydrates involves the storage and transportation of natural gas in hydrate form. Due to their outstanding storage capacity ($1m^3$ of gas hydrates may contain as much as 160 SCM of gas), gas hydrates are considered suitable systems for these kinds of tasks. Besides, the storage and

transportation of natural gas in hydrate form is much safer than the gaseous or compressed liquid forms due to the fact they will not ignite in case of an accident; in addition, the decomposition process can be carried out at low temperature making the combustion highly unlikely. Gudmundsson et al. (1996) developed a feasibility study for a natural gas large scale facility considering production plant, hydrate carriers and regasification plant. According to their results, the capital cost of the hydrate system was 24% lower than its equivalent in LNG system.

It is also possible to form gas hydrates in reverse micelles (Nguyen et al., 1989; Rao et al. 1990; Phillips et al., 1991; Giraldo, 2008); this system provides a means for *in-situ* control of the droplet size (hydrate formation removes water from the reverse micelles thus, decreasing the mean micellar size), which in turn can be used to manipulate the properties of any material that has been formed in the water droplet (nanoparticles, catalysts, semiconductors etc).

Rising levels of greenhouse gases (GHG) in the atmosphere has been a great concern for most of the nations around the world. This fact has stimulated considerable research in methods to curb or sequester the CO_2 emissions. As such, the capture of CO_2 in the hydrate form constitutes a novel and promising method for reducing the concentration of CO_2 in the atmosphere; since, as mentioned previously it is possible to replace the methane molecule with carbon dioxide (Hirohama, 1996; Ota, 2005). These previous studies provide the starting point of the current research and it will be elaborated in more detail in the following section.

2.2 Intrinsic Kinetics

The intrinsic kinetics of gas hydrate formation/decomposition has been studied specially in aqueous, laboratory systems. The following sections present the studies related to the problem into consideration.

2.2.1 CO_2 Hydrate Formation

Clarke et al. (2005) studied the intrinsic kinetics of CO_2 formation in a semibatch reactor equipped with an in-situ particle size analyzer. Their measurements were carried out at temperatures ranging from 274 to 279K and pressures ranging 1.6 to 3MPa. It was found that the intrinsic rate constants using a modified version of the model of Englezos et al (1987) that incorporates the measured particle size data varied from $3.214*10^{-3}$ to $3.423*10^{-3}$ mol/m^2Pa s. However, since these experiments were done, new and important modifications have been implemented such as the inclusion of the Raman spectroscopy and a better system to remove background noise from the particle size analyzer.

Bergeron et al. (2008) determined experimentally the average reaction rate constant of the CO_2 hydrate formation in a semibatch stirred-tank reactor with particle size analyzer. Experiments were carried out at temperatures between 275.3 and 279.4K and pressures ranging from 2014 to 3047kPa. Using their own kinetic model, the reaction rate constant was found to increase from $1.8*10^{-8}$ to $1.8*10^{-7}$ m/s.

2.2.2 CO_2 Hydrate Dissociation

Clarke et al. (2004) obtained experimental data on the rate of decomposition of CO_2 gas hydrates in a semi-batch stirred tank reactor with an in-situ particle analyzer. Data were measured at temperatures ranging from 274 to 281K and pressures ranging from 1.4 to 3.3MPa. By applying their kinetic model it was obtained that the activation energy is 102.88 kJ/mol and the intrinsic rate constant is $1.83*10^{8}$ mol/m^2 Pa s.

2.2.3 CH_4 Hydrate Dissociation

Kim et al. (1987) studied the kinetics of methane hydrate decomposition in a semibatch stirred-tank reactor at temperatures and pressures ranging from 274 to 283K and 0.17 to 6.97MPa. Their results indicated that the rate of decomposition is strongly dependent on the temperature, hydrate particle surface area and the difference of fugacity

of methane at equilibrium pressure and the decomposition pressure. These findings allowed them to develop an intrinsic model for hydrate decomposition.

Clarke et al. (2001), carried out an experimental study on the kinetics of methane dissociation. The experiments were conducted at temperatures ranging from 274.65 to 281.15 K and at pressures between 3.1 and 6.1 MPa. The obtained intrinsic rate constant of decomposition and the activation energy were respectively 36000 mol/m^2.Pa.s and 81 kJ/mol.

2.2.4 CH_4/CO_2 Mixture Hydrate Formation/Decomposition

Malegaonka (1996) determined kinetic data for gas hydrate formation from mixtures of methane and carbon dioxide in a semi-batch stirred tank reactor using the Englezos model (1987). His results showed that the rate constant of carbon dioxide is higher than for methane.

At the best of my knowledge measurements for hydrate decomposition have not been done yet.

2.3 Replacing Methane with CO_2 in Clathrate Hydrate

Ohgaki et al. (1996) were the first who experimentally showed the possibility of producing methane gas from its hydrate by injecting carbon dioxide. During the exchange of these gases at 280K, they observed the mole fraction of carbon dioxide in the hydrate phase to be more than that in the gas phase.

Hirohama et al. (1996) measured the recovering rate from CH_4-hydrate using liquid CO_2 at 274-277K and 4-5 MPa. The composition of the hydrate measured at the end of their experiment indicated that CO_2 hydrate was formed with the water that had been encaging the recovered CH_4. Likewise, they described mathematically the phenomenon for the first time by applying non-equilibrium thermodynamics.

Komai et al (1999) studied the kinetics of replacement of CH_4 molecule in the CH_4-hydrate by using CO_2 gas. The experiments were carried out at 3.5MPa and 276K achieving after 12h a 90% concentration of CO_2 in the hydrate phase.

Uchida et al. (2001) used Raman spectroscopy to study the mechanism and the kinetics of the replacement of CH_4-hydrate by CO_2-hydrate at 271K and 2.9MPa. Their experiments revealed that an induction period of 50h was required so that CO_2 molecules replace CH_4 molecules in the hydrate structure. Likewise, it was showed that the replacement occurs mainly in the large cavities but the presence of CO_2 might cause a collapse of the small lattice which would explain the reduction of CH_4 in the small cages.

Komai et al. (2003) carried out replacement experiments on CO_2 and CH_4 gas hydrates at 2 MPa and 1-2°C. Their results indicated that the replacement can be achieved within a period of 12h, based on their results the ratio of occupancy for CO_2/CH_4 gas hydrates in the replaced hydrate samples were 40-45% and the final concentration of methane in the hydrate phase was 20%.

Lee et al. (2003) calculated that at the equilibrium the ratio between the large and small occupancies for methane changes from 1.26 to 0.23 and estimated that at least 64% of methane is recoverable. In order to prove this, experiments were performed at 270K and 6MPa reaching a pseudo-equilibrium condition after 5h and recovering only 50%; they attributed this fact to the sample morphology.

Ota et al. (2005) studied the dynamics of CH_4 replacement with saturated liquid CO_2 at 273.2K and 3.6MPa using in situ Raman spectroscopy. Their results showed that CH_4 in the hydrate gradually moved to the liquid CO_2 phase while CO_2 in the liquid phase penetrated into the hydrate; likewise it was found that the decomposition of the large cage in the CH_4 hydrate proceeded faster than that of the small cage.

Ota et al. (2005) studied the effect of the temperature on the dynamics of the replacement at 3.25MPa and temperatures ranging from 271.5K to 275.5K. According to their results, the amount of CH_4 hydrate decomposition was found to be almost proportional to that of CO_2 hydrate formation and the temperature had a positive effect on the recovery of CH_4. Likewise, based on the rate measurements, it was determined the overall rate constants and activation energies of 14.5kJ/mol for CH_4 hydrate decomposition and 73.3kJ/mol for CO_2 hydrate formation after a given initial period of 10h.

Jadhawar et al (2005) performed for the first time an experimental investigation on replacing methane in the hydrates structures with carbon dioxide in porous media. Their results showed that the rate of methane recovery almost double (12.55% vs 7.97%) when the experiment was done at 10.8°C and a pressure above the saturation pressure of CO_2, compared to the test results at 2°C with a pressure below CO_2 saturation pressure.

Graue et al. (2006) used Magnetic Resonance Imaging to verify experimentally that methane hydrate in porous sandstone spontaneously converts to CO_2 hydrate when exposed to liquid CO_2 at high pressure and low temperature. It was also confirmed that without heating, an exchange process between CO_2 and methane occurred allowing the injected CO_2 to be stored as hydrate resulting in spontaneous production of methane with no associated water production.

Park et al. (2006) studied the direct sequestration of CO_2 and N_2 mixtures into structure I CH_4 hydrates. By using CNMR and Raman spectra, it was determined that 23% of CH_4 in the hydrate was replaced with N_2 whereas 62% of CH_4 is replaced with CO_2. Accordingly, approximately 85% of CH_4 encaged in saturated CH_4 hydrate is recovered. This fact, allowed them to conclude that the replacement of CH_4 with N_2+CO_2 proceeds more effectively in hydrate structures than in the case of using only pure CO_2.

Ota et al. (2007) studied the effect of the pressure on the CH_4-CO_2 replacement in CH_4 hydrate with high pressure CO_2. Experiments were carried out at 273.2K and at initial pressures of 3.2, 5.4 and 6.0MPa using an in-situ laser Raman Spectroscopy in order to monitor the reaction. Their results showed that replacement rates increased with increasing pressures up to 3.6MPa with no further change at higher pressures (6MPa). Likewise, it was determined that the rates were dependent on the pressure and phase conditions with the driving force being strongly related to fugacity differences of the two guest components between fluid and hydrate phases.

Stevens et al. (2008) compared experimentally two approaches (depressurization vs replacement with CO_2) for releasing methane from methane hydrate in porous sandstone. Based on their results, it was concluded that depressurization produced total recovery of methane in a faster way than replacement, with a major limitation of the associated water produced which can destabilize underground structure. Likewise, replacement reaction was carried out at 277K and 8.37MPa, under these conditions, 70% of the total methane was recovered (after 500h) with the advantage that no-water is produced and the underground keeps its stability.

Yang et al. (2008) conducted experiments at different temperature and pressure conditions, in the presence or absence of excess water, in the presence of gaseous or liquid CO_2. Likewise, silica glass beads and a kaolinite-sand mixture were used as porous media. Their results showed a higher methane recovery at high temperature and pressure, inside the methane hydrate stability zone (HSZ) and outside the CO_2 (HSZ). Likewise, it was established that the presence of free water and kaolinite-sand as porous media reduced the recovery rate.

Chapter Three: EXPERIMENTAL STUDY

3.1 EXPERIMENTAL DESIGN

The successful exploitation of methane hydrates by sequestering carbon dioxide requires an understating of the hydrodynamics of carbon dioxide injection and transport to the methane hydrate accumulation; thermodynamics and kinetics of formation and dissociation of the hydrates of methane, carbon dioxide and their mixtures, which are function of temperature, pressure, pore media characteristics and mole fraction of carbon dioxide and methane in the mixture. Likewise, it is necessary to understand the effect of viscosity and density differences between the injecting carbon dioxide and the dissociated methane gas; interfacial mass transfer between the two; interfacial tension between the different phases; type of porous media; pore size distribution; saturation of the different phases in the sediment and water salinity (Goel, 2006). Considering the enormous number of variables involved in this phenomenon, only a part of them will be considered in this study.

3.1.1 Kinetics Experiments

Experiments will be conducted to obtain data on the kinetics of gas hydrates formation/dissociation. Temperatures will range from 274 to 278K and pressures will be chosen according to the three phase equilibrium line as shown in figure 3.1, 3.2 and 3.3. Previous studies (Alotaibi, 2009) on this equipment showed that a stirring rate of 700 rpm is enough to consider that the heat and mass transfer resistances are negligible.

Two mixtures compositions that will be evaluated in this work are:

- 40%CO_2, 60%CH_4
- 60%CO_2, 40%CH_4

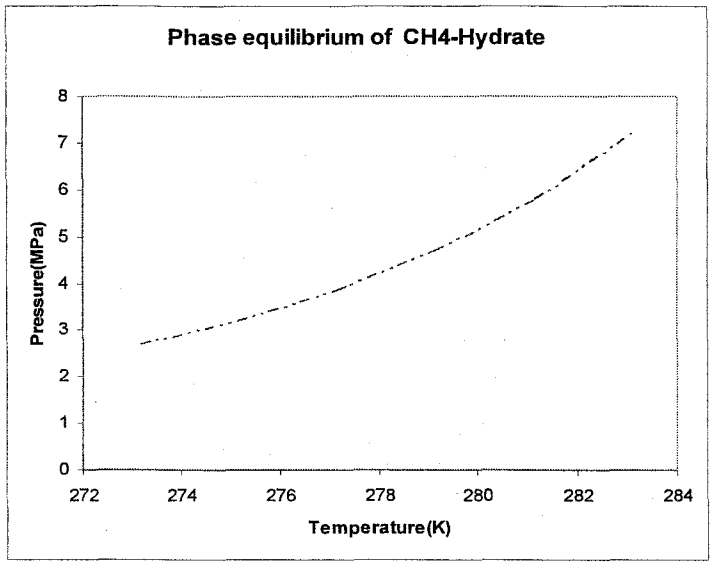

Figure 3-1 Methane Hydrate Equilibrium

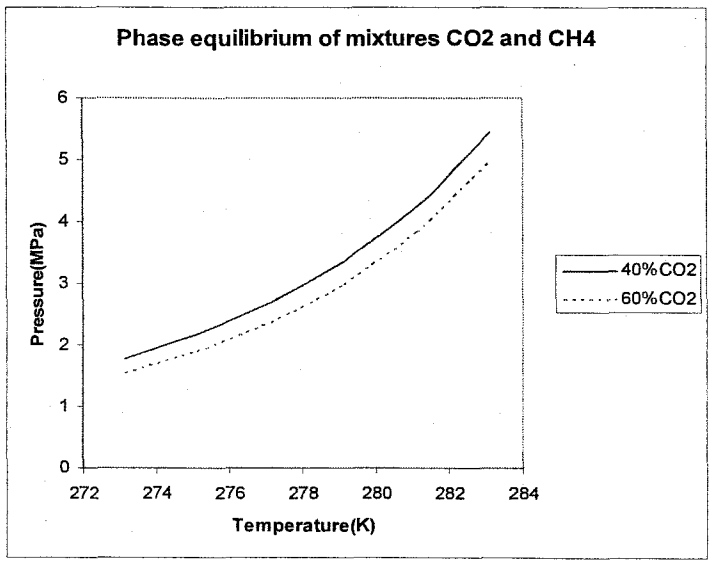

Figure 3-2 Methane/CO_2 Mixture Hydrate Equilibrium

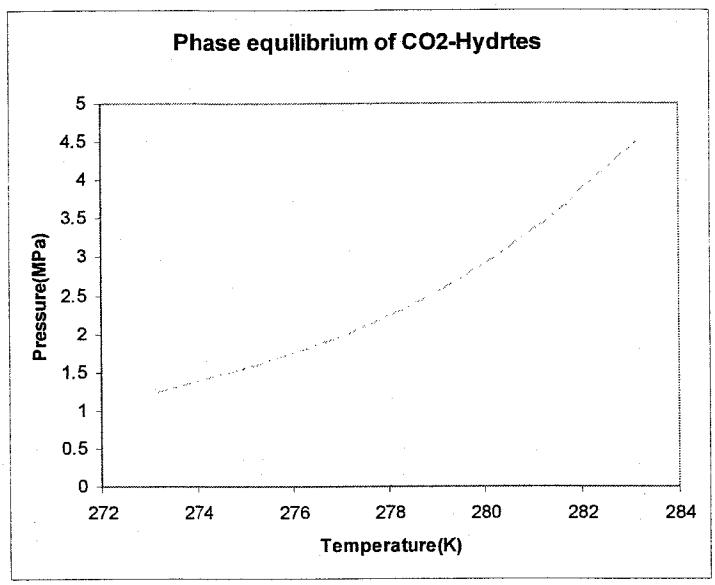

Figure 3-3 CO_2 Hydrate Equilibrium

With these compositions and with the data for pure components the whole spectrum for this mixture is covered. These curves were generated using Adisasmito correlation (1991)

3.1.2 Replacing Methane with CO_2 in Clathrate Hydrate

As mentioned previously the objective of this part is to carry out an experimental study of the conversion of methane hydrate into CO_2 hydrate in porous media. In order to do that, a systematic approach to plan the experiments will be adopted.

- *Objective of the Experiment*: To quantify the CH_4 recovery and CO_2 sequestration when a constant flow rate of CO_2 is passed through CH_4 hydrate in porous media.
- *Relevant Background:* Figure 3.4 presents the experimental conditions where CO_2-CH_4 replacement has been carried out according to the literature. As noticed, most of the experiments haven been performed in bulk hydrate phase (squares) and just few of them in porous media (triangles). All the experiments shown have been carried out in batch reactors. Likewise, it is very likely that the CH_4-CO_2

replacement reaction rate will be controlled by different mechanisms such as: heat and mass transfer, intrinsic kinetics and fluid flow.

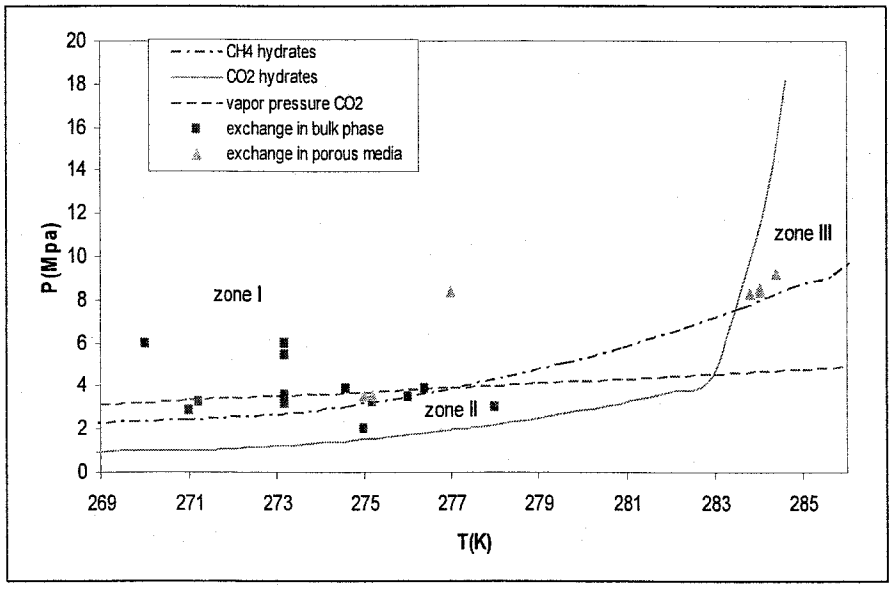

Figure 3-4 CH_4-CO_2 Replacement Reported in the Literature

- *Response Variables:* Two variables are required to meet the objective of this work.

  Y1: Number of moles of CH_4 freed during the replacement reaction

  Y2: Number of moles of CO_2 trapped during the replacement reaction

- *Control Variables*: From the thermodynamic point of view, CO_2 replacement can occur at different conditions (see figure 3.4).The temperature and pressure may be inside both Hydrate Stability Zone (HSZ), zone I; or outside methane HSZ and inside CO_2 HSZ, zone II; or inside methane HSZ and outside CO_2 HSZ, zone III. For the purpose of this research two factors will be studied: Temperature and CO_2 flow rate and zone II was chosen due to the fact that few experimental data are reported in the literature and the equipment available is not designed to work with liquid CO_2. The operating temperature will range from 273.5K to 278.5K. Regarding the CO_2 flow rate, the operating range will be kept low in order to

allow the CO_2 to replace the methane and to avoid any deformation in the porous media due to excessive flow. Thus, the flows will vary from 10-100 cm^3/min

- *Held-Constant Factors*: These are controllable factors whose effect will not be determined in this study. Their value will be kept in a particular setting.
  - ✓ Back Pressure: 2MPa
  - ✓ Initial Water Saturation: 20%
  - ✓ Porous medium: sand
  - ✓ Initial Porosity: 30%
- *Interactions:* It can not be determined a-priori a possible interaction between the two control factors. If there is any, it will be defined after carrying out the experiments.
- *Experimental Design*: Central composite design (CCD) has been chosen to determine effect of temperature and CO_2 flow rate on the response variables. This kind of design can be divided in three parts.
  - ✓ Two-level factorial design: This portion will contribute in estimating linear effects and two-factor interactions.
    Factors: 2 (Temperature-CO_2 flow rate)
    Levels: 2 (273.5-278.5K; 10-100 cm^3/min)
    Total blocks: 1
  - ✓ Center point: It contains replications at the center point (276K; 45cm^3/min). Once, this point has been measured it is possible to perform an ANOVA analysis to determine the presence of curvature in the response variable. If so, the axial portion of the CCD is required
  - ✓ Axial portion: These points will contribute to determine the curvature of the system.
    Design Table:

Run	Temp	Flow Rate
1	1	1
2	-1	1
3	1	-1

4	-1	-1
5	0	0
6	1	0
7	-1	0
8	0	1
9	0	-1

Based on the results obtained in these experiments, it will possible to fit a first/second order model that represents the response variables.

3.2 EXPERIMENTAL APPARATUS

3.2.1 Intrinsic Kinetics System

The equipment to be used in this study is essentially the same as that used by Al-Otaibi (2009). This apparatus consists of an isothermal, isobaric stirred tank reactor (CSTR), three bias reservoirs, a supplier reservoir and a collection reservoir. The temperature is maintained at a constant value by immersing the reactor in a circulating glycol cooling bath. The reactor pressure is kept constant by adjusting the flow rate from the supply reservoir or to the collection reservoir through a control valve depending on whether hydrates are being formed or decomposed. The three bias reservoirs are used for the differential pressure transducer cells to accurately measure the pressure in the reactor, supply and collection reservoirs. In addition, the system is equipped with an in-situ particle size analyser is a Lasentec model D600x which will provide a particle chord length distribution which is function of the true particle diameter distribution; these data are to be used in the determination of the intrinsic rate constants. Figure 3.5 shows a schematic of the apparatus.

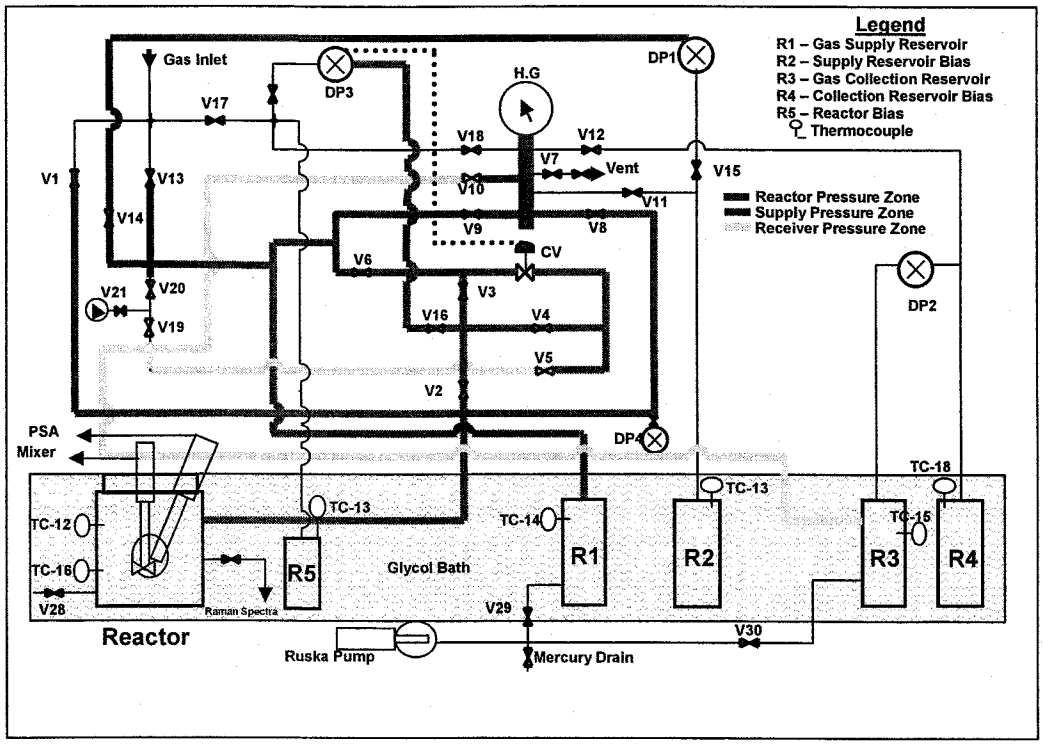

Figure 3-5 Schematic of the Apparatus for Intrinsic Kinetics

3.2.2 CH_4-CO_2 Replacement System

The equipment used in this part is essentially the same as that used by Kumar (2005) and consists of a Jerguson cell packed with the selected porous medium and immersed in a constant temperature glycol bath. This cell possesses connections for four thermocouples and two pressures transducers to follow the phenomena to be studied. The whole system is located inside an insulated metallic cabinet to minimize heat transfer form the surroundings. For the purpose of the current study some modifications need to be implemented in order to carry out the experiments:

- ✓ Mass flow controller will be installed after the CO_2 cylinder in order to keep constant the injection flow rate.
- ✓ Gas connections for gas chromatograph
- ✓ Produced gas collection system will be replaced by a pressure vessel with a pressure transducer. The current system is based on water displacement, thus part of the CO_2 collected will be dissolved in the water which can

introduce some error in the measurements. In addition the amount of gas to be collection is big which makes the current system unsuitable for the study.

Figure 3.6 presents a schematic representation of the system:

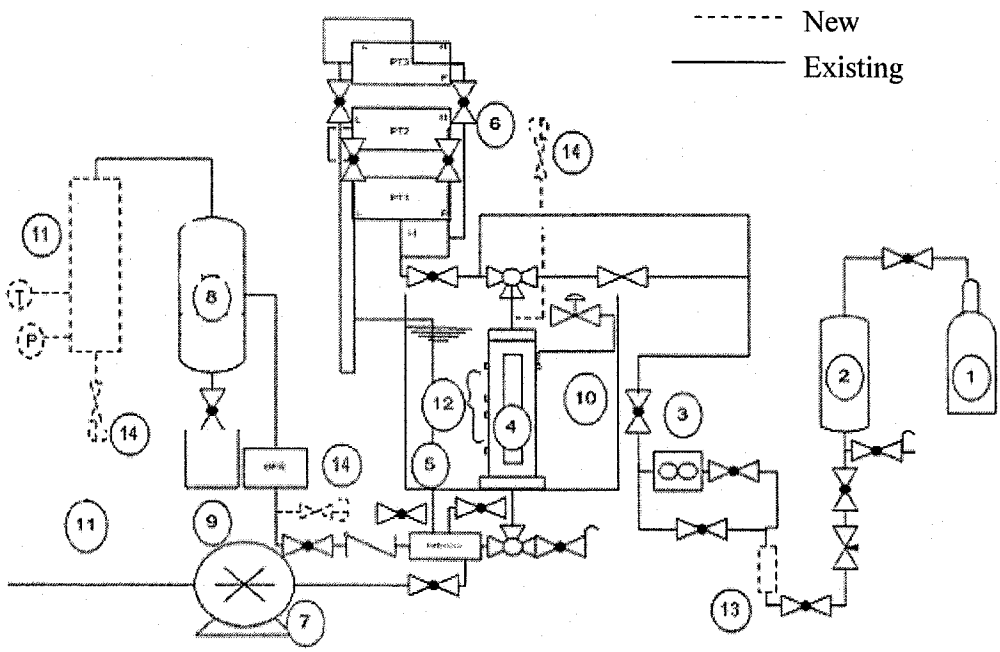

1. Gas cylinder
2. Vessel (damper)
3. Mass flow meter
4. Jergusson cell
5. Temperature controlled bath
6. Pressure transducer
7. Vaccum pump
8. Separator
9. Water collection unit
10. Water injection port
11. Gas collection unit
12. Thermocouple ports
13. Mass flow controller
14. Gas chromatograph sampling connection

Figure 3-6 Schematic Apparatus for CH_4-CO_2 Replacement

3.3 Experimental Procedure

3.3.1 Intrinsic Kinetics.

3.3.1.1 Hydrate Formation

The experimental procedure for the current study can be divided into two steps: gas dissolution and hydrate particle growth; the methodology is identical to that followed by Clarke and Bishnoi (2005) and Alotaobi (2009) which can be summarized as follow:

All reservoirs are purged with the experimental gas several times to ensure no gas from previous experiments is leftover. The reactor is then flushed several times with ultra pure water. The water used is first de-ionized through a purification system using (Millipore-Simplicity) model and then water is distilled for further purification. The reactor is then charged with 280 ml of the ultra clean water. After the water reaches thermal stability; at the desired operating temperature, the experimental gas is introduced slowly into the system. Reactor and supply cell bias reservoir (R2) are filled to the desired experimental pressure (above the three phase equilibrium pressure), while the reactor bias reservoir (R5) and the gas supply cell (R1) are charged to pressures 2 and 4 bar higher than experimental pressure, respectively. Then, data acquisition system is started, and given some time to get consistent readings, roughly 3 minutes, then, the controller is set to auto mode, and the stirrer is gradually increased from 0 to the desired stirring rate. Then, the FBRM is started. The data acquisition system records temperatures and pressures using LabView software.

3.3.1.2 Hydrate Decomposition

The procedure to carry out hydrate decomposition is an extension of the hydrate formation. After the formation step has proceeded for sufficient time, the stabilisation period is initiated by reducing the pressure in the reactor to a value slightly above the three phase equilibrium pressure. At this point the driving force for hydrate growth is negligible. This, it is possible to measure a steady state particle size distribution. The

stabilisation pressure is maintained until the number of particles approach a constant value. Subsequently, pressure is reduced to a value below the three phase equilibrium pressure.

3.3.2 CH_4-CO_2 Replacement System

In order to carry out the experimental design proposed above, the following experimental procedure will be adopted:

- Calibrate measuring devices (pressure and temperature)
- Charge the system with porous media
- Verify that the system is leak proof
- Measure the porosity
- Measure the absolute permeability of the medium
- Charge the system with water according to the water saturation required
- Allow enough time to permit even distribution of the water
- Inject CH_4 in order to form CH_4-hydrates
- Determine the amount of CH_4 in the hydrates
- Purge CH_4 in gas phase by CO_2
- Measure the composition in the gas phase
- Initiate the experiment injecting a constant flow of CO_2
- Monitor the gas composition at the exit of the reactor via GC for a limited period of time
- Stop the experiment
- Measure pressure, temperature and composition in the reactor and in the gas collection unit
- Decompose the hydrates and measure the amount of CO_2 and CH_4 in the hydrates.

All the data required will be compiled in table 3.1. Likewise, pressure, temperature and CH_4/CO_2 composition will be measured periodically in the reactor and in the collection reservoir:

Data to be collected during the experiments

Porous medium:
Total volume of the reactor
Porosity (ϕ)
Water Saturation (Sw)
Permeability of the porous media

	Run 1	Run 2	Notes
Formation of CH4-hydrates			
H2O charged			
Initial Pressure			
Initial Temperature			
Initial Volume of the Gas			ϕ-Sw
Initial mol			Calculated using an equation of state
Final Pressure			
Final Temperature			
Final Volume of the Gas			Vinitial, include correction for difference in density (water-hydrate)
Final mol			Calculated using an equation of state
CH4 in the hydrates			initial mol-final mol
Experimental Nh			nH2O/nCH4
Reported Nh			
H2O remained free			
Permeability of the medium with hydrates			
Purging CH4 by CO2			
CO2 flow rate			Using totalizer
Composition of the gas phase			Using GC. Verify that CH4 has been removed
Experiment			
fill table attached			
Stop the Experiment			
Pressure			
Temperature			
xCH4			
xCO2			
Volume of the gas			ϕ–Sw
moles of CO2 in the gas phase			
moles of CH4 in the gas phase			
Reduce pressure to the atmosphere			
Volume			ϕ-Sw
xCH4			
xCO2			
moles of CO2 in the gas+hydrate phases			
moles of CH4 in the gas+hydrate phases			
moles of CO2 in the hydrate phases			
moles of CH4 in the hydrate phases			

Table 3-1 Data Sheet for the CH_4-CO_2 Replacement

Chapter Four: MODELING OF CO_2-CH_4 REPLACEMENT REACTION IN CH_4-HYDRATE IN POROUS MEDIA

A general model was developed to study the characteristics of CO_2-CH_4 reaction replacement when a CO_2 gas is injected at constant flow rate. The numerical results of the methane produced in the cell during the exchange will then be compared to the experimental data in order to get a better understating of this phenomenon.

The model considers the following assumptions:

- Steady state of CO_2 injection will be supplied
- Reactor is an unsteady-state open system
- Phases involved are: gas/aqueous/hydrate
- Components: CH_4, CO_2, H_2O, CH_4HYD, CO_2HYD
- Darcy's law will be used to describe the fluid flow in porous media.
- Relative permeability curves and capillary pressure are calculated using Hong's correlation (Hong, 2003).
- STARS is chosen as the tool to solve the mass and energy balances. Its suitability to represent gas hydrates has been proven by others authors (Wilder, 2008; Uddin et al[a, b], 2008; Uddin et al, 2006).

In order to use STARS as a modeling tool, the kinetics of gas hydrate decomposition has to be transformed into a suitable format.

Kinetics of methane hydrate decomposition follows the Clarke-Bishnoi model:

$$-\frac{1}{V}\frac{dn_{CH4HYD}}{dt} = k_d A_{dec}(f_e - f_{CH4})$$

$A_{dec} = \Phi_f S_H A_{SH}$; $A_{SH}=3.75*10^5$ m^2 of hydrate/m^3 of hydrate (Matsuda, 2002)

$k_d = k_d^0 \exp\left(\frac{-E}{RT}\right)$ where E=81kJ/mol and $k_d^0= 3.6*10^4$ mol/m^{2}Pa s

$f_{CH4}=\varphi P$; $f_e=\varphi P_e$; Assuming that the system behaves as an ideal gas the $\varphi=1$. This assumption will be verified according to the experimental conditions (see results section).

$$-\frac{1}{V}\frac{dn_{CH4HYD}}{dt}=k_d^0\exp\left(\frac{-E}{RT}\right)(\Phi_f S_H A_{SH})(P_e-P_{CH4})$$

$$-\frac{1}{V}\frac{dn_{CH4HYD}}{dt}=\frac{k_d^0 A_{SH}}{\rho_{CH4HYD}}\exp\left(\frac{-E}{RT}\right)(\Phi_f S_H \rho_{CH4HYD})P_e\left(1-\frac{P_{CH4}}{P_e}\right)$$

$$P_e(kPa)=a\exp\left(\frac{b}{T(^\circ C)-C}\right)=9.02E15\exp\left(\frac{-7881.79}{T+273.15}\right)$$

$$-\frac{1}{V}\frac{dn_{CH4HYD}}{dt}=\frac{k_d^0 A_{SH}a}{\rho_{CH4HYD}}\exp\left(\frac{-E-bR}{RT(K)}\right)(\Phi_f S_H \rho_{CH4HYD})\left(1-\frac{P_{CH4}}{P_e}\right)$$

For CO_2 decomposition:

$P_e(kPa)=9.02E15\exp\left(\frac{-8073.66}{T+273.15}\right)$; E=103kJ/mol and k_d^0= 1.83*10^8 mol/m^{2}Pa s.

4.1 Modeling CH_4-CO_2 replacement in CH_4-hydrates.

This model includes all three rate-controlling mechanisms (multiphase fluid flow in porous media, kinetics of replacement and heat transfer) that govern CO_2-CH_4 replacement reaction.

4.1.1 Governing Equations

The equations that govern the process of CH_4-CO_2 replacement in CH_4-hydrate are:

1. *Material Balance:* Accumulation=input-output+production

- For CH_4:

$$\frac{\partial(\rho_{CH4}\Phi_f S_g)}{\partial t}=-\frac{\partial(\rho_{CH4}u_g)}{\partial x}+r_{CH4}$$

- For CO_2:

$$\frac{\partial(\rho_{CO2}\Phi_f S_g)}{\partial t}=-\frac{\partial(\rho_{CO2}u_g)}{\partial x}-r_{CO2}$$

- For water: It would depend if there is a production or consumption

$$\frac{\partial(\rho_w \Phi_f S_w)}{\partial t} = -\frac{\partial(\rho_w u_w)}{\partial x} - (r_{CO2} - r_{CH4})$$

- For CH_4HYD

$$\frac{\partial(\rho_{CH4HYD} \Phi_f S_H)}{\partial t} = -r_{CH4}$$

- For CO_2HYD

$$\frac{\partial(\rho_{CO2HYD} \Phi_f S_H)}{\partial t} = r_{CO2}$$

2. *Energy Balance*: Accumulation= input-output+production+Q-W

$$\frac{\partial(\rho_{rock}(1-\Phi_f)U_{rock} + \rho_H \Phi_f S_H U_H + \rho_g \Phi_f S_g U_g + \rho_w \Phi_f S_w U_w)}{\partial t} = -\frac{\partial(\rho_g u_g H_g + \rho_w u_w H_w)}{\partial x} + \frac{\partial}{\partial x}\left(k_m \frac{\partial T}{\partial x}\right) + Q + \Delta H_R r_{CH4} + \Delta H_R r_{CO2}$$

4.1.2 Kinetics

Although, the kinetics of this process is not well understood, it seems likely that CH_4-hydrate dissociates before CO_2 hydrate formation for the operating region chosen. In addition, CH_4-hydrate decomposition is stimulated by the heat released from CO_2-hydrate formation (Oghaki et al. 1996).

$$CH_4(H_2O)_n \rightarrow CH_4 + nH_2O \quad \Delta H_d = 54.19 \text{kJ/mol}$$

$$CO_2 + nH_2O \rightarrow CO_2(H_2O)_n \quad \Delta H_f = -57.66 \text{ kJ/mol}$$

The kinetics of CH_4 hydrate decomposition will be now compositional dependent since a mixture of gases is present in the gas phase, thus:

$f_{CH4}=\varphi y_{CH4}P$; $f_{CO2}=\varphi y_{CO2}P$; following the same procedure showed before, it is possible to obtain the following expression:

$$-\frac{1}{V}\frac{dn_{CH4HYD}}{dt} = \frac{k_d^0 A_{SH} a}{\rho_{CH4HYD} P} \exp\left(\frac{-E-bR}{RT(K)}\right)(\Phi_f S_{CH4HYD} \rho_{CH4HYD})(y_{CH4} P)\left(1-\frac{P}{P_e}\right)$$

For CO_2 hydrate formation, the procedure is analogous to the dissociation, however $A_{dec} = \Phi_f S_w A_{SH}$

$$\frac{1}{V}\frac{dn_{CO2HYD}}{dt} = k_{fCO2} A_{dec}(f_{CO2} - f_e)$$

$$\frac{1}{V}\frac{dn_{CO2HYD}}{dt} = \frac{k_{fCO2} A_{SH}}{\rho_W P} P_e(\Phi_f S_W \rho_W)(y_{CO2} P)\left(\frac{P}{P_e} - 1\right)$$

In this case, the CO_2 hydrate formation is inhibited by the presence of CH_4 in the gas mixture (equilibrium curve shifts depending on the gas composition) which implies that some CH_4 will be reacting with water to form the hydrate structure. Thus, the formation of CH_4-hydrate has also to be considered taking into account that the equilibrium pressure would be the one in the mixture.

$$CH_4 + nH_2O \rightarrow CH_4(H_2O)_n \quad \Delta H_d = -54.19 kJ/mol$$

$$\frac{1}{V}\frac{dn_{CH4HYD}}{dt} = \frac{k_{fCH4} A_{SH}}{\rho_W P} P_e(\Phi_f S_W \rho_W)(y_{CH4} P)\left(\frac{P}{P_e} - 1\right)$$

Kinetics constants for CH_4 hydrate and CO_2 hydrate formation are taken from Englezos (1987) and Clarke (2005) respectively.

The equation for the equilibrium pressure presented below was fitted to the correlation reported by Adisasmito (1991)

$$P_e(kPa) = \frac{9.02E15}{(1 + 1.0511 y_{CO2})^{0.9585}} \exp\left(\frac{-7896.076}{T + 273.15}\right)$$

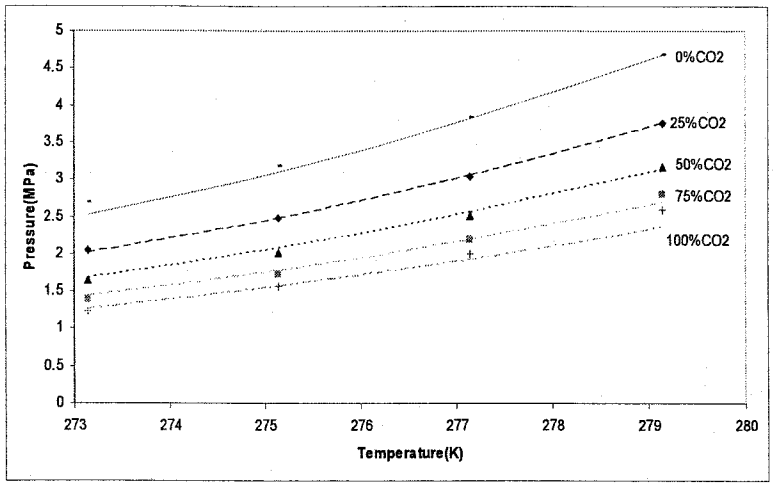

Figure 4-1. Phase Equilibrium of mixtures CO_2 and CH_4. Data points represent results obtained using Adisasmito's correlation.

4.1.3 Results

In order to verify the suitability of STARS to simulate this type of process, initially the CH_4-hydrate and CO_2-hydrate decomposition will be simulated and compared with previous works (Hong, 2003; Kumar, 2005). The results presented below are modeled as one-dimensional processes for comparison purposes (previous works were done this way) and because experimentally it will only be possible to obtain information in one direction.

a. Modeling CH_4 hydrate decomposition (Hong, 2003)

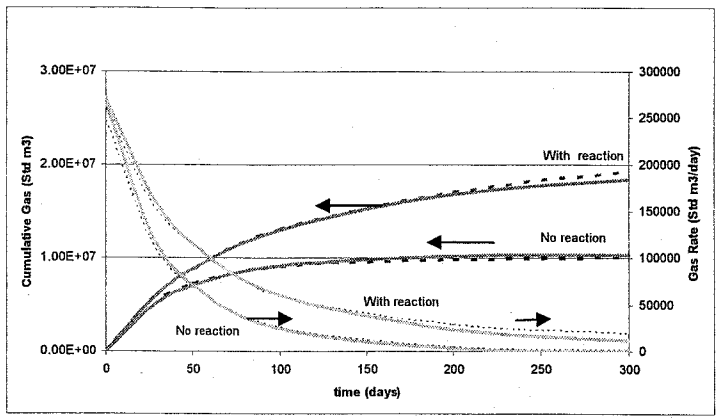

Figure 4-2 Gas production in CH4 hydrate dissociation. Gas production from a single well located at the centre of a 200m radius cylindrical reservoir. Pi=6913kPa, Ti=10C, BHP=4000kPa, S_H=0.6. Adiabatic system. Dashed lines represent Hong's work. At these conditions, the fugacity coefficient calculated using the TB EOS is 0.98.

b. Modeling CO_2 hydrate decomposition (Kumar, 2005)

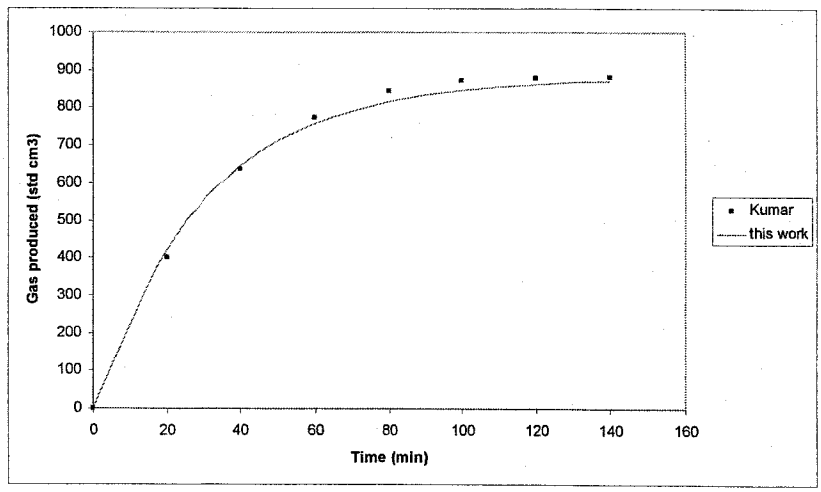

Figure 4-3 Gas production in CO2 hydrate dissociation. Gas production from a cell packed glass beads. P_i=2412kPa, T_i=3.6C, BHP=1654kPa, SH=0.187, T_{bath}=3.6C. Non-adiabatic system. At these conditions, the fugacity coefficient calculated using the TB EOS is 0.88.

In order to check the behaviour of the system during the replacement reaction, the experimental set up used in the lab and described by Kumar (2005) is modeled in STARS. Operational and initial conditions are shown in figure 4.4

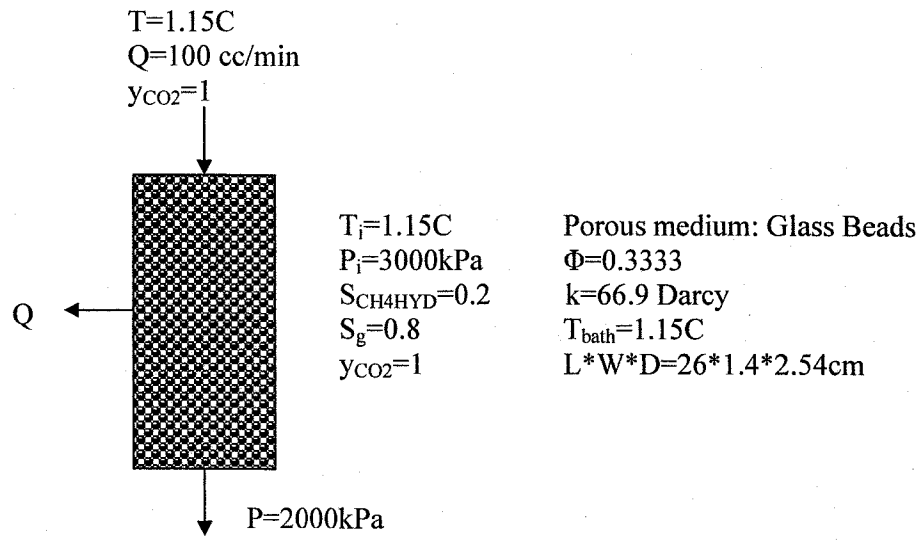

Figure 4-4 Schematic representation and initial conditions of the replacement experiment (Base Case)

The results are presented in figures 4.5, 4.6 and 4.7

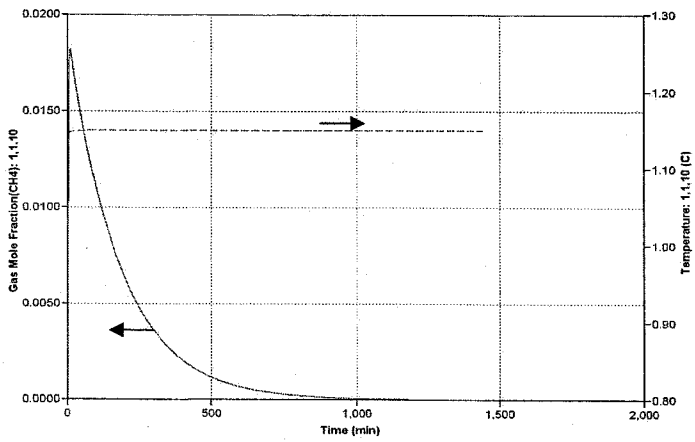

Figure 4-5 CH4 Mole fraction in the gas phase and Temperature profile during the Base Case

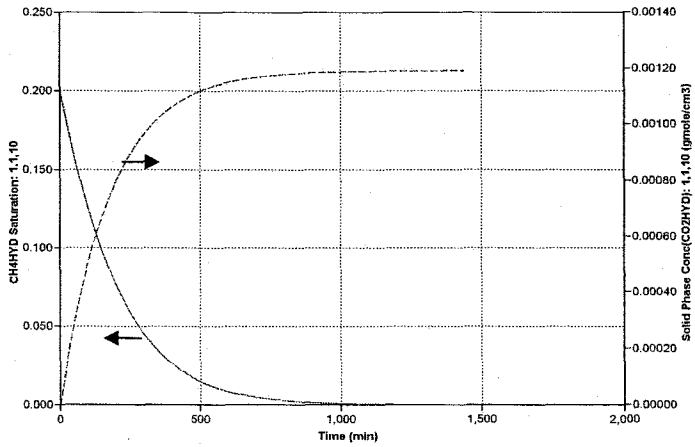

Figure 4-6 CH_4 and CO_2 Hydrates profile during the Base Case

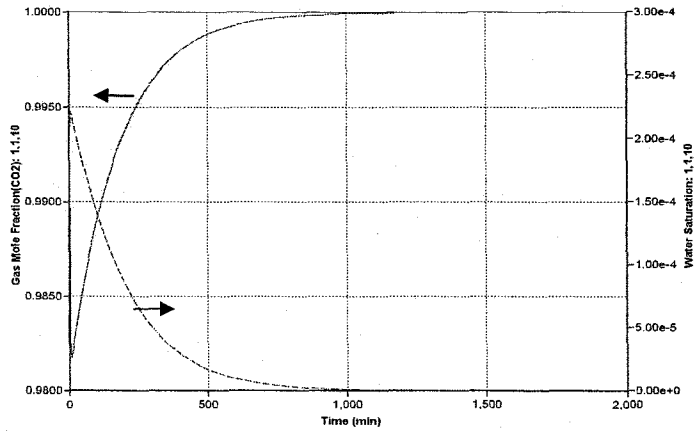

Figure 4-7 CO_2 Mole fraction in the gas phase and water saturation profile during the Base Case

The following conclusions can be made from the results presented through figures 4.5 to 4.7

- These graphs show that at the beginning of the process a fast decomposition of CH_4-hydrate occurs followed by the formation of CO_2-hydrate which can be inferred by the temperature drop and the increase of water saturation.
- The system recovers quickly its initial temperature. This is due to the fact that the equipment is immersed in a constant temperature bath and that the CH_4-hydrate heat of decomposition and CO_2-hydrate heat of formation are very similar.

- Water saturation is always very low, meaning that all the water is almost being consumed as soon it is produced.
- Gas composition of CH_4 increases at the beginning of the process and tend to fade with time due to it is constantly removed of the system.
- Total conversion of CH_4-hydrate is achieved at approximately 1000 min

To verify the effect of some of the process variables, four additional cases are presented:

I. Effect of CO_2 flow rate injection: Q_{CO2}=10 cm^3/min

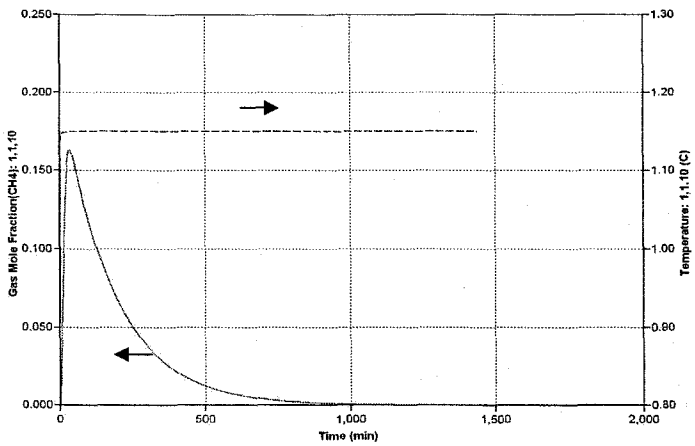

Figure 4-8 CH4 moles fraction in the gas phase and temperature profile during the alternative I

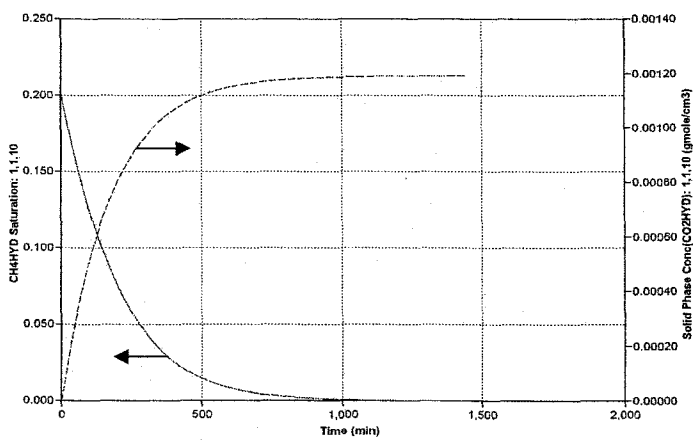

Figure 4-9 CH_4 and CO_2 hydrates saturation profile during the alternative I

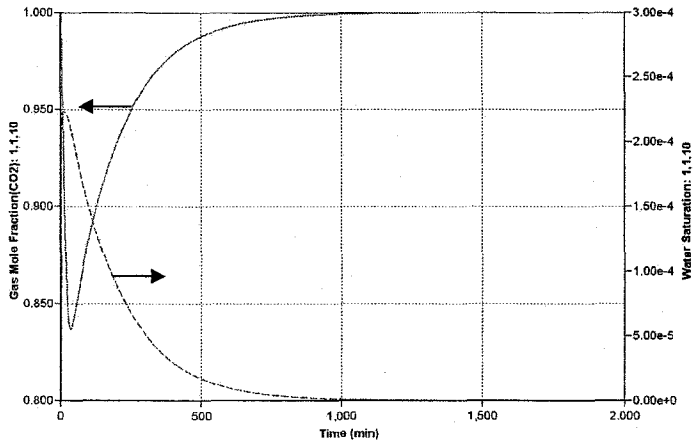

Figure 4-10 CO_2 moles fraction in the gas phase and water saturation profile during the alternative I

From these graphs, it can be seen that by reducing the CO_2 flow rate from $100cm^3/min$ to $10cm^3/min$ does not really affect the kinetics of exchange; however, in this case it was assumed that mass transfer resistance is negligible. This will be checked during the experiments. The small variations on the decomposition and formation rates are due to the different composition in the gas mixture.

II. Effect of external heat transfer: Q=0 J/s

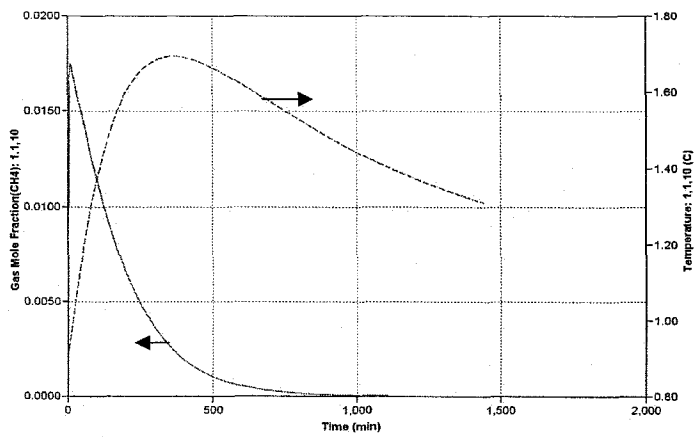

Figure 4-11 CH4 moles fraction in the gas phase and temperature profile during the alternative II

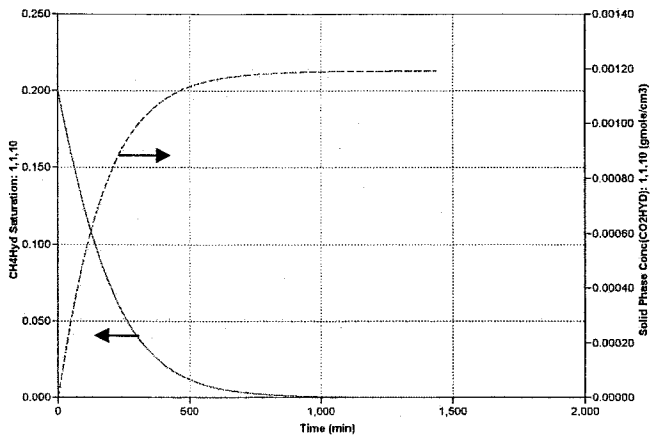

Figure 4-12 CH_4 and CO_2 hydrates saturation profile during the alternative II

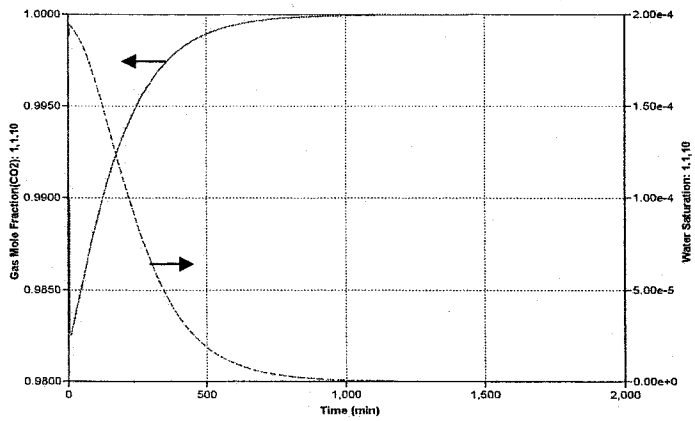

Figure 4-13 CO_2 Mole fraction in the gas phase and water saturation profile during the alternative II

These graphs show that even if the system is completed insulated, the rate of replacement is not affected significantly, this result can be explained by the fact the heat of decomposition of CH_4-Hydrate is very similar to the heat of formation of CO_2-Hydrate, making the temperature change very small. This can be noticed in the temperature profile, where initially there is a fast drop in temperature due to the initial decomposition to subsequently increase to a maximum of 1.7C and finally the temperature starts decreasing once again in a smooth way, due to the continuous entrance of fresh CO_2.

III. Effect of permeability: 10 mD (in presence of hydrate)

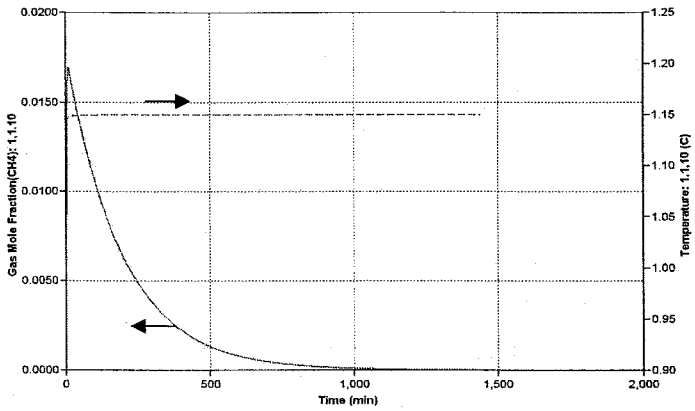

Figure 4-14 CH4 mole fraction in the gas phase and temperature profile during the alternative III

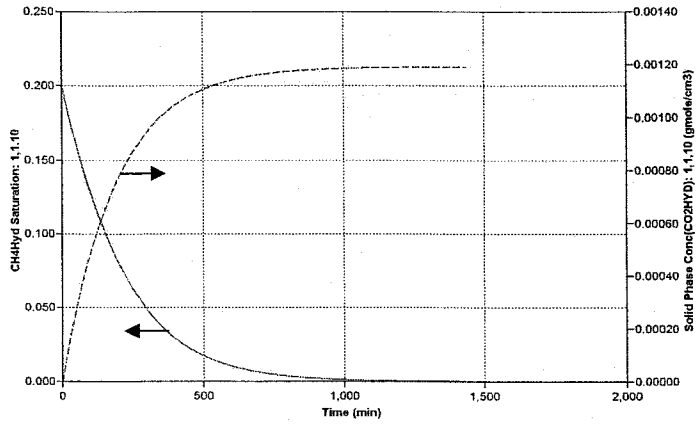

Figure 4-15 CH_4 and CO_2 hydrate saturation profile during alternative III

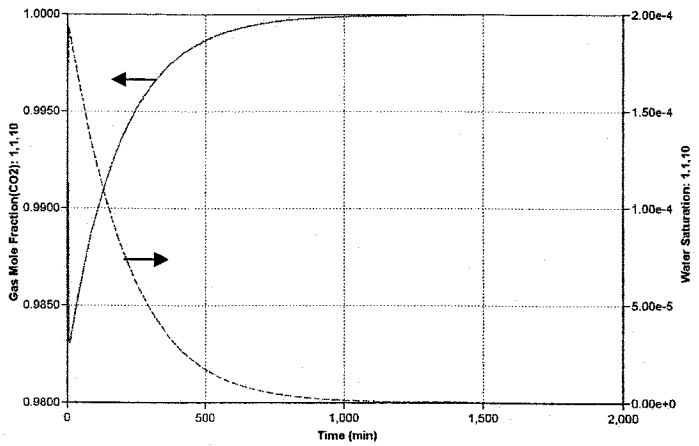

Figure 4-16 CO2 mole fraction in the gas phase and water saturation profile during alternative III

These curves showed similar behaviour when compared to the base case, however, despite the fact the permeability was reduced drastically the rate of replacement was reduced only by a 5%. Thus, for this system, the fluid flow is not the controlling mechanism.

IV. Effect of Kinetics: Although the kinetics constants have been previously established, the area exposed to reaction is an important factor that plays a key role in the kinetics. Thus, assuming $A_{SH} = 1.875*10^{-5}\ m^{-1}$

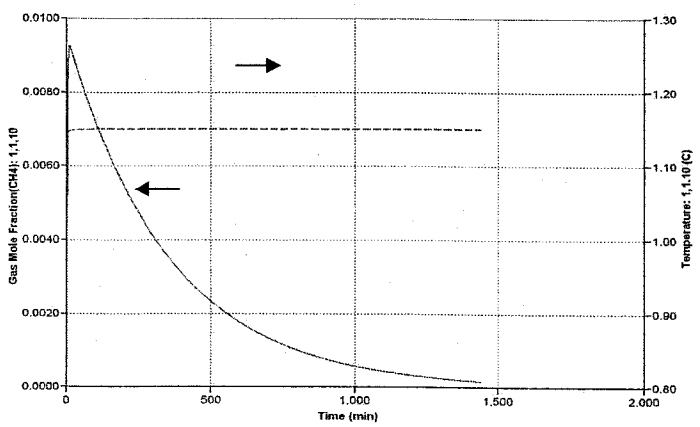

Figure 4-17 CH_4 mole fraction in the gas phase and temperature profile during the alternative IV

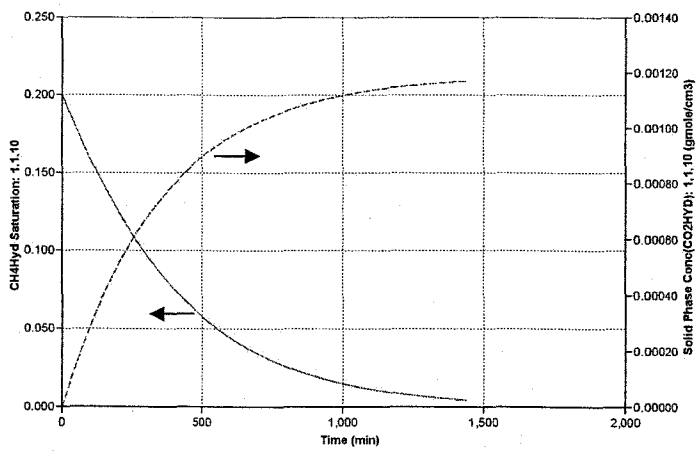

Figure 4-18 CH_4 and CO_2 Hydrate saturation profile during the alternative IV

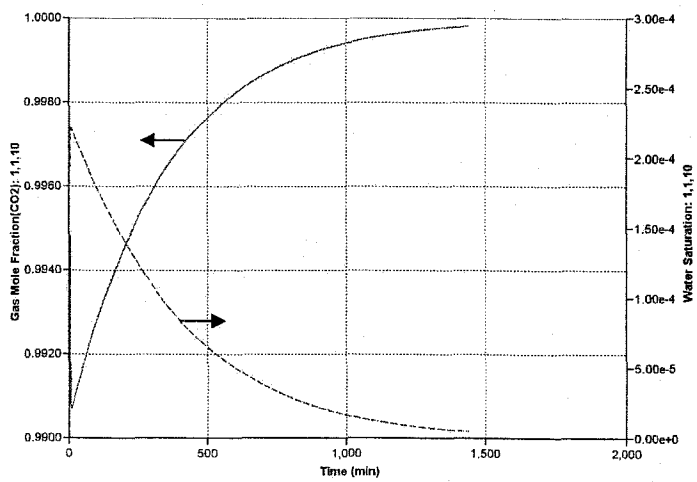

Figure 4-19 CO_2 mole fraction in the gas phase and water saturation profile during the alternative IV

These graphs show that the effect of the surface plays a key role in the overall process of CH_4-CO_2 replacement, by reducing the reaction area, the rate of decomposition diminishes significantly. The following table 4.1, presents some of the results on how CH_4-Hydrate saturation changes with time

Time (min)	Case Base	Alternative I	Alternative II	Alternative III	Alternative IV
0	0.2	0.2	0.2	0.2	0.2
178	0.084	0.084	0.082	0.088	0.132
536	0.012	0.012	0.010	0.014	0.052
715	0.004	0.004	0.003	0.006	0.032

Table 4-1. Comparative table of CH_4 hydrate saturation.

Based on these results, it is possible to conclude that the controlling mechanism is the intrinsic kinetics; in particular, the determination of the reaction area of hydrates in the porous media will affect considerably the final model.

Chapter Five: FUTURE WORK

Further experiments on determining intrinsic kinetics constants for methane hydrate dissociation as well as the processes of formation/dissociation of CH_4/CO_2 mixtures and pure CO_2 will be carried out.

Experimental work on CH_4-CO_2 replacement on CH_4-hydrate in porous media will continue.

Numerical simulation results will be compared with the experimental results and the model will be modified if necessary to match the experimental data.

References

Adisasmito, S; Frank, R.; Sloan D.; "Hydrates of carbon dioxide and methane mixtures"; Journal of chemical engineering data; v 36; n 1; p 68-71; 1991.

Alotaibi, F.; "Determination of the intrinsic kinetics of decomposition of hydrates formed from mixtures of nitrogen and carbon dioxide using in-situ particle size analysis", MSc. Thesis, University of Calgary, 2005.

Alotaibi, F.; "Kinetics Studies of Gas Hydrate Formation Using In-situ Particle Size Analysis and Raman Spectroscopy", PhD. Thesis, University of Calgary, 2009.

Bergeron, S.; Servio, P.; "Reaction rate constant of CO2 hydrate formation and verification of old premises pertaining to hydrate growth kinetics"; AIChE Journal, v 54, n 11, p 2964-2970, 2008.

Clarke, M.; Bishnoi, P.R.; Determination of the activation energy and intrinsic rate constant of methane gas hydrate decomposition; Canadian Journal of Chemical Engineering, v 79, n 1, p 143-147, 2001.

Clarke, M.; Bishnoi, P.R.; "Determination of the intrinsic rate constant and activation energy of CO2 gas hydrate decomposition using in-situ particle size analysis"; Chemical Engineering Science, v 59, n 14, p 2983-2993, 2004

Clarke, M.; Bishnoi, P.R. ; "Determination of the intrinsic kinetics of CO2 gas hydrate formation using in situ particle size analysis"; Chemical Engineering Science, v 60, n 3, p 695-709, 2005

Collett, T. ; Kuuskraa, A.; "Emerging U.S. gas resources - 4. Hydrates contain vast store of world gas resources"; Oil and Gas Journal, v 96, n 19, p 90-95, 1998.

Energy Information Administration form the US government, www. eia.doe.gov/oiaf/ ieo/ nat_gas.html , 2009.

Englezos, P.; Kalogerakis, N.; Dholabhai, P.D.; Bishnoi, P.R. "Kinetics of formation of methane and ethane gas hydrates. Chemical Engineering Science, v 42, n 11, p 2647-2658, 1987.

Giraldo, C.; "Measurement and Thermodynamic Modeling of Ethane and Carbon Dioxide Gas Hydrate Incipient Conditions in Reverse Micelles", MSc. Thesis, University of Calgary, 2008

Goel, N.; In situ methane hydrate dissociation with carbon dioxide sequestration: Current knowledge and issues; Journal of Petroleum Science and Engineering, v 51, n 3-4, p 169-184; 2006

Graue, A.; Kvamme, B.; Baldwin, B.A.; Stevens, J.; Howard, J.; Aspenes, E.; Ersland, G.; Huseb, J.; Zornes, D.; "CO_2 storage in natural-gas-hydrate reservoirs benefits from associated methane production"; JPT, Journal of Petroleum Technology; v 58; n 8; p 65-67; 2006

Gudmundsson, J., Borrehaug, A., "Frozen Hydrate for Transport of Natural Gas", Proc. 2nd Int. Conf. on Natural Gas Hydrates, 415−422, (1996).

Hirohama S., Shimoyama Y., Wakabayashi A., Tatsuta S., and Nishida N., "Conversion of CH4-Hydrate to CO2-Hydrate in liquid CO2", Journal of Chemical Engineering of Japan, v 29, n6, pp 1014-1020, 1996.

Hong, H.; "Modeling of gas production form hydrates in porous media", MSc. Thesis, University of Calgary, 2003.

Jadhawar P., Yang J., Jadhawar J., and Tohidi B., "Preliminary Experimental Investigation on Replacing Methane in Hydrate Structure with Carbon Dioxide in Porous Media", 5th International Conference on Gas Hydrates, Throndheim, Norway, p 1006-1011, 2005.

Kim, H.C. ; Bishnoi, P.R.; Heidemann, R.A.; Rizvi, S.S.H.; Kinetics of methane hydrate decomposition"; Chemical Engineering Science, v 42, n 7, p 1645-1653, 1987.

Komai, T.; Yamamoto, Y.; Ohga, K.; "Dynamics of reformation and replacement of CO2 and CH4 gas hydrates"; Third International Conference on Gas Hydrates, Salt Lake City, USA; p 272-280; 1999.

Komai, T.; Kawabe, Y.; Kawamura, T; Yoon, J.Extraction of Gas Hydrates Using CO2 Sequestration; Proceedings of the International Offshore and Polar Engineering Conference, p 321-326, 2003

Kumar A.; "Formation and dissociatin of gas hydrates in porous media", MSc. Thesis, University of Calgary, 2005.

Lee H., Seo Y., Moudrakovski I., and Ripmeester J., "Recovering Methane from Solid Methane Hydrate with Carbon Dioxide", Angewwandte Chemie International Edition, v42, p 5048-5051, 2003.

Majorowicz, J.A. and Osadetz, K.G.; "Gas hydrate distribution and volume in Canada"; American Association of Petroleum Geologists Bulletin, v 85, n 7, p 1211-1230, 2001

Nguyen, H., Phillips, J., John, V.T, "Clathrate Formation in Reversed Micellar Solutions", Journal of Physical chemistry, v93, n25, 8123-8126, 1989.

Oghaki, K.; Takano, K. Sangawa, H.; Matsubara T. and Nakano S.; "Methane exploitation by carbon dioxide from gas hydrates-phase equilibria for CO_2-CH_4 mixed hydrate system"; Journal of chemical engineering of Japan; v 29; n3; p 478-483, 1996.

Ota, M.; Morohashi, K.; Abe, Y.; Watanabe, M.; Lee R.; Innomata, H.; "Replacement of CH_4 in the hydrate by use of liquid CO2"; Energy Conversion and Management, v46, n 11-12, p 1680-1691, 2005.

Ota, M.; Abe, Y.; Watanabe, M.; Smith Jr., R..; Inomata, H.;Methane recovery from methane hydrate using pressurized CO2; Fluid Phase Equilibria, v 228-229, p 553-559; 2005.

Ota, M.; Saito, T.; Aida, T.; Watanabe, M.; Sato, Y.i; Smith, L.; Inomata, H.; "Macro and microscopic CH4-CO2 replacement in CH 4 hydrate under pressurized CO2"; AIChE Journal, v 53, n 10, p 2715-2721, 2007.

Park, Y; Kim, Y; Lee, W; Huh, G; Park, P; Lee, J; Lee H; "Sequestering carbon dioxide into complex structures of naturally occurring gas hydrates"; :Proc Natl Acad Sci; v103; n 34; p 12690-12694; U S A; 2006.

Phillips, J., Nguyen, H., John, V.T., "Protein Recovery from Reversed Solutions Through Contact with a Pressurized Gas Phase", Biotechnol. Prog., v7, p 43-48, 1991.

Rao, A., Nguyen, H., John, V.T., "Modification of Enzyme Activity in Reversed Micelles Through Clathrate Hydrate Formation", Biotechnol. Prog., v6, p 465-471, 1990.

Stevens, J.; Howard, J; Baldwin B.; Ersland, G.; Husebo, J.; Graue, A; " Experimental hydrate formation and gas production scenarios based on CO2 sequestration"; Proceedings of the 6th international conference on gas hydrates; Vancouver, 2008.

Uchida, T.; Takeya, S.; Ebimuna, T.; Narita, H.; "Replacing methane with CO2 in clathrate hydrate: Obaservations using raman spectroscopy"; Greenhouse gas control technologies, 2001.

Uddin, M; Coombe D.; Wright F.; "Modeling of CO2-Hydrate formation in geological reservoirs by injection of CO2"; Journal of Energy Resources Technology, v 130, p 0325021- 03250211; 2008.

Uddin, M; Coombe D.; Law D.; "Numerical studies of gas hydrate formation and decomposition in a geological reservoir"; Journal of Energy Resources Technology, v 130, p 0325011- 03250114; 2008.

Uddin, M; Coombe D.; Law D.; Gunter W.; "Numerical studies of gas hydrate formation and decomposition in a geological reservoir"; SPE Gas Technology Symposium; SPE 100460; Calgary; p 1-13; 2006.

Yang J., Chapoy A., and Tohidi B., "Thermodynamic Conditions and Kinetics of Integrated Methane Recovery and Carbon Dioxide Sequestration", Offshore Technology Conference, Houston, USA, p 976-982, 2008.